

AD-A280 478

ON PAGE

Form Approved
OMB No. 0704-0188**1**Public
gathe
collec
Data

ge 1 hour per response, including the time for reviewing instructions, searching existing data sources, collection of information. Send comments regarding this burden estimate or any other aspect of this Washington Headquarters Services, Directorate for Information Operations and Reports, 1215 Jefferson Management and Budget, Paperwork Reduction Project (0704-0188), Washington, DC 20503.

1. AGENCY USE ONLY (Leave blank)		2. REPORT DATE 26 March 1994		3. REPORT TYPE AND DATES COVERED Final Report: 15 Dec 90 to 14 Dec 93	
4. TITLE AND SUBTITLE Modeling and Control of Intelligent Flexible Structures				5. FUNDING NUMBERS AFOSR-91-0181	
6. AUTHOR(S) Daniel J. Inman					
7. PERFORMING ORGANIZATION NAME(S) AND ADDRESS(ES) The Research Foundation of the State University of New York on Behalf of the University of Buffalo P. O. Box 9 Albany, NY 12201-0009				8. PERFORMING ORGANIZATION REPORT NUMBER AFOSR-TR- 94 0353	
9. SPONSORING/MONITORING AGENCY NAME(S) AND ADDRESS(ES) AFOSR/NA Bldg. 410 Bolling AFB, DC 20332-6448				10. SPONSORING/MONITORING AGENCY REPORT NUMBER	
11. SUPPLEMENTARY NOTES 94 6 20 039					
12a. DISTRIBUTION/AVAILABILITY STATEMENT Approved for public release; distribution unlimited.					
13. ABSTRACT (Maximum 200 words) The research effort reported here summarizes the issues and discoveries of a three year effort to examine the modeling and control of intelligent structures for aerospace applications. Intelligent structures or smart structures or more appropriately, active structures are defined here in a narrow sense as structures with highly integrated sensors and actuators (piezoceramic elements in this case). The major control thrust is vibration suppression. The issues of interest are a) is the complexity of a smart structure control system worth it, b) how detailed must modeling be to produce effective results, and c) does the choice of a control law make a significant difference on the response. The results show clearly that improved models and complex control strategies form the most effective combination. The results show three experimental examples which clearly indicate the usefulness and advantages of smart structures over conventional vibration suppression methodologies. In particular, active structures improve overall efficiency in cases involving both flexible and rigid body control. In addition, some tangent results on nonlinear control, control in the presence of uncertainties and control of thermoelastic systems are presented.					
14. SUBJECT TERMS smart intelligent structure, slewing, solar arrays, antenna, structural control, nonlinear controller, thermo-elastic response, critical speed control.				15. NUMBER OF PAGES 25	
				16. PRICE CODE	
17. SECURITY CLASSIFICATION OF REPORT unclassified		18. SECURITY CLASSIFICATION OF THIS PAGE unclassified		19. SECURITY CLASSIFICATION OF ABSTRACT unclassified	
				20. LIMITATION OF ABSTRACT UL	

94-18972
DTIC
SELECTED FOR
S B D
JUN 21 1994

AFOSR-JR 94 0353

Approved for public release;
distribution unlimited.

Modeling and Control of Intelligent Flexible Structures

Final Technical Report

March 1994

AFOSR-91-0181

by

Daniel J. Inman

Department of Engineering Science and Mechanics

Virginia Polytechnic Institute and State University

Blacksburg, VA 24061-0219

(703) 231-4709 FAX (703) 231-4574 email INMAND@vtvml.cc.vt.edu

DTIC QUALITY INSPECTED 2

TABLE OF CONTENTS

1. Introduction	1
2. Summary of Smart Structures Results	1
3. Results on Nonlinear Modal Control	4
4. Results on Control of Uncertain Systems	6
5. Control of Critical Speeds	7
6. Control of a Thermoelastic Systems	8
7. References	10
8. Where the Objectives Meet?	11
9. Publications	11
10. Personnel Supported	12
11. Coupling Activities	12
12. Appendix	15
A. 1st Year Annual Report	15
B. 2nd Year Annual Report	33
C. Papers Produced in the 3rd Year	121

Accession For	
NTIS GRA&I	<input checked="" type="checkbox"/>
DTIC TAB	<input type="checkbox"/>
Unannounced	<input type="checkbox"/>
Justification	
By _____	
Distribution/ _____	
Availability Codes	
Dist	Avail and/or Special
A-1	

1. INTRODUCTION

The results obtained under the support of this grant are divided into four categories corresponding to sections 2-5. The main thrust of the proposed and funded research has been the modeling and control of intelligent flexible structures. Two previous reports (Appendix I and II) delineate the efforts and results of the funded research during the first two years of support. The present document focuses on the results of the last year of support. In addition to results obtained while focusing on the objectives at hand (see section 7), general results were obtained which are not directly related to the proposed objectives. These results are related to the discovery of a nonlinear modal control method presented in section 3, a deterministic methodology for treating the control of uncertainty in structures presented in section 4, and the control of critical speeds in rotating machines as discussed in section 5. Section 6 reviews some preliminary results in the control of thermoelastic systems.

In addition to the summary presentation of results, this report concludes with a discussion of the original objectives, in section 9 and whether or not these have been met (they have), and a list of publications under AFOSR support in section 9. Section 10 lists the graduate students supported under the 3 years of this grant and section 10 discusses coupling activities and technology transfer effectuated while under AFOSR support. The appendix contains the first two annual technical reports for this award to provide completeness.

2. SUMMARY OF SMART STRUCTURE RESULTS

A substantial amount of research effort has been put forth in the area of smart structures and intelligent material systems over the last decade, often without regard for application. The work reported here examined a common example of a smart structure, i.e., the infamous cantilevered beam in bending with either a surface mounted or embedded piezoceramic actuators and sensors, and the application of this configuration to control unwanted vibration in a variety of configurations common to satellites. In particular, results for three applications point out natural, and perhaps unique, solutions to the vibration suppression problem,

provided by a smart structures approach. The first of these three examples consists of the slewing motion of a flexible beam through its bending direction around a rigid hub driven by a motor. Such motions are common in space and robotics applications. The addition of a piezoceramic based closed loop system is shown to significantly impact the power and performance of the slewing configuration.

The second application examines the vibration suppression of slewing frames similar to those used as solar panels on satellites. Such frames are rich in coupled bending and torsion and known to vibrate excessively while slewing. The torsional motion is not able to be suppressed by use of the rigid body actuator (motor) as is conventional. Here piezoceramics mounted directly on the frame are shown to render the torsional motion controllable providing an order of magnitude improvement in system performance. Thus, a smart structure approach is shown to provide a solution to a difficult vibration suppression problem not solvable by conventional sensors and actuators. Both theoretical prediction and experimental verification is provided. Power consumption is shown to be minimal, and in fact, less in some cases.

The third application examines the vibration suppression of a ribbed antenna similar to those used on satellites (e.g. TDRSS). Such structures exhibit repeated and nearly repeated natural frequencies. Hence, controllability becomes an issue and again a smart structures approach provides a low cost natural solution to a practical vibration problem. Again both experimental and theoretical results were obtained.

The results obtained under the support of this grant are summarized in several journal papers and proceeding articles by the author's graduate students (Leo and Inman, 1994, Leo and Inman, 1993a, b, 1992a, b, Garcia and Inman, 1990, Dosch et al., 1993a, b, 1992, Inman and Garcia, 1992, Garcia et al. 1991). These results indicate a clear, logical use of smart structures to solve vibration suppression problems in situations where conventional sensors and actuators are not applicable. From a control theory point of view, the use of smart structures is beneficial because it allows the control designer to approach full state feedback

in the design of a given system without resorting to state estimation. In addition, the use of smart structures allows placement of sensors and actuators at almost any location allowing a maximum use of the concept of controllability and observability. From a mechanical design point of view, use of smart structures offers an order of magnitude reduction in settling times for a small expenditure of power.

The specific results delineated in the Appendix B as well as in the refereed papers are:

- a smart structure approach allows sensors and actuators to be placed throughout a structure or machine, allowing one to approach full state feedback.
- because sensors and actuators can be placed almost anywhere within a structure or machine, they can be placed at points of maximum controllability and observability, rendering very low power consumption in active control.
- in cases where rigid body motion is controlled along with flexible motion, the use of smart structures can actually reduce total power consumption for equivalent performance. Alternatively, the smart structure approach can be use to provide increased performance.
- in cases where repeated modal frequencies require multiple actuator/sensors for controllability, smart structures provide a natural solution.
- complex modeling issues can be avoided by using positive position feedback (PPF) control as robustness depends only upon measurements of the open loop eigenvalues.
- the better the model, the more sophisticated the control law can be and the better the performance.

Power Consumption While not yet published, it is clear from the results of experiments that using smart structures involves a very small increase in total power consumption. In some cases, the total power actually decreases (Garcia and Inman 1990). The power consumption

in slewing solar panel experiments indicate that an increase in power of 0.3 watts (i.e., from 121.53 to 121.83 watts) results in a substantial increase in performance. In particular, if the damping ratios of the closed loop motor control are compared to the closed loop motor control with smart structures attached (Leo and Inman) a dramatic improvement in performance is observed. In particular, the use of rotational rigid body actuators exhibit low controllability in torsion whereas the addition of piezoceramic actuators provide a drastic increase in performance under combined rigid/smart structure control. The damping ratio for the smart structural control system

- increases by a factor of 15 in the 1st torsional mode
- increases by a factor of 23 in the 2nd torsional mode
- increases by a factor of 6 in the 1st plate mode

and 1.5 times in the second bending mode. This represents a large improvement in performance for a very small increase in power during a 30° slew maneuver.

Additional Results The main results in this section are reported in appendix B. In addition, several journal papers have been accepted and are included in appendix C along with copies of the appropriate conference papers.

3. RESULTS IN NONLINEAR MODAL CONTROL

Although not part of the original objective, the personnel funded by this support and also funded by ARO (DJI) determined a new method of providing closed loop control for weakly nonlinear systems which does not require any linearization.

This work extended the work of Shaw and Pierre (1992) on nonlinear normal modes to include the case of forced response. This allows the nonlinear normal mode method to be applied to the feedback control problem providing a new method of controlling nonlinear systems. The proposed method uses the transformation proposed by Shaw and Pierre for

homogeneous systems written in state space form. The coordinate transformation for the forcing vector is defined in the state space and related to the physical coordinate system. The results is a pseudo modal decoupling transformation of a nonlinear inhomogeneous system. Although interesting in its own statement, this transformation also provides a nonlinear modal control scheme. This result is applied to a known coupled two degree of freedom oscillator with a cubic stiffness term. The results illustrate the design of a nonlinear modal control law.

The concept that nonlinear modes with nonlinear modal equations exist for some set of nonlinear systems has been accepted intuitively by many for quite some time. It wasn't until 1964 when Rosenberg presented the first paper on nonsimilar normal modes that it became possible to solve even the simplest nonsimilar normal mode system. Many perturbation methods have been developed to approximate the deviation of a nonlinear mode from a corresponding linear mode. However, only the Shaw and Pierre method utilizes the definition of nonsimilar nonlinear modes as invariant manifolds. This method allows the straight forward computation of nonsimilar nonlinear normal modes and their corresponding mode shapes. Although algebraically tedious, this method lends itself to programming using algebraic manipulation packages such as Mathematica[©] and MACSYMA[©].

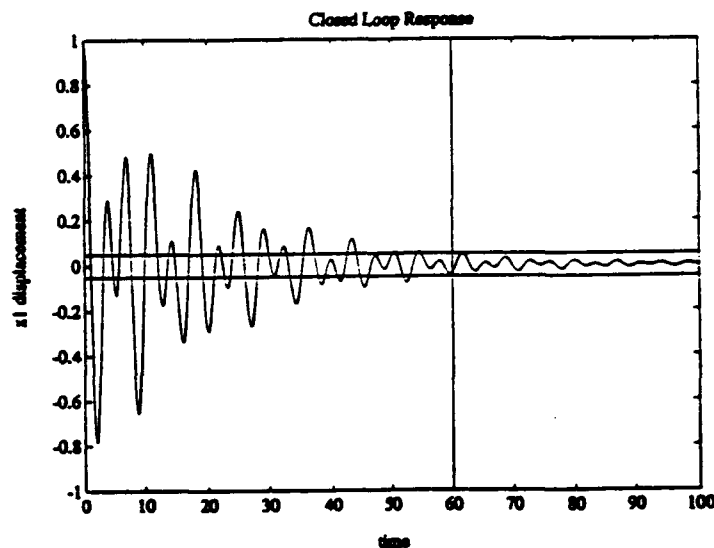


Figure 1. The displacement time response of one mass of a 2 degree of freedom oscillator with cubic nonlinear using nonlinear feedback modal control. The open loop system is undamped.

4. RESULTS ON THE CONTROL OF UNCERTAIN SYSTEMS

Convex optimization techniques have been developed to design feedback control laws for structures with uncertain transient inputs. The uncertain disturbances are modeled deterministically as convex sets of functions. Three types of models have been considered; one which bounds the total energy of the disturbance, another which bounds the instantaneous energy, and a third that limits the maximum and minimum values of the input. Each of these models provide an alternative to the usual statistical description (i.e. expected value). Expressions for the maximum response are derived for each model. The optimal feedback control law is found via the solution of an infinite dimensional optimization by an affine parameterization of all stabilizing controllers. The parameterization maintains convexity and converges to the unique solution as the number of terms in the approximation is increased. The techniques have been illustrated on a simple model of an unconstrained flexible structure.

As an application of the usefulness of this method, it has been used to design collocated control laws for the small-scale model of a flexible antenna used in section 2. The objective of the active control is to minimize the response of a single rib to a disturbance occurring at a remote location on the structure. Two separate designs are examined. The first is standard Linear Quadratic Gaussian (LQG) control, whereby the H_2 norm of the transfer matrix is minimized via the solution of two Riccati equations. Unfortunately, this type of design does not exploit the favorable attributes of sensor/actuator collocation, resulting in control laws that are not robust to model uncertainty and structural variations. An optimization approach to H_2 optimal design is presented that bounds the phase of the control law, thereby increasing its robustness. The optimization is shown to be convex, providing important guarantees on solution accuracy and convergence. Control laws designed with both procedures have been experimentally implemented on the antenna testbed. The results illustrate the advantages of designing H_2 optimal controllers that are bounded in phase.

Experimental implementation of H_2 optimal controllers designed via constrained convex

optimization illustrated the robustness achieved by bounding the phase of the compensator. In comparison with standard Linear Quadratic Gaussian (LQG) designs, they remained stable in the presence of structural variations and model uncertainty. The loss of performance that resulted from constraining the optimization could be compared to a trade-off curve that represented all achievable LQG solutions. In this way, convex optimization proved to be effective method of studying the trade-offs associated with constraining the phase of the controller.

Although the results of the initial effort are encouraging, many questions arose regarding the convex optimization approach to control design. For example, the optimal solutions were found to be sensitive to the choice of functions used in the Q parameterization. Furthermore, the optimization seemed to exhibit convergence properties when the constraint on the control effort became large. Checking the phase constraint at discrete points (even for a fine grid) introduced errors into the control design. Finally, the pole-zero cancellation procedure used in this paper was a rather ad hoc method of order reduction, the reasons why more advanced methods were ineffective needs to be investigated. Future work involves studying these topics and also generalizing the phase constraints to control systems with more than one sensor and actuator. The details of these results are reported in Leo and Inman (1994, a,b), which appear in Appendix C.

5. CONTROL OF CRITICAL SPEEDS

A method has been researched for suppressing the resonances that occur as a rotating machine is spun-up from rest to its operating speed. This proposed method invokes "stiffness scheduling" so that the resonant frequency of the system is shifted during spin-up so as to be distant from the excitation frequency. A strategy for modulating the stiffness through the use of shape memory alloy has been derived.

Most common applications of "smart materials" actuators involves obliging them to undergo some generalized displacement in response to a specified stimulus. A slightly dif-

ferent approach is used in an application in which a modulus rather than a displacement is manipulated.

The results, using a very simple model a rotatory machine, clearly indicate that stiffness scheduling can reduce critical speed amplitude during run up. In particular, it is shown in Parker, Segalman and Inman (1993) that the critical speed amplitude is reduced by 1/3 of its open loop value by the use of shape memory alloys and the stiffness scheduling control law. This work was supported by DOE (Parker, Segalman) and Inman's time was paid in part by ARO, in part by AFOSR under this grant.

6. CONTROL OF THERMOELASTIC SYSTEMS

Thermally induced vibrations remain largely uncontrolled while their presence can significantly affect the stability of structures. Thermal effects are important in space applications and in other structures required to operate in environments where large temperature gradients are common. In the satellite industry, thermally induced vibrations are a recurring problem which affect the stability and the proper operation of satellites. The vibrations are typically caused by the rapid heating of satellite appendages during normal orbital flight. At the day-night and night-day orbital transitions, sudden heating produces temperature gradients which result in time dependent thermal moments. These thermally induced moments can cause significant undesirable vibrations in the satellite. Numerous satellites have been lost as a result of this problem and, therefore, it is important to find a method to satisfactorily suppress these vibrations and to minimize their effect on the operation of the spacecraft. The purpose of this work was to investigate thermally induced transverse vibrations in flexible satellite appendages with the expectation that the results will be useful to the satellite industry.

Consider, for example, a typical solar array found on most satellites. The solar array is made up of two booms, a rigid bar and a solar blanket. The two booms are usually cantilevered to a rotating shaft at one end and to the rigid bar at the other end. The

solar blanket is a membrane stretched between the rigid bar and the rotating shaft. The thermal disturbances generated in this structure result from the temperature gradients in the two booms. The magnitudes of the thermal disturbances from the solar blanket and the rigid bar are insignificant when compared to those generated in the booms. For this reason, the dynamics of the boom were investigated. Each boom can be approximated as a simply supported beam in transverse vibration. Assuming that the Euler-Bernoulli beam assumptions hold, linear equations of motion were obtained which include a time dependent thermal moment term. The thermal effects appear as a disturbance (a time varying thermal moment) in the equations of motion and they also appear in the boundary conditions. Knowing the temperature distribution in the beam and the material parameters, the thermal moment can be calculated. In solving for the temperature distribution, a classical heat transfer approach was taken, where the motion of the structure does not affect the temperature distribution. That is, an uncoupled thermal structural analysis was performed where the beam was assumed rigid for the purpose of calculating the temperature distribution and neither the incidence of the heat flux nor the actual structural deformations affected the solution.

It was determined that a distributed control force would be most suitable to suppress the thermally induced vibrations. Therefore, a piezoelectric sensor/actuator pair was added to the model and two different control methods were applied. In the first case, an LQR controller was used to suppress the vibrations. The results for the controlled case showed a significant improvement in time response over the uncontrolled case. In the uncontrolled case, the magnitude of the vibrations remained largely unchanged for times longer than one minute, since very little damping was included in the model. Adding LQR control to the system, the vibrations were suppressed in less than one second. This was possible, since the beam examined was very small (i.e., low inertia). In the second case, positive position feedback was used to control the vibrations. The results were similar to the LQR case. A significant amount of damping was added to the model through active control. The results of the study

indicate that it is possible to model and control thermally induced vibrations in a simply supported beam. The results suggest that the problems of thermally induced vibrations encountered in the satellite industry can be solved using currently available technology.

7. REFERENCES

Dosch, J. J., Leo, D. J. and Inman, D. J., 1992, "Comparison of Vibration Control Schemes for a Smart Antenna," Proceedings of the 31st IEEE Conference on Decision and Control, pp. 1815-1820.

Dosch, J., Leo, D. J. and Inman, D. J., 1993a, "Modeling and Control for Vibration Suppression of a Flexible Smart Structures," in *Dynamics and Control Structures in Space II*, ed. Kirk, C. L. and Hughes, P. C., pp. 603-618.

Dosch, J., Leo, D. J. and Inman, D. J., 1994, "Modeling and Control for Vibration Suppression of a Flexible Smart Structure," *AIAA Journal of Guidance, Control and Dynamics* to appear.

Garcia, E. and Inman, D. J., 1990. "Advantage of Slewing an Active Structure," *Journal of Intelligent Material Systems and Structures*, Vol. 1, No. 4, pp. 261-272.

Garcia, E., Dosch, J. and Inman, D. J., 1992, "The Application of Smart Structures to the Vibration Suppression Problem," *Journal of Intelligent Material Systems and Structures*, Vol. 3, No. 4, pp. 659-667.

Inman, D. J. and Garcia, E., 1991, "Vibration Suppression Using Smart Structures," *Smart Structures and Materials*, ed. Haritos, G. K., and Srinivassan, A. V., AMD Vol. 123, ASME, pp. 167-172, 1991 Winter Annual Meeting (invited).

Leo, D. J. and Inman, D. J., 1992a, "Control of a Flexible Frame in Slewing," Proceedings of the American Control Conference, pp. 2535-2539.

Leo, D. J. and Inman, D. J., 1992b, "Smart Slewing Frames," Proceedings of the First European Conference on Smart Structures.

Leo, D. J. and Inman, D. J., 1993a, "Modeling and Control of a Slewing Frame Containing Self-Sensing Active Members," *Smart Materials and Structures*, Vol. 2, pp. 82-95.

Leo, D. J. and Inman, D. J., 1993b, "Active Control of a Slewing Frame Using Smart Structures," Conference on Modern Practice in Stress and Vibration Analysis, Ed. J. L. Wearing, Sheffield Academic Press, April 1993b, pp. 203-214.

Leo, D. J. and Inman, D. J., 1994, "Pointing Control and Vibration Suppression of a Slewing Flexible Frame," *AIAA Journal of Guidance and Control*, to appear.

Leo, D. J. and Inman, D. J., 1994a, "Linear Control Design for Structures with Uncertain Transient Disturbances," to appear, AIAA Dynamics Specialized Conference, April 1994.

Leo, D. J., and Inman, D. J., 1994b, "Convex Controller Design for Vibration Suppression of a Flexible Antenna," International Conference on Intelligent M????, Williamsburg, VA.

Parker, G. G., Segalman, D. J., and Inman, D. J., 1993, "Vibration Suppression by Modulation of Elastic Modulus Using Shape Memory Alloy," *Proceedings ASME B? Vibrations and Noise Conference*, Vol. 58, pp. 1-10.

Shaw, S. W., and Pierre, C., 1992, "Normal Modes for Nonlinear Vibratory Systems," *Journal of Sound and Vibration*, to appear.

Slater, J. C., 1993, *Nonlinear Modal Control*, Ph.D. Thesis, State University of New York at Buffalo, Buffalo, NY.

Slater, J. C. and Inman, D. J., 1993, "Forced Response of Nonlinear Systems for Modal Control," Meeting.

Vakakis, A. F., 1991, *Analysis and Identification of Linear and Nonlinear Normal Modes in Vibrating Systems*, Ph.D. Thesis, California Institute of Technology, Pasadena, California.

8. WERE THE OBJECTIVES MET?

A comparison between the funded objectives and the resulting research illustrates that these objectives have been met, precisely. In particular, a theoretical and experimental investigation of the modeling and control of smart aerospace like structures for vibration suppression has been performed and the issues have been identified (see section 2). The only issue not specifically completed is a rigorous comparison of smart structural control to passive damping. This was not performed as result of others have clearly indicated the advantage of smart materials over passive devices.

9. PUBLICATIONS

This section lists those journal articles in pressure, print or under review during the award period. Only those manuscripts submitted to archival journals are listed.

Banks, H.T. and Inman, D.J., "On Damping Mechanisms in Beams," *ASME Journal of Applied Mechanics*, Vol. 58, No. 3, September 1991, pp. 716-723.

Banks, H.T. and Inman, D.J., "On the Significance of Modeling Internal Damping in the Control of Structures," *AIAA Journal of Guidance, Control and Dynamics*, Vol. 15, No. 6, Nov.-Dec. 1992, pp. 1509-1512.

Banks, H. T., Wang, Y., Inman, D. J. and Slater, J.C., "Approximation and Parameter Identification for Damped Second Order Systems with Unbanded Input Operation," *Control: Theory and Applied Technology*, submitted, May 1993.

Banks, H. T., Wang, Y., and Inman, D. J., "Bending and Shear Damping in Beams: Frequency Domain Estimation Techniques," *Journal of Vibration and Acoustics*, to appear.

Ben-Haim, Y. and Inman, D. J., "Vibration Control with Unknown Disturbances Represented by Convex Models of Uncertainty," *Journal of Dynamic Systems, Measurement and Control*, submitted April 1993.

Crassidis, J. L., Leo, D. J., Mook, D. J. and Inman, D. J., "Robust Identification on Vibration Suppression of Flexible Structures," *AIAA Journal of Guidance and Control*, to appear.

Dosch, J.J., Inman, D.J. and Garcia, E., "A Self Sensing Piezoelectric Actuator for Collocated Control," *Journal of Intelligent Materials, Systems and Structures*, Vol. 3, No.

1, January 1992, pp. 166-185.

Dosch, J. J., Leo, D. J. and Inman, D. J., 1993b, "Modeling of a Smart Antenna for Active Vibration Suppression," Proceedings of the 11st International Modal Analysis Conference, pp. 1418-1424.

Garcia, E., Dosch, J. and Inman, D. J., 1991, "The Application of Smart Structures to the Vibration Suppression Problem," Proceedings of the Second Joint Japan-US Conference on Adaptive Structures.

Garcia, E. and Inman, D.J., "On the Modeling of the Slewing Control of a Flexible Structure," *AIAA Journal of Guidance, Control and Dynamics*, Vol. 114, No. 4, July-August 1991, pp. 736-742.

Leo, D. J. and Inman, D. J., "Modeling and Control of a Slewing Frame Containing Self-Sensing Active Members," *Smart Materials and Structures*, Vol. 2, pp. 82-95, 1993.

Leo, D. J. and Inman, D. J., "Pointing Control and Vibration Suppression of a Slewing Flexible Frame," *AIAA Journal of Guidance and Control*, to appear.

Ross, A.D.S. and Inman, D.J., "Design Criteria for Predicting Damping in Underdamped Linear Lumped Parameter Systems," *AIAA Journal of Guidance, Control and Dynamics*, Vol. 14, No. 5, September/October 1991, pp. 1033-1039.

Slater, J. C. and Inman, D. J., "Transfer Function Modeling of Damping Mechanisms in Distributed Parameter Models," *Mechanics Research Communications*, Vol. 20, No. 4, pp. 287-292, 1993.

Yae, H. and Inman, D.J., "Model Reduction in a Subset of the Original States," *Journal of Sound and Vibration*, Vol. 155, No. 1, March 1992, pp. 165-176.

Yae, K.H. and Inman, D.J., "Control Oriented Order Reduction of Finite Element Models," *ASME Journal of Dynamic Systems, Measurement and Control*, to appear.

Zimmerman, D.C., Inman, D.J. and Juang, J - N, "Vibration Suppression Using a Constrained Rate-Feedback Threshold Control Strategy," *ASME Journal of Vibration and Acoustics*, Vol. 113, No. 3, July 1991, pp. 345-353.

10. PERSONNEL SUPPORTED

Professional personnel supported in full or part under this grant are the principal investigator, Daniel J. Inman, and the following graduate students: Donald Leo, Ralph Rietz, Jeffrey Dosch, and Ephraim Garcia.

11. COUPLING ACTIVITIES

Dr. Inman gave invited departmental seminars and public lectures on activities funded under this grant at the following organizations: PCB Electronics, Inc., ASME Nigam Mohawk Section, Mercedes Benz Sensor-Actuator Group, Kodak Government Systems Group,

NASA Langley Research Center, University of Michigan, University of Illinois, Virginia Tech, University of Northern Illinois, Carnegie Mellon University, Pennsylvania State University, Wright State University, University of Waterloo, Rensselaer Polytechnic Institute, University of Kentucky and the Catholic University of America. In addition, Dr. Inman taught two short courses in the US and one in Taiwan on smart structures and presented over 27 papers at national and international conferences. A list of conference papers follow:

Banks, H. T., Wang, Y., Inman, D. J. and Slater, J. L., "Variable Coefficient Distributed Parameter System Models for Structures with Piezoceramic Actuators and Sensors," Proceedings of the 31st IEEE Conference on Decision and Control, December 1992, pp. 1803-1808.

Crassidis, J. L., Leo, D. J., Mook, D. J. and Inman, D. J., "Robust Identification and Control of a Flexible Structure," Proceedings Guidance Navigation and Control Conference, August 1993.

Cudney, H.H., Inman, D.J. and Oshman, Y., "Distributed Structural Control Using Multi Layered Piezoelectric Actuators," Proceedings of the AIAA 31st Structures, Dynamics and Materials Conference, 1990, pp. 2257-2265.

Dosch, J. J., Calamita, J. P. and Inman, D. J., "Performance of a Programmable Structure," Proceedings 1993 SPIE Conference on Smart Structures and Materials *MATHEMATICS IN SMART STRUCTURES*, ed. H. T. Banks, Vol. 1919, February 1993, pp. 151-156.

Dosch, J., Leo, D. J. and Inman, D. J., "Modeling and Control for Vibration Suppression of a Flexible Smart Structure," in *Dynamics and Control Structures in Space II*, ed. Kirk, C. L. and Hughes, P. C., pp. 603-618, September 1993.

Dosch, J. J., Leo, D. J. and Inman, D. J., "Comparison of Vibration Control Schemes for a Smart Antenna," Proceedings of the 31st IEEE Conference on Decision and Control, December, 1992, pp. 1815-1820.

Dosch, J. J., Leo, D. J. and Inman, D. J., "Modeling of a Smart Antenna for Active Vibration Suppression," Proceedings of the 11th International Modal Analysis Conference, February 1993, pp. 1418-1424.

Garcia, E., Dosch, J. and Inman, D.J., "The Application of Smart Structures to the Vibration Suppression Problem," Proceedings of the Second Joint Japan-US Conference on Adaptive Structures, November 1991.

Garcia, E., Dosch, J. and Inman, D.J., "Feedback Control of an Active Antenna Structure," Proceedings of the 8th VPI&SU Symposium on Dynamics and Control of Large Structures, May 1991, pp. 291-298.

Garcia, E., Dosch, J. and Inman, D.J., "Vibration Attenuation in an Active Antenna Structure," Proceedings Recent Advances in Active Control of Sound and Vibration, April 1991, pp. 535-542.

Garcia, E. and Inman, D.J., "Control Formulations for Vibration Suppression of Active Structures in Slewing Motions," ASME 1990 Winter Annual Meeting. (Invited) *Advances in Dynamic and Control of Flexible Spacecraft and Space Based Manipulators*. Ed. Joshi, Alberts and Kakad, DSC Vol. 20- pp. 1-5.

Garcia, E., and Inman, D. J., "Modeling of Actuator-Structure Interaction in the Slewing

of a Flexible Structure," Proceedings of the 1990 American Controls Conference, San Diego, California, May 23-25, 1990.

Inman, D. J., "Model Correction Using Frequency Data," International Conference on Structural Dynamics Modeling, Test, Analysis and Correlation, NAFEMS, July 1993, pp. 349-358.

Inman, D. J. and Garcia, E., "Vibration Suppression Using Smart Structures," *Smart Structures and Materials*, ed. Haritos, G. K., and Srinivassan, A. V., AMD Vol. 123, ASME, 1991 pp. 167-172. 1991 ASME Winter Annual Meeting. (invited)

Inman, D.J., Garcia, E. and Pokines, B., "Vibration Suppression and Slewing Control of a Flexible Structure," Proceedings of the 4th NASA Workshop on Computation Control of Flexible Aerospace Systems, July 1990, Part II, pp. 663-672.

Inman, D.J., Garcia, E. and Dosch, J., "Vibration Suppression Using Smart Structures," *Smart Structures and Materials*, ed. Haritos, G.K. and Srinivasan, A.V., AMD, Vol. 123, 1991, ASME, pp. 167-172.

Inman, D.J. and Garcia, E., "Smart Structures for Vibration Suppression," Proceedings of the 4th International Conference on Recent Advances in Structural Dynamics, Southampton, UK, July 1991, pp. 139-155.

Leo, D.J. and Inman, D.J., "Control of a Flexible Frame in Slewing," Proceedings of the American Control Conference, June 1992, pp. 2535-2539.

Leo, D.J. and Inman, D.J., "Smart Slewing Frames," Proceedings of the First European Conference on Smart Structures, May 1992.

Leo, D. J. and Inman, D. J., "Control System Design for a Smart Slewing Frame," Proceedings of the Second Conference on Recent Advances in Active Control of Sound and Vibration," April 1993, pp. 717-728.

Leo, D. J. and Inman, D. J., "Active Control of a Slewing Frame Using Smart Structures," Conference on Modern Practice in Stress and Vibration Analysis, Ed. J. L. Wearing, Sheffield Academic Press, April 1993, pp. 203-214.

Leo, D. J., Crassidis, J. L., Inman, D. J., and Mook, D. J., "Experimental Study of Structural Uncertainties in an H_∞ Design," Ninth VPI&SU Symposium on Dynamics and Control of Large Structures, May 1993.

Rietz, R. W. and Inman, D. J., "Comparison of Linear and Nonlinear Control on a Distributed Parameter System," in *Vibration and Control of Mechanical Systems*, ed. Tan, C. A., Bergman, L. A. and Yang, B., ASME Vol. 61, 1993, pp. 43-50.

Segalman, D. J., Parker, G. G. and Inman, D. J., "Vibration Suppression by Modulation of Elastic Modulus Using Shape Memory Alloy," in *Intelligent Structures, Materials and Vibration*, ed. Shahinapoor, M. and Tzou, H. S., ASME Vol. 58, 1993, pp. 1-5.

Slater, J. C., and Inman, D. J., "Forced Response of Nonlinear Systems for Modal Control," ASME Applied Mechanics Summer Meeting, *Recent Developments in Stability, Vibration and Control of Structural Systems*, ed. A. Guran, ASME AMD Vol. 167, June 1993.

Van Norstrand, W. C., Knowles, G. J. and Inman, D. J., "Active Constrained Layer Damping for Micro-Satellites," in *Dynamics and Control of Structures in Space II*, ed. Kirk, C. L. and Hughes, P. C., pp. 667-681, September 1993.

Yae, K. H. and Inman, D.J., "Control Oriented Order Reduction of Finite Element Models," Proceedings of the 1991 Joint Automatic Control Conference, May 1991, pp. 2187-2189.

APPENDIX A
1st Year Annual Report

REPORT DOCUMENTATION PAGE

Form Approved
OMB No. 0704-0188

Public reporting burden for this collection of information is estimated to average 1 hour per response, including the time for reviewing instructions, searching existing data sources, gathering and maintaining the data needed, and completing and reviewing the collection of information. Send comments regarding this burden estimate or any other aspect of this collection of information, including suggestions for reducing this burden, to Washington Headquarters Service, Directorate for Information Operations and Reports, 1215 Jefferson Davis Highway, Suite 1204, Arlington, VA 22202-4302, and to the Office of Management and Budget, Paperwork Reduction Project (0704-0188), Washington, DC 20503.

1. AGENCY USE ONLY (Leave blank)		2. REPORT DATE 11 March 92	3. REPORT TYPE AND DATES COVERED Annual Technical Report: 15 Dec 90 to 14 Dec 91	
4. TITLE AND SUBTITLE Modeling and Control of Intelligent Flexible Structures - slewing frames			5. FUNDING NUMBERS G AFOSR-91-0181	
6. AUTHOR(S) Daniel J. Inman and Donald Leo				
7. PERFORMING ORGANIZATION NAME(S) AND ADDRESS(ES) The Research Foundation of the State University of New York on Behalf of the University of Buffalo PO Box 9 Albany, NY 12201-0009			8. PERFORMING ORGANIZATION REPORT NUMBER	
9. SPONSORING/MONITORING AGENCY NAME(S) AND ADDRESS(ES) AFOSR/NA Bldg. 410 Bolling AFB, DC 20332-6448			10. SPONSORING/MONITORING AGENCY REPORT NUMBER	
11. SUPPLEMENTARY NOTES				
12a. DISTRIBUTION/AVAILABILITY STATEMENT unlimited			12b. DISTRIBUTION CODE	
13. ABSTRACT (Maximum 200 words) The modeling and experimental investigation of a smart slewing frame is reported. The smart, or active, frame consist of a flexible 11 bay two dimensional frame with a piezoceramic strut connected to ground through a rotational electric motor providing the slewing motion. The slewing motion induces relatively uncontrollable torsional vibration. The active frame member renders the torsional model controllable and proves a natural application of smart structure technology. Noncolocated and colocated control laws are implemented using the active strut as both a sensor and an actuator. The relative effectiveness of several structural control laws in suppressing torsional motion is discussed				
14. SUBJECT TERMS smart intelligent structure, slewing, frame, structural control			15. NUMBER OF PAGES 16	
			16. PRICE CODE	
17. SECURITY CLASSIFICATION OF REPORT unclassified	18. SECURITY CLASSIFICATION OF THIS PAGE unclassified	19. SECURITY CLASSIFICATION OF ABSTRACT unclassified	20. LIMITATION OF ABSTRACT UL	

Modeling and Control of Intelligent Flexible Structures - Slewing Frames

1. Introduction

In recent years, there has been a large amount of research on slewing structures against a fixed base. These structures present challenging control problems since the action of slewing induces residual vibrations. These vibrations can degrade performance when strict pointing and tracking requirements are to be maintained.

Until now, most of the work has concentrated on the slewing of flexible beams. For the most part, these structures exhibit only bending motion when excited [1-3]. Recently, research performed by Sakawa and Luo [4] studied the control of a flexible beam with an eccentric tip mass. This tip mass induced torsional vibrations when slewed, adding a new dimension to the control problem. They presented motor control schemes designed to simultaneously slew the structure and suppress vibrations.

The effort described here also examines the problem of slewing a structure that exhibits bending and torsional vibrations. The structure studied is not a flexible beam, though, but a frame that models the dynamics of a solar array. The torsional motion induced when slewed is relatively uncontrollable using colocated motor control. Smart structure technology will be applied in an attempt to suppress this motion. Namely, a piezoceramic strut placed in the frame will render these modes controllable. A number of different control laws will be experimentally verified.

2. Slewing Frame Testbed

A slewing frame was constructed to provide an experimental testbed for control. The frame consisted of thin-walled circular aluminum tubing (Figure 1). Slewing actuation was provided by an Electro-Craft 670 dc motor. Angular rate and position sensors could be used for analog motor control.

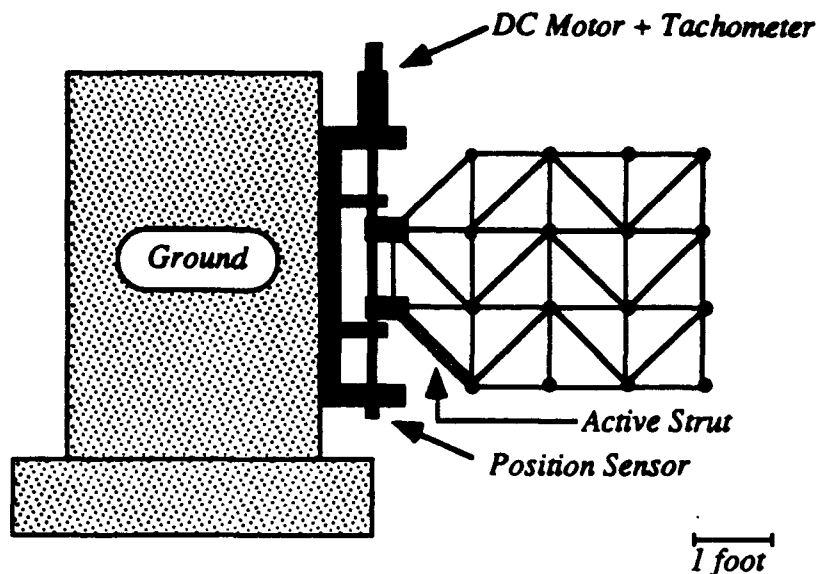


Figure 1. Slewing Frame Testbed.

An active strut was designed and inserted into the slewing frame. It consisted of a flat aluminum bar layered with four piezoceramics on each side. Each ceramic was a Model G-1195 from Piezo Electric Products with dimensions 2.5" x 0.75" x 0.01". The strut was configured so that it could be used as a sensor, an actuator, or as a collocated sensor/actuator pair. Figure 2 is a drawing of the active strut. The output from the active strut is proportional to the strain induced in the member. Conversely, the active strut produced a bending moment proportional to the command input.

A number of computers were available for control and data acquisition. A Comdyna GP-6 analog computer was used for position control of the frame and various signal operations (summation, subtraction, etc.). Control laws for the active strut were implemented on an Optima 3 digital controller sampling at 1500 Hz. Finally, data acquisition and frequency analysis was performed using a Tektronix 2630 Fourier Analyzer.

The objective of the experiments was to slew the frame in a reasonable amount of time while minimizing unwanted vibrations. Due to the configuration of the structure, bending and torsional vibrations were induced when a maneuver was performed. The rest of this paper will deal with the modeling and control aspects of this problem.

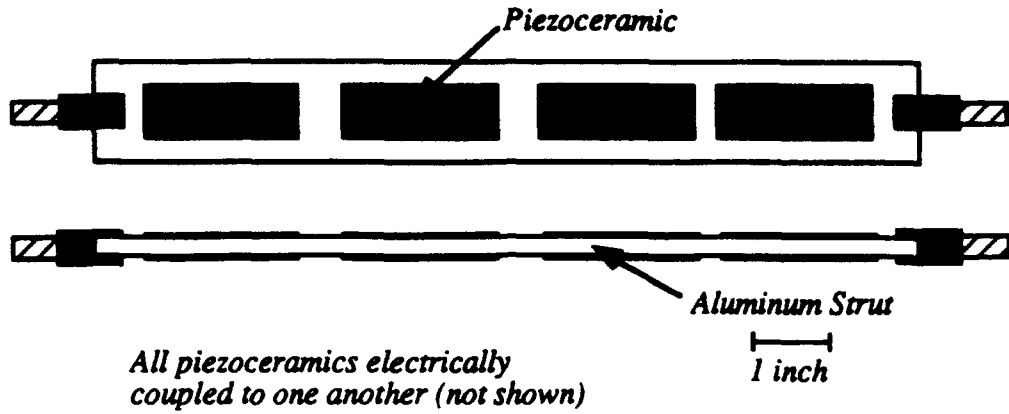


Figure 2 Piezoceramic Active Strut.

3. Modeling and Analytical Results

A linear model of the slewing frame was developed so that a number of control laws could be tested analytically. In physical coordinates, this model takes the form [3]

$$\begin{bmatrix} [M] & I_b \\ I_b^T & I_s \end{bmatrix} \begin{Bmatrix} \ddot{q} \\ \ddot{\theta} \end{Bmatrix} + \begin{bmatrix} [K] & 0 \\ 0 & 0 \end{bmatrix} \begin{Bmatrix} q \\ \theta \end{Bmatrix} = \{f\} \quad (1)$$

where M and K are the mass and stiffness matrices of the structure, respectively, I_s is the rigid body inertia about the slewing axis, and I_b is part of the interaction between the rigid body and flexible motion. The physical coordinates of the structure are denoted q , and the rigid body rotation is symbolized by θ . f is a matrix of applied forces and the overdot represents differentiation with respect to time.

To correctly model the interaction between the motor and the structure, pinned-free natural frequencies and mode shapes were used. The mass and stiffness matrices were built using finite elements and a modal test was performed to verify analytical results [5]. By collecting the normalized mode shapes into a matrix S_m , equation (1) was transformed into modal coordinates by assuming $q = S_m r$ and premultiplying by S_m^T . This yields

$$\begin{bmatrix} [I] & \tilde{I}_b \\ \tilde{I}_b^T & I_s \end{bmatrix} \begin{Bmatrix} \ddot{r} \\ \ddot{\theta} \end{Bmatrix} + \begin{bmatrix} [\Lambda] & 0 \\ 0 & 0 \end{bmatrix} \begin{Bmatrix} r \\ \theta \end{Bmatrix} = \{S_m^T f\} \quad (2)$$

A is a matrix of the form $\text{diag}\{\omega_1^2, \omega_2^2, \dots, \omega_N^2\}$, and $\tilde{I}_b = S_m^T I_b$. I is an $N \times N$ identity matrix, where N is the number of flexible modes in the model.

The active strut was modeled as a moment generator [6]. For simplicity, it was assumed to span the entire length of the strut. Although not a rigorous model of the piezoelectric effect, it did produce satisfactory results.

To study the slewing frame, a 16 mode model was developed using finite elements. The boundary condition was chosen to be pinned-free, and the natural frequencies and mode shapes were verified by a modal test. Initially, a simple Proportional-Derivative (PD) controller of the form

$$G_{pd}(s) = -K_v \dot{\theta} - K_p \theta$$

was used for position control of the frame. The gains were set to values that produced an adequate step response. Due to the nature of the boundary condition, this controller also added damping to certain flexible modes. This occurs because the pinned-free condition allows a large amount of interaction between the structure and the motor. In the model, the damping in the motor is added to the flexible motion through the applied loads vector f . Consequently, derivative action on the motor also produces an increase in damping in the flexible motion. Results of an analytical study where $K_p = 2.5$ and $K_v = 6.5$ are given in Table 1. All modes were initially assumed to be undamped.

This study reveals that a simple PD motor control adds a significant amount of damping to the bending modes. This is consistent with previous results [7]. Table 1 also shows that the torsional motion is still relatively undamped.

Table 1. Natural Frequencies and Damping Ratios in the flexible modes using PD control.

Mode	$\omega_d(\text{Hz})$	ζ % Critical
Torsional	4.37	0.41
Bending	8.87	11.24
Torsional	15.47	0.50
Plate	19.79	0.3
Bending	27.53	5.10

In an attempt to control the first torsional mode of the slewing frame, an analysis was performed using the active strut as a sensor and an actuator. Various control laws were attempted. The two that performed the best were Generalized Structural Filtering (GSF) and Positive Position Feedback (PPF). Analytical designs were obtained using the model. They indicated that the damping in the first torsional mode could be increased to 5.7 % using the GSF method and to 8.5 % using PPF control. Details of the actual designs will be presented in the following section.

4. Experimental Results

Analytical results indicated that the torsional motion of the frame was difficult to suppress using colocated motor control. Further studies revealed that by using an active strut, these torsional vibrations could be rendered controllable. Experimental results support these conclusions and provide studies in the design of active control systems for flexible structures.

Three levels of control were implemented on the slewing frame. The first consisted of a simple PD compensator for the motor. This was necessary in order to position the frame and suppress the bending vibrations. Next, a non-colocated control law was designed to adequately damp the dominant torsional motion. Finally, a colocated controller using the active strut was implemented and the results were compared to the non-colocated case. Figure 3 is a schematic of the overall control architecture.

Proportional-Derivative Motor Control

The first control law studied was a simple PD compensator of the form given in equation (3). The $\dot{\theta}$ term was the tachometer output, and θ was the signal from the potentiometer. The reference command was a step input of 1 volt. This corresponded to a 30° slewing maneuver. The active strut was only used as a sensor for these experiments.

A typical response of the frame position is shown in Figure 4. The settling time for the slew maneuver is about 6 seconds. In addition to controlling the position of the frame, the PD compensator has the desirable effect of suppressing the bending motion. Unfortunately, the torsional motion is still relatively undamped, even with quite a lot of derivative action on the motor. Table 2 lists the natural frequencies and damping ratios for the case of experimental PD control. It shows that the colocated motor control suppresses

the dominant bending motion but leaves the torsional mode lightly damped. This trend is similar to the results obtained analytically with the FEM model.

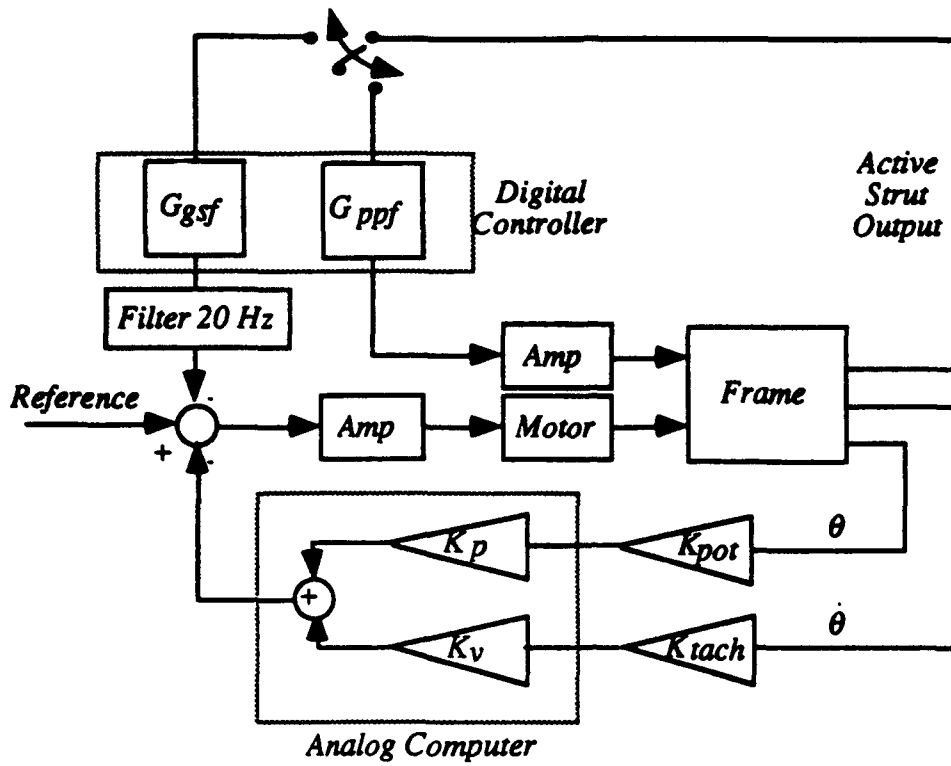


Figure 3. Slewing Frame Control Architecture.

Table 2. Natural frequencies and damping ratios for experimental PD control.

Mode	$\omega_d(\text{Hz})$	ζ % Critical
Torsional	4.32	0.82
Bending	7.68	9.18
Torsional	14.11	1.26
Plate	20.76	0.94
Bending	26.25	1.32

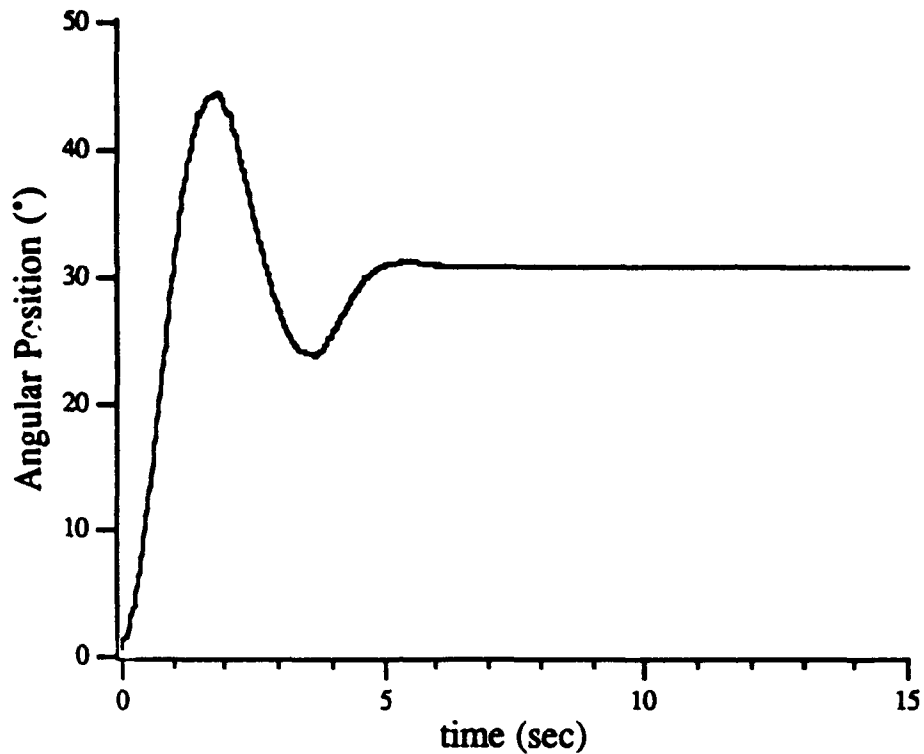


Figure 4. Frame Step Response ($K_p = 2.5$, $K_v = 6.5$).

Table 2. Natural frequencies and damping ratios for experimental PD control.

Mode	$\omega_d(\text{Hz})$	ζ % Critical
Torsional	4.32	0.82
Bending	7.68	9.18
Torsional	14.11	1.26
Plate	20.76	0.94
Bending	26.25	1.32

During this maneuver, the sensor output of the active strut during a 30° slew is shown in Figure 5. This illustrates the lightly damped torsional mode. The 4.32 Hz vibration does not settle for over 30 seconds, well after the slewing maneuver is over.

One problem that became important during the experiments was static friction in the motor and bearings. This problem is evident in Figure 4. The sudden stop of the slewing maneuver is due to the fact that the motor cannot overcome the dry friction in the system. This problem was even more important when control laws were implemented to suppress

the torsional motion of the frame. This will be discussed in the next section on non-colocated control.

Non-Colocated Control using the Active Strut

To supplement the PD compensator, a non-colocated controller was designed to add damping to the torsional mode. The design tool was a method called Generalized Structural Filtering (GSF). The GSF method uses non-minimum phase second order filters to successively stabilize structural poles. The design is done iteratively, using 'classical' techniques of root locus and Bode plots. For a detailed description of GSF control, see [8].

For this particular application, the design steps were as follows. Initially, a transfer function was taken between the motor input and the active strut output. A commercially available Recursive Least Squares package used the time domain data to obtain a pole-zero

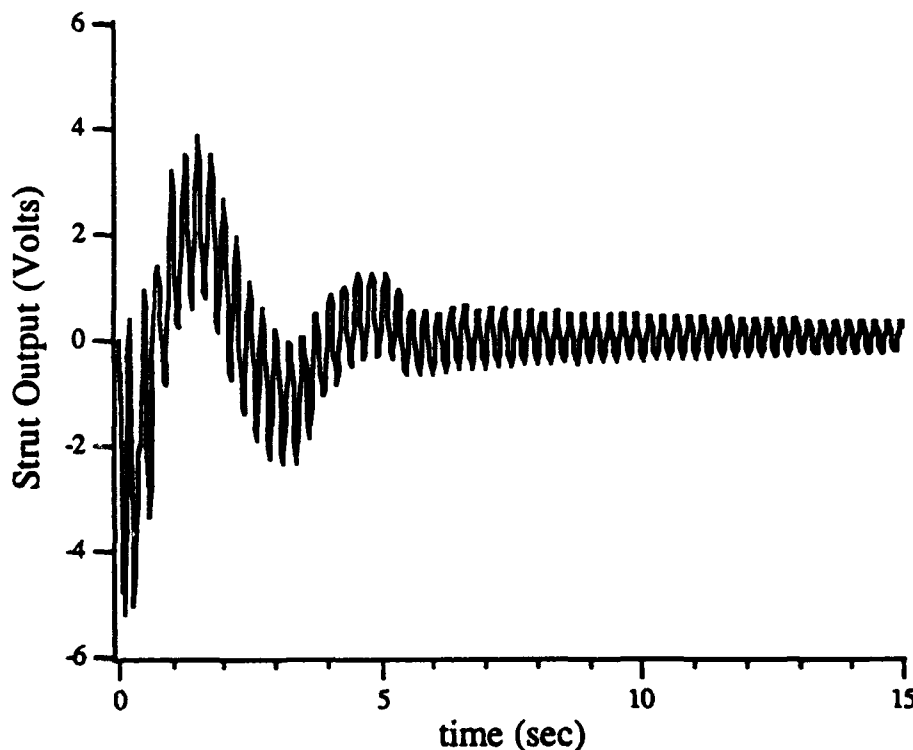


Figure 5. Active strut output for 30° slew maneuver with only PD control.

model [9]. From this model, root locus and Bode plots could be used to design a compensator. The objective of the design was to add damping to the torsional motion without destabilizing higher frequency dynamics. In an attempt to attenuate the high

frequency content of the control signal, it was filtered at 20 Hz with an Ithaca 24 dB/octave low-pass filter. A number of designs were attempted, with varying degrees of success. Each design was tested experimentally by feeding back the active strut output into the dc motor and performing a slewing maneuver. All but the final compensator caused instabilities in the flexible motion when experimentally implemented. The final GSF controller took the form

$$G_{gsf}(s) = .07 \frac{(s/20+1)(s - 29.5 + j 34.2)}{(s/40+1)(s + 26.0 + j 30.4)} \quad (4)$$

Equation (4) is the combination of a simple lead and a non-minimum phase filter. Figure 6 shows the response of the structure during a 30° slewing maneuver with GSF control on. The torsional motion is adequately damped out, i.e., by the time the slewing is over (≈ 7 s), the vibrations have ceased.

Even though this method damps out the torsional motion during a slew maneuver, the deadband in the motor makes it ineffective for disturbance rejection. If some type of input was applied to the frame (e.g. thermal shock of a solar panel) when it was not slewing, the controller could not react until it overcame the static friction in the system. Thus, the static friction limits the effectiveness of this non-colocated control.

To alleviate this problem, one of two things could be done. Quite simply, the first solution is to reduce the static friction by using better hardware. The less of a deadband, the more effective this type of controller will be. But since all real systems have static friction, a more practical approach would be to put both the sensor and actuator on the flexible structure [10]. If this is done, then the vibration suppression of the torsional motion would be independent of the slewing actuator. This colocated controller could suppress vibrations during a slew maneuver as well as reject disturbances. The last experiment deals with this type of design.

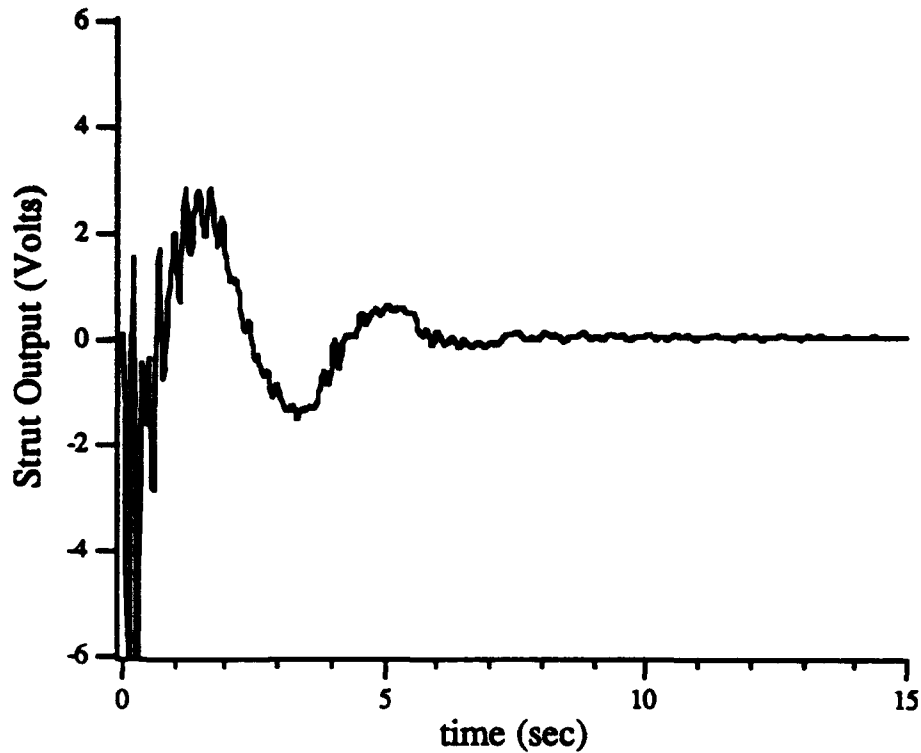


Figure 6. Structural response using GSF control during a 30° slew.

Control using the Active Strut as a Colocated Sensor Actuator

The final control strategy was to use the active strut as a colocated sensor/actuator. The design method was Positive Position Feedback (PPF). It is a type of second order filtering which has good robustness and stability properties [11].

The objective is the same as before, suppress the torsional motion without destabilizing higher modes. For the colocated case, stability boundaries are much better defined since the phase of the transfer function lies between 0 and -180° over most of the frequency range. Use of PPF control allowed for a much easier design process. Only two iterations were necessary to obtain a satisfactory result, as opposed to the five or needed for GSF control.

$$G_{ppf}(s) = 0.7 \frac{\omega_f^2}{s^2 + 2 \zeta_f \omega_f s + \omega_f^2} \quad (5)$$

$$\omega_f = 33.14 \text{ rad/s} \quad \zeta_f = 0.15$$

Implementation of this control law increased the damping in the torsional mode from about 0.82% to 3.8% critical, almost a factor of 5 better. The slewing response (Figure 7) is not as impressive as the one for the non-colocated control (Figure 6), but it is independent of the motor. With this type of control, disturbance rejection is achieved since the active strut serves as the actuator as well as the sensor.

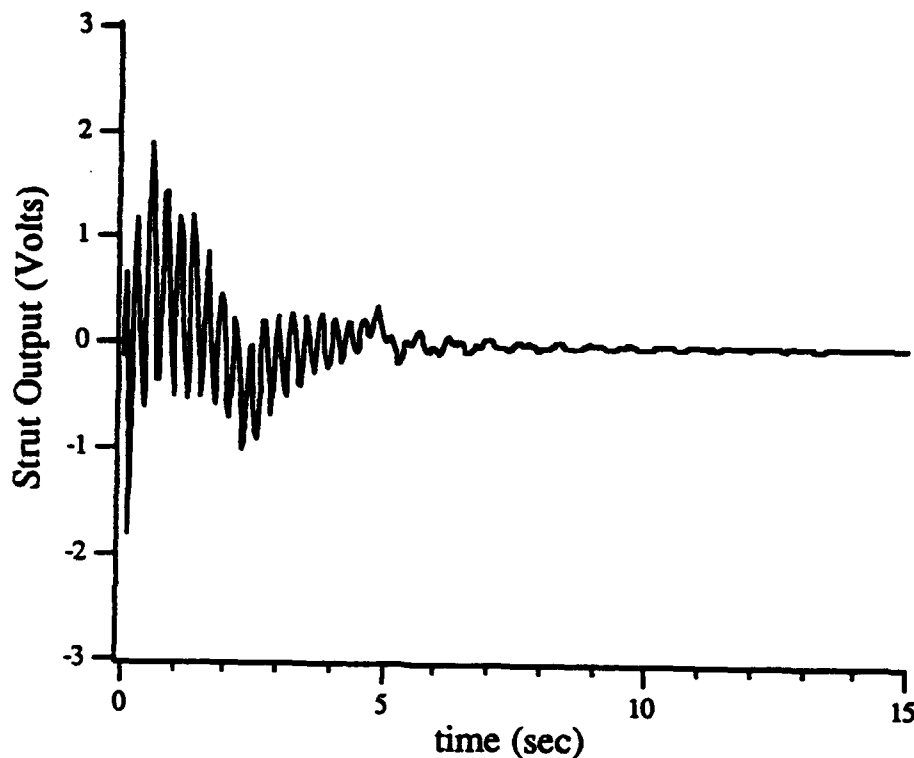


Figure 7. Structural response using PPF control on the active strut. Slew maneuver is 30° .

This last control experiment illustrates an important point about slewing an active structure. The advantages are that a number of separate colocated sensor/actuator pairs can be used for both vibration suppression and disturbance rejection. This alleviates the problem that the static friction played when using non-colocated control and allows more flexibility in designing control laws. This was especially apparent in this case, since the dominant torsional motion was not well controlled by motor control alone.

6. Objectives

The global objective of the proposed work is to model and experimentally verify the slewing of a smart/intelligent beam and a slewing active frame system complete with actuator dynamics, passive damping mechanisms and smart (piezoactive) system components.

The approach to be taken in modeling is to combine distributed parameter equations for the actuating and sensing piezoelectric devices with those of the flexible structure by using Euler Lagrange Equations. This approach also allows for the natural inclusion of the slewing actuator's dynamics. To date, only simple proportional control has been illustrated in the literature and at various laboratories. The approach here uses segmented actuators and sensors to produce a multi-input multi-output system so that modern control methods such as optimal control (minimum time/tracking) can be implemented and tested. They will be used to determine the design producing the most favorable closed loop response. The prediction will be experimentally verified.

The approach taken for the slewing frame is finite element based. Both passive constrained layer damping treatments and piezoactive treatments will be used to replace a frame element. A piezoactive frame element will be constructed and modeled to produce an active frame longeron. The active frame element is a unique concept which produces bending control in the frame which will be combined with the slewing motor control to produce desired vibrations suppression for improved performance.

7. Status

The significant accomplishment during this reporting period is the theoretical prediction and experimental verification that torsional modes in slewing two dimensional flexible structures require the use of a secondary piezoceramic actuators (smart structure) in order to reduce jitter and increase the closed loop performance.

The slewing of a structure that exhibited bending and torsional motion was examined. An analytical model predicted difficulty in suppressing the torsional vibration using a collocated controller located at the slewing actuator. This was experimentally verified on a testbed that consisted of a flexible frame slewed by a dc motor. An active strut was built by layering piezoceramic material on a flat aluminum bar. This strut was placed in the frame and a number of control experiments were performed. A non-collocated controller was designed using Generalized Structural Filtering techniques. This adequately suppressed the torsional vibrations but did not provide any disturbance rejection due to static friction in the system. Positive Position Feedback was then implemented using the active strut as a collocated sensor/actuator. Since this control scheme was independent of the motor, it was not limited by the static friction. Having two separate collocated controllers, one on the motor and one on the active strut, provided both vibration suppression during slewing and disturbance rejection.

8. Publications

This section list journal publications prepared or appearing in print while the PI was under partial support of this award.

Starek, L., Inman, D.J. and Kress, A., "A Symmetric Inverse Vibration Problem," ASME Journal of Vibration and Acoustics, to appear

Banks, H.T. and Inman, D.J., "On the Significance of Modeling Internal Damping in the Control of Structures," AIAA Journal of Guidance, Control and Dynamics, to appear.

Yae, K.H. and Inman, D.J., "Control Oriented Order Reduction of Finite Element Models," ASME Journal of Dynamic Systems, Measurement and Control, to appear.

Dosch, J.J., Inman, D.J. and Garcia, E., "A Self Sensing Piezoelectric Actuator for Collocated Control," Journal of Intelligent Materials, Systems and Structures, Vol. 3, No. 1, January 1992, pp. 166-185.

Starek, L. and Inman, D.J., "On Inverse Problems with Rigid Body Modes," ASME Journal of Applied Mechanics, December 1991, Vol. 50. pp. 1101-1104.

Ross, A.D.S. and Inman, D.J., "Design Criteria for Predicting Damping in Underdamped Linear Lumped Parameter Systems," AIAA Journal of Guidance, Control and Dynamics, Vol. 14, No. 5, September/October 1991, pp. 1033-1039.

Yae, H. and Inman, D.J., "Model Reduction in a Subset of the Original States," Journal of Sound and Vibration, Vol. 153, No. 3, 22 March 1992, to appear.

Banks, H.T. and Inman, D.J., "On Damping Mechanisms in Beams," ASME Journal of Applied Mechanics, Vol. 58, No. 3, September 1991, pp. 716-723.

Minas, C. and Inman, D.J., "A Note on Pole Placement of Mechanical Systems," ASME Journal of Vibration and Acoustics, Vol. 113, No. 3, July 1991, pp. 420-421.

Zimmerman, D.C., Inman, D.J. and Juang, J-N, "Vibration Suppression Using a Constrained Rate-Feedback Threshold Control Strategy," ASME Journal of Vibration and Acoustics, Vol. 113, No. 3, July 1991, pp. 345-353.

Garcia, E. and Inman, D.J., "On the Modeling of the Slewing Control of a Flexible Structure," AIAA Journal of Guidance, Control and Dynamics, Vol. 114, No. 4, July-August 1991, pp. 736-742.

9. Personnel Supported

Professional personnel associated with the research effort are Mr. Donald Leo and Dr. Daniel J. Inman. Mr. Ralph Rietz was also supported during part of the grant period.

10. Coupling Activities

The following is a list of papers presented at meetings, conferences and seminars during the award period by the PI as well as those submitted and accepted.

Leo, D.J. and Inman, D.J., "Control of a Flexible Frame in Slewing," Proceedings of the American Control Conference, June 1992.

Leo, D.J. and Inman, D.J., "Smart Slewing Frames," Proceedings of the First European Conference on Smart Structures, May 1992.

Pokines, B., Belvin, W.K. and Inman, D.J., "A Variable Stiffness Strut Using Strain Induced Bending for Vibration Suppression in the Evolutionary Model," Proceedings of the 33rd AIAA SDM Conference, April 1992, to appear.

Pokines, B., Belvin, W.K. and Inman, D.J., "Static and Dynamic Characteristics of Piezoceramic Strut," Proceedings of the 5th NASA/DOD Controls - Structure Interaction Technology Conference, March 1992.

Slater, J.C., Belvin, W.K. and Inman, D.J., "A Comparison of Viscoelastic Damping Models," Proceedings of the 5th NASA/DOD Controls - Structure Interaction Technology Conference, March 1992.

Garcia, E., Dosch, J. and Inman, D.J., "The Application of Smart Structures to the Vibration Suppression Problem," Proceedings of the Second Joint Japan-US Conference on Adaptive Structures, November 1991.

Johnson, D., Brown, G.V. and Inman, D.J., "Force Analysis of Magnetic Bearings," International Symposium on Magnetic Suspension Technology, August 19-23, 1991.

Inman, D.J., Garcia, E. and Dosch, J., "Vibration Suppression Using Smart Structures," *Smart Structures and Materials*, ed. Haritos, G.K. and Srinivasan, A.V., AMD, Vol. 123, 1991, ASME, pp. 167-172.

Starek, L. and Inman, D.J., "Inverse Problems in Vibration Generating Symmetric Coefficient Matrices," *Vibration Analysis - Analytical and Computational*, Ed Haug, et al., ASME DE-Vol. 37, pp. 13-18, 1991

Inman, D.J., "Estimation, Model Correction and Inverse Problems," Proceedings 13th IMAC World Congress on Computation and Applied Mathematics, Dublin, Ireland, July 1991.

Inman, D.J. and Garcia, E., "Smart Structures for Vibration Suppression," Proceedings of the 4th International Conference on Recent Advances in Structural Dynamics, Southampton, UK, July 1991, pp. 139-155.

Slater, J.C. and Inman, D.J., "Transfer Function Modeling of Damped Mechanisms in Viscoelastic Plates," Proceedings of the 32nd AIAA Structures, Structural Dynamics and Material Conference, April 1991, Part 3, pp. 2381-2383.

Slater, J.C., Inman, D.J. and Belvin, W.K., "Modeling of Constrained Layer Damping in Trusses," Proceedings of Damping 91, February 1991.

Yae, K. and Inman, D.J., "Control Oriented Order Reduction of Finite Element Models," Proceedings of the 1991 Joint Automatic Control Conference, May 1991, pp. 2187-2189.

Garcia, E., Dosch, J. and Inman, D.J., "Feedback Control of an Active Antenna Structure," Proceedings of the 8th VPI&SU Symposium on Dynamics and Control of Large Structures, May 1991.

Garcia, E., Dosch, J. and Inman, D.J., "Vibration Attenuation in an Active Antenna Structure," Proceedings Recent Advances in Active Control of Sound and Vibration, April 1991, pp. 535-542.

Johnson, D., Inman, D.J. and Horner, G.C., "An Active Suspension system for Space Structure Dynamic Testing," Proceedings Recent Advances in Active Control of Sound and Vibration, April 1991, pp. 567-578.

Starek, L. and Inman, D.J., "Solution of the Model Correction Problem Via Inverse Methods," Proceedings of the 9th International Modal Analysis Conference, April 1991, pp. 352-355.

Inman, D.J., "Introduction to Matrices in Modal Analysis," Proceedings of the 9th International Modal Analysis Conference, April 1991, pp. 1410-1414.

Garcia, E. and Inman, D.J., "Control Formulations for Vibration Suppression of Active Structures in Slewing Motions," ASME 1990 Winter Annual Meeting. (Invited) *Advances in Dynamic and Control of Flexible Spacecraft and Space Based Manipulators*. Ed. Joshi, Alberts and Kakad, DSC Vol. 20- pp. 1-5.

Yae, K.H. and Inman, D.J., "Flexible-Body Dynamics Modelling with a Reduced-Order Model," *Advances in Design Automation*, Vol II, Optimal Design and Mechanical Systems Analysis, ed. B. Ravani, ASME DE-Vol, 23-2, 1990, pp. 87-92.

Umrand, J.W. , Inman, D.J. and Banks, H.T., "Damping in Coupled Rotation and Bending - an Experiment," Proceedings of the 1991 Joint Automatic Control Conference, May 1991, Vol. III, pp. 2994-2999. (Invited)

Cudney, H.H., Inman, D.J. and Oshman, Y., "Distributed Structural Control Using Multi Layered Piezoelectric Actuators," Proceedings of the AIAA 31st Structures, Dynamics and Materials Conference, 1990, pp. 2257-2265.

In addition, the author taught a one day short course on *Control Methods for Smart Structures* on November 1991, just prior to conference on Adaptive Material and Structures. Several Air Force officers attended this course. The author also presented "Smart Structures - Where's the Beef," at the October 1991 AFOSR Contractors Meeting in Dayton, Ohio and served on a smart structures panel discussion which preceded the structures contractors meeting.

11. References

[1] Juang, J.N., Horta L.G., and Robertshaw H.H., "A Slewing Control Experiment for Flexible Structures," *J. of Guidance, Control and Dynamics*, v 9 n5, Sept-Oct 1986, pp. 599-607.

[2] Cannon, R.H., and Schmitz, E., "Initial Experiments on the End-Point Control of a Flexible One-Link Robot," *Intl. J. of Robotics Research*, v3 n3, Fall 1984, pp. 62-75.

[3] Garcia, E., and Inman, D.J., "Modeling of the Slewing Control of a Flexible Structure", *J. of Guidance, Control, and Dynamics*, v14 n4, July-Aug 1991, pp. 736-742.

[4] Sakawa, Y., and Luo, Z.H., "Modeling and Control of Coupled Bending and Torsional Vibrations of Flexible Beams," *IEEE Trans. on Automatic Control*, v 34 n9, Sept. 1989, pp. 970-977.

- [5] Leo, D.J. and Inman, D.J., "Smart Slewing Frames," *Proc. of the 1st European Conference on Smart Structures and Materials*, Glasgow, Scotland, 1992 (to appear).
- [6] Fanson, J.L., and Caughey, T.K., "Positive Position Feedback Control for Large Space Structures," *Proc. of the 28th Structural, Dynamics, and Materials Conference*, 1987, pp. 588-98.
- [7] Garcia, E., "On the Modeling and Control of Slewing Flexible Structures," Ph.D. dissertation, State University of New York at Buffalo, 1989.
- [8] Wie, B., and Byun, K.W., "New Generalized Structural Filtering Concept for Active Vibration Control Synthesis," *J. of Guidance, Control, and Dynamics*, v12 n2, Mar-Apr 1989, pp. 147-155.
- [9] *TurboPac User's Guide*, Tektronix, Campbell, CA.
- [10] Garcia, E., and Inman, D.J., "Advantages of Slewing an Active Structure," *J. of Intelligent Material Systems and Structures*, v1 n3, July 1990, pp. 261-272.
- [11] Goh, C.J., and Caughey, T.K., "On the Stability Problem Caused by Finite Actuator Dynamics in the Colocated Control of Large Space Structures," *Int. J. of Control*, v 41 n3, 1985, pp. 787-802.

APPENDIX B
2nd Year Annual Report

REPORT DOCUMENTATION PAGE

Form Approved
OMB No. 0704-0188

Public reporting burden for this collection of information is estimated to average 1 hour per response, including the time for reviewing instructions, searching existing data sources, gathering and maintaining the data needed, and completing and reviewing the collection of information. Send comments regarding this burden estimate or any other aspect of this collection of information, including suggestions for reducing this burden, to Washington Headquarters Services, Directorate for Information Operations and Reports, 1215 Jefferson Davis Highway, Suite 1204, Arlington, VA 22202-4302, and to the Office of Management and Budget, Paperwork Reduction Project (0704-0188), Washington, DC 20503.

1. AGENCY USE ONLY (Leave blank)	2. REPORT DATE 20 March 93	3. REPORT TYPE AND DATES COVERED Technical Report: 15 Dec 91 to 14 Dec 92
----------------------------------	-------------------------------	--

4. TITLE AND SUBTITLE Modeling and Control of Intelligent Flexible Structures - Smart Uses of Intelligent Structures	5. FUNDING NUMBERS AFOSR-91-0181
--	-------------------------------------

6. AUTHOR(S) Daniel J. Inman	
---------------------------------	--

7. PERFORMING ORGANIZATION NAME(S) AND ADDRESS(ES) The Research Foundation of the State University of New York on Behalf of the University of Buffalo PO Box 9 Albany, NY 12201-0009	8. PERFORMING ORGANIZATION REPORT NUMBER
--	---

9. SPONSORING/MONITORING AGENCY NAME(S) AND ADDRESS(ES) AFOSR/NA Bldg. 410 Bolling AFB, DC 20332-6448	10. SPONSORING/MONITORING AGENCY REPORT NUMBER
--	---

11. SUPPLEMENTARY NOTES

12a. DISTRIBUTION/AVAILABILITY STATEMENT unlimited	12b. DISTRIBUTION CODE
---	------------------------

13. ABSTRACT (Maximum 200 words) A great deal of attention has been generated in the past five years regarding the use of smart/intelligent materials and structures. Much attention has been given to the technical and scientific details of various materials, material systems and structural configurations. Less attention has been given to the control aspects unique to such systems. The efforts of the last year of this program have focused on active structures based on piezoelectric devices used to control vibrations. A unique feature of the configurations considered here as applications, is that the use of sensors and actuators integrated into structural components may provide the only feasible method of suppressing undesirable vibration in such structures. The effort of the second year of funding reported here has focused on a) on comparing various control methods on slewing frames, b) on controlled systems with repeated or nearly repeated natural frequencies as typified by ribbed antenna systems, and c) on using a nonlinear controller to improve the efficiency of controlling coupled flexible-rigid body vibration. The work reported here is largely experimental in that the control laws considered are those proposed by other researchers in the theoretical community. However, some modification of these methods is required in order to actually implement them.

14. SUBJECT TERMS smart intelligent structure, slewing, solar arrays, antenna, structural control, nonlinear controller	15. NUMBER OF PAGES 84
	16. PRICE CODE

17. SECURITY CLASSIFICATION OF REPORT unclassified	18. SECURITY CLASSIFICATION OF THIS PAGE unclassified	19. SECURITY CLASSIFICATION OF ABSTRACT unclassified	20. LIMITATION OF ABSTRACT UL
---	--	---	----------------------------------

**Modeling and Control of Intelligent Flexible Structure
- Smart Uses of Intelligent Structures**

AFOSR Technical Report

**Daniel J. Inman
Department of Engineering Science and Mechanics
Virginia Polytechnic Institute and State University
Blacksburg, VA 24061**

March 1993

TABLE OF CONTENTS

1. Introduction	1
2. Slewing Frames	1
3. Modeling and Control of Systems with Nearly Repeated Modes	6
4. Experimental Use of Nonlinear Controllers	9
5. References	17
6. Review of Objectives and Status	19
7. Publications	19
8. Personnel Supported	20
9. Coupling Activities	20
10. Appendix	21

**Modeling and Control of Intelligent Flexible Structure
- Smart Uses of Intelligent Structures**

AFOSR Technical Report

1. Introduction

A great deal of attention has been generated in the past five years regarding the use of smart/intelligent materials and structures. Much attention has been given to the technical and scientific details of various materials, material systems and structural configurations. Less attention has been given to the control aspects unique to such systems. The efforts of the last year of this program have focused on active structures based on piezoelectric devices used to control vibrations. A unique feature of the configurations considered here as applications, is that the use of sensors and actuators integrated into structural components may provide the only feasible method of suppressing undesirable vibration in such structures.

The effort of the second year of funding reported here has focused on a) on comparing various control methods on slewing frames, b) on controlled systems with repeated or nearly repeated natural frequencies as typified by ribbed antenna systems, and c) on using a nonlinear controller to improve the efficiency of controlling coupled flexible-rigid body vibration. The work reported here is largely experimental in that the control laws considered are those proposed by other researchers in the theoretical community. However, some modification of these methods is required in order to actually implement them.

2. Slewing Frames

Space frames present a useful model of the solar panel system common to most satellites. They also present a rich theoretical abstraction of a fairly common practical problem which is best solved by the use of smart structures. As an example of such a practical problem, recall the Hubble Space Telescope (HST) experience. Rapid temperature changes induced rather serious vibration in the HST's solar panels rendering the telescope disfunctional for long periods of time. The problem was eventually reduced to tolerable levels by implementing active control using the panels rigid body actuator. However this problem could have easily

been prevented by implementing a smart structural system in the original design. The basic difficulty with the current design is that the rigid body actuator associated with rotating the solar array and/or extending the solar array cannot control torsional modes of vibration, or plate modes, and solar arrays are rich with such vibration. While the work presented here is distinct from the HST configuration, the problem is generic to any solar panel on any satellite system.

The problem statement is simple: how does one control torsional vibration with a rigid body actuator? The answer is that you don't. Rather a smart structures approach is used. The generic laboratory structure considered is given in Figure 1. This device simulates the dynamics of slewing solar arrays. The modeling, hardware development and initial control development for this structure is given in the previous AFOSR report [1] and is not repeated here. The modeling is also paraphrased in the appended papers [2,3].

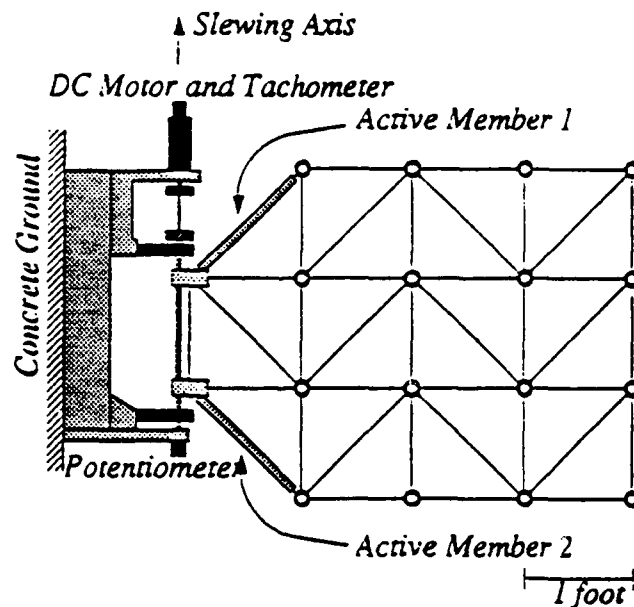


Figure 1 The testbed for slewing solar panel dynamics and control

In the initial study of slewing solar arrays given in [1], the problem of the uncontrollability of the torsional and plate modes was discovered in physical terms from testing. In the subsequent year the lack of controllability was normalized using a number of criteria [4]. The

results are summarized in Table 1 which lists the controllability index suggested by

Table 1: Relative controllability index for solar panel. The larger the index the more controllable the indicated mode is.

Mode	Motor Control Only	Smart Strut Only
1st Torsion	0.692	1.374
1st Bending	14.287	0.571
2nd Torsion	1.029	2.751
1st Plate	1.262	3.225
2nd Bending	6.513	2.808

Hamdan and Nayfeh [4]. Note that the torsional modes and the plate modes with the motor (rigid body actuator) as the only control input have very low relative controllability index indicating that the primary rigid body actuator will not be able to easily control these modes. The second column of the table indicates that by using an active member as just one of the elements of the frame, the torsional and plate modes become controllable.

With the structural control system rendered controllable several control designs were attempted and compared. First a performance comparison was made between collocated and noncollocated control. A second comparison was made between traditional proportional-derivative control and μ synthesis/ H^∞ methodology.

The initial study comparing the results of collocated versus noncollocated control involve designing a controller that provides satisfactory step response (i.e., simultaneously slew the frame and suppress vibration). Important performance criteria here include minimizing the settling time and overshoot of the frame's hub position as well as suppressing the structural vibration induced during the maneuver.

Here three control laws are compared to determine if collocated or uncollocated control configuration should be used. The noncollocated control configuration consists of using the rigid body actuator as the control input and the smart structure as a sensor only. The particular control law chosen to implement is the Generalized Structural Filtering (GSF)

method proposed by Wei [5] coupled with PD control. This control configuration is compared to a collocated configuration using the smart structure as both a sensor and an actuator. The control law implemented in the collocated case is the Positive Position Feedback (PPF) method [6,7] coupled with PD control. The results of these two implementations are given in Figure 2 which also lists the results of using just PD control without a smart structure.

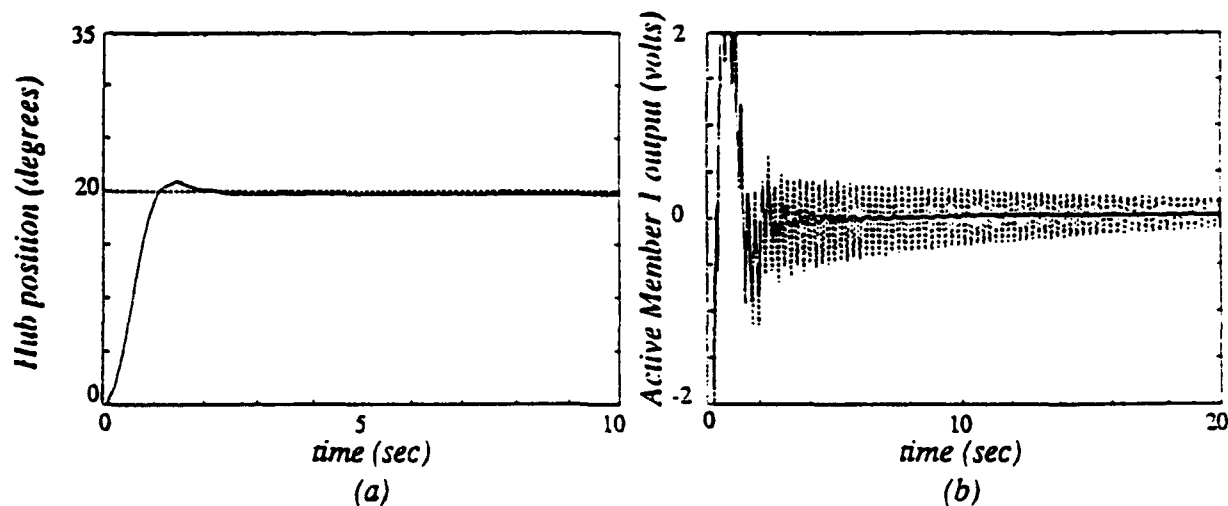


Figure 2 Comparison of collocated versus noncollocated hardware configurations

The figure shows clearly the following results

- PD control alone does not suppress vibration
- using the smart structure as a sensor only to produce noncollocated PD control using GSF suppresses vibration, but does so at the expense of large overshoot and no stability robustness with respect to model error
- collocated control using PD and PPF give low overshoot, controls torsional vibration and is robust with respect to model error

Details of this result can be found in Leo and Inman [8].

Now consider a comparison between two collocated, control laws: μ -synthesis [9-10] and PD control. Since it is the industry standard to model using finite elements (FEM) a finite element model of the test structure is used here as well. The basic problem with FEM's is that they generally contain some error when compared with physical experiments. Hence,

the control laws used must be robust with respect to model error, if they are to be applied to real and/or experimental devices as is the case here. Two pointing control laws are examined:

- proportional derivative control
- a compensation design with μ -synthesis combined with PPF

Basically, the PD controller is simple to design, and certainly a favorite of practicing engineers, but lacks robustness. The μ synthesis approach when combined with PPF produces a high performance closed loop response with good stability robustness to parameter uncertainties.

Pointing control and vibration suppression in a slewing frame structure was achieved by designing two independent control laws. Vibration suppression of the first torsional mode was attained by using a piezoceramic active member in a collocated feedback loop. The Positive Position Feedback control law was robust against model error and increased the damping in the target mode by a factor of ten. This is because the closed loop stability of a PPF control law depends only on knowledge of the structure's frequencies and structural frequencies are the physical quantity which has the most accurate measure from tests. Two separate pointing controllers were examined: a simple Proportional-Derivative compensator and a more sophisticated design using μ -synthesis techniques. Structural singular value plots illustrated that the PD compensator was sensitive to the high frequency dynamics of the frame. When experimentally implemented, this control law destabilized the system as predicted by the robust stability analysis. After changing the position and velocity gains, the system remained stable but produced unsatisfactory results (16% steady state error or 55% overshoot). The pointing controller designed with μ -synthesis techniques resulted in a superior step response. During a 20° slewing maneuver, this design produced a step response with 7% overshoot, 2 second settling time, and less than 2% steady state error. With the supplementary PPF control loop closed, the structural vibrations were suppressed 4 seconds after the hub position came to rest. Without the supplementary control, the frame vibrated for over 30 seconds after the end of the slewing maneuver.

The major contribution here is that the experimental implementation of a smart structural control system requires a robust control formulation, and that smart structures need to be used in controlling a certain class of devices with dynamics similar to those found in solar arrays common to satellites.

3. Modeling and Control of Systems with Nearly Repeated Modes

Control of systems with repeated or nearly modes is a relatively common problem addressed in the large flexible spacecraft discipline. Here, however a hardware solution is proposed to this problem using the capability of smart structures. Modern control theory calls for one actuator for each repeated mode. Here this is made possible by integrating piezoceramic devices throughout the structure, using them as sensors and actuators and developing an appropriate control and modeling scheme.

To explain this approach, an experimental model of an 8-ribbed antenna, common to satellites is used. Figure 3 shows a schematic of the experimental test bed. Such antenna

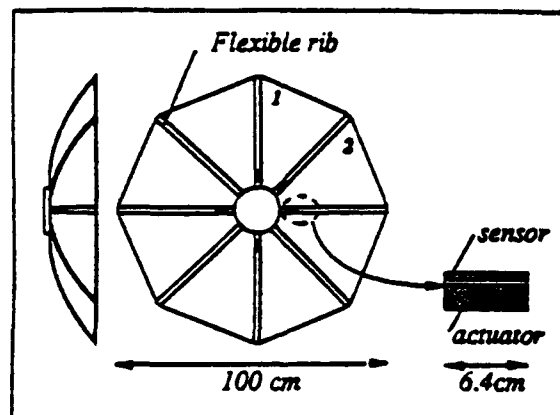


Figure 3 An experimental smart antenna illustrating (at left) the bowed ribs and (at right) the location and size of the integrated sensors and actuators

exhibit substantial repeated natural frequencies. Such structures, because of their unique curvature, are difficult to model using standard finite element methods. Rather a lumped model as pictured in Figure 4 is used. This model uses spring stiffeners for the antenna's

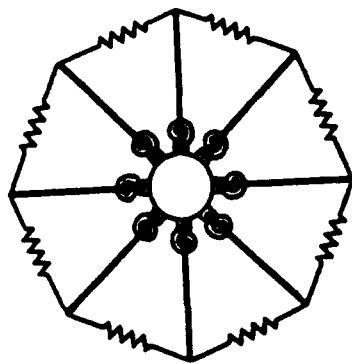


Figure 4 An 8 degree of freedom lumped mass model of the ribbed antenna in the previous figure. The hub at the center is assumed rigid.

connections, torsional springs for hub connection and models the ribs themselves as lumped masses. This model displays most of the important dynamics of the experimental apparatus. Figure 5 illustrates a comparison between the analytical model obtained from Figure 4 and

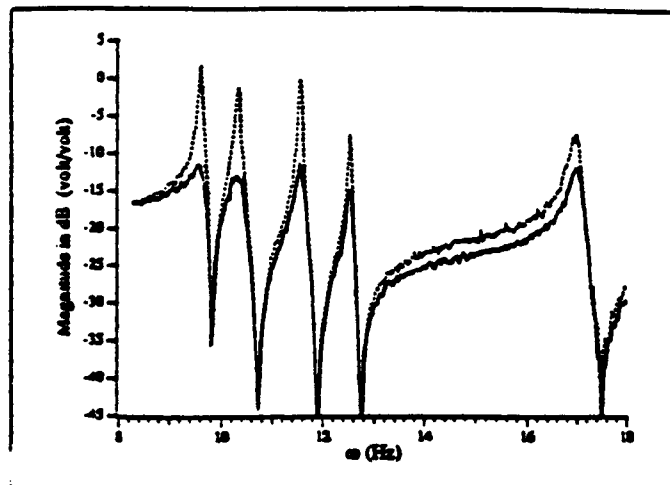


Figure 5 Experimental (solid line) and theoretical transfer function (dotted line) magnitude plots for the antenna.

the experimental magnitude plot of the structure. The agreement is very good in magnitude but poor in high frequency phase. The details are presented in [11]. Two different control schemes were used for implimenting active vibration suppression for this system. They are

Positive Position Feedback (PPF) and the Active Vibration Absorber (AVA) method. Each method takes advantage of the structure of second order system to claim closed loop stability in the face of high gain. The work here shows that these two methods are related, as PPF is a subset of AVA and that AVA actually suffers from high gain instability when applied to systems with unmodeled high frequency dynamics such as a ribbed antenna. This is illustrated clearly in Figure 6. Each of these methods have been modified to take advantage

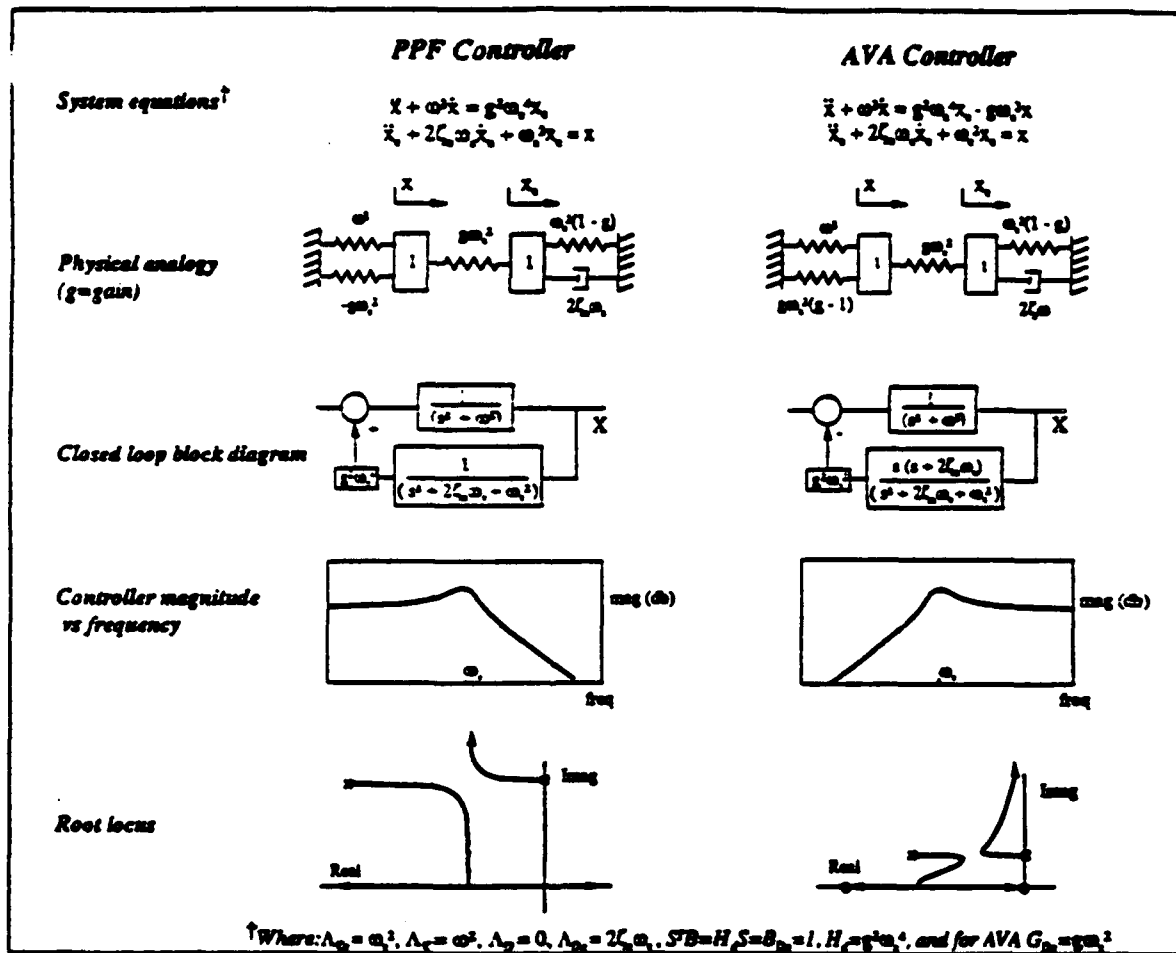


Figure 6 Comparison of PPF and AVA for the single degree of freedom case of displacement feedback. Note the high gain instability for AVA.

of recent results in stability of second order systems by using symmetrizability conditions [12] and new definite tests [13]. As detailed in [14], two second order controllers have been developed and experimentally implemented on the antenna testbed. Theoretical stability

bounds were also derived, with PPF control being conditionally stable and AVA control being unconditionally stable. An important difference between the two types of control was that a PPF filter rolls off at higher frequencies while the AVA controller maintains a constant gain. The roll off characteristic of PPF is an advantage since it makes it less sensitive to unmodeled dynamics. In real systems, that stability of the AVA control is determined by the high frequency response of the structure, which is often not known with any accuracy.

Both types of control were successfully implemented on the smart antenna. The performance of PPF and AVA were compared on a SISO design using one active rib. Each design consisted of only one second-order controller since numerical simulations indicated that there was no significant advantage in using multiple filters. Both types of control were able to increase the damping in the target modes. PPF control produced better results since it was not limited by unmodeled dynamics. Unfortunately, the SISO controller did not adequately address the problem of repeated natural frequencies. A MIMO controller was implemented using PPF control on ribs 1 and 2. Not only did not the MIMO controller improve the overall performance, it was able to add damping to a repeated mode at 9.7 Hz.

4. Experimental Use of Nonlinear Controllers

A comparison between linear control and nonlinear control of a distributed parameter system (experimental) consisting of a slewing flexible beam was performed. The experimental research sought to determine the advantage of nonlinear control over linear control for a linear distributed parameter system.

The strongest argument for using nonlinear control is that it can significantly improve the performance over linear control schemes. This can be shown in simulations, where the step response rise time, settling time and overshoot are significantly smaller than the response when linear control is used. Lewis [15] showed the response of a second order system can be improved by constructing a variable damping. He used position times velocity feedback to eliminate overshoot and improve the settling time of a positional servomechanism. More

recently, Castelazo and Lee [16] proposed using the same type of feedback to improve the response of a slewing beam system. They considered a nonlinear feedback, where state positions and state velocities were multiplied. A heuristic method was proposed to tune the nonlinear feedback gains and the resulting performance was better than the performance provided by an optimal linear controller. They provided simulation results for a slewing beam to verify the method. Others, such as Kuo and Wang [17], have proposed using nonlinear controllers to improve the robustness of a more complicated two link manipulator.

Initially, the purpose of this work was to experimentally verify the simulation results found by Castelazo and Lee. However, to insure global stability, their proposed feedback required a simple modification. Also, implementing full state feedback is difficult and as a result, proportional plus derivative feedback control, which lends itself well to experimentation, was chosen for this purpose. Angular position and angular velocity are easily measured on the experimental apparatus. The nonlinear feedback consisted of the angular position times the angular velocity and the objective was to show that the system using nonlinear feedback provided better results than the system using the best available linear feedback.

Table 2 Total Energy Input to the Motor for the Simulated 30°
Slewing Manuever using the Identified Plant Model

Linear	17.4J
Nonlinear	12.1J
% reduction	30.6%

Comparing this result to the theoretical model simulations shows a significant difference. The maximum power for the theoretical model simulations was approximately 245 W and for the pole zero model simulations, the peak power input was 95 W. For both models, the motor current was the first constraint to be exceeded. That is, at some instant of time for both models, the motor current exceeded its maximum allowed value. Therefore, the

difference in the power plots lies in the simulated armature voltages. Along with this, the energy consumption found in the theoretical model simulations was more than two times that of the pole zero model simulations. These observations emphasize that the difference between the two models lies in the mode shapes, which can be explained as follows. First, the armature voltage is a function of the controller gains and the controller gains were much larger for the theoretical model simulations. The magnitude of the terms in the theoretical model feedback matrices were small (they are functions of the mode shapes), therefore, large gains were required to produce adequate results. Large gains translate to large voltages in the motor. This explains the sizable difference in the energy results. Also, much more damping was present in the pole zero model, while the damping matrix of the theoretical model (which is a function of the mode shapes) was small. Larger derivative feedback gains, which are not necessary for the pole zero model simulations, are required for the theoretical model to make up for this inadequacy. Perhaps including internal (material) damping in the theoretical model or increasing the term corresponding to the bearing friction in the model would produce closer results for the two models. For the simulations using the theoretical model, increasing the feedback gains increases the motor voltage, resulting in larger energy consumption results. These observations imply that the main difference in the models is found in the assumed mode shapes and the lack of an internal damping model for the beam.

The simulation results using the pole zero model were the most promising results obtained up to this point. These simulations used a model obtained from data of the experimental system and therefore, they provide the most optimistic result that the simulated observations can be implemented on a real system.

Simulations are valuable in examining the dynamics of systems. In this work, simulating various forms of feedback and using different plant models provided valuable information about the system before any experiments were attempted. A PD controller was constructed for the slewing beam and an experiment was performed. Then, the nonlinear feedback was added to the controller and another experiment was performed.

It is important to note that this study was initially conducted to verify, through experimentation, that the proposed nonlinear feedback control could be used to improve the response of slewing beam systems. A natural extension of this investigation was to determine the cost of the improvement in performance. There may be other control strategies which provide similar responses while using even less energy. The purpose now is to show that it is possible to reduce the energy requirements of this system with no loss in performance. We have found through simulations and, as will be seen, through experimentation that even when there is no visual improvement in the performance as measured with respect to settling time or rise time or overshoot, there is a significant improvement in the energy required when the proposed nonlinear control is used in addition to the linear control.

The controllers were implemented in the same manner as in the simulations. The beam tip acceleration was measured and used as an indicator of the closed loop performance. Angular position at the slewing axis was measured with a potentiometer and angular velocity was measured with a tachometer mounted at the motor and input to an analog computer, where the PD and PD plus nonlinear controllers were constructed. An EAI 2000 analog computer manufactured by Electronic Associates, Inc. was used. The output signal from the analog computer was amplified and input to the motor. A block diagram of the closed loop system is given in Figure 7. The controller gains were adjusted until the fastest settling time was obtained. The time responses are shown below for the PD controlled slewing beam. The beam is given an angular displacement of 30° and slewed to 0° . The beam tip acceleration versus time is shown in Figure 8. The instantaneous power versus time curve was obtained by multiplying the time histories of the motor voltage and current together.

The proportional gain determined in the experiments was the same as the proportional gain in the pole zero model simulations. The derivative gain was smaller in the experiments than in the simulations, since the settling time increased and the amplifier saturated when higher gains were used.

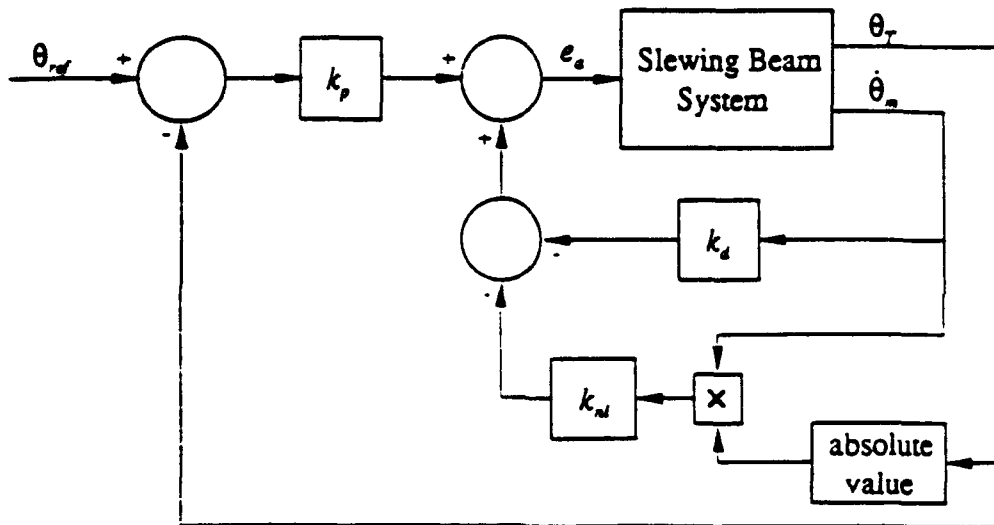


Figure 7 Closed loop PD plus nonlinear feedback control system.

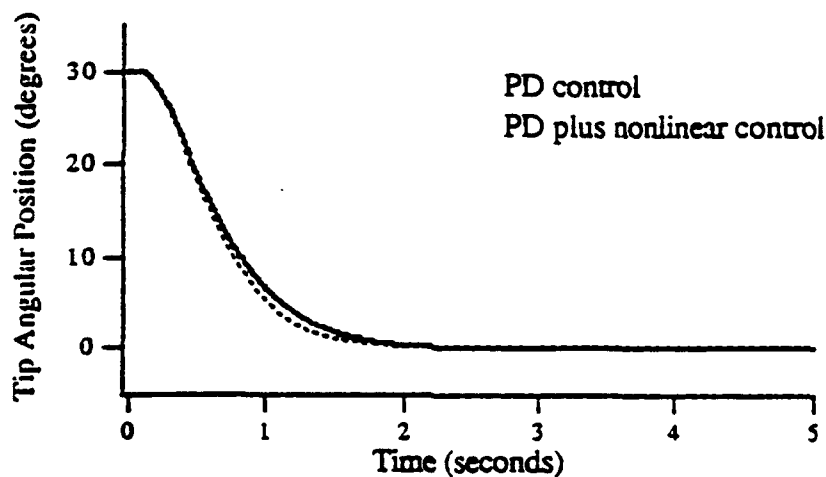


Figure 8 Beam tip acceleration versus time.

These experimental responses are comparable to the simulated responses. In general, the experimental result shows less damping than the simulation. The overshoot is larger and the settling time is also larger than the simulation predicted. As mentioned earlier, it was believed that the damping in the pole zero model was larger than the actual system. These results confirm this belief. The settling times of the angular position at the slewing axis and

of the beam tip are approximately 2 seconds each. Integrating under the power curve, the total energy input to the motor for the PD controlled system was 16.3J.

Next, nonlinear feedback was added to the PD controller established above. The nonlinear feedback is the absolute value of the angular position multiplied by the angular velocity and the nonlinear feedback gain. The result is subtracted from the PD feedback signal to obtain the nonlinear control system.

The settling times of the angular position and tip acceleration are seen to be approximately 2 seconds. Integrating under the power curve, the total energy input to the motor for the nonlinear feedback system was 13.7J.

The nonlinear feedback gain was set at a small value since larger nonlinear gains saturated the amplifier. For the PD case only, setting the proportional and derivative feedback gains lower produced time responses with larger overshoot and longer settling times. As a result of the lower PD gains, the nonlinear feedback gain could be set to larger values and significant improvements in overshoot and settling time were obtained, confirming the observations discussed earlier. Thus, it was verified that the proposed nonlinear feedback control could be used to improve the closed loop performance of the linear system. The plots are not included here since the objective of this work was to find the best experimental PD controller, then add as much nonlinear feedback as possible (before saturating the amplifier) and compare the energy requirements of each system.

Consider the experimental time responses. The angular position and beam tip acceleration settled in 2 seconds for both the linear and nonlinear control systems implemented. There was a small decrease in overshoot in the angular position for the nonlinear feedback result, but this is not readily apparent in the figures shown. In general, the angular position shows an underdamped response for both the linear and nonlinear feedback results. Now, consider the time responses of the beam tip acceleration. The nonlinear feedback result shows a small decrease in magnitude of the peak accelerations. This is the

same result noticed in the simulations performed.

Finally, the power plots that the system using nonlinear feedback required less energy than the system using the linear feedback alone. The peak magnitude of the instantaneous power input to the system decreased by approximately 10%. Integrating under the instantaneous power versus time curves gives the total energy input to the motor during the control maneuver. The results are shown in Table 3. A 15.6 % decrease in energy resulted for the system using nonlinear control than for the system using linear control, while the performance was virtually the same for both control methods. Therefore, it is possible to add nonlinear feedback of the form proposed here to a linearly controlled system and save energy, while obtaining the same performance in every other respect.

Table 3 Total Energy Input to the Motor for the
Experimental 30° Slewing Maneuver

Linear	16.3J
Nonlinear	13.7J
% reduction	15.6%

Figures 9-12 illustrate the effectiveness of the nonlinear controller.

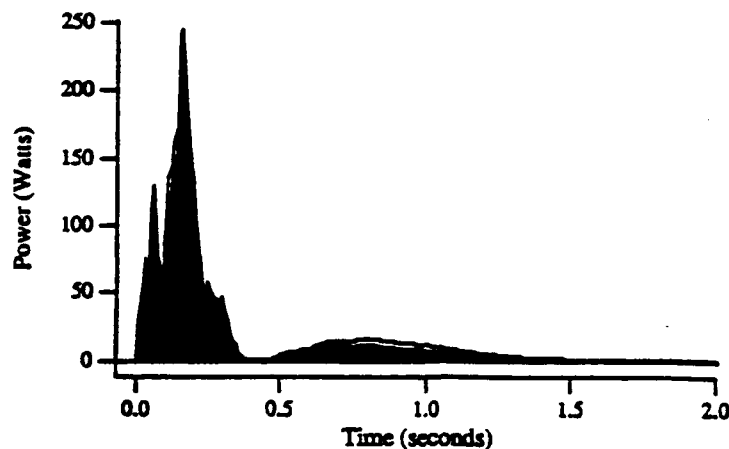


Figure 9 Instantaneous power versus time.

Initially, the purpose of this work was to experimentally verify that a specific nonlinear feedback control could be used to improve the performance of a closed loop system using

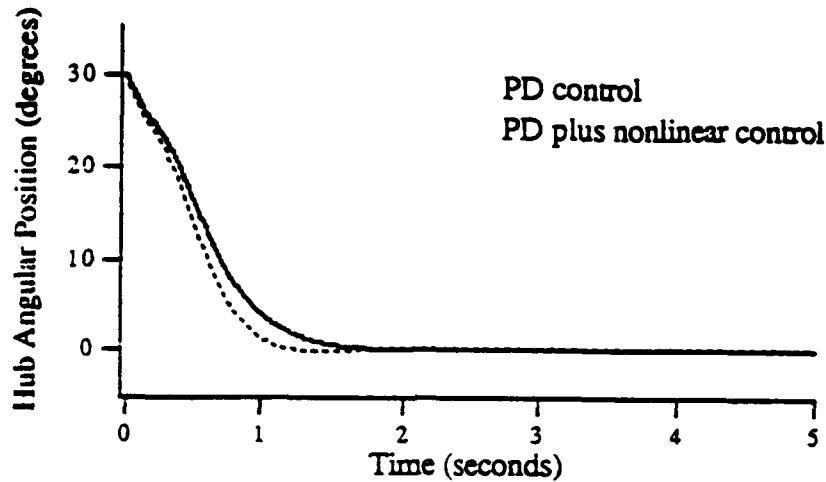


Figure 10 Angular position at the slewing axis versus time (nonlinear feedback).

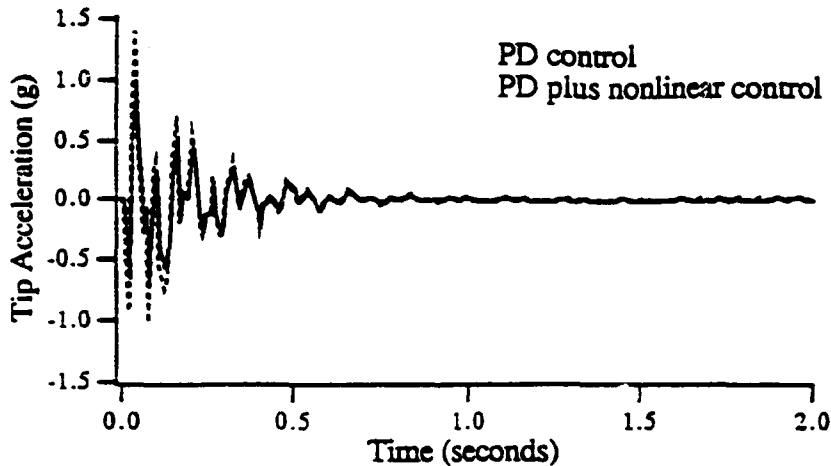


Figure 11 Beam tip acceleration versus time (nonlinear feedback).

linear control. A slewing beam system was chosen to implement the nonlinear control. Before experimenting with the system, simulations were run to find an acceptable controller to implement.

Two different controllers were studied, an LQR and a PD controller. Simulation results showed that large increases in performance (settling time and overshoot) for the nonlinear system were not obtained within the system constraints. Usually, the motor current reached its upper limit first. However, it was noticed that the control effort required by the system using nonlinear control was less than that required by the system using the linear control.

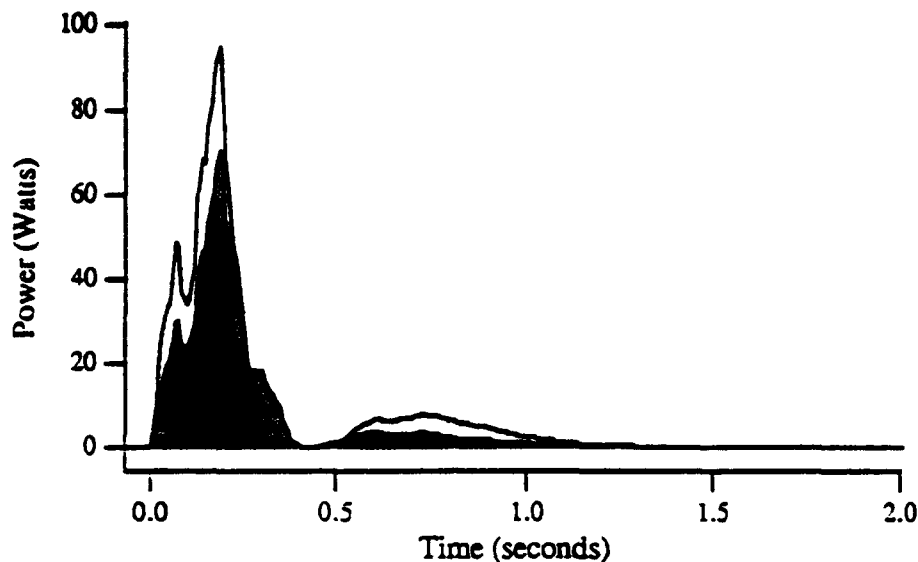


Figure 12 Instantaneous power versus time (nonlinear feedback).

The objective of this work then changed to experimentally verify that this type of nonlinear control used less energy than the linear control when all other measures of performance were virtually unchanged.

The PD result was verified experimentally. The best performance for the linear control was an underdamped response. Adding the nonlinear feedback showed no significant improvement in performance. However, when the control efforts were compared, the nonlinearly controlled system required much less energy than the system using linear control. The conclusion reached was that the nonlinear feedback control proposed here can significantly save energy, even when no other change in performance is perceived.

5. References

- [1] Inman, D. J., Leo, D. J., "Modeling and Control of Intelligent Flexible Structures - Slewing Frame," AFOSR Annual Technical Report, 11 March 92.
- [2] Leo, D. J. and Inman, D. J., "Control of a Flexible Frame in Slewing," *Proc. of the American Control Conference*, 1991, Vol. 3, pp. 2535-2539, Chicago, IL.
- [3] Leo, D. J. and Inman, D. K., "Modeling and Control Simulations of a Slewing Frame Containing Active Members," submitted to the *Smart Materials and Structures Journal* 1993.

- [4] Hamdan, A. M. A., Nayfeh, A. H., "Measures of Model Controllability and Observability for First and Second Order Linear Systems," *AIAA Journal*, Vol. 12, No. 3, May-June 1989, pp. 421-428.
- [5] Wie, B., and Byun, K. W., "New Generalized Structural Filtering Concept for Active Vibration Control Synthesis," *J. of Guidance, Control, and Dynamics*, Vol. 12, No. 2, pp. 147-155, 1989.
- [6] Fanson, J. L., and Caughey, T. K., "Positive Position Feedback Control for Large Space Structures," *Proc. of the 28th Structural, Dynamics, and Materials Conference*, pp. 58898, 1987.
- [7] Goh, C. J., and T. K., "On the Stability Problem Caused by Finite Actuator Dynamics in the Colocated Control of Large Space Structures," *Int. J. of Control*, Vol. 41, No. 3, pp. 787-802, 1985.
- [8] Leo, D. J., "Active Control of a Slewing Frame," M.S. Thesis, Dept. of Mechanical and Aerospace Engineering, State University of New York at Buffalo, 1992.
- [9] Balas, G., *et al*, μ -Analysis and Synthesis Toolbox, The Math Works, Inc.
- [10] Stein, G., and Doyle, J. C., "Beyond Singular Values and Loop Shaping," *Journal of Guidance, Control, and Dynamics*, 14(1): pp. 5-15.
- [11] Dosch, J. J., Leo, D. J. and Inman, D. J., "Modeling of a Smart Antenna for Active Vibration Suppression," *Proceeding 11th International Model Analysis Conference*, pp. 1418-1424, 1993.
- [12] Inman, D. J., "Dynamics of Asymmetric Non Conservative Systems," *ASME Journal of Applied Mechanics*, Vol. 50, No. 1, pp. 199-203, 1983.
- [13] Kerr, T. H., "Misstatements of the Test for Positive Semidefinite Matrices," *AIAA Journal of Guidance, Control, and Dynamics*, Vol. 13, No. 3, pp. 571-572, 1990.
- [14] Dosch, J. J., Leo, D. J. and Inman, D. J., "Comparison of Vibration Control Schemes for a Smart Structure," *IEEE Conference on Decision and Control Proceedings*, 1992, pp. 1815-1820.
- [15] Lewis, J. B., "The Use of Nonlinear Feedback to Improve the Transient Response of a Servomechanism," *AIEE Transactions*, Vol. 71, Part II, 1953, pp. 449-453.
- [16] Castelazo, I. A., and Lee, H., "Nonlinear Compensation for Flexible Manipulators," *Journal of Dynamic Systems, Measurement and Control*, Vol. 112, 1990, pp. 62-68.
- [17] Kuo, C. Y., and Wang, Shay-Ping, T., "Nonlinear Robust Hybrid Control of Robotic Manipulators," *Journal of Dynamic Systems, Measurement, and Control*, Vol. 112, pp. 49-54.

6. Review of Objectives and Status

The objectives of the proposed work for the second year of funding have been met. In particular it was proposed to develop and experimentally verify and implement vibration suppression control in coupled rigid flexible systems and systems with repeated modes. This has been accomplished. It remains during the third year to publish these results in journals and to finish implementing the nonlinear "smart" controller, as well as developing the associated theory.

7. Publications

This section lists journal publications prepared or in print while the PI was under partial support of this award, only those in archival journals are listed.

Leo, D. J. and Inman, D. J., "Modeling and Control of a Slewing Frame Containing Self-Sensing Active Members," *Smart Materials and Structures*, to appear.

Banks, H. T., Wang, Y., and Inman, D. J., "Bending and Shear Damping in Beams: Frequency Domain Estimation Techniques," *Journal of Vibration and Acoustics*, to appear.

Yae, K.H. and Inman, D.J., "Control Oriented Order Reduction of Finite Element Models," *ASME Journal of Dynamic Systems, Measurement and Control*, to appear.

Slater, J. C. and Inman, D. J., "Transfer Function Modeling of Damping Mechanisms in Distributed Parameter Models," *Mechanics Research Communications*, to appear.

Garcia, E., Dosch, J. and Inman, D. J., "The Application of Smart Structures to the Vibration Suppression Problem," *Journal of Intelligent Material Systems and Structures*, Vol. 3, No. 4, October 1992, pp. 659-667.

Starek, L., Inman, D.J. and Kress, A., "A Symmetric Inverse Vibration Problem," *ASME Journal of Vibration and Acoustics*, Vol. 114, Oct. 1992, pp. 564-568.

Banks, H.T. and Inman, D.J., "On the Significance of Modeling Internal Damping in the Control of Structures," *AIAA Journal of Guidance, Control and Dynamics*, Vol. 15, No. 6, Nov.-Dec. 1992, pp. 1509-1512.

Yae, H. and Inman, D.J., "Model Reduction in a Subset of the Original States," *Journal of Sound and Vibration*, Vol. 155, No. 1, March 1992, pp. 165-176.

Dosch, J.J., Inman, D.J. and Garcia, E., "A Self Sensing Piezoelectric Actuator for Collocated Control," *Journal of Intelligent Materials, Systems and Structures*, Vol. 3, No. 1, January 1992, pp. 166-185.

8. Personnel Supported

The professional personnel associated with this research effort are Mr. Donald J. Leo, Mr. Ralph Riets and Mr. Jeffrey J. Dosch (all Ph.D. students) and the PI, Dr. Daniel J. Inman.

9. Coupling Activities

Dr. Inman gave invited lectures on the topics of this proposal at

- ASME Niagra Mohawk Section (Albany, N.Y.)
- Rensselaer Polytechnic Institute (Troy, N.Y.)
- Virginia Tech (Blacksburg, VA)
- University of Illinois (Champaign, IL)

In Addition the following lists papers presented at professional meetings (*indicates invited)

*"Programmable Structures" SPIE Meeting on Smart Materials, Albuquerque, New Mexico, Feb. 1993.

"Model Correction Using Constrained Eigenstructure Assignment," 11th International Modal Analysis Conference, February 1993, Orlando, Florida.

*Dosch, J. J., Leo, D. J. and Inman, D. J., "Comparison of Vibration Control Schemes for a Smart Antenna," Proceedings of the 31st IEEE Conference on Decision and Control, to appear December, 1992.

Shulz, M. J. and Inman, D. J., "Model Correction Using Constrained Eigenstructure Assignment," Proceedings of the 11th International Modal Analysis Conference, February 1993, pp. 941-948.

Slater, J., Inman, D. J. and Belvin, W. K., "A Survey of Modern Methods for Modeling Frequency Dependent Damping in Finite Element Models," Proceedings of the 11th International Modal Analysis Conference, February 1993, pp. 1508-1512.

Dosch, J. J., Leo, D. J. and Inman, D. J., "Modeling of a Smart Antenna for Active Vibration Suppression," Proceedings of the 11th International Modal Analysis Conference, February 1993, pp. 1418-1424.

*Leo, D.J. and Inman, D.J., "Control of a Flexible Frame in Slewing," Proceedings of the American Control Conference, June 1992.

Leo, D.J. and Inman, D.J., "Smart Slewing Frames," Proceedings of the First European Conference on Smart Structures, May 1992.

Pokines, B., Belvin, W.K. and Inman, D.J., "A Variable Stiffness Strut Using Strain Induced Bending for Vibration Suppression in the Evolutionary Model," Proceedings of the 33rd AIAA SDM Conference, April 1992.

*Pokines, B., Belvin, W.K. and Inman, D.J., "Static and Dynamic Characteristics of Piezoceramic Strut," Proceedings of the 5th NASA/DOD Controls — Structure Interaction Technology Conference, March 1992.

Slater, J.C., Belvin, W.K. and Inman, D.J., "A Comparison of Viscoelastic Damping Models," Proceedings of the 5th NASA/DOD Controls — Structure Interaction Technology Conference, March 1992.

10. Appendix

The following contains references [2], [3], [11] and [14] which contain the details of the work presented here.

CONTROL OF A FLEXIBLE FRAME IN SLEWING

Donald J. Leo
Daniel J. Inman

Department of Mechanical and Aerospace Engineering
State University of New York at Buffalo
Buffalo, NY, 14260

Abstract

Many satellites require the use of slewing solar panels. A laboratory model of a slewing frame is presented here as an article for testing control laws for such solar arrays. A slewing frame presents a challenging control problem because the primary action of slewing induces torsional vibration which is relatively uncontrollable with respect to the slewing actuator. An experimental investigation of controlling this structure for combined slewing and vibration suppression is presented. The frame is modeled using finite element methods verified by experimental modal analysis. Analytical results indicate that the torsional motion can be suppressed by including an active strut in the feedback loop. Non-colocated and colocated control laws are implemented using the active strut as a sensor and an actuator. The relative effectiveness of each design in suppressing the torsional motion is discussed.

1. Introduction

In recent years, there has been a large amount of research on slewing structures. These structures present challenging control problems since the action of slewing induces residual vibrations. These vibrations can degrade performance when strict pointing and tracking requirements are to be maintained.

Until now, most of the work has concentrated on the slewing of flexible beams. For the most part, these structures exhibit only bending motion when excited [1-3]. Recently, research performed by Sakawa and Luo [4] studied the control of a flexible beam with an eccentric tip mass. This tip mass induced torsional vibrations when slewed, adding a new dimension to the control problem. They presented motor control schemes designed to simultaneously slew the structure and suppress vibrations.

This work will also examine the problem of slewing a structure that exhibits bending and torsional vibrations. The structure studied is not a flexible beam, though, but a frame that models the dynamics of a solar array. The torsional motion induced when slewed is relatively uncontrollable using colocated motor control. Smart structure technology will be applied in an attempt to suppress this motion. Namely, a piezoceramic strut placed in the frame will render these modes controllable.

A number of different control laws will be experimentally verified.

2. Slewing Frame Testbed

A slewing frame was constructed to provide an experimental testbed for control. The frame consisted of thin-walled circular aluminum tubing (Figure 1). Slewing actuation was provided by an Electro-Craft 670 dc motor. Angular rate and position sensors could be used for analog motor control.

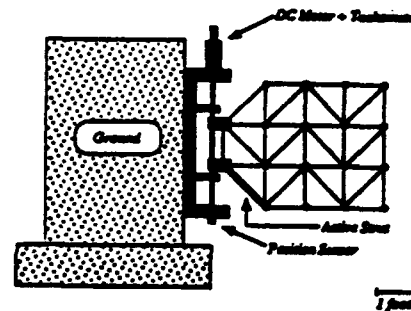


Figure 1: Slewing Frame Testbed

An active strut was designed and inserted into the slewing frame. It consisted of a flat aluminum bar layered with four piezoceramics on each side. Each ceramic was a Model G-1195 from Piezo Electric Products with dimensions 2.5" x 0.75" x 0.01". The strut was configured so that it could be used as a sensor, an actuator, or as a colocated sensor/actuator pair. Figure 2 is a drawing of the active strut. The output from the active strut is proportional to the strain induced in the member. Conversely, the active strut produced a bending moment proportional to the command input.

A number of computers were available for control and data acquisition. A Comdyna GP-6 analog computer was used for position control of the frame and various signal operations (summation, subtraction, etc.). Control laws for the active strut were implemented on an Optima 3 digital controller sampling at 1500 Hz. Finally, data acquisition and frequency analysis was performed using a Tektronix 2630 Fourier Analyzer.

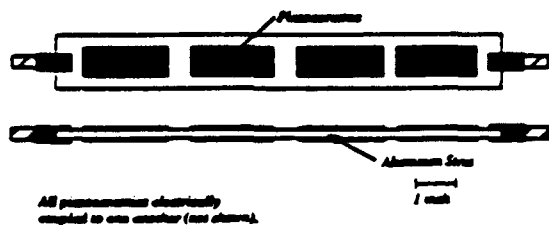


Figure 2: Piezoceramic Active Strut

The objective of the experiments was to slew the frame in a reasonable amount of time while minimizing unwanted vibrations. Due to the configuration of the structure, bending and torsional vibrations were induced when a maneuver was performed. The rest of this paper will deal with the modeling and control aspects of this problem.

3. Modeling and Analytical Results

A linear model of the slewing frame was developed so that a number of control laws could be tested analytically. In physical coordinates, this model took the form [3]

$$\begin{bmatrix} [M] & I_b \\ I_b^T & I_s \end{bmatrix} \begin{Bmatrix} \ddot{q} \\ \ddot{\theta} \end{Bmatrix} + \begin{bmatrix} [K] & 0 \\ 0 & 0 \end{bmatrix} \begin{Bmatrix} q \\ \theta \end{Bmatrix} = \{f\} \quad (1)$$

where M and K are the mass and stiffness matrices of the structure, respectively, I_s is the rigid body inertia about the slewing axis, and I_b is part of the interaction between the rigid body and flexible motion. The physical coordinates of the structure are denoted q , and the rigid body rotation is symbolized by θ . f is a matrix of applied forces and the overdot represents differentiation with respect to time.

To correctly model the interaction between the motor and the structure, pinned-free natural frequencies and mode shapes were used. The mass and stiffness matrices were built using finite elements and a modal test was performed to verify analytical results [5]. By collecting the normalized mode shapes into a matrix S_m , equation (1) was transformed into modal coordinates by assuming $q = S_m r$ and premultiplying by S_m^T . This yields

$$\begin{bmatrix} [I] & \bar{I}_b \\ \bar{I}_b^T & I_s \end{bmatrix} \begin{Bmatrix} \ddot{r} \\ \ddot{\theta} \end{Bmatrix} + \begin{bmatrix} [\Lambda] & 0 \\ 0 & 0 \end{bmatrix} \begin{Bmatrix} r \\ \theta \end{Bmatrix} = \{S_m^T f\} \quad (2)$$

Λ is a matrix of the form $\text{diag}(\omega_1^2, \omega_2^2, \dots, \omega_N^2)$, and

$\bar{I}_b = S_m^T I_b$. I is an $N \times N$ identity matrix, where N is the number of flexible modes in the model.

The active strut was modeled as a moment generator [6]. For simplicity, it was assumed to span the entire length of the strut. Although not a rigorous model of the piezoelectric effect, it did produce satisfactory results.

To study the slewing frame, a 16 mode model was developed using finite elements. The boundary condition was chosen to be pinned-free, and the natural frequencies and mode shapes were verified by a modal test. Initially, a simple Proportional-Derivative (PD) controller of the form

$$G_{pd}(s) = -K_v \dot{\theta} - K_p \theta \quad (3)$$

was used for position control of the frame. The gains were set to values that produced an adequate step response. Due to the nature of the boundary condition, this controller also added damping to certain flexible modes. This occurs because the pinned-free condition allows a large amount of interaction between the structure and the motor. In the model, the damping in the motor is added to the flexible motion through the applied loads vector f . Consequently, derivative action on the motor also produces an increase in damping in the flexible motion. Results of an analytical study where $K_p = 2.5$ and $K_v = 6.5$ are given in Table 1. All modes were initially assumed to be undamped.

Table 1: Natural Frequencies and Damping Ratios in the flexible modes using PD motor control.

Mode	ω_d (Hz)	ζ % Critical
Torsional	4.37	0.41
Bending	8.87	11.24
Torsional	15.47	0.50
Plate	19.79	0.53
Bending	27.53	5.10

This study reveals that a simple PD motor control adds a significant amount of damping to the bending modes. This is consistent with previous results [7]. Table 1 also shows that the torsional motion is still relatively undamped.

In an attempt to control the first torsional mode of the slewing frame, an analysis was performed using the active strut as a sensor and an actuator. Various control laws were attempted. The two that performed the best were Generalized Structural Filtering (GSF) and Positive Position Feedback (PPF). Analytical designs were obtained using the model. They indicated that the damping in the first torsional mode could be increased to

5.7 % using the GSF method and to 8.5 % using PPF control. Details of the actual designs will be presented in the following section.

4. Experimental Results

Analytical results indicated that the torsional motion of the frame was difficult to suppress using colocated motor control. Further studies revealed that by using an active strut, these torsional vibrations could be rendered controllable. Experimental results support these conclusions and provide studies in the design of active control systems for flexible structures.

Three levels of control were implemented on the slewing frame. The first consisted of a simple PD compensator for the motor. This was necessary in order to position the frame and suppress the bending vibrations. Next, a non-colocated control law was designed to adequately damp the dominant torsional motion. Finally, a colocated controller using the active strut was implemented and the results were compared to the non-colocated case. Figure 3 is a schematic of the overall control architecture.

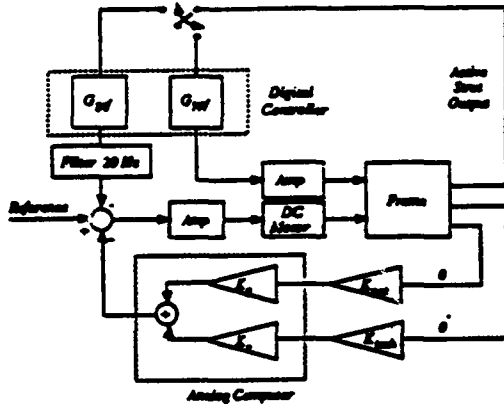


Figure 3: Slewing Frame Control Architecture

Proportional-Derivative Motor Control

The first control law studied was a simple PD compensator of the form given in equation (3). The $\dot{\theta}$ term was the tachometer output, and θ was the signal from the potentiometer. The reference command was a step input of 1 volt. This corresponded to a 30° slewing maneuver. The active strut was only used as a sensor for these experiments.

A typical response of the frame position is shown in Figure 4. The settling time for the slew maneuver is about 6 seconds. In addition to controlling the position of the frame, the PD compensator has the desirable effect of suppressing the bending motion. Unfortunately, the torsional motion is still relatively undamped, even with quite a lot of derivative action on the motor. Table 2 lists the natural frequencies and

damping ratios for the case of experimental PD control. It shows that the colocated motor control suppresses the dominant bending motion but leaves the torsional mode lightly damped. This trend is similar to the results obtained analytically with the FEM model.

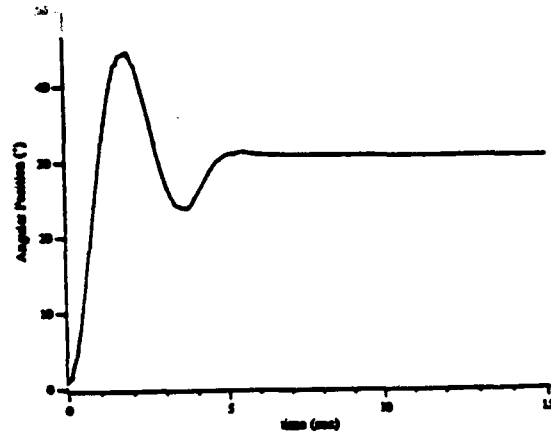


Figure 4: Frame Step Response ($K_p = 2.5$, $K_v = 6.5$)

Table 2: Natural frequencies and damping ratios for experimental PD control.

Mode	ω_d (Hz)	ζ % Critical
Torsional	4.32	0.82
Bending	7.68	9.18
Torsional	14.11	1.26
Plate	20.76	0.94
Bending	26.25	1.32

During this maneuver, the sensor output of the active strut during a 30° slew is shown in Figure 5. This illustrates the lightly damped torsional mode. The 4.32 Hz vibration does not settle for over 30 seconds, well after the slewing maneuver is over.

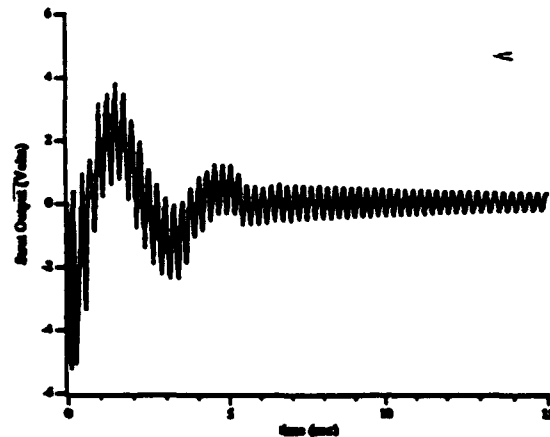


Figure 5: Active strut output for 30° slew maneuver with only PD control.

One problem that became important during the experiments was static friction in the motor and bearings. This problem is evident in Figure 4. The sudden stop of the slewing maneuver is due to the fact that the motor cannot overcome the dry friction in the system. This problem was even more important when control laws were implemented to suppress the torsional motion of the frame. This will be discussed in the next section on non-colocated control.

Non-Colocated Control using the Active Strut

To supplement the PD compensator, a non-colocated controller was designed to add damping to the torsional mode. The design tool was a method called Generalized Structural Filtering (GSF). The GSF method uses non-minimum phase second order filters to successively stabilize structural poles. The design is done iteratively, using 'classical' techniques of root locus and Bode plots. For a detailed description of GSF control, see [8].

For this particular application, the design steps were as follows. Initially, a transfer function was taken between the motor input and the active strut output. A commercially available Recursive Least Squares package used the time domain data to obtain a pole-zero model [9]. From this model, root locus and Bode plots could be used to design a compensator. The objective of the design was to add damping to the torsional motion without destabilizing higher frequency dynamics. In an attempt to attenuate the high frequency content of the control signal, it was filtered at 20 Hz with an Ithaca 24 dB/octave low-pass filter. A number of designs were attempted, with varying degrees of success. Each design was tested experimentally by feeding back the active strut output into the dc motor and performing a slewing maneuver. All but the final compensator caused instabilities in the flexible motion when experimentally implemented. The final GSF controller took the form

$$G_{gsf}(s) = 0.7 \frac{(s/20+1)(s - 29.5 \pm j34.2)}{(s/40+1)(s + 26.0 \pm j30.4)} \quad (4)$$

Equation (4) is the combination of a simple lead and a non-minimum phase filter. Figure 6 shows the response of the structure during a 30° slewing maneuver with GSF control on. The torsional motion is adequately damped out, i.e., by the time the slewing is over (= 7 s), the vibrations have ceased.

Even though this method damps out the torsional motion during a slew maneuver, the deadband in the motor makes it ineffective for disturbance rejection. If some type of input was applied to the frame (e.g. thermal shock of a solar panel) when it was not slewing, the controller could not react until it overcame the static friction in the system. Thus, the static friction limits the effectiveness of this non-colocated control.

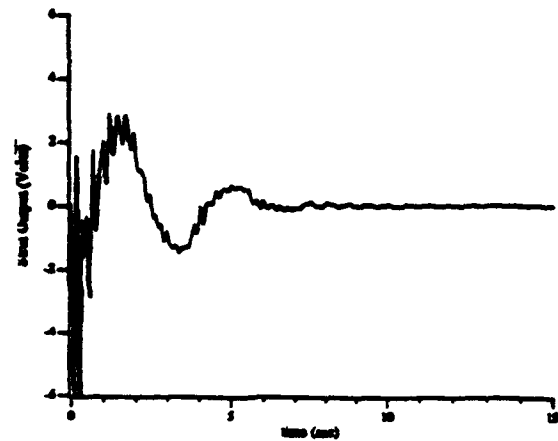


Figure 6: Structural response using GSF control during a 30° slew.

To alleviate this problem, one of two things could be done. Quite simply, the first solution is to reduce the static friction by using better hardware. The less of a deadband, the more effective this type of controller will be. But since all real systems have static friction, a more practical approach would be to put both the sensor and actuator on the flexible structure [10]. If this is done, then the vibration suppression of the torsional motion would be independent of the slewing actuator. This colocated controller could suppress vibrations during a slew maneuver as well as reject disturbances. The last experiment deals with this type of design.

Control using the Active Strut as a Colocated Sensor Actuator

The final control strategy was to use the active strut as a colocated sensor/actuator. The design method was Positive Position Feedback (PPF). It is a type of second order filtering which has good robustness and stability properties [11].

The objective is the same as before, suppress the torsional motion without destabilizing higher modes. For the colocated case, stability boundaries are much better defined since the phase of the transfer function lies between 0 and -180° over most of the frequency range. Use of PPF control allowed for a much easier design process. Only two iterations were necessary to obtain a satisfactory result, as opposed to the five or needed for GSF control.

$$G_{ppf}(s) = 0.7 \frac{\omega_f^2}{s^2 + 2\zeta_f \omega_f s + \omega_f^2} \quad (3)$$

$$\omega_f = 33.14 \text{ rad/s} \quad \zeta_f = 0.15$$

Implementation of this control law increases the damping in the torsional mode from about 0.82% to 3.8% critical, almost a factor of 5 better. The slewing response (Figure 7) is not as impressive as the one for

the non-colocated control (Figure 6), but it is independent of the motor. With this type of control, disturbance rejection is achieved since the active strut serves as the actuator as well as the sensor.

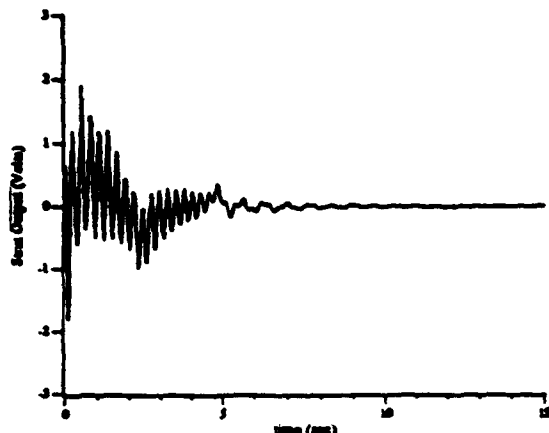


Figure 7: Structural response using PPF control on the active strut. Slew maneuver is 30° .

This last control experiment illustrates an important point about slewing an active structure. The advantages are that a number of separate colocated sensor/actuator pairs can be used for both vibration suppression and disturbance rejection. This alleviates the problem that the static friction played when using non-colocated control and allows more flexibility in designing control laws. This was especially apparent in this case, since the dominant torsional motion was not well controlled by motor control alone.

5. Conclusions

The slewing of a structure that exhibited bending and torsional motion was examined. An analytical model predicted difficulty in suppressing the torsional vibration using a colocated controller located at the slewing actuator. This was experimentally verified on a testbed that consisted of a flexible frame slewed by a dc motor. An active strut was built by layering piezoceramic material on a flat aluminum bar. This strut was placed in the frame and a number of control experiments were performed. A non-colocated controller was designed using Generalized Structural Filtering techniques. This adequately suppressed the torsional vibrations but did not provide any disturbance rejection due to static friction in the system. Positive Position Feedback was then implemented using the active strut as a colocated sensor/actuator. Since this control scheme was independent of the motor, it was not limited by the static friction. Having two separate colocated controllers, one on the motor and one on the active strut, provided both vibration suppression during slewing and disturbance rejection.

Acknowledgement

This work is supported under AFOSR grant number 91-0181 under the direction of Dr. Spencer Wu.

References

- [1] Juang, J.N., Horta L.G., and Robertshaw H.H., "A Slewing Control Experiment for Flexible Structures," *J. of Guidance, Control and Dynamics*, v 9 n5, Sept-Oct 1986, pp. 599-607.
- [2] Cannon, R.H., and Schmitz, E., "Initial Experiments on the End-Point Control of a Flexible One-Link Robot," *Int. J. of Robotics Research*, v3 n3, Fall 1984, pp. 62-75.
- [3] Garcia, E., and Inman, D.J., "Modeling of the Slewing Control of a Flexible Structure", *J. of Guidance, Control, and Dynamics*, v14 n4, July-Aug 1991, pp. 736-742.
- [4] Sakawa, Y., and Luo, Z.H., "Modeling and Control of Coupled Bending and Torsional Vibrations of Flexible Beams," *IEEE Trans. on Automatic Control*, v 34 n9, Sept. 1989, pp. 970-977.
- [5] Leo, D.J. and Inman, D.J., "Smart Slewing Frames," *Proc. of the 1st European Conference on Smart Structures and Materials*, Glasgow, Scotland, 1992 (to appear).
- [6] Fanson, J.L., and Caughey, T.K., "Positive Position Feedback Control for Large Space Structures," *Proc. of the 28th Structural, Dynamics, and Materials Conference*, 1987, pp. 588-98.
- [7] Garcia, E., "On the Modeling and Control of Slewing Flexible Structures," Ph.D. dissertation, State University of New York at Buffalo, 1989.
- [8] Wie, B., and Byun, K.W., "New Generalized Structural Filtering Concept for Active Vibration Control Synthesis," *J. of Guidance, Control, and Dynamics*, v12 n2, Mar-Apr 1989, pp. 147-155.
- [9] *TurboPac User's Guide*, Tektronix, Campbell, CA.
- [10] Garcia, E., and Inman, D.J., "Advantages of Slewing an Active Structure," *J. of Intelligent Material Systems and Structures*, v1 n3, July 1990, pp. 261-272.
- [11] Goh, C.J., and Caughey, T.K., "On the Stability Problem Caused by Finite Actuator Dynamics in the Colocated Control of Large Space Structures," *Int. J. of Control*, v 41 n3, 1985, pp. 787-802.

MODELING AND CONTROL SIMULATIONS OF A SLEWING FRAME CONTAINING ACTIVE MEMBERS

Donald J. Leo*
Daniel J. Inman**

**Research Assistant
Department of Mechanical and Aerospace Engineering
State University of New York at Buffalo
Buffalo, NY, 14260*

***Samuel Herrick Professor
Department of Engineering Science and Mechanics
Virginia Polytechnic Institute and State University
Blacksburg, VA, 24061*

ABSTRACT

A testbed consisting of a flexible frame slewed by a dc motor is modeled for active vibration suppression. This presents a challenging control problem since the primary action of slewing induces both bending and torsional vibrations in the structure. Inserted into the frame are two active members that can be used as self-sensing actuators in feedback control loops. First, a model for the slewing frame is developed using Lagrange's equations and finite element approximations. The interactions between the structure and the slewing actuator are then derived from the equations for a dc motor. Similar expressions are obtained for the forces applied to the structure by the active elements. A detailed model of the self-sensing actuator is provided which includes the terms due to actuator and sensor dynamics. A theoretical study is then conducted to obtain control laws that simultaneously slew the frame and suppress the residual vibrations. Simulation results indicate that the dc motor is effective in slewing the frame and suppressing the bending motion but not the torsional motion. Hence, the torsional vibrations are suppressed using the active members in colocated feedback loops.

1. Introduction

The slewing of flexible structures is a challenging control problem due to the coupling between the rigid body and elastic motion. The primary action of rotating the flexible body induces vibrations that cause a considerable degradation in system performance. This problem is important in the space structures community due to the high flexibility and strict performance requirements of future space missions.

Much of the research performed in this area has concentrated on implementing active control laws to simultaneously slew the structure and suppress vibrations. Early work performed by Juang, Horta, and Robertshaw (1986) examined the active control of a large slewing beam. They developed a model for the structure and used a dc motor as the actuator in a feedback loop. Vibration suppression was obtained by mounting a strain gage onto the beam and using it as a non-colocated sensor. A similar approach was taken by Garcia (1989), except that only angular rate and position signals were used for feedback control. Simple Proportional-Derivative control laws were able to suppress the vibrations of a slewing beam due to the large interaction between the motor and the structure. A Lyapunov based control strategy was developed by Junkins, Rahman, and Bang (1990) for the reorientation of a rigid hub with four flexible appendages. An improvement in performance was achieved by shaping the input to the slewing actuator. Another Lyapunov based method was introduced by Fujii, Ohtsuka, and Udou (1991). Experimental results were presented indicating that vibration suppression could be improved by using a method they called Mission Function Control.

In all of the previously mentioned work, the slewing actuator was used to simultaneously rotate the structure and suppress vibrations. This strategy was effective, in part because the structure being slewed was a simple beam. If the structure exhibited more complex dynamic behavior, the slewing actuator might not be able to suppress all of the

flexible modes. It would be desirable, and in some cases even necessary, to have separate sensors and actuators available for feedback control.

Recent advances in smart structure technology provide a means for integrating actuators and sensors into a slewing structure. This is accomplished by replacing passive members of the structure by active elements. The active members contain piezoceramic material, thereby enabling them to be used as sensors and actuators for control. Recently, Dosch, Inman, and Garcia (1992) demonstrated the concept of using a single piece of piezoceramic to simultaneously sense the vibrations and apply a moment to a cantilever beam. This is important in the control of flexible structures since the resulting sensor and actuator are perfectly colocated with one another. With regards to the slewing problem, Garcia and Inman (1990) showed that integrating a piezoceramic sensor/actuator into a slewing beam can improve performance and reduce the peak power of the motor.

This paper examines the modeling and control of a slewing structure that contains integrated actuators and sensors. The structure is not a beam, but a frame that models the complex dynamics of a flexible appendage such as a solar array. Two of the passive frame members have been replaced with active elements: aluminum bars with piezoceramic material bonded to the surface. Characteristics of the piezoceramics allow these active elements to be used as colocated sensor/actuators. The active members are an integral part of the control system since the torsional motion of the frame is not suppressed by the slewing actuator.

The paper is organized in the following manner. First, a model for the frame is developed using Lagrange's equations and finite element approximations. The interaction between the structure and the motor is obtained by considering the equations for a dc motor. A model of the active members is developed which includes the dynamics

associated with a self-sensing actuator. Finally, control system design for the slewing frame is studied using the model and the actual parameters of the testbed.

MODELING OF A SLEWING STRUCTURE USING FINITE ELEMENTS

The model for the slewing frame is derived from Lagrange's equations and finite element approximations. The advantages of using the finite element approach is that it can easily handle the complex geometry of the frame. The governing equations for the complete structure are obtained by first considering a single element slewing about an axis, as shown in Figure 1.

The motion of this element consists of a rigid body rotation, $\theta(t)$, and an elastic deformation, $\hat{u}(\hat{x}, t)$. A torsional rotation about the \hat{x} axis also exists, and is denoted $\hat{\phi}(\hat{x}, t)$. The two ends of the beam are called the *nodes* of the element. Node i is a fixed distance r_i from the origin of the inertial coordinate system, XYZ . The rigid body is constrained to lie in a plane, xz , which is rotating with respect to the Z axis with an angular velocity $\dot{\theta}(t)$.

Another set of coordinates, the $\hat{x}\hat{y}\hat{z}$ frame, is attached to the rigid body of the slewing element. The origin of $\hat{x}\hat{y}\hat{z}$ is chosen to be Node i and \hat{x} is the centroidal axis of the rigid body. Since the element is constrained to be in the xz plane, the y and \hat{y} axes are parallel. Thus, the orientation of the element with respect to the rotating xyz frame can be described by a single angle γ .

The arbitrary deformation, $\hat{u}(\hat{x}, t)$, and torsion about the \hat{x} axis, $\hat{\phi}(\hat{x}, t)$, can be expanded into the following form:

$$\hat{u}(\hat{x}, t) = \begin{bmatrix} \hat{u}_x \\ \hat{u}_y \\ \hat{u}_z \end{bmatrix} = \Psi_u(\hat{x})\hat{q}(t) \quad (1)$$

$$\hat{\phi}(\hat{x}, t) = \Psi_\phi(\hat{x})\hat{q}(t)$$

where $\hat{q}(t)$ is a 12 x 1 vector of independent generalized coordinates. The matrix $\Psi_u(\hat{x})$ is a 3 x 12 matrix of basis functions, and $\Psi_\theta(\hat{x})$ is a 1 x 12 vector basis functions [Cook and Malkus (1989)]. The set of generalized coordinates are chosen to be the three translations and three rotations at each node of the element. This choice assumes that the rotations are small, i.e., they can be added as vectors.

The Lagrangian of this slewing element is obtained and Lagrange's Equations are used to derive the governing equations [Leo (1992)]. They take the following form:

$$\begin{bmatrix} \hat{M} & \hat{I}_b \\ \hat{I}_b^T & \hat{I}_r \end{bmatrix} \begin{Bmatrix} \ddot{\hat{q}}(t) \\ \ddot{\theta}(t) \end{Bmatrix} + \begin{bmatrix} \hat{K} & 0 \\ 0 & 0 \end{bmatrix} \begin{Bmatrix} \hat{q}(t) \\ \theta(t) \end{Bmatrix} = \hat{Q}_m + \hat{Q}_{pe} \quad (2)$$

where \hat{M} and \hat{K} are the 12 x 12 mass and stiffness matrices of the finite element, respectively. The structural inertia of the element about its slewing axis is denoted \hat{I}_r , and \hat{I}_b is a 12 x 1 vector that couples the elastic deformation to the rigid body rotation. The non-conservative forces due to the motor and the piezoelectrics are denoted \hat{Q}_m and \hat{Q}_{pe} , respectively. The assumptions made during the derivation are that the element can be modeled as an Euler-Bernoulli beam, that the cross-section is symmetric, and that the geometric and material properties are independent of \hat{x} . The expressions for each of the terms in equation (2) is placed in the Appendix of this work.

The governing equations of the slewing frame are assembled from equation (2) by substituting

$$\begin{Bmatrix} \hat{q}(t) \\ \theta(t) \end{Bmatrix} = \mathbf{CB} \begin{Bmatrix} \mathbf{q}(t) \\ \theta(t) \end{Bmatrix} \quad \mathbf{C} = \begin{bmatrix} \mathbf{C}_e & 0 \\ 0 & 1 \end{bmatrix} \quad \mathbf{B} = \begin{bmatrix} \mathbf{B}_e & 0 \\ 0 & 1 \end{bmatrix} \quad (3)$$

into the expression and pre-multiplying by $\mathbf{B}^T \mathbf{C}^T$. The matrix \mathbf{C}_e is the transformation between the element coordinates and the global frame of reference. The operator \mathbf{B}_e transforms the element coordinates into the corresponding global degrees of freedom. It

has the dimension $12 \times N_{def}$, where N_{def} is the number of degrees of freedom in the complete model. The final set of equations has the form

$$\begin{bmatrix} \mathbf{M} & \mathbf{I}_b \\ \mathbf{I}_b^T & \mathbf{I}_s \end{bmatrix} \begin{Bmatrix} \ddot{\mathbf{q}}(t) \\ \ddot{\theta}(t) \end{Bmatrix} + \begin{bmatrix} \mathbf{K} & \mathbf{0} \\ \mathbf{0} & \mathbf{0} \end{bmatrix} \begin{Bmatrix} \mathbf{q}(t) \\ \theta(t) \end{Bmatrix} = \mathbf{Q}_m + \mathbf{Q}_s \quad (4)$$

where

$$\mathbf{M} = \sum_{i=1}^{N_e} \mathbf{B}_i^T \mathbf{C}_i^T \hat{\mathbf{M}}_i \mathbf{C}_i \mathbf{B}_i \quad \mathbf{K} = \sum_{i=1}^{N_e} \mathbf{B}_i^T \mathbf{C}_i^T \hat{\mathbf{K}}_i \mathbf{C}_i \mathbf{B}_i$$

$$\mathbf{I}_b = \sum_{i=1}^{N_e} \mathbf{B}_i^T \mathbf{C}_i^T \hat{\mathbf{I}}_{bi} \quad \mathbf{I}_s = \sum_{i=1}^{N_e} \hat{\mathbf{I}}_{si}$$

$$\mathbf{Q}_m = \sum_{i=1}^{N_e} \mathbf{B}_i^T \mathbf{C}_i^T \hat{\mathbf{Q}}_{mi} \quad \mathbf{Q}_s = \sum_{i=1}^{N_e} \mathbf{B}_i^T \mathbf{C}_i^T \hat{\mathbf{Q}}_{si}$$

The number of elements in the slewing model is denoted N_e . The assembly of the governing equations is more computationally efficient if the *direct assembly* approach is used [Cook and Malkus (1989)].

2. Modeling the Motor/ Structure Interaction

Modeling the interaction between the motor and the structure has always received considerable attention in the slewing literature [Juang, et al, (1986), Garcia and Inman (1991)]. The derivation presented here is similar to the previous work in most respects, except that earlier research concentrated on obtaining expressions for distributed parameter systems, not finite element models.

First, consider the model for a DC motor shown in Figure 2. The motor is connected through a set of gears to the slewing structure. The armature voltage and current are denoted $e_a(t)$ and $i_a(t)$, respectively. The pertinent motor parameters are the inductance, L_a , the resistance, R_a , the torque constant, K_n , and the back-EMF K_b . The motor has an inertia I_m and a viscous friction coefficient B_v . A set of gears with ratio N_2/N_1 are placed between the motor shaft and the structure. The rotation of the structure is denoted $\theta_s(t)$. The

expression for the torque produced on the structure can be derived from Kirchoff's laws and summation of torques [Kuo (1987)]:

$$\tau = N_s K_a i_a(t) - I_m N_s^2 \ddot{\theta}_s(t) - B_s N_s^2 \dot{\theta}_s(t) \quad (5)$$

where the armature current is related to the command voltage by

$$L_a \frac{di_a(t)}{dt} + R_a i_a(t) = -K_b N_s \dot{\theta}_s(t) + e_a(t) \quad (6)$$

For convenience, the gear ratio N_2/N_1 is denoted N_s .

The next step is to choose a boundary constraint for the finite element model. For the slewing frame, the boundary constraint is chosen to be pinned-free. Thus, the rotational degrees of freedom of the shaft that lies along the slewing axis are unconstrained. These are the $\theta_s(t)$ rotations, using the notation of the previous section. Assuming that the torque acts at the i^{th} node of the structure, the total rotation at that node can be written as:

$$\theta_s(t) = \theta_m(t) + \theta(t) \quad (7)$$

A diagram of this concept for a single element is shown below in Figure 1. The total rotation at the root is a combination of the rigid body rotation and the rotation due to the flexibility. The non-conservative virtual work due to the motor torque, δW_m , is

$$\delta W_m = \tau \delta \theta_s(t) = \tau \delta \theta_m(t) + \tau \delta \theta(t) \quad (8)$$

Equation (7) can be rewritten as a vector multiplied by the generalized coordinates of the system

$$\theta_s(t) = \theta_m(t) + \theta(t) = \mathbf{F}_m^T \begin{Bmatrix} \mathbf{q}(t) \\ \theta(t) \end{Bmatrix} \quad (9)$$

where the $1 \times N_{\text{dof}}$ vector \mathbf{F}_m^T has a one in the i^{th} column and a one in the last column.

The virtual work can now be written as

$$\delta W_m = \tau F_m^T \begin{Bmatrix} \delta q(t) \\ \delta \theta(t) \end{Bmatrix} \quad (10)$$

where $\tau F_m^T = Q_m$ from equation (4).

With the expression for the virtual work, the equations of motion can be rewritten as:

$$\begin{bmatrix} M & I_b \\ I_b^T & I_r \end{bmatrix} \begin{Bmatrix} \ddot{q}(t) \\ \ddot{\theta}(t) \end{Bmatrix} + \begin{bmatrix} K & 0 \\ 0 & 0 \end{bmatrix} \begin{Bmatrix} q(t) \\ \theta(t) \end{Bmatrix} = F_m \tau + Q_m \quad (11)$$

Equation (9) is substituted into the DC motor equations to yield

$$\begin{aligned} \tau &= N_s K_t i_a(t) - I_m N_s^2 F_m^T \begin{Bmatrix} \ddot{q}(t) \\ \ddot{\theta}(t) \end{Bmatrix} - B_s N_s^2 F_m^T \begin{Bmatrix} \dot{q}(t) \\ \dot{\theta}(t) \end{Bmatrix} \\ L_s \frac{di_a(t)}{dt} + R_s i_a(t) &= -K_b N_s F_m^T \begin{Bmatrix} \dot{q}(t) \\ \dot{\theta}(t) \end{Bmatrix} + e_a(t) \end{aligned} \quad (12)$$

These expressions are substituted into equation (11) and, after some manipulation, they can be written as

$$\begin{Bmatrix} M & I_b \\ I_b^T & I_r \end{Bmatrix} + I_m N_s^2 G_m \begin{Bmatrix} \ddot{q}(t) \\ \ddot{\theta}(t) \end{Bmatrix} + B_s N_s^2 G_m \begin{Bmatrix} \dot{q}(t) \\ \dot{\theta}(t) \end{Bmatrix} + \begin{bmatrix} K & 0 \\ 0 & 0 \end{bmatrix} \begin{Bmatrix} q(t) \\ \theta(t) \end{Bmatrix} = F_m K_t N_s i_a(t) + Q_m \quad (13)$$

$$L_s \frac{di_a(t)}{dt} + R_s i_a(t) = -K_b N_s F_m^T \begin{Bmatrix} \dot{q}(t) \\ \dot{\theta}(t) \end{Bmatrix} + e_a(t)$$

where G_m is the gain matrix associated with the motor. It has the form

$$G_m = F_m F_m^T = \begin{bmatrix} G_{m1} & G_{m2} \\ G_{m2}^T & G_{m3} \end{bmatrix} \quad G_{m1} \text{ is order } N_{def} \times N_{def} \quad (14)$$

One final step needs to be performed to obtain the open loop model of the slewing frame. Since the boundary constraints are chosen to be pinned-free, there exists a zero frequency mode in the mass and stiffness matrices. This mode is already accounted for by the rigid body coordinate, $\theta(t)$. To eliminate this redundant mode, equation (13) is transformed from physical coordinates into modal coordinates. This transformation is calculated by solving the following free vibration problem [Inman (1989)]

$$\{M + N_s^2 I_m G_{m1}\} \ddot{q}(t) + Kq(t) = 0 \quad (15)$$

and normalizing the mode shapes such that

$$\begin{aligned} S_s^T \{M + N_s^2 I_m G_{m1}\} S_s &= I \\ S_s^T K S_s &= \Omega = \text{diag}(\omega_i^2) \end{aligned} \quad (16)$$

where S_s is a matrix of the *elastic* modes of the frame. It is not square since the zero frequency mode has been eliminated. The squares of the remaining non-zero natural frequencies, denoted ω_i^2 , are the diagonal elements of the matrix Ω . Equation (13) can be transformed into modal coordinates by substituting the following transformation

$$\begin{Bmatrix} q(t) \\ \theta(t) \end{Bmatrix} = \begin{bmatrix} S_s & 0 \\ 0 & 1 \end{bmatrix} \begin{Bmatrix} r(t) \\ \theta(t) \end{Bmatrix} = T \begin{Bmatrix} r(t) \\ \theta(t) \end{Bmatrix} \quad (17)$$

into the equation and pre-multiplying by T^T . The result is

$$\begin{aligned} \begin{bmatrix} I & S_s^T (I_b + N_s^2 I_m G_{m2}) \\ (I_b^T + N_s^2 I_m G_{m2}^T) S_s & I_s + N_s^2 I_m \end{bmatrix} \begin{Bmatrix} \dot{r}(t) \\ \dot{\theta}(t) \end{Bmatrix} + \begin{Bmatrix} T^T B_s N_s^2 T + D_{prop} \\ \end{Bmatrix} \begin{Bmatrix} \dot{r}(t) \\ \dot{\theta}(t) \end{Bmatrix} \\ + \begin{bmatrix} \Omega & 0 \\ 0 & 0 \end{bmatrix} \begin{Bmatrix} r(t) \\ \theta(t) \end{Bmatrix} = T^T F_m K_r N_s^T i_s(t) + T^T Q_m \end{aligned} \quad (18)$$

$$L_s \frac{di_s(t)}{dt} + R_s i_s(t) = -K_s N_s^T F_m^T T \begin{Bmatrix} \dot{r}(t) \\ \dot{\theta}(t) \end{Bmatrix} + e_s(t)$$

A damping matrix, D_{prop} , is added to the system to account for the inherent damping in the structure. It is a diagonal matrix of the form

$$D_{prop} = \begin{bmatrix} \text{diag}(2\zeta_i \omega_i) & 0 \\ 0 & 0 \end{bmatrix} \quad (19)$$

where ζ_i are the modal damping ratios.

3. Modeling of the Self-Sensing Active Members

One of the major issues of this study is the ability of smart structure technology to improve the performance of the slewing frame. As mentioned in section 2, two members of the frame have piezoceramic material bonded to the surface, thereby enabling them to be used sensors or actuators. To model these active members, expressions for voltage output and applied moment of the piezoceramics must be developed.

The actuator equation is derived for a pair of piezoceramics bonded to a flat beam, as shown in Figure 3. Assuming that the beam is in pure bending, the expression for the moment applied by the piezoceramics is [Dosch, et al, (1992)]:

$$M(\hat{x}, t) = K_a v_a(t) [h(\hat{x} - \hat{x}_1) - h(\hat{x} - \hat{x}_2)] \quad (20)$$

where \hat{x}_1 and \hat{x}_2 are the location of the ends of the piezoceramic pair. The heaviside step function defines the region of the beam covered by the piezoceramics. The applied voltage is denoted $v_a(t)$ and the actuator constant, K_a is expressed in terms of the geometric and material properties of the beam and ceramic:

$$K_a = b d_{31} Y_p (t_{ps} + t_c) \quad (21)$$

The thickness of the piezoceramic and the strut are denoted t_{ps} and t_c , respectively. The width of the strut is labeled b , and Y_p is Young's modulus. The dielectric constant of the ceramic is denoted d_{31} .

The expression for the virtual work produced by the pair of piezoceramics is [Fanson (1987)]:

$$\delta W_{\pi} = \delta \int_0^L M(\hat{x}, t) \frac{\partial^2 \hat{u}_y(\hat{x}, t)}{\partial \hat{x}^2} d\hat{x} \quad (22)$$

where L is the length of the beam.

Substituting for $\hat{u}_y(\hat{x}, t)$ as defined in equation (1), the previous expression can be rewritten as

$$\delta W_{\pi}^i = \int_0^L M(\hat{x}, t) [\Psi_{\pi}^{\prime i}(\hat{x}) \delta \hat{q}(t)] d\hat{x} \quad (23)$$

The superscript i indicates that the expression is for the i^{th} piezoceramic pair, and the prime notation signifies differentiation with respect to \hat{x} . Integration of the preceding equation yields

$$\delta W_{\pi}^i = K_a v_a(t) [\Psi_{\pi}^{\prime}(\hat{x}_2^i) - \Psi_{\pi}^{\prime}(\hat{x}_1^i)] \delta \hat{q}(t) \quad (24)$$

The virtual work done by all four piezoceramic pairs is

$$\delta W_{\pi} = K_a v_a(t) \sum_{i=1}^4 \{ \Psi_{\pi}^{\prime}(\hat{x}_2^i) - \Psi_{\pi}^{\prime}(\hat{x}_1^i) \} \delta \hat{q}(t) \quad (25)$$

Equation (25) assumes that all of the piezoceramics have the same actuator constant and applied voltage. The expression can be transformed into global coordinates by substituting

$$\delta \hat{q}(t) = C_s B_s \delta q(t) \quad (26)$$

into the equation. This leads to

$$\delta W_{\pi} = K_a v_a(t) \sum_{i=1}^4 \{ \Psi_{\pi}^{\prime}(\hat{x}_2^i) - \Psi_{\pi}^{\prime}(\hat{x}_1^i) \} C_s B_s \delta q(t) \quad (27)$$

The non-conservative work term associated with the active strut can now be written as

$$\begin{aligned}
Q_{\mu} &= \mathbf{B}_{\mu}^T \mathbf{C}_{\mu}^T \left[\sum_{i=1}^4 \{ \Psi_{\mu}^{\prime T}(\hat{x}_2^i) - \Psi_{\mu}^{\prime T}(\hat{x}_1^i) \} \right] K_{\mu} v_{\mu}(t) \\
&= \mathbf{F}_{\mu} K_{\mu} v_{\mu}(t)
\end{aligned} \tag{28}$$

A similar expression is derived for the voltage output of the active member, $v_{\mu}(t)$. The expression is

$$v_{\mu}(t) = K_{\mu} \left[\frac{\partial \hat{u}_y(\hat{x}_2, t)}{\partial \hat{x}} - \frac{\partial \hat{u}_y(\hat{x}_1, t)}{\partial \hat{x}} \right] \tag{29}$$

where

$$K_{\mu} = \frac{Y_p d_{31} b y_c}{C_p} \text{ Volt/rad}$$

the term y_c is the distance from the neutral axis of the strut to the middle of the ceramic and C_p is the constant strain capacitance of the material.

Performing an analysis similar to the one for the actuator equation results in the following expression for the piezoceramic voltage of the active strut:

$$\begin{aligned}
v_{\mu}(t) &= K_{\mu} \left[\sum_{i=1}^4 \{ \Psi_{\mu}^{\prime}(\hat{x}_2^i) - \Psi_{\mu}^{\prime}(\hat{x}_1^i) \} \right] \mathbf{C}_{\mu} \mathbf{B}_{\mu} \mathbf{q}(t) \\
&= K_{\mu} \mathbf{F}_{\mu}^T \begin{Bmatrix} \mathbf{q}(t) \\ \theta(t) \end{Bmatrix} \\
&= K_{\mu} \mathbf{F}_{\mu}^T \mathbf{T} \begin{Bmatrix} \mathbf{r}(t) \\ \theta(t) \end{Bmatrix}
\end{aligned} \tag{30}$$

4. Dynamics of the Self-Sensing Actuator

The idea of using a single piezoceramic to simultaneously sense and actuate was previously presented by Dosch, Inman, and Garcia (1992). The importance of this concept is that the actuator and sensor are perfectly colocated. Sensor/actuator collocation is very attractive when designing active control schemes for flexible structures since it is inherently

more stable than non-colocated control. Self-sensing actuation is accomplished by the use of a bridge circuit connected to the piezoceramic active member. Use of this circuit introduces dynamics into the feedback loop that can have an effect on the open and closed properties of the system.

The circuit studied in this work was originally presented by Dosch, et al (1992) as a means of simultaneously sensing strain and applying a force. Other versions of this circuit are able to sense strain rate, but for this work, only the strain sensor is examined (Figure 4). The sensor voltage is the difference between $v_1(t)$ and $v_2(t)$, which are the voltages at the two terminals shown in Figure 4. In the Laplace domain, the sensor voltage is

$$V_s(s) = \frac{RC_p^*s}{1 + R(C_p^* + C_2)s} V_m(s) + \left[\frac{RC_p^*s}{1 + R(C_p^* + C_2)s} - \frac{RC_2s}{1 + R(C_3 + C_4)s} \right] V_c(s) \quad (31)$$

Likewise, the voltage applied to the piezoceramic is the difference between $v_a(t)$ and $v_1(t)$:

$$\begin{aligned} V_a(s) &= V_c(s) - \left[\frac{RC_p^*s}{1 + R(C_p^* + C_2)s} V_m(s) + \frac{RC_p^*s}{1 + R(C_p^* + C_2)s} V_c(s) \right] \\ &= \frac{1 + RC_2s}{1 + R(C_p^* + C_2)s} V_c(s) - \frac{RC_p^*s}{1 + R(C_p^* + C_2)s} V_m(s) \end{aligned} \quad (32)$$

The result of equation (31) can be substituted into the previous expression. After manipulation, the actuator voltage can be written

$$V_a(s) = \frac{1 + RC_2s}{1 + R(C_3 + C_4)s} V_c(s) - V_s(s) \quad (33)$$

A block diagram between the control voltage, $v_c(t)$, and the self-sensing output, $v_s(t)$, can be obtained from the results of the previous two sections (Figure 5). In Figure 5, the following notation is used:

$$E_1(s) = \frac{1 + RC_4s}{1 + R(C_3 + C_4)s}$$

$$E_2(s) = \frac{RC_p s}{1 + R(C_p + C_2)s}$$

$$E_3(s) = \frac{R^2(C_p C_4 - C_3 C_2)s^2 + R(C_p - C_3)s}{[1 + R(C_p + C_2)s][1 + R(C_3 + C_4)s]}$$

The block diagram of the self-sensing actuator illustrates the dynamics associated with using the circuit in a feedback loop. The actuator voltage across the piezoceramics is a combination of the input voltage and a feedback proportional to the sensor signal. Similarly, the output of the circuit is a combination of the piezoceramic voltage and an input feedthrough term. Nominally, the circuit parameters are chosen such that $C_3 = C_p$ and $C_2 = C_4$. In this situation, the feedthrough term is identically zero and the sensor output is simply a high-passed filtered version of the piezoceramic voltage. The corner frequency of the high-pass filter depends on the constant strain capacitance of the strut and the choice of C_2 . The actuator dynamics have the form of a lag filter, thus attenuating the high frequency content of the control signal. Even in the nominal case, the sensor output feedback term is still present in the open loop dynamics.

Of course, the circuit parameters are not always tuned perfectly to one another. In the original work by Dosch, et al (1992), this situation is referred to as a 'mistuned' self-sensing actuator. Not tuning the parameters correctly can have a significant effect on the transfer function between the control voltage and the sensor output [Anderson, Hagood, and Goodcliffe (1992)]. Studying the problems associated with mistuning the circuit is a direction for future research. A simple consequence of capacitor mismatch is illustrated in the simulations later on in Section 7 of this paper.

5. The Slewing Frame Testbed

A frame slewed by a dc motor is presented as a testbed for experiments in the control of slewing flexible structures. Due to its configuration, the action of rotating the frame about an axis causes both bending and torsional vibrations. The frame consists of individual elements of thin-walled circular aluminum tubing. Each member is 0.635 cm in diameter and has a wall thickness of 0.124 cm. The elements are joined at octagonal nodes that are also made of aluminum. Each member is pinned and bolted into the node to eliminate looseness in the joints. The frame is mounted onto the larger steel shaft by bolting two of the nodes into aluminum clamps.

The slewing actuator is an Electro-Craft 670 dc motor. The shaft of the motor is coupled to a steel shaft with a diameter of 0.635 cm, which in turn is connected to another steel shaft of diameter 1.270 cm. The smaller shaft can easily be removed so that gears can be placed between the motor and the structure. A tachometer housed inside the motor measures angular rate, and a potentiometer attached to the bottom of the larger steel shaft produces a signal proportional to angular position. The whole slewing rig is attached to a large concrete block that serves as ground. Figure 6 is a diagram of the slewing frame testbed.

Two of the passive elements of the frame have been replaced by active elements. The active members are flat aluminum bars that have four strips of piezoceramic material bonded to each side (see Figure 3). The piezoceramics are model G-1195 from Piezo Electric Products and have dimensions 6.350 cm x 1.905 cm x 0.025 cm. Each ceramic is glued to the member with Duro Depend II adhesive. All of the piezoceramics are electrically coupled to one another to create one sensor/ actuator. On both active members, the aluminum beam is used as a ground for the underside of all the ceramics.

The parameters for both the dc motor and the active members are listed in Table 1.

Table 1: Parameters for the slewing actuator and active members.

d_{31}	190 e-12	m/Volt	K_t	0.11298	(N-m)/Amp
b	0.0254	m	K_b	0.11298	V/rad/sec
y_c	2.86 e-3	m	I_m	3.53e-4	kg-m ²
C_p	0.275 e-6	F	L_s	0.002	H
t_{pe}	3.175 e-3	m	R_s	0.63	Ohms
t_s	2.54 e-4	m	Y_p	6.3 e10	N/m ²

6. Open Loop Modeling Results

To validate the open loop model, analytical results are compared to experimentally obtained frequency response functions. Magnitude plots of the slewing frame are determined by inputting a random signal of bandwidth 20 Hz into the motor and measuring the tachometer output and sensor voltage of active member 2. A Tektronix 2630 Fourier Analyzer performs the data acquisition and frequency analysis.

Results of the open loop tests and the corresponding analytical transfer functions are shown in Figure 7. For the analytical results, the first 20 modes of the FEM model are used and a proportional damping ratio of 0.001 is assumed. In the case of the tachometer output, the model is very accurate over the frequency range considered. The damping exhibited in the mode at approximately 7.1 Hz is due to the dry friction in the motor and bearings. This phenomenon only occurs in the region around the zero position of the frame. During a maneuver, this mode is lightly damped since the motor is free from the dry friction. The model of the transfer function between the motor and active member 2 shows adequate fidelity over approximately the first 10 Hz. Subsequent error is attributed to the sensitivity of the expression for the sensor voltage (equation 30) to the position of the four actuators along the active member. Also, the model for the sensor voltage of the piezoelectrics is only an approximation, since it assumes that the piezoelectrics are in pure

bending and neglects effects such as the bonding layer. In spite of this, the model maintains the correct pole-zero pattern over the 0 to 20 Hz frequency range. Comparing the analytical to the experimental transfer functions illustrates that any control law must account for the uncertainties that exist in the model.

The transfer function between the motor and the tachometer reveals that the first torsional mode at 4 Hz is not very prominent. This has ramifications in the control system design, since this indicates a pole-zero cancellation at that frequency. Pole-zero cancellation does not occur between the motor and the active member, though, leading to a large peak on the magnitude plot at 4 Hz (see Figure 7b). These features can be related to the controllability and observability measures of the motor, tachometer, and active member [Inman and Leo (1992)]. Their effect on the control of the slewing frame is presented in the next section.

7. Control Simulations

The objective of this study is to develop control schemes for the slewing frame. The primary action of the frame is a rotation about its slewing axis, which, due to the flexibility and low inherent damping of the structure, induces vibrations that do not decay for a considerable amount of time. Using the model developed in this paper, control laws are designed that simultaneously slew the frame and suppress the vibrations. The control simulations are divided into two sections. The first simulation involves designing a controller that provides satisfactory step response. Important performance criteria include minimizing the settling time and overshoot of the frame's hub position, as well as the structural vibrations induced during the maneuver. A second section involves control design for a tracking maneuver. Here, it is important to keep the error between the input command and the hub position within a prescribed tolerance while simultaneously suppressing the residual vibrations.

Control Design for a Step Input

First consider the case of designing a controller to obtain satisfactory step response of the frame's hub position. The input command to the motor is constant at 0.742 volts, which corresponds to a 15° slewing maneuver. Three designs are studied. The first is a simple Proportional-Derivative controller using the slewing actuator and angular rate and position feedback. The second control law has a non-colocated control loop using active member 2 in addition to the PD compensator. The final control scheme involves two separate colocated controllers, one loop closed around the motor and the other loop closed around active member 2. All designs are performed using the nominal model shown in the previous section. Robustness is checked by closing the control loops around models that have slightly higher and lower natural frequencies [see Table 2]. While not an exhaustive search, this check is an indicator to how well the controllers can tolerate uncertainty. As pointed out in the previous section, errors in the model do exist and must be accounted for in the control design.

Table 2: First three natural frequencies (in Hz) for the nominal model, the open loop experiment, and the perturbed models used for stability analysis during the simulations.

	Nominal	Exp.	Model 1	Model 2
1st torsional	4.21	3.97	4.33	4.09
1st bending	7.17	7.12	7.33	7.00
2nd torsional	13.90	14.24	14.30	13.53

Proportional-Derivative Control

The procedure for designing this type of controller is rather straightforward, since both angular rate and position measurements are available. The form for the control law is

$$e_s(t) = K_p[\theta_{ref} - \theta(t)] - K_d\dot{\theta}(t) \quad (34)$$

where $\theta(t)$ and $\dot{\theta}(t)$ are the outputs of the potentiometer and tachometer, respectively. The reference voltage, θ_{ref} , is set to 0.742 volts, a command for a 15° slew. After iterating on

the controller gains, values of $K_p = 2.5$ and $K_v = 40$ produce a satisfactory step response without exceeding the voltage limits on the motor (see Figure 8). The overshoot of the hub position is less than 5 % and the settling time is approximately 4 seconds.

The importance of examining this control design lies in its inability to suppress the torsional motion of the frame. This results in substantial residual vibrations after the end of the slewing maneuver, as illustrated by the output of active member 2 in Figure 8. This problem is due to the pole-zero cancellation that occurs in the transfer function between the motor and the tachometer/potentiometer outputs (the potentiometer output is essentially the integral of the transfer function shown in Figure 7). As listed in Table 3, the PD compensator successively adds damping to the first bending mode, but leaves the torsional modes lightly damped. The ability to suppress the bending motion of the frame is due to the large interaction between the motor and the structure, as evidenced in the open loop magnitude plots (Figure 7).

Proportional-Derivative Compensation with Supplementary Non-Colocated Control

A natural extension of simple PD control is to use an active member as a non-colocated sensor for a supplementary feedback loop. The function of the supplementary control is to suppress the torsional motion of the frame while the PD compensator provides a satisfactory step response. Using the active member in this manner leads to the design of a control law for a non-colocated sensor and actuator. Similar actuator/sensor arrangements have been used in the past [Juang, *et al.*, (1986), for example], but with different design strategies and on structures that did not exhibit torsional vibrations.

Control law development is performed using a method called Generalized Structural Filtering (GSF). A detailed treatment of the GSF method is presented in Wie and Byun (1989). In its basic form, Generalized Structural Filtering is a classical control approach to active vibration suppression in that frequency domain and root locus techniques are used to

find a suitable compensator. The design for the slewing frame is accomplished in the following manner. First, the model is used to find the transfer function between the motor input and the output of active member 2, with the PD control loop closed. Closing the first loop is important since it greatly effects the dynamics of the structure. The first stage of the design involves introducing a fourth order Butterworth Lowpass Filter into the forward loop with a corner frequency of 20 Hz. This attenuates the high frequency content of the signal but causes substantial phase lag in the target region, 0 to 20 Hz. Following the procedure outlined in Wie and Byun (1989), a lead filter is then placed in the compensator to recover phase around the frequency of the first torsional mode (4 Hz). Finally, parameters of a non-minimum phase second order filter are chosen to actively damp the first torsional mode. The final form for the control law is

$$e_a(t) = 2.5[\theta_{ref} - \theta(t) - v_{gsf}(t)] - 40\dot{\theta}(t) \quad (35)$$

where $v_{gsf}(t)$ is the output of the GSF compensator. In the Laplace domain, it takes the form

$$V_{gsf}(s) = \frac{0.025 \left(\frac{s}{15.8 \pm j42.1} + 1 \right) \left(\frac{s}{20} + 1 \right)}{\left(\frac{s}{48.1 \pm j116} + 1 \right) \left(\frac{s}{116 \pm j48.1} + 1 \right) \left(\frac{s}{14 \pm j37.5} + 1 \right) \left(\frac{s}{40} + 1 \right)} V_{m2}(s) \quad (36)$$

A root locus plot for the GSF design is shown in Figure 9a. From the roots locus, a gain of 0.025 is chosen since it increases the damping in the first torsional mode. An important feature of the root locus is that the damping in the first bending mode is being decreased as a result of the supplementary control loop. This is an unattractive feature of this method. The time responses of the slewing frame with supplementary control are shown in Figure 8. The rigid body response has slightly greater overshoot due to the added control effort in the motor. The motor voltages with and without supplementary control are similar, although a higher frequency component is added to the input due to the GSF compensator

(Figure 8b). The marked difference with this control scheme is the suppression of the residual vibrations in the frame. With the supplementary control, the structural vibrations are negligible at the end of the slewing maneuver, which contrasts sharply with the case when there is only PD compensation (Figure 8c). The addition of the non-colocated GSF controller enables the suppression of the first torsional mode of the frame.

The robustness of this control strategy is checked by closing the loop around the perturbed models shown in Table 2. For both cases, an instability in the first torsional mode results. This is illustrated in Figure 8d, where it shows that the frame is still vibrating almost forty seconds after the slewing maneuver is over. This vibration is due to the mode at 4 Hz being marginally stable. Checking the robustness in this manner indicates that the non-colocated control design is sensitive to the uncertainties that are bound to exist in the model. Attempts at redesigning the control law in light of these results could be made, but a more practical approach to achieving performance and robustness specifications is detailed in the next section.

Proportional-Derivative Compensation with Supplementary Colocated Control

The final design for satisfactory step response uses active member 2 as both a sensor and an actuator to provide vibration suppression. As in the previous case, a PD compensator is used to slew the frame, with the colocated control loop acting as supplementary feedback. The control law chosen for the active member is Positive Position Feedback. Much like the GSF method, Positive Position Feedback (PPF) consists of second order filters tuned to suppress specific structural modes. For a detailed treatment of the design procedure, the reader is referred to Fanson and Caughey (1987). PPF control is chosen since it is easy to design and is robust with respect to unmodeled dynamics [Goh and Caughey (1985)]. It has also been experimentally implemented in

previous work [Fanson and Caughey (1987), Dosch, *et al.*, (1992)]. In the Laplace domain, the form of the PPF controller is

$$V_e(s) = \left\{ \sum_{i=1}^{N_f} \frac{\omega_{\beta i}^2}{s^2 + 2\zeta_{\beta i} \omega_{\beta i} s + \omega_{\beta i}^2} \right\} V_{m2}(s) \quad (37)$$

The parameters for the filter design are found using root locus techniques (see Figure 9b). The design procedure for PPF control is more straightforward than for the GSF method and requires much less iteration. In this case, the first torsional mode is targeted for suppression. An important feature of the control law is that the spillover into the high frequency modes of the system is almost negligible due to the controller roll-off. This contrasts with the GSF design, which decreases the damping in the first bending mode. After performing the analysis, the following control law is obtained

$$e_a(t) = 2.5[\theta_{ref} - \theta(t)] - 40\dot{\theta}(t)$$

$$V_{e2}(s) = \frac{65(29)^2}{s^2 + 2(0.08)(29)s + (29)^2} V_{m2}(s) \quad (38)$$

The first part of equation (38) is simply the PD compensator designed in the previous section, the second part is the PPF controller using active member 2 as a colocated sensor/actuator. A simulated slewing maneuver is shown in Figure 10. The hub position response and motor voltage are essentially the same with and without PPF control. This is to be expected since the feedback loop is independent of the motor. With the supplementary control loop, the structural vibrations in the frame are suppressed by the time the slewing maneuver is over (Figure 10c). The damping out of the torsion is not as fast as with the GSF controller, but this is due to the fact that the motor is a much more powerful actuator. During the design, the achievable damping was limited by the peak value of the active member control effort, which is approximately 100 volts (Figure 10d).

Two robustness tests are performed on this control scheme. The first check is to close the feedback loops around the perturbed models listed in Table 2. For both cases, the system remains stable. This represents a major advantage over the non-colocated control, which results in an unstable system in the presence of model error. A second robustness check is performed by intentionally 'mistuning' the self-sensing actuator capacitor values by $\pm 5\%$, $\pm 10\%$, and $\pm 20\%$. Again the system maintains stability, but performance is adversely affected. The damping achieved by the PPF design is sensitive to the mistuning of the self-sensing actuator circuit. The settling time of the structural vibrations is increased from 4 seconds to slightly over 10 seconds if the capacitor values are off by $\pm 10\%$ (Figure 10c). This mistuning also increases the control effort of the active member (Figure 10d). Sensitivity to capacitor mismatch could represent an obstacle to implementation of the circuit in future experiments.

Table 3: Comparison of the results for the three separate simulations.

<i>Control Law</i>	<i>PD</i>	<i>PD + GSF</i>	<i>PD + PPF</i>
<i>Damping (%)</i>			
1st torsional	0.2	8.2	4.8
1st bending	6.1	4.8	6.1
2nd torsional	0.4	0.5	0.4
<i>Rigid Body Response</i>			
settling time (seconds)	4 seconds	4 seconds	4 seconds
overshoot (degrees)	0.7	1.1	0.4
<i>Stability Robustness¹</i>	Yes	No	Yes ²

¹ Defined as being stable with the perturbed models listed in Table 2.

² Capacitor mismatch causes loss of damping in torsional mode, but not instability.

Discussion of the Simulation Results

These simulations indicate the inability of a motor control law to suppress the torsional motion of the slewing frame. This is a result of a pole-zero cancellation that occurs between the motor input and the angular rate and position sensors. Physically, this means that the interaction between the input torque and the torsional modes is small. These modes can be suppressed, though, by integrating actuators and sensors into the structure.

In one control law, the active member is used solely as a sensor in a non-colocated feedback loop. This achieves the desired vibration suppression, but is difficult to design and does not maintain stability in the presence of model error. Another approach is to use the active member in a colocated feedback loop, taking advantage of the piezoelectrics ability to actuate. This leads to a rather simple design that has negligible spillover into the higher modes. It is also more robust with respect to model uncertainty. Its only drawback is a sensitivity to capacitor mismatch in the self-sensing circuit. This 'mistuning' does not lead to instability, but only a decrease in damping of the torsional mode. The results of these simulations are consistent with initial experiments on the slewing frame [Leo and Inman (1992)].

Control Design for a Tracking Maneuver

The concept of using two independent control laws to achieve performance is now extended to a more complicated slewing maneuver. Instead of a simple step input, the command into the slewing actuator now consists of a series of three 5° ramp maneuvers followed by a smooth return to the zero position (Figure 11). It is assumed that the hub position is at an initial angle of -5° . It is desired to keep the error between the hub position and the command as small as possible throughout the maneuver, and always less than 0.5° after the first ramp input.

The control law is a combination of PID compensation using the dc motor as the actuator and a PPF filter using active member 2 as a colocated sensor/ actuator. For convenience and to show the flexibility of the control law design, the parameters for the PPF filter are chosen to be the same as found in the previous section. Integral compensation is added to the motor controller to limit the tracking error. After iterating on the gain values, the following control is used in the simulation:

$$e_a(t) = 20[\theta_{ref} - \theta(t)] - 75\dot{\theta}(t) - 10\int \theta(t)$$

$$V_{c2}(s) = \frac{65(29)^2}{s^2 + 2(0.08)(29)s + (29)^2} V_{m2}(s) \quad (39)$$

The position gain is higher than for the step input case to speed up the system response. Adding the integral control action improves the tracking ability of the system, and the derivative component reduces overshoot. Increasing K , too much, though, can slow the system down and degrade performance. The PPF filter parameters have not been changed from the step input design. The ability of the hub position to track the reference input is shown in Figure 11. Except for the initial slew, the hub error is kept to less than 0.5° throughout the maneuver (Figure 12a). Because of the initial condition on the hub position, the structure is excited at the outset of the slew. Without the colocated control loop, structural vibrations occur and do not decay until after 50 seconds. As expected, the torsional vibrations are suppressed by the PPF control loop and the active member output is much smoother (Figure 12c). Combining the PID compensator with a colocated control law has produces satisfactory tracking and reduces the structural vibrations considerably.

8. Conclusions and Future Work

Integrating active members into complicated slewing structures is an effective means of suppressing vibrations during and after maneuvers. This is the result of a modeling and simulation study of a slewing frame. The distinctive feature of the slewing frame is that there exists torsional modes that cannot be controlled using feedback loops consisting of the slewing actuator and angular rate and position sensors. Vibration suppression can be achieved by using active members as sensors in non-colocated feedback loops, but this yields a difficult design that is sensitive to model error. A superior approach is to use the active members in colocated feedback loops with robust control laws such as Positive Position Feedback. When used in conjunction with a simple Proportional-Derivative

compensator, this design produces satisfactory slewing maneuvers and simultaneously suppresses the structural vibrations.

Future work on this topic includes experimentally implementing active control schemes and studying the effects of actuator and sensor dynamics. The problem of controlling the slewing frame is well suited to the study of MIMO control systems. How the closed loop performance is affected by the dynamics of the motor and self-sensing actuators is currently being investigated.

Appendix

The equations of motion for the slewing element shown in Figure 1 are given by equation (2). They are expressed in element coordinates and form the basis for the model assembly described in Section 2. The element mass and stiffness matrices are

$$\hat{M} = \frac{\rho A_e L_e}{420} \begin{bmatrix} 140 & 0 & 0 & 0 & 0 & 0 & 70 & 0 & 0 & 0 & 0 & 0 \\ & 156 & 0 & 0 & 0 & 22L_e & 0 & 54 & 0 & 0 & 0 & -13L_e \\ & & 156 & 0 & -22L_e & 0 & 0 & 0 & 54 & 0 & 13L_e & 0 \\ & & & \frac{140I_p}{A_e} & 0 & 0 & 0 & 0 & 0 & \frac{70I_p}{A_e} & 0 & 0 \\ & & & & 4L_e^2 & 0 & 0 & 0 & -13L_e & 0 & -3L_e^2 & 0 \\ & & & & & 4L_e^2 & 0 & 13L_e & 0 & 0 & 0 & -3L_e^2 \\ & & & & & & 140 & 0 & 0 & 0 & 0 & 0 \\ & & & & & & & 156 & 0 & 0 & 0 & -22L_e \\ & & & & & & & & 156 & 0 & 22L_e & 0 \\ & & & & & & & & & \frac{140I_p}{A_e} & 0 & 0 \\ & & & & & & & & & & 4L_e^2 & 0 \\ & & & & & & & & & & & 4L_e^2 \end{bmatrix}$$

sym

$$\begin{matrix} \hat{x}_1 & \hat{y}_1 & \hat{z}_1 & \hat{\phi}_1 & \hat{\theta}_{y1} & \hat{\theta}_{z1} & \hat{x}_2 & \hat{y}_2 & \hat{z}_2 & \hat{\phi}_2 & \hat{\theta}_{y2} & \hat{\theta}_{z2} \end{matrix}$$

The last line of the above matrix indicates the element coordinate the node refers to. Any lumped masses at the nodes are added to the diagonal elements of the mass matrix. A mass at *node i* is added to the (1,1), (2,2), and (3,3) elements, a mass at *node j* is added to the (7,7), (8,8) and (9,9) elements.

$$\hat{K} = \begin{bmatrix} \hat{K}_{11} & \hat{K}_{12} \\ \hat{K}_{12}^T & \hat{K}_{22} \end{bmatrix}$$

where

$$\hat{K}_{11} = \begin{bmatrix} \frac{EA}{L_s} & 0 & 0 & 0 & 0 & 0 \\ & \frac{12EI_s}{L_s^3} & 0 & 0 & 0 & \frac{6EI_s}{L_s^2} \\ & & \frac{12EI_s}{L_s^3} & 0 & -\frac{6EI_s}{L_s^2} & 0 \\ & & & \frac{GJ}{L_s} & 0 & 0 \\ & sym & & & \frac{4EI_s}{L_s} & 0 \\ & & & & & \frac{4EI_s}{L_s} \end{bmatrix}$$

$$\hat{K}_{12} = \begin{bmatrix} -\frac{EA}{L_s} & 0 & 0 & 0 & 0 & 0 \\ 0 & -\frac{12EI_s}{L_s^3} & 0 & 0 & 0 & \frac{6EI_s}{L_s^2} \\ 0 & 0 & -\frac{12EI_s}{L_s^3} & 0 & -\frac{6EI_s}{L_s^2} & 0 \\ 0 & 0 & 0 & -\frac{GJ}{L_s} & 0 & 0 \\ 0 & 0 & \frac{6EI_s}{L_s^2} & 0 & \frac{2EI_s}{L_s} & 0 \\ 0 & -\frac{6EI_s}{L_s^2} & 0 & 0 & 0 & \frac{2EI_s}{L_s} \end{bmatrix}$$

$$\hat{K}_{22} = \begin{bmatrix} \frac{EA}{L_s} & 0 & 0 & 0 & 0 & 0 \\ & \frac{12EI_s}{L_s^3} & 0 & 0 & 0 & -\frac{6EI_s}{L_s^2} \\ & & \frac{12EI_s}{L_s^3} & 0 & \frac{6EI_s}{L_s^2} & 0 \\ & & & \frac{GJ}{L_s} & 0 & 0 \\ & sym & & & \frac{4EI_s}{L_s} & 0 \\ & & & & & \frac{4EI_s}{L_s} \end{bmatrix}$$

The rigid body inertia about the slewing axis is:

$$\hat{I}_s = \rho A L_s [r_s^2 + r_s \cos \gamma L_s + \frac{1}{3} L_s^2 \cos^2 \gamma] + m_s r_s^2 + m_j (r_s + L_s \cos \gamma)^2$$

The interaction vector for the slewing element is:

$$\hat{i}_s = \left(\frac{\rho A_s L_s}{60} \right) \begin{bmatrix} 0 \\ 3(3L_s \cos \gamma + 10r_s) \\ 0 \\ 0 \\ 0 \\ L(2L_s \cos \gamma + 5r_s) \\ 0 \\ 3(7L_s \cos \gamma + 10r_s) \\ 0 \\ 0 \\ 0 \\ 0 \\ -L(3L_s \cos \gamma + 5r_s) \end{bmatrix}$$

The following notation is used for the appendix:

- ρ density of the element
- A_s cross-sectional area of the element
- L_s element length
- I_p polar moment of inertia of the cross-section
- I_x, I_y moments of inertia
- GJ torsional stiffness of the cross-section
- m_i, m_j lumped masses at nodes i and j , respectively
- r_z distance from z axis to node i
- γ angle between x and \hat{x} axes.

References

- Anderson, E., Hagood, N., Goodcliffe, J., 1992, "Self-Sensing Piezoelectric Actuation: Analysis and Application to Controlled Structures," *Proc. of the 33rd Structures, Structural Dynamics and Materials Conference*, pp. 2141-2155.
- Cook, R.D., Malkus, D.S., Plesha, M.E., 1989, *Concepts and Applications of Finite Element Analysis*, 3rd ed., New York, NY, Wiley and Sons.
- Dosch, J., Inman, D.J., and Garcia, E., 1992, "A Self-Sensing Piezoelectric Actuator for Colocated Control," *J. of Intelligent Material Systems and Structures*, v3 n1, pp. 166-185.
- Fanson, J.L., and Caughey, T.K., 1987, "Positive Position Feedback Control for Large Space Structures," *Proc. of the 28th Structural, Dynamics, and Materials Conference*, pp. 588-98.
- Fujii, H., Ohtsuka, T., Udou, S., 1991, "Mission Function Control for a Slew Maneuver Experiment," *AIAA J. of Guidance, Control, and Dynamics*, v.14, n5, pp. 986-1000.
- Garcia, E., 1989, "On the Modeling and Control of Slewing Flexible Structures," PhD Dissertation, Dept. of Mechanical and Aerospace Engineering, State University of New York at Buffalo.
- Garcia, E., and Inman, D.J., 1990, "Advantages of Slewing an Active Structure," *J. of Intelligent Material Systems and Structures*, v1, n3, pp. 261-272.
- Garcia, E., and Inman, D.J., 1991, "Modeling of the Slewing Control of a Flexible Structure," *AIAA J. of Guidance, Control, and Dynamics*, v14, n4, pp. 736-742.

- Goh, C.J., and Caughey, T.K., 1985, "On the Stability Problem Caused by Finite Actuator Dynamics in the Colocated Control of Large Space Structures," *Int. J. of Control*, v 41 n3, pp. 787-802.
- Inman, D.J., 1989, *Vibration, with Control, Measurement, and Stability*, Englewood Cliffs, NJ, Prentice Hall.
- Inman, D.J., and Leo, D.J., 1992, "Controllability Issues in Smart Structural Control Systems," presented at the *Society of Engineering Science 29th Annual Technical Meeting*.
- Juang, J.N., and Horta, L.G., Robertshaw H.H., 1986, "A Slewing Control Experiment for Flexible Structures," *AIAA J. of Guidance, Control, and Dynamics*, v9, n5, pp. 599-607.
- Junkins, J.L., Rahman, Z., and Bang, H., 1990, "Near-Minimum-Time Maneuvers of Flexible Vehicles: A Lyapunov Control Law Design Method," *Mechanics and Control of Large Flexible Structures* (ed. Junkins, J.L.), AIAA Press, pp. 565-593.
- Kuo, B.C., 1987, *Automatic Control Systems*, 5th ed., Englewood Cliffs, NJ, Prentice Hall.
- Leo, D.J., 1992, "Active Control of a Slewing Frame," M.S. Thesis, Dept. of Mechanical and Aerospace Engineering, State University of New York at Buffalo.
- Leo, D.J., and Inman, D.J., 1992, "Control of a Flexible Frame in Slewing," *Proc. of the American Control Conference*.
- Wie, B., and Byun, K.W., 1989, "New Generalized Structural Filtering Concept for Active Vibration Control Synthesis," *J. of Guidance, Control, and Dynamics*, v12, n2, pp. 147-155.

Figure Captions

Figure 1: (a) A flexible element slewing about an axis. The dotted line represents the rigid body and the solid line is the elastic deformation. (b) A single element slewing about an axis. The total rotation at the root is a combination of rigid body and elastic motion.

Figure 2: Model of a dc motor connected through gears to a slewing structure.

Figure 3: (a) Piezoceramic pair bonded to a flat beam. (b) Piezoceramic active member.

Figure 4: Self-sensing actuator as presented by Dosch, Inman, and Garcia (1992).

Figure 5: Block diagram of the self-sensing actuator with the inclusion of the circuit dynamics.

Figure 6: Slewing frame testbed showing the location of the active members, angular rate and position sensors, and the dc motor.

Figure 7: Open loop magnitude plots of the slewing frame from 0 to 20 Hz. The experimental response (dotted) exhibits damping in the 7.1 Hz mode due to dry friction in the motor. (a) Tachometer/ Motor input. (b) Sensor output of active member 2/ Motor input.

Figure 8: Simulated step responses for the slewing frame with PD control (dotted) and PD with supplementary GSF feedback (solid). (a) Hub position. (b) Motor control voltage. (c) Output of active member 1. (d) Output of member 2 showing instability due to model error.

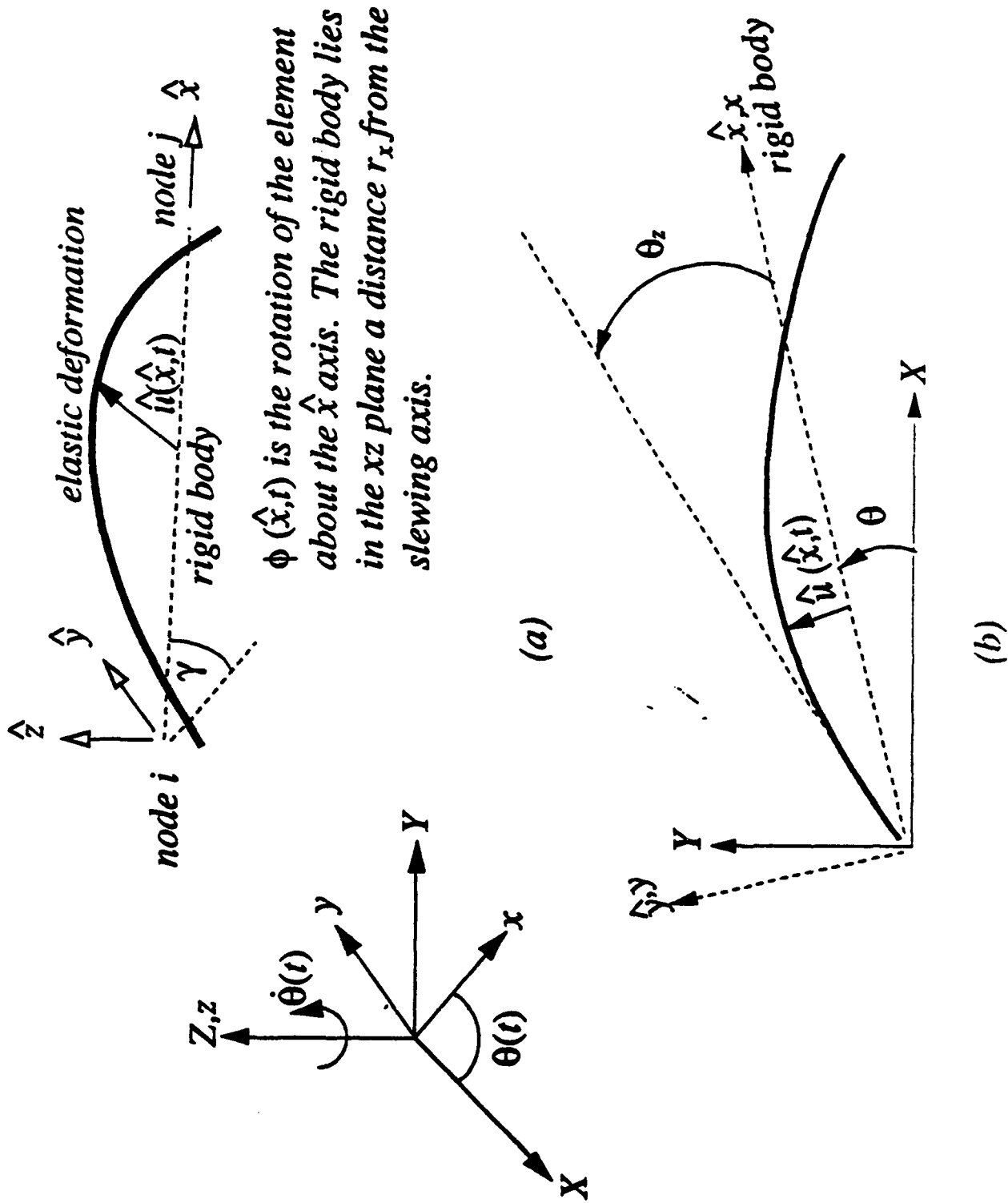
Figure 9: Root locus plots for the GSF design (a) and the PPF design (b). The PPF controller does not exhibit the spillover into the higher modes that occurs in the GSF compensation.

Figure 10: Simulated time responses for PD control with supplementary PPF feedback. (a) Hub position. (b) Motor control voltage. (c) Sensor output of active member 1. (d) Active member 2 control voltage. The capacitor mismatch in the self-sensing circuit causes a loss of damping in the torsional mode (dotted line in (c) and (d)).

Figure 11: Input command (dotted) and hub position (solid) for the tracking maneuver.

Figure 12: Simulated time responses for a tracking maneuver without supplementary feedback (solid) and with supplementary feedback (dotted). (a) Hub position error. (b) Motor control voltage. (c) Sensor output of active member 1. (d) Active member 2 control effort.

Fig 1



$\phi(\hat{x}, t)$ is the rotation of the element about the \hat{x} axis. The rigid body lies in the xz plane a distance r_x from the slewing axis.

(a)

(b)

Fig 2.

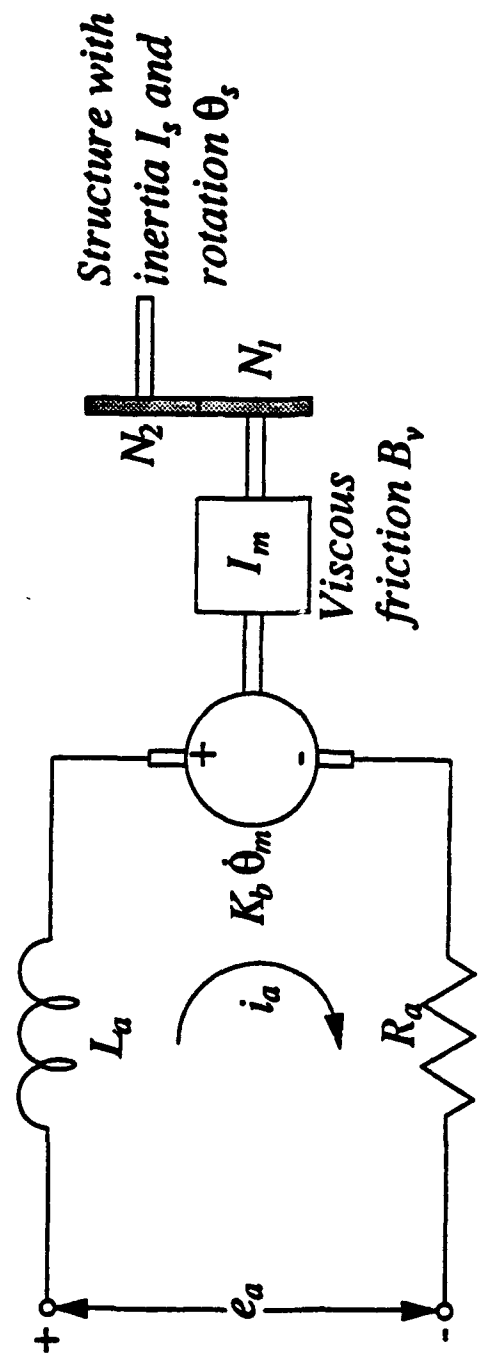
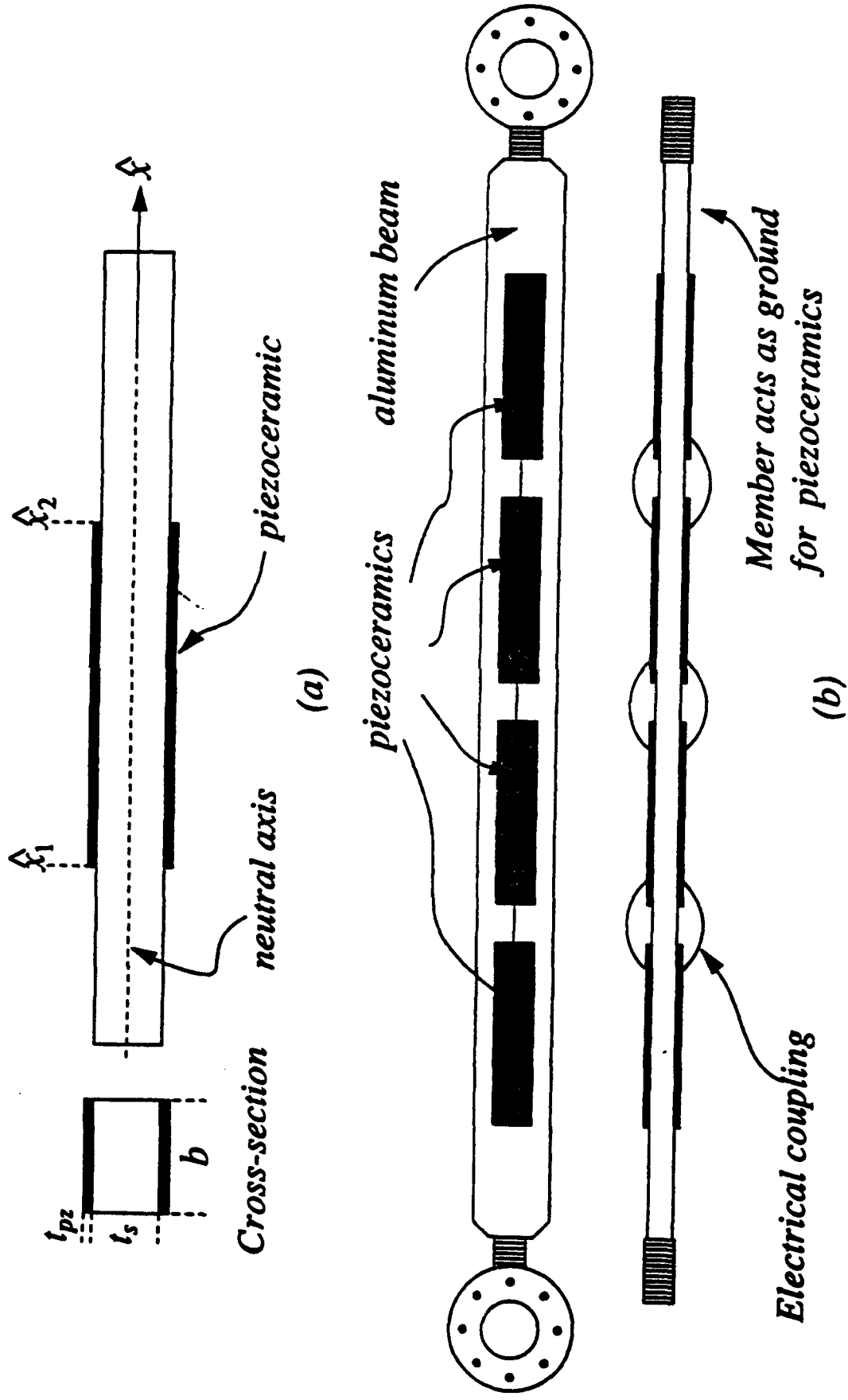


Fig 5



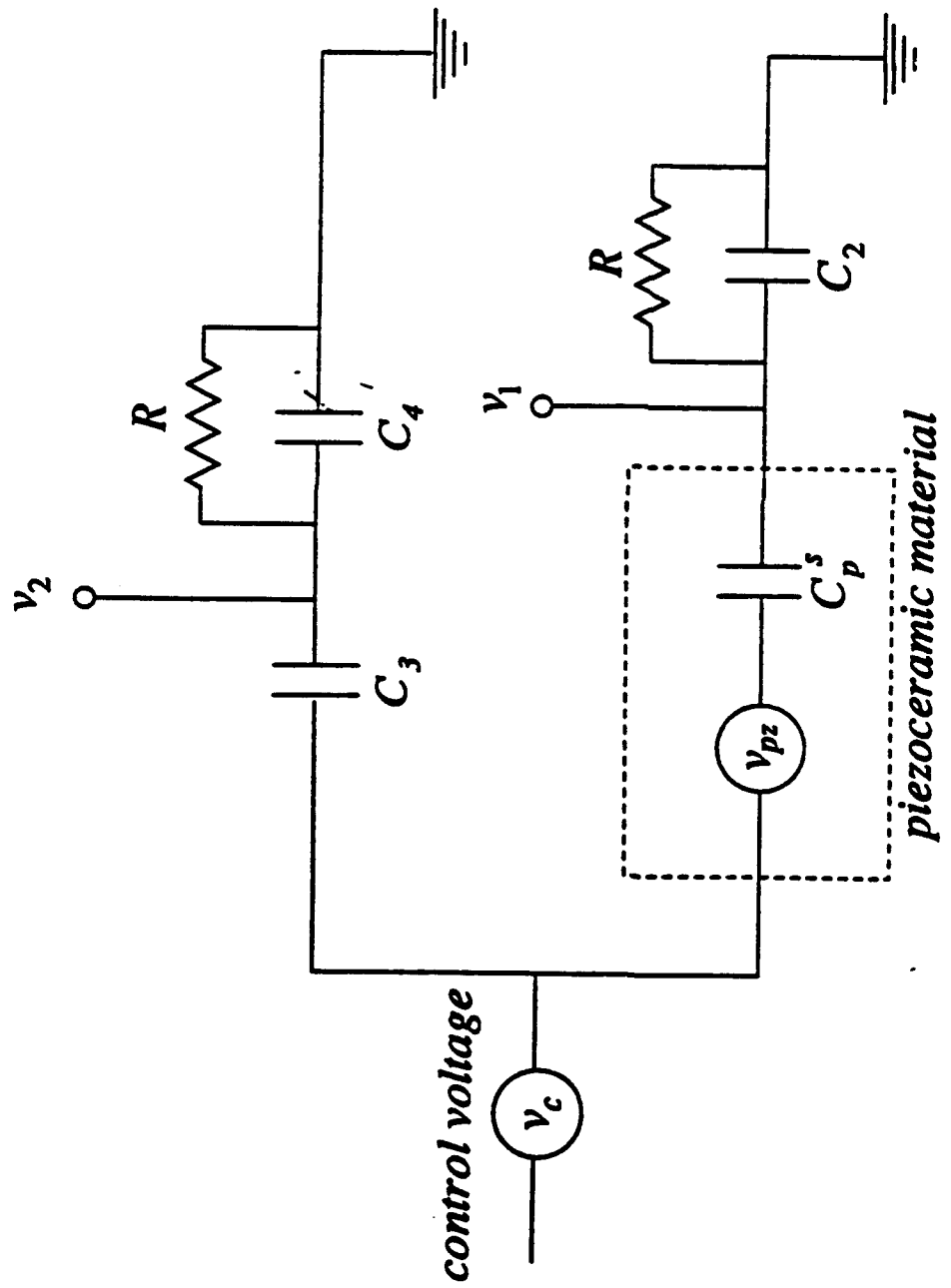


Fig 5

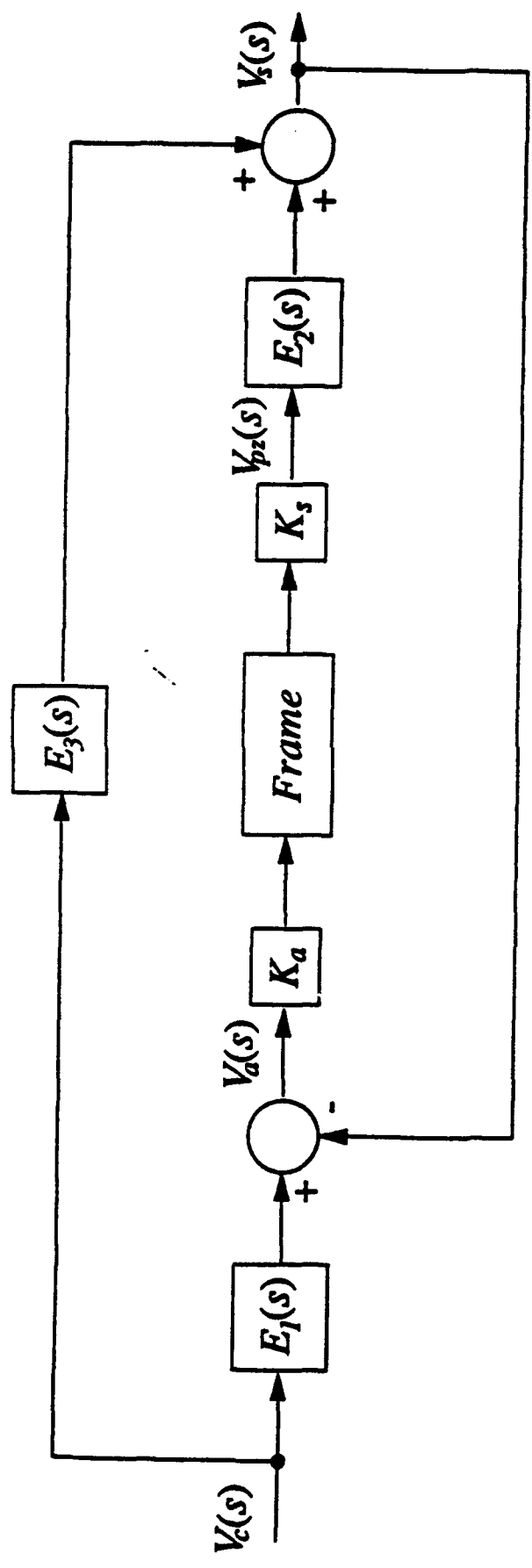


Fig 6.

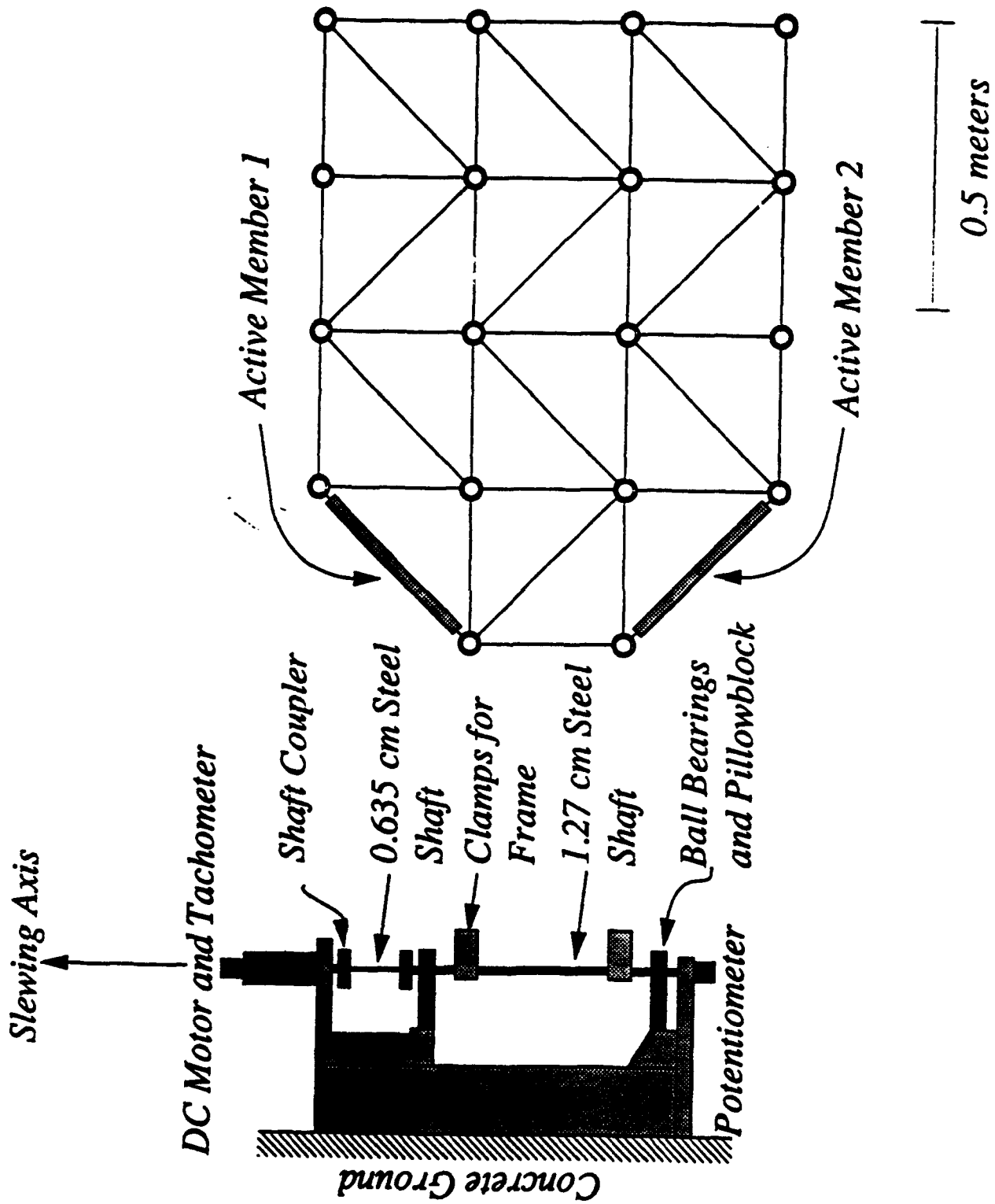
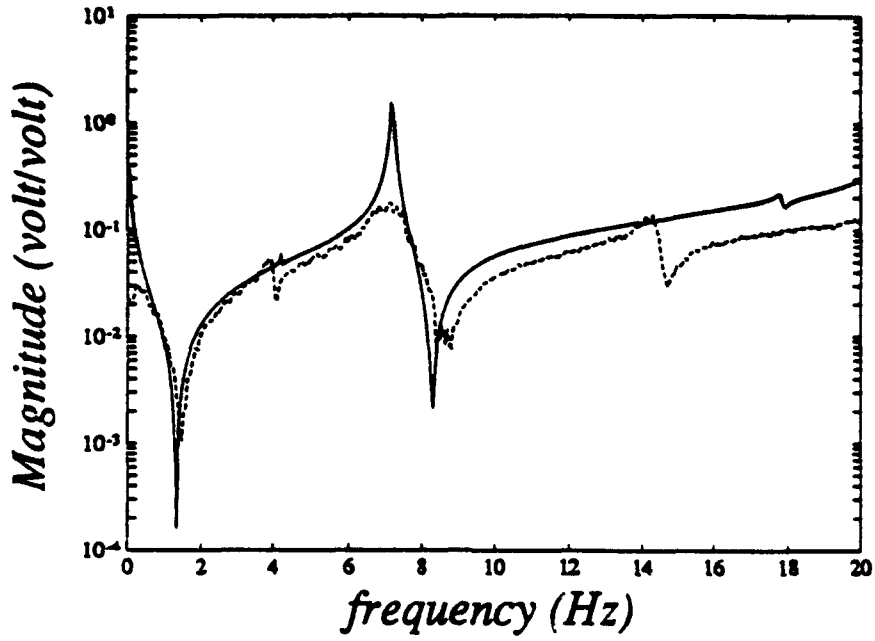
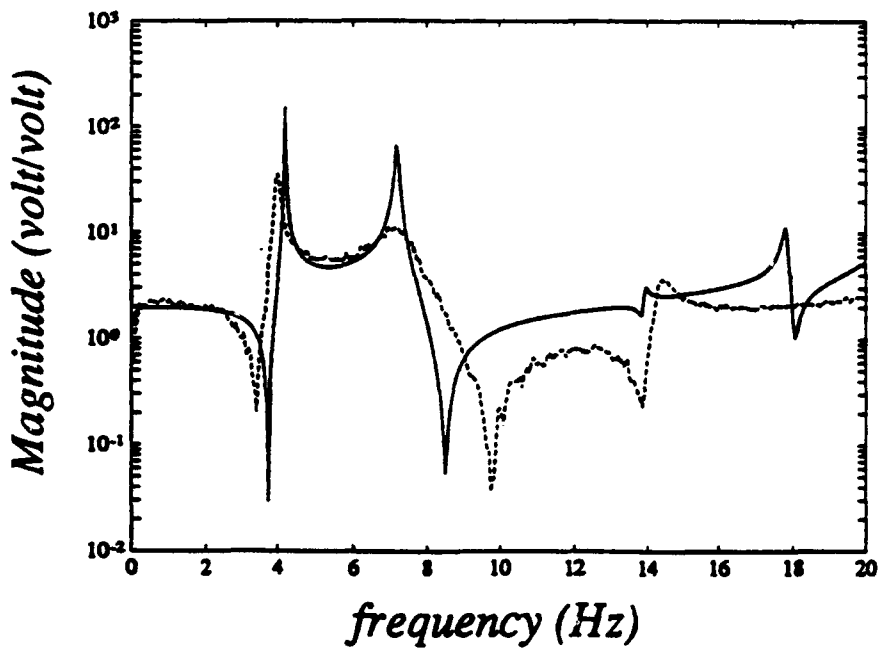


Fig 7

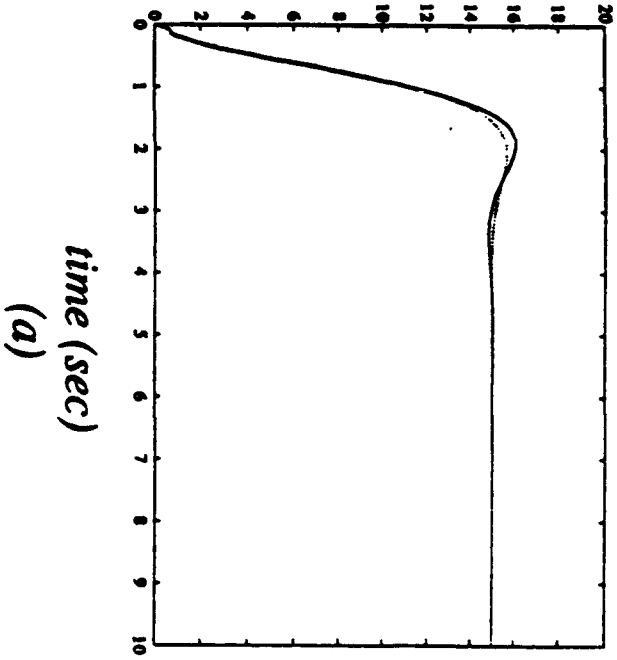


(a)



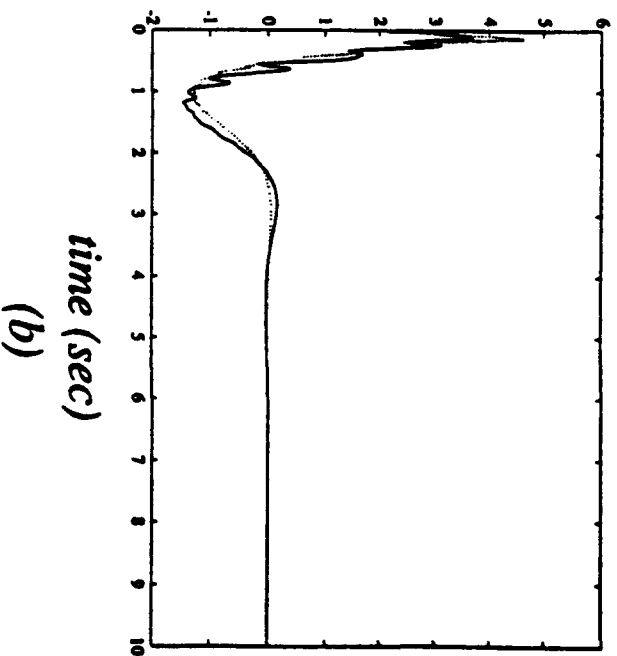
(b)

Hub Position (degrees)



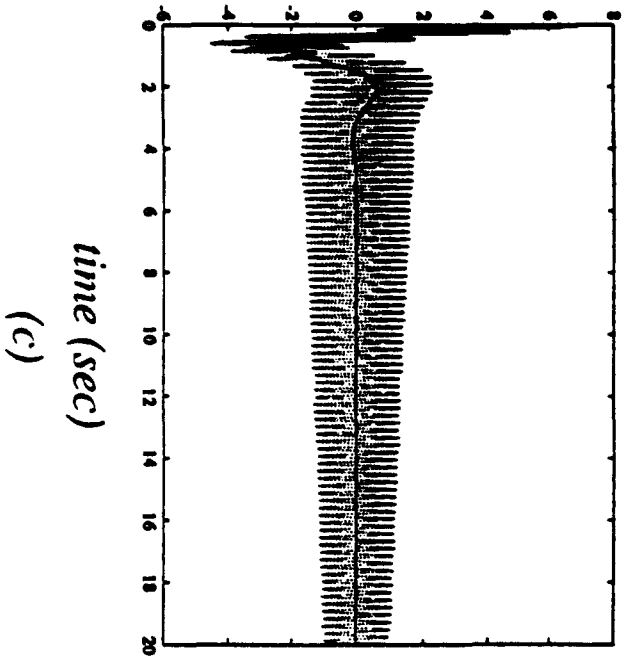
time (sec)
(a)

Motor Effort (volts)



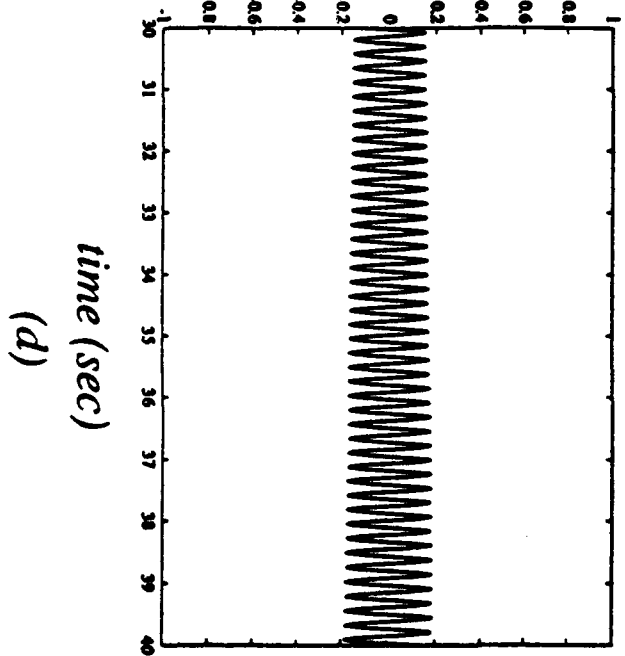
time (sec)
(b)

Sensor Output (volts)



time (sec)
(c)

Sensor Output (volts)



time (sec)
(d)

Fig 9

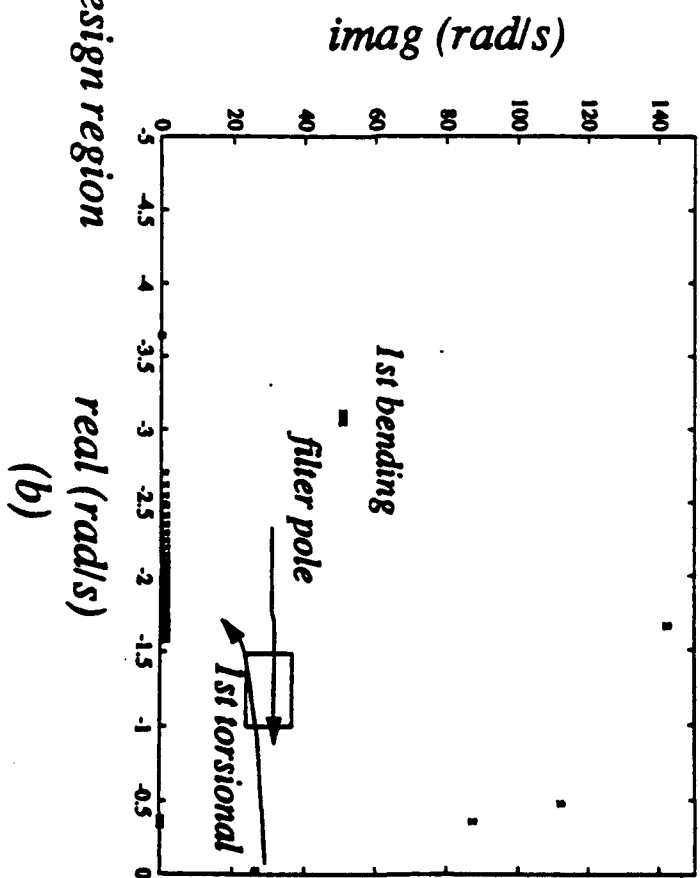
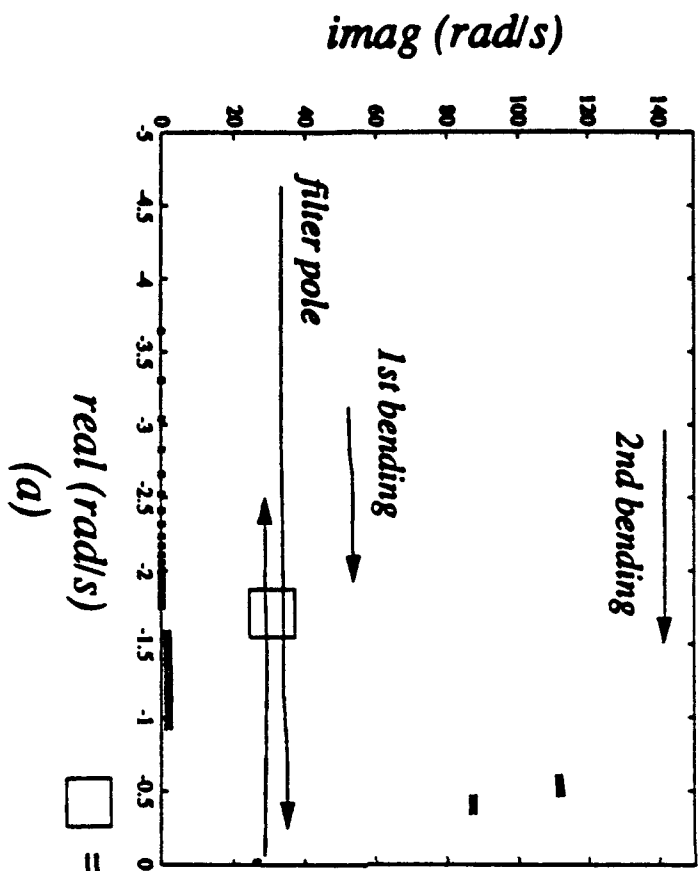
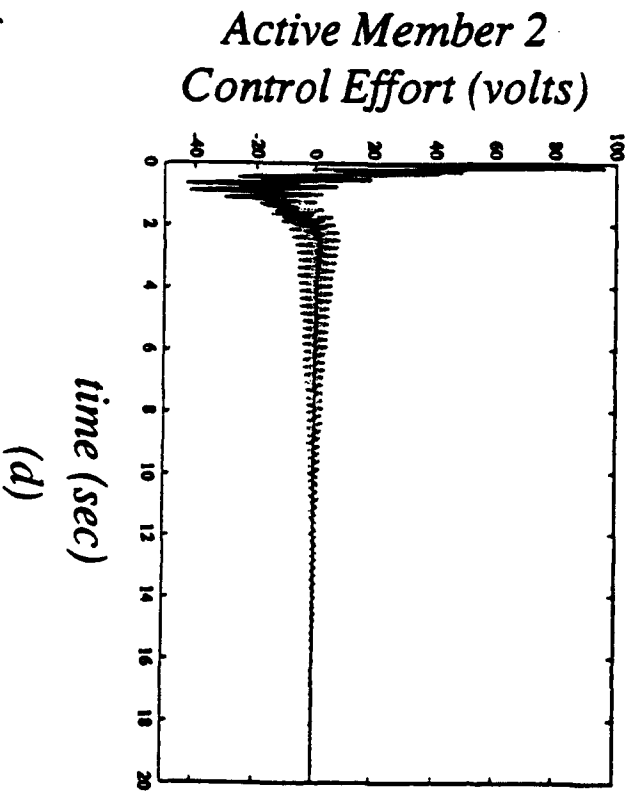
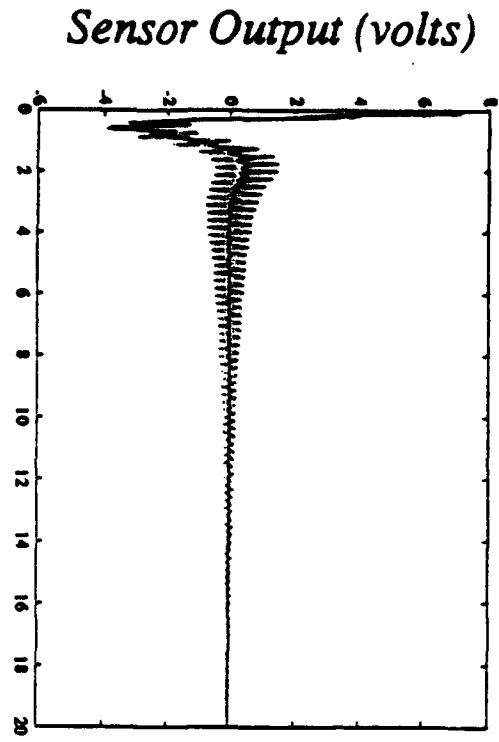
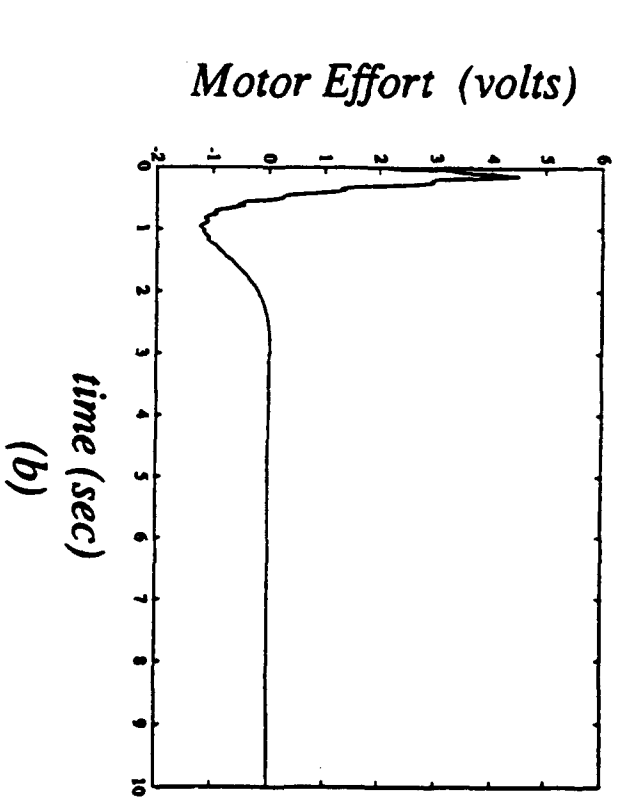
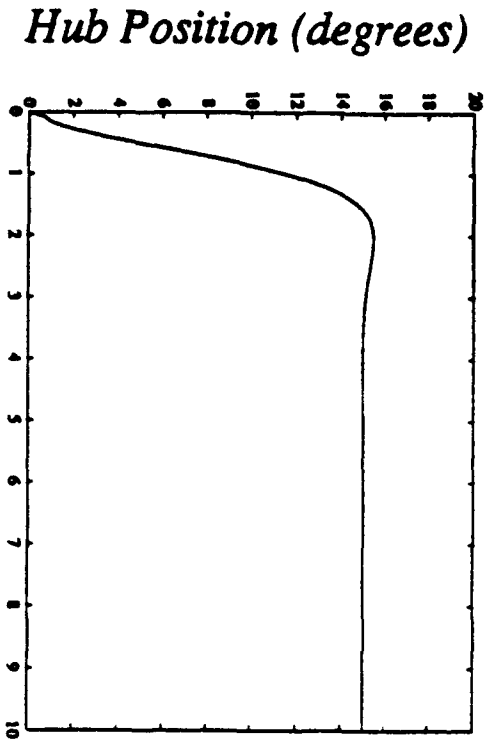
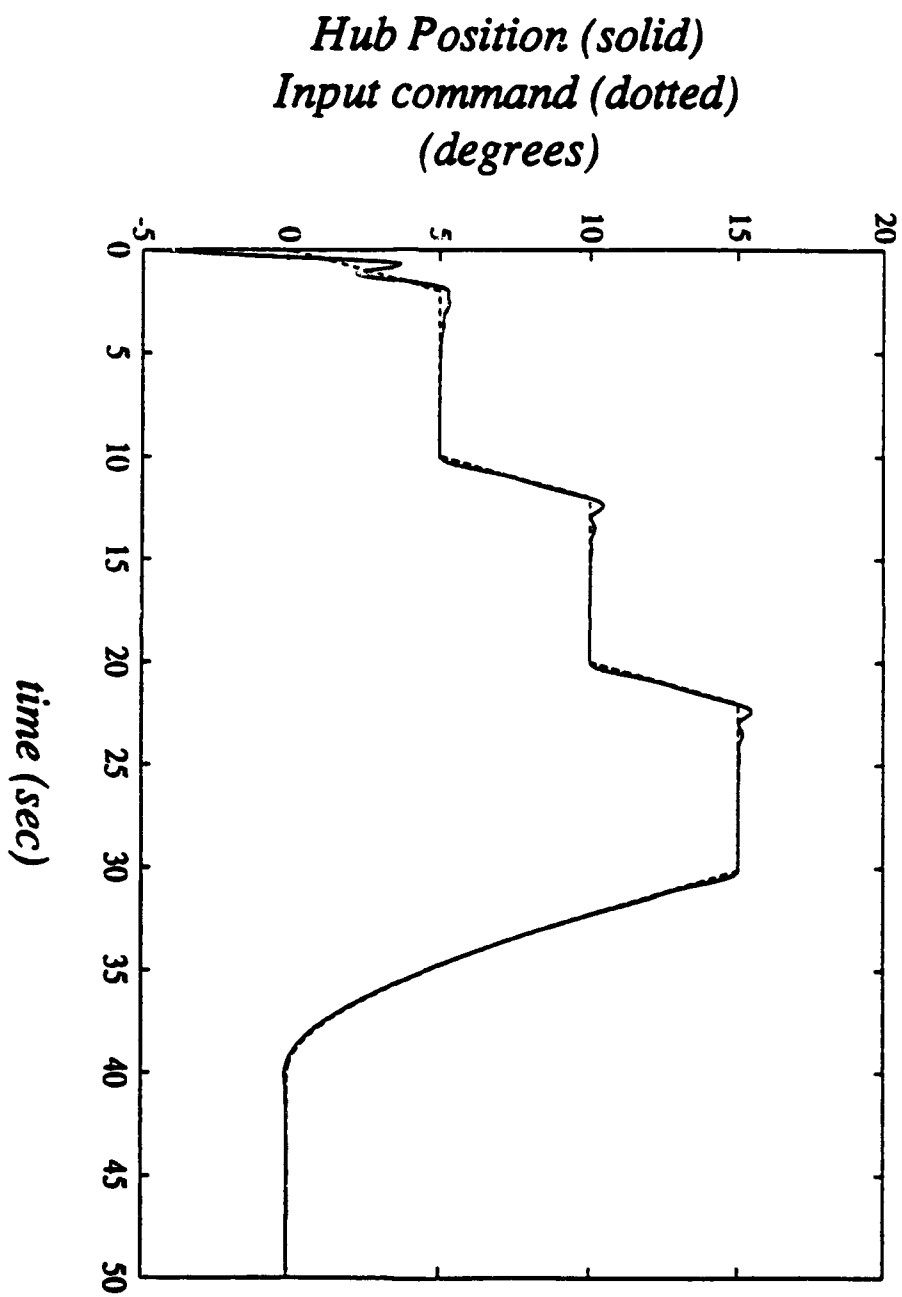
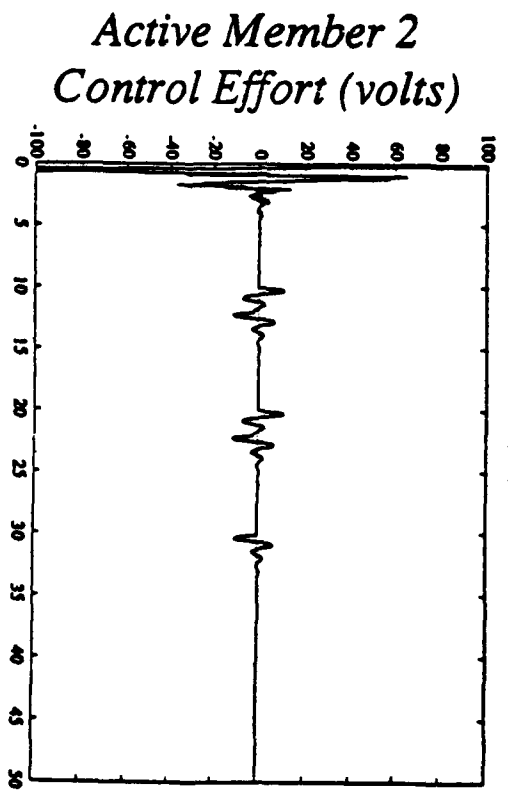
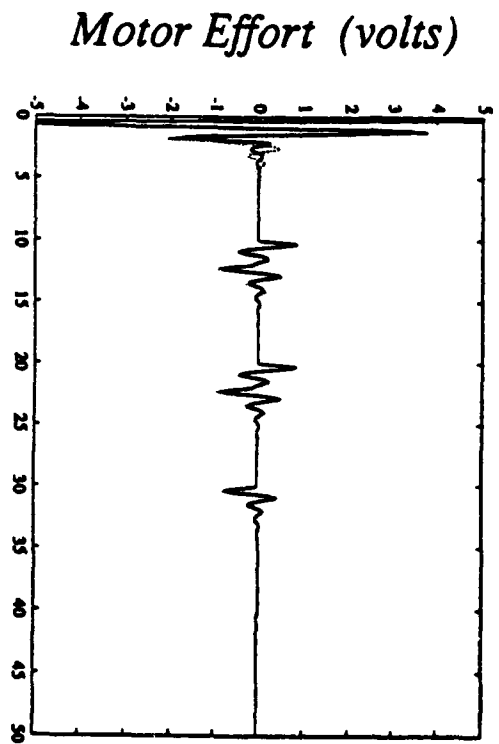
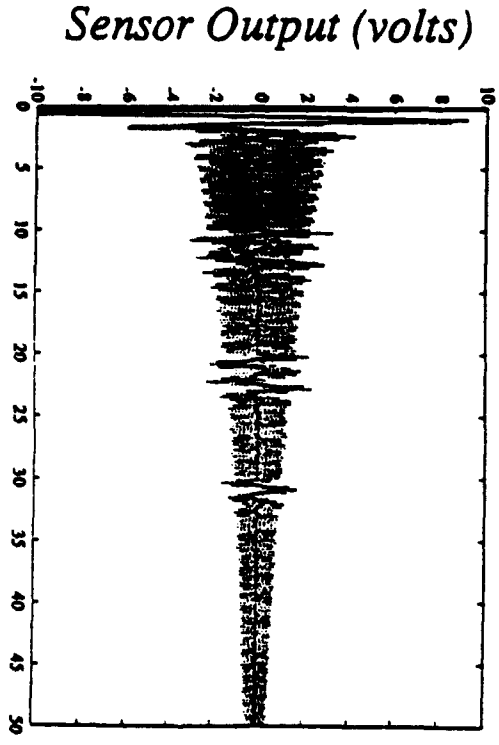
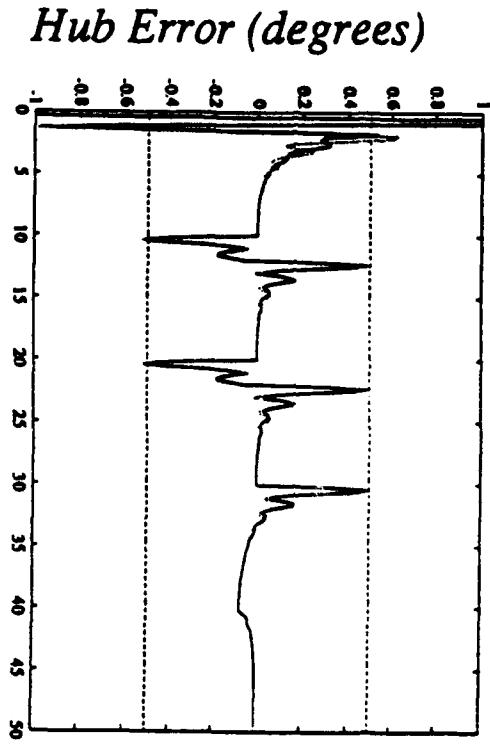


Fig 10







MODELING OF A SMART ANTENNA FOR ACTIVE VIBRATION SUPPRESSION

Jeffrey Dosch*

Donald Leo*

Daniel Inman†

* Research Assistant
Department Of Mechanical & Aerospace Engineering
State University of New York at Buffalo
Buffalo, NY 14260

† Samuel Herrick Professor
Department of Engineering Science and Mechanics
Virginia Polytechnic Institute and University
Blacksburg, VA 24061

Abstract

This paper discusses modal analysis of structures with repeated eigenvalues and eigenvectors. Equations are derived for systems with and without driving point information. In the case where driving point residues are available, an eigenvalue of multiplicity q can only be identified using q inputs. The derivation is verified on a simple model of a smart antenna. An identification of the model is also performed using the Eigensystem Realization Algorithm (ERA). Modal parameters are identified accurately using ERA but the resulting model contains errors in the phase of the input/output transfer functions. Modal tests and the Modal Assurance Criteria are used to distinguish between repeated and distinct modes of a smart antenna. The need for an accurate model is discussed in relation to the problem of active vibration suppression.

Nomenclature

M	mass matrix
C	viscous damping matrix
K	stiffness matrix
u	input vector
y	displacement vector
\dot{y}, \ddot{y}	derivative of y with respect to time
G, H	symmetric state space matrices, in eq (3)
f	input vector, in eq.(3)
Ψ	transformation matrix in eq. (4)
Λ	diagonal matrix of eigenvalues
λ_r	r^{th} eigenvector
Φ	matrix of mode shapes (columns)
ϕ_r	r^{th} mode shape
ϕ_{ir}	r^{th} mode shape's i^{th} modal participation factor
r_{ij}	experimental residue, i^{th} output, j^{th} input, r^{th} mode
A	modal state space state matrix
B	modal state space input matrix
C_o	modal state space observation matrix
D	modal state space direct transmission matrix
s	Laplace variable = $j\omega$
T	transformation matrix
0	zero matrix
$()^T$	transpose
$()^*$	complex conjugate

1. INTRODUCTION

An accurate model of an active structure is fundamental to the understanding of the problem of control structure interaction. An active, or smart structure, contains a number of integrated sensors and actuators that allow the structure to perform precision pointing, sighting, placement, or vibration

suppression to a degree of accuracy or performance which is not easily achieved with a passive structure. In the initial stages of design a Finite Element Model (FEM) is adequate. The FEM allows the engineer to address such issues as optimal actuator and sensor placement, size and power requirements of the actuators, and open and closed loop performance comparisons. Typically the FEM will accurately predict the natural frequencies of the structure and give a general idea of the structure's mode shapes (at least at low frequencies). The FEM will less accurately predict input/output transfer function parameters such as the zeros and the phase versus frequency response. In addition standard FEM methods make no predictions of the damping in the system.

To design a stable high authority controller the model must accurately reflect the dynamics of structure. The FEM can be improved by incorporating experimental test data (model updating) or an identified model can be derived based entirely on experimental tests. The latter approach is taken in this paper using two methods. The first method is a model based on modal analysis techniques and the second is identified using the Eigensystem Realization Algorithm (ERA) [1].

2. MODEL IDENTIFICATION USING MODAL ANALYSIS

The purpose of modal analysis is to obtain the structure's modal parameters: the eigenvalues (damping and natural frequency) and the eigenvectors (mode shapes). The modal parameters can be used to construct a modal model. A model based on modal analysis has two advantages over other model identification techniques. The modal model retains a simple physical correspondence between the identified model and the structure which is lost in many state space based identification methods. Another advantage is that an initial assumption of the of the structure's dynamics allows the modal parameters to be identified from a relatively small number experimental transfer function measurements. In modal analysis it is assumed that the structure's dynamics are represented by:

$$M\ddot{y} + C\dot{y} + Ky = u \quad (1)$$

where M , C and K are symmetric and positive semidefinite matrices, y is vector of displacements and u is a vector of inputs. It is also assumed that the structure is time invariant, the modes are distinct, and a driving point transfer function (collocated sensor and actuator) is available. There are methods available to be used on structures which do not conform to these assumptions: Ewins [2] discusses the problem of using modal identification on non-linear systems and Inman [3] discusses modal identification for asymmetric M , C and K matrices. In this paper the issues of model

identification when there are repeated eigenvalues and when the a driving point transfer function is not available are addressed.

In modal analysis of a passive structure, structural inputs are obtained from a hammer or a shaker, and structural outputs are obtained by attaching accelerometers or strain gauges. An active structure has actuators and sensors as an integral part of the structure. Here the excitation points needed for modal analysis are the actuators of the active structure and the structural outputs are the built in sensors. In an active structure such as the smart antenna which uses piezoelectric materials for both the sensors and the actuators (this structure is discussed later in the paper), any given piezoelectric sensor and actuator element can be used as an actuator or as a sensor during modal analysis.

It is well known that when the eigenvalues are distinct and the structure is of the form given by equation (1) then the modal parameters can be identified from a single column of the receptance matrix. This is equivalent to saying that the modal parameters can be obtained from experimental transfer functions between a single input and m sensor outputs. When the eigenvalues are not distinct or when a collocated transfer function is not available then in order to identify the structure, multiple inputs are required. Each of these cases is discussed in the following sections.

Modeling When Eigenvalues Are Distinct

Equation (1) can be put into a symmetric state space format:

$$G\dot{q} - Hq = f \quad (2)$$

where:

$$q = \begin{bmatrix} y \\ \dot{y} \end{bmatrix}, G = \begin{bmatrix} C & M \\ M & 0 \end{bmatrix}, H = \begin{bmatrix} -K & 0 \\ 0 & M \end{bmatrix}, f = \begin{bmatrix} u \\ 0 \end{bmatrix} \quad (3)$$

There exists a transformation matrix Ψ orthogonal with respect to G which will diagonalize the system in (2):

$$\Psi^T G \Psi = I, \quad \Psi^T H \Psi = \begin{bmatrix} \Lambda & 0 \\ 0 & \Lambda^* \end{bmatrix} \\ \Lambda = \text{diag}(\lambda_r), \quad \Lambda^* = \text{diag}(\lambda_r^*) \quad (4)$$

The transformation matrix Ψ is partitioned in the following manner:

$$\Psi = \begin{bmatrix} \Phi & \Phi^* \\ \Phi\Lambda & \Phi^*\Lambda^* \end{bmatrix} \quad (5)$$

Where the columns of Φ are the mode shape vectors of the system given in (1) and the rows of Φ are the modal participation vectors.

Substituting the transformation $q = \Psi x$ into equation (2) results in the diagonal equation:

$$\dot{x} = \begin{bmatrix} \Lambda & 0 \\ 0 & \Lambda^* \end{bmatrix} x + \Psi^T f \quad (6)$$

Equation (6) can be cast in the familiar state space formulation:

$$\dot{x} = Ax + Bu \\ y = C_o x + Du \quad (7)$$

where:

$$A = \begin{bmatrix} \Lambda & 0 \\ 0 & \Lambda^* \end{bmatrix}, B = \begin{bmatrix} \Phi^T \\ \Phi^{*T} \end{bmatrix}, C_o = \begin{bmatrix} \Phi \\ \Phi^* \end{bmatrix} \quad (8)$$

and D is the direct transmission matrix. The objective of the modal modeling is to identify the A , B , C_o and D matrixes in equation (8). The columns of C_o (also the rows of B) are the mode shapes and are designated c_r where r can take values from 1 to $2n$ (n is the number of DOF retained in the model). The columns of B (and the rows of C_o) are the modal participation vectors and are designated b_i where i can take values from 1 to m (m is the number of measurement locations). Note that in the identified model the number of columns of B is not necessarily equal to $2n$ but will instead depend on the number of experimental measurement locations. The i th element of the r th row of Φ is designated ϕ_{ir} and is called the modal participation factor. Taking the Laplace Transform of (7) and substituting (8) results in an input/output relationship involving the receptance matrix α :

$$Y(s) = C_o (sI - A)^{-1} B U(s) + D U(s) \quad (9)$$

$$Y(s) = \alpha(s) U(s) \quad (10)$$

$$\alpha(s) = \begin{bmatrix} \Phi & \Phi^T \end{bmatrix} \begin{bmatrix} (sI - \Lambda)^{-1} & 0 \\ 0 & (sI - \Lambda^*)^{-1} \end{bmatrix} \begin{bmatrix} \Phi \\ \Phi^* \end{bmatrix} - D \quad (11)$$

It follows from equation (10) that the transfer function between the i th output and the j th input is:

$$\frac{Y_i(s)}{U_j(s)} = \sum_{r=1}^n \frac{\phi_{ir} \phi_{jr}}{s + \lambda_r} + \sum_{r=1}^n \frac{\phi_{ir}^* \phi_{jr}^*}{s + \lambda_r^*} + d_{ij} \quad (12)$$

The numerators of (12) may have both real and imaginary parts and in the normal mode assumption (proportional damping) the numerators will be purely imaginary. The experimental transfer function between the i th output and j th input is measured to be:

$$\frac{Y_i(s)}{U_j(s)} = \sum_{r=1}^n \frac{A_{ijr}}{s + \lambda_r} + \sum_{r=1}^n \frac{A_{ijr}^*}{s + \lambda_r^*} + k_{ij} \quad (13)$$

The modal participation factors ϕ_{ir} are identified by equating the residues of the experimental transfer function (which are the numerators of equation (13)) to the residues of the assumed model's transfer function (which are the numerators of equation (12)). Only a single column of the receptance matrix $\alpha(s)$ needs to be measured to provide sufficient equations to determine all $m \cdot n$ modal participation factors ϕ_{ir} . This is equivalent to saying that only a single input is needed in obtaining the required transfer functions. Equating the numerators of equation (12) with the numerators of equation (13) and using the input $j = \beta$ results in:

$$\phi_{ir} \phi_{\beta r} = A_{i\beta r}, \quad i = 1 \text{ to } m, \quad r = 1 \text{ to } n \quad (14)$$

which describes $m \cdot n$ equations and $m \cdot n$ unknowns. There is a closed form solution to the equations described by (14). The equation involving the driving point $j = \beta$ is solved and $\phi_{j\beta}$ is found. The modal participation factor $\phi_{j\beta}$ is then the "seed" for solving the remaining equations.

A single input $j = \beta$ is the minimum requirement to identify the structure only if the structure is controllable from the input $j = \beta$. The structure is controllable from the input $j = \beta$ if all of the modal participation terms in the modal participation vector b_j are not zero (4). If the structure is not controllable from $j = \beta$ then more than a single input will be required to identify the structure.

The elements of the modal state space model's (equations (7) and (8)) B and C matrices are determined by equation (14). The A matrix is simply a diagonal matrix of the identified eigenvalues. The elements of the D matrix d_{ij} are determined by setting the residual term in equation (13) equal to the residual term in equation (12): $d_{ij} = k_{ij}$. For many structures only the diagonal terms d_{ij} will be non-zero. Each diagonal term relates to a collocated transfer function which may have an equal number of poles and zeros in the measurement.

Driving Point Not Available

When the driving point is not available equation (14) will reduce to $(m-1) \cdot n$ equations and $m \cdot n$ unknowns:

$$\phi_{j\beta} = A_{ij} \quad i=1 \text{ to } m \quad i \neq \beta \quad r=1 \text{ to } n \quad (15)$$

A transfer function from an additional input $j = \gamma$ and a single output i will yield an additional n equations:

$$\phi_{i\gamma} = A_{ij} \quad i \neq \beta \quad i = \gamma \quad r=1 \text{ to } n \quad (16)$$

Equation (15) together with equation (16) yield $m \cdot n$ equations and $m \cdot n$ unknowns.

Eigenvalues Repeated When the Eigenvectors Linearly Independent

Here we show that when the eigenvalues are repeated with a multiplicity of 2 then a minimum of 2 inputs are required to identify the modal participation terms $\phi_{j\beta}$.

It is important to keep in mind that when the eigenvalues are distinct the rows of the B matrix (the mode shapes) are uniquely determined from experimental data. When the eigenvalues are repeated, there are an infinite number of mode shape solutions associated with the repeated eigenvalue, and each of these solutions is related to another solution by an orthogonal similarity transformation. Thus for the system given by equations (7) and (8) there exists an orthogonal similarity transformation T such that:

$$\dot{x} = T^T q \quad T^T A T = A \quad \tilde{B} = T^T B \quad (17)$$

Note that the A matrix (the matrix of eigenvalues) is unaffected by the transformation while certain rows of the B matrix are transformed and other rows are unaffected. Those rows of B which are associated with distinct eigenvalues are unaffected by the transformation T and those rows associated with repeated eigenvalues may be transformed. This result is best shown by a simple example. Given is the following

system with distinct eigenvalues a and c and repeated eigenvalue b :

$$\dot{x} = A x + B u$$

$$A = \begin{bmatrix} a & & & \\ & b & & \\ & & b & \\ & & & c \end{bmatrix} \quad B = \begin{bmatrix} d_1 & d_2 & d_3 & d_4 \\ e_1 & e_2 & e_3 & e_4 \\ f_1 & f_2 & f_3 & f_4 \\ g_1 & g_2 & g_3 & g_4 \end{bmatrix} \quad (18)$$

An orthogonal similarity transformation is arbitrarily chosen to be:

$$T = \begin{bmatrix} 1 & 0 & 0 & 0 \\ 0 & \cos \theta & -\sin \theta & 0 \\ 0 & \sin \theta & \cos \theta & 0 \\ 0 & 0 & 0 & 1 \end{bmatrix} \quad (19)$$

Applying the transformation $x = T^T q$ to equation (18) it is found that $T^T T = I$, $T^T A T = A$ and:

$$\tilde{B} = T^T B = \begin{bmatrix} d_1 & d_2 & d_3 & d_4 \\ e_1 \cos \theta - f_1 \sin \theta & e_2 \cos \theta - f_2 \sin \theta & e_3 \cos \theta - f_3 \sin \theta & e_4 \cos \theta - f_4 \sin \theta \\ e_1 \sin \theta + f_1 \cos \theta & e_2 \sin \theta + f_2 \cos \theta & e_3 \sin \theta + f_3 \cos \theta & e_4 \sin \theta + f_4 \cos \theta \\ g_1 & g_2 & g_3 & g_4 \end{bmatrix} \quad (19)$$

Note that the first and fourth rows of \tilde{B} are the same as the first and fourth rows of B . These are the row associated with the distinct modes. Note also that any single element of the repeated mode shapes can be arbitrarily set to zero by judicious choice of the transformation T . For instance the element in the second row first column of \tilde{B} will be equal to zero if θ is chosen such that $\theta = \tan^{-1}(e_1/f_1)$. We will use this property to obtain an extra equation in solving for the modal participation factors.

Here we examine the transfer function from a structure with repeated modes. Assume the first p modes are repeated with a multiplicity of 2 and the remaining modes are distinct. The transfer function between input j and output i is then:

$$\frac{Y_i(s)}{U_j(s)} = \sum_{r=1}^p \frac{{}_1\phi_{j\beta} \phi_{i\beta} + {}_2\phi_{j\beta} \phi_{i\beta}}{s + \lambda_r} + \sum_{r=1}^p \frac{{}_1\phi_{j\beta} \phi_{i\beta} + {}_2\phi_{j\beta} \phi_{i\beta}}{s + \lambda_r} + \sum_{r=p+1}^{2m-p} \frac{\phi_{j\beta} \phi_{i\beta}}{s + \lambda_r} + \sum_{r=p+1}^{2m-p} \frac{\phi_{j\beta} \phi_{i\beta}}{s + \lambda_r} + d_{ij} \quad (20)$$

The subscript preceding $\phi_{j\beta}$ (either a 1 or a 2) is used to differentiate between modes associated with a repeated eigenvalue r . Equating the numerator terms in equation (20) with the numerator terms in the experimental transfer function equation (13) and using the input $j = \beta$ results in:

$${}_1\phi_{\beta 1} \phi_{\beta 1} + {}_2\phi_{\beta 2} \phi_{\beta 2} = A_{ij} \quad i=1 \text{ to } m \quad r=1 \text{ to } p \quad (21)$$

which yields $2m \cdot p$ unknowns and $m \cdot p$ equations. An additional $p(m-1)$ equations can be obtained by using a second input $j = \gamma$:

$${}_1\phi_{\beta 1} \phi_{\beta 1} + {}_2\phi_{\beta 2} \phi_{\beta 2} = A_{ij} \quad i=1 \text{ to } m, \quad i \neq \beta \quad r=1 \text{ to } p \quad (22)$$

which together with equation (21) yield $2m-p$ equations. Another p equations are obtained by arbitrarily setting:

$$1\phi_1 = 1\phi_2 = 1\phi_3 = \dots = 1\phi_p = 0 \quad (23)$$

Equations (21), (22) and (23) yield the $2m-p$ equations necessary to solve for the elements ϕ_{ij} using experimental transfer functions. Note that in order to obtain a determined set of equations it is necessary to use 2 inputs. The procedure described by equations (21), (22) and (23) can be extended to show that when an eigenvalue is repeated with a multiplicity of q , then a minimum of q input locations are necessary to obtain a determined set of equations provided that the system is controllable from the chosen q inputs. If the system is not controllable from the chosen q inputs then additional input locations or location will be needed to identify the structure.

Solving equations (21), (22) and (23) will also reveal whether a mode is repeated or distinct. If it is found from the solution of (21), (22) and (23) that the r^{th} mode shape is a vector of zeros, i.e. $1\phi_r = 0$, then this mode is distinct and the assumption of a repeated mode is incorrect.

Driving Point Not Available

When the driving point is not available, then the input $j = \beta$ will provide $(m-1)p$ equations:

$$1\phi_{r1}\phi_{r\beta} + 2\phi_{r2}\phi_{r\beta} = A_{r\beta} \quad r=1 \text{ to } m, \quad i=\beta \quad r=1 \text{ to } p \quad (24)$$

An additional $(m-2)p$ equations are obtained from a second input location $j = \gamma$:

$$1\phi_{r1}\phi_{r\gamma} + 2\phi_{r2}\phi_{r\gamma} = A_{r\gamma} \quad r=1 \text{ to } m, \quad i=\beta \quad i=\gamma \quad r=1 \text{ to } p \quad (25)$$

The remaining necessary equations can be obtained by measuring three transfer functions from a third input $j = \delta$:

$$1\phi_{r1}\phi_{r\delta} + 2\phi_{r2}\phi_{r\delta} = A_{r\delta} \quad r=1 \text{ to } 3, \quad i=\beta \quad i=\gamma \quad i=\delta \quad r=1 \text{ to } p \quad (26)$$

Equations (24), (25) and (26) together with equation (23) describe $2m-p$ equations and $2m-p$ unknowns.

3. ISSUES IN IDENTIFICATION AND CONTROL

The Benchmark System

The benchmark system is used for comparison of identification schemes on a known reference (Figure 1). Each of the eight rigid spokes is connected by a pin joint and a torsional spring to the rigid hub. Each of the spokes is connected at the end opposite to the pin to its neighboring spoke by a linear spring (a small angle assumption is made for rotation about the pin). The torsional springs represent the stiffness of the antenna rib and the linear springs represent the coupling between the ribs. When the coupling is small, the ribs act independently, when the coupling is high repeated or nearly repeated modes are found. Each of the torsional springs is given a slightly different value to represent the manufacturing tolerance of the rib stiffness. Simulated transfer functions are measured between the inputs at spokes 1 and 2 and the outputs at spokes 1, 2 and 3. From

any one SISO a maximum of 5 modes are identified 2 of which are distinct and 3 of which are repeated.

Modal Model

A verification of the modal analysis technique is performed using the benchmark system as a reference. Using the residuals from the simulated transfer functions, the modal participation vectors are correctly identified using equations (21)-(23). In solving the equations no assumptions are made about which modes are distinct and which modes are repeated. In the solution, the 2 modes shapes associated with a repeated mode form a linearly independent pair. The 2 solved mode shapes associated with a distinct mode are a non-zero modeshape, which is the correct modeshape, and a modeshape consisting of a vector of zeros, which can be discarded in the model.

ERA Model

After verifying the modal analysis method on the benchmark system, the Eigensystem Realization Algorithm (ERA) is used to obtain a 2 input 3 output state-space model. The objective is to determine whether ERA can accurately identify the modal parameters of a system which exhibits closely spaced and nearly repeated eigenvalues. The advantage of ERA over the modal analysis method is that it uses the time data directly to form the model. It is not necessary to perform any type of identification to obtain the SISO transfer functions.

Whether identifying the benchmark system or the actual structure, the method of acquiring the ERA model is as

follows. The system is excited by a random signal input into the first actuator and the desired sensor measurements are obtained. This process continues for all of the necessary actuator/sensor relationships. After all of the tests are complete, an FFT algorithm uses the time data to calculate the impulse response of the system. The results are input into an ERA program which forms the state-space model of the system. The algorithms used for this procedure are available in the SOCI Toolbox [5].

In terms of the natural frequencies and damping ratios, ERA is able to accurately identify all but one of the parameters. From the singular values of the Hankel matrix, the order of the state-space model is chosen to be 16, as it should be. Except for the fact that ERA did not identify the 3.3397 Hz mode, the identified natural frequency and damping ratios show good agreement with the actual values [Table 1]. Of course, it must be remembered that the time data for this analysis is noise-free, a characteristic that won't be present in an experiment.

Table 1. Actual and ERA identified natural frequencies and damping ratios for the benchmark system.

Actual		Identified	
ω (Hz)	ζ (%)	ω (Hz)	ζ (%)
1.5804	1.0070	1.5800	1.2006
1.9935	0.7984	1.9443	0.5381
1.9973	0.7968	1.9965	0.8072
2.7501	0.5787	2.0085	0.8102
2.7504	0.5787	2.7391	0.5312
3.3375	0.4769	2.7400	0.5522
3.3397	0.4766	3.3366	0.5700
3.5539	0.4478	3.5544	0.3630

Although ERA identified most of the natural frequencies and damping ratios correctly, the resulting transfer functions contain error in both the magnitude and the phase. Figure 2 compares the actual SISO transfer function between sensor 1 and actuator 1 and the one obtained from the identified model. The magnitude matches over most of the frequency range, but a large error exists in the phase. If the identified model is the basis for a control system design, this error in the phase is a major concern. A vibration suppression scheme based on the identified model would be fundamentally different than one designed from the actual transfer functions.

The Smart Antenna

The structure under examination is an eight ribbed smart antenna, as shown in Figure 3. At the clamped end of 5 of the ribs, a single piece of piezoceramic is bonded to each side of the beam. Each piezoceramic has dimensions 0.0152 x 6.4 x 2.3 cm and is separated into two electrically isolated strips, the larger area is used for actuation, the smaller area is for sensing (Piezo Product material G1195). Control laws are implemented using an Optuma 3 digital controller and data acquisition is performed on a Tektronix 2630 Fourier Analyzer. The sensor for the modal tests is an optical probe from Philtec.

To identify which natural frequencies of the antenna are repeated, two separate modal tests are performed. For the first modal analysis, the piezoceramic on rib 1 is used as an excitation source, and the displacement at the tip of each rib is measured with the optical probe. The natural frequencies, damping ratios, and residues are then calculated using the

STAR Modal Analysis package [Table 2]. A second modal test is performed in the same manner, except that the actuator located on rib 2 provides the excitation.

Table 2. Natural frequencies (in Hz) of the five modal peaks, as calculated from the two inputs.

Mode	Input 1	Input 2
1	9.66	9.71
2	10.41	10.44
3	11.51	11.63
4	12.58	12.58
5	17.23	17.25

The results of the individual tests are used to determine which of the antenna's eigenvalues are repeated and which are distinct. From any one SISO transfer function, only five modal peaks are well defined. Thus, each test yields modal parameters for five modes. Since there are eight ribs in the antenna, there are eight eigenvalues with associated eigenvectors in the first modal cluster. Since only five modal peaks are visible on any one SISO transfer function, two of the modes are distinct and three are repeated. To find the repeated modes, the eigenvectors that correspond to the same modal peaks from the two separate transfer functions are compared in terms of the Modal Assurance Criterion (MAC) [2]. If the MAC is very close to zero, this indicates that the eigenvectors are linearly independent and the corresponding eigenvalue is repeated. If the MAC is close to one, then the two eigenvectors differ only by a scalar, and the eigenvalue could be distinct. This second test is not definitive since an eigenvalue could have a MAC value of one and still be repeated.

The results of the MAC tests for the two separate data sets are listed in Table 3. For the first two modes, the eigenvectors that are excited from input 1 are definitely orthogonal to those that result from an excitation at input 2. Conversely, the fifth mode is the same irregardless of the location of the input, therefore the corresponding eigenvalue is distinct. For the remaining two modes, the results are not as clear. By examining the mode shapes that result from the two separate excitations, it is determined that mode 4 is distinct and the third mode is repeated. This conclusion is supported by the results of the Modal Assurance test.

Table 3. The MAC comparison for the two separate modal tests. The higher the value, the larger the correlation between the modes from the two inputs.

		Input 2				
		1	2	3	4	5
Input 1	1	0.02				
	2		0.16			
	3			0.62		
	4				0.82	
	5					0.94

The difference between repeated and distinct modes can be illustrated by examining the mode shapes that result from the two separate inputs. Figure 4a is the fifth mode shape resulting from an input at rib 1, and Figure 4b is the same mode excited by an input at rib 2. To the degree of experimental accuracy, the shape of the mode is independent of the location of the input, which means that the corresponding eigenvalue is distinct. This is consistent with the MAC value being 0.94 for these two modes [Table 3]. The next part of Figure 4 contains the modes that result from an excitation at the second natural frequency. From Figures 4c and 4d, it's clear that the mode shapes change depending on the location of the input. This indicates that the corresponding eigenvalue is repeated, which again is consistent with the MAC result.

The procedures for identifying the smart antenna with modal analysis or ERA are similar but there is one important difference. Both are based on random input/ random output time domain responses between all of the necessary actuator and sensor locations. For the modal analysis approach, the number of measurements is affected by the availability of driving point residues. Once the individual input/ output responses are obtained, the transfer functions are identified using a Recursive Least Squares program. The transfer functions are expanded into the pole-zero form of equation (13) and the identification of the antenna is completed by the approach derived in section 1. If ERA is used, no SISO identification is necessary. Once the time data between all of the inputs and outputs is acquired, the impulse responses are obtained by use of an inverse FFT. The ERA algorithm can then be used to find the state-space model. Although at first it seems cumbersome to identify SISO transfer functions in order to do the modal analysis, this might turn out to be an advantage because the individual transfer functions are forced to be accurate before the identification is performed.

Although a full experimental identification and control of the smart antenna has not been performed, preliminary results illustrate the importance of obtaining an accurate MIMO model. Previous studies show that simple SISO models can be used in conjunction with collocated control laws to obtain an increase in structural damping [6]. Unfortunately, the

increase in damping achieved is limited due to the existence of closely spaced and repeated modes. In the future, it is desired to use both collocated and non-collocated control laws to obtain a larger increase in the closed loop damping. For these types of control schemes, it is very important to have an accurate model. As discussed in section 2, it might be difficult to achieve the necessary accuracy using a time domain technique such as ERA. The next step in our modeling study is to apply the modal analysis approach developed in section 1 to an experimental identification of the smart antenna.

4. CONCLUSIONS

A modal analysis technique that identifies MIMO models of structures that contain repeated or nearly repeated eigenvalues was presented. The method is an extension of the well established procedure that applies if the eigenvalues of the system are distinct. For a system containing repeated eigenvalues with multiplicity q , it is necessary to have q inputs for the modal tests. Equations were derived for the systems where the driving point residues are available as well as for systems with no driving point information.

Comparisons were made between the modal analysis approach and the Eigensystem Realization Algorithm. The modal analysis technique is based on the availability of SISO transfer functions of the necessary input/output relationships. Accurate SISO models are easily obtained with time domain identification techniques such as Recursive Least Squares. These transfer functions are expanded and the resulting residues form the basis for the modal analysis. In contrast, ERA uses the time domain data directly and returns the modal parameters as well as a state-space model. A study conducted on a simple model indicated that ERA identified the natural frequencies and damping ratios well, but had difficulty matching both the magnitude and phase of the actuator/sensor transfer functions.

Preliminary experimental results on identification and control of a smart antenna were also presented. Two modal tests were performed and the repeated modes of the structure were identified using the Modal Assurance Criterion. The importance of understanding the nature of the repeated modes was discussed in relation to designing active vibration schemes for the smart antenna.

Acknowledgments

The authors are thankful for the support of NASA Fellowship number NGT 50541 under the direction of Dr. W. Keith Belvin and AFOSR grant number 9010181 under the direction of Dr. Spencer Wu. The authors would also like Mark Holcomb for performing the modal tests.

References

[1] Juang, J.-N., and R.S. Pappa, "An Eigensystem Realization Algorithm for Modal Parameter Identification and Model Reduction," *Journal of Guidance, Control, and Dynamics*, Vol. 8, No. 5, pp. 620-627, 1985.

[2] Ewins, D.J., *Modal Testing: Theory and Practice*, John Wiley & Sons Inc., 1986.

[3] Inman, D.J., "Modal Analysis For Assymmetric Systems", *Proceedings of the 1st International Modal Analysis Conference*, pp. 705-708, 1982

[4] Hughes, P.C., Skelton, R.E. "Controllability and Observability of Linear Matrix-Second-Order Systems," *Journal of Applied Mechanics*, Vol. 47, pp. 415-420, 1980.

[5] Juang, J.-N., Horta, L.G., Phan, M., "System Observer/Controller Identification Toolbox, User's Guide," NASA Langley Research Center, Hampton, VA, Dec., 1991.

[6] Dosch, J.J., Leo, D.J., Inman, D.J., "Comparison of Vibration Control Schemes For a Smart Antenna," *31st Conference on Decision and Control*, Dec., 1992.

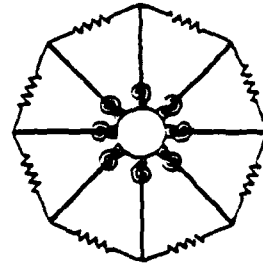
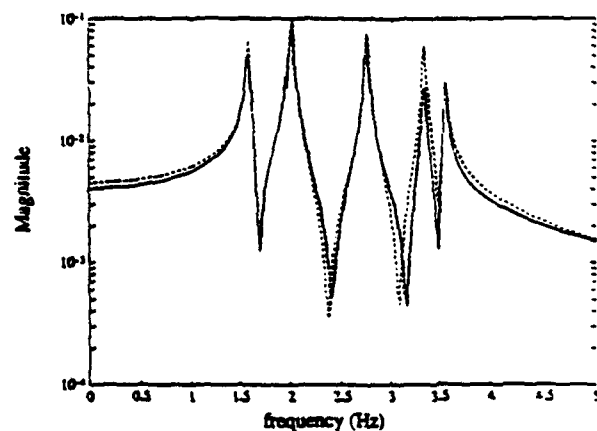


Figure 1. Benchmark system for comparing identification methods. The eight degree of freedom lumped parameter system displays much of the dynamic response characteristics found in the flexible antenna.



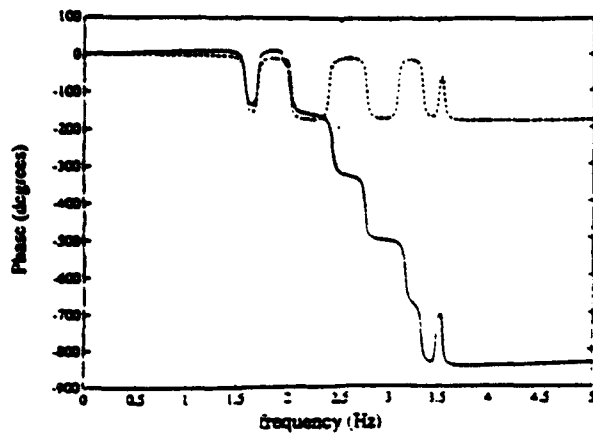


Figure 2. Comparison between an actual (dotted) and ERA (solid) identified transfer function for the benchmark system. The model agrees well in terms of the magnitude, but the phase contains significant error.

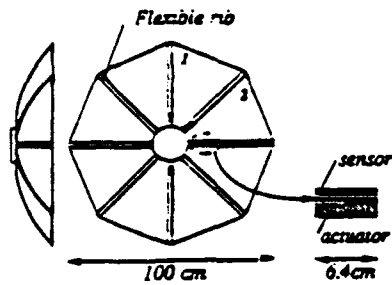


Figure 3. The smart antenna test structure. Location and design of the piezoceramics are shown.

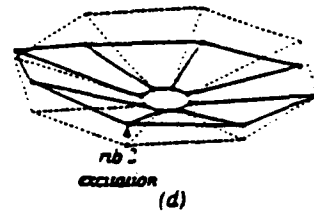
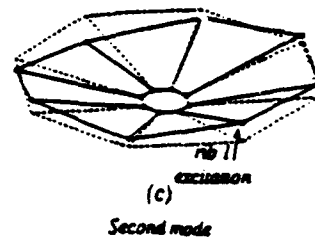
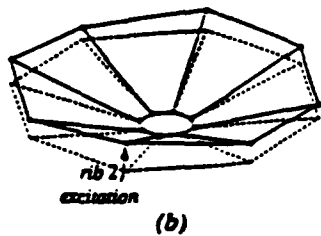
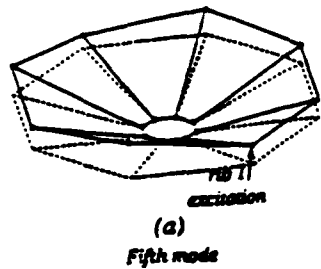


Figure 4. A comparison of the mode shapes of the antenna from two separate inputs. The fifth mode is distinct, since the shape is independent of the input location (a and b). For the second mode, the shape is dependent on the location of the input (c and d), therefore it is a repeated mode.

COMPARISON OF VIBRATION CONTROL SCHEMES FOR A SMART ANTENNA

Jeffrey J. Dosca[†] Donald J. Leo[†] Daniel J. Inman^{*}

[†] Department Of Mechanical & Aerospace Engineering
State University of New York at Buffalo
Buffalo, NY 14260

^{*} Samuel Herrick Professor
Department of Engineering Science and Mechanics
Virginia Polytechnic Institute and University
Blacksburg, VA 24061

ABSTRACT

Two active vibration control schemes, Positive Position Feedback (PPF) and Active Vibration Absorber (AVA), are experimentally implemented with an eight ribbed smart antenna. Mounted on five of the eight ribs are collocated piezoceramic sensor/ actuator pairs creating a multi-input multi-output control structure. A SISO pole zero model of one of the antenna ribs is identified. The design parameters for the AVA and PPF controllers are numerically optimized from simulations of the SISO model. The design parameters found in the SISO simulations are then implemented in the MIMO structure. Theoretical stability bounds for collocated and non-collocated control for both the PPF and AVA control schemes are also presented.

1. INTRODUCTION

Vibration suppression of a flexible antenna is complicated by existence of closely spaced modes and repeated natural frequencies. A further difficulty is that the configuration of such structures makes the use of standard actuators such as proof masses and torque wheels infeasible. These problems can be overcome by applying smart structure technology combined with control laws that exploit the benefits of sensor/ actuator collocation. Distributed sensors and actuators such as piezoceramic material are well suited to this problem. [1]. They can be readily integrated into the structure without significantly increasing the weight or compromising structural integrity. Another important feature of the smart structure approach is that the sensor and actuator can be virtually collocated with one another. In this situation, control laws such as Positive Position Feedback (PPF) [2] and Active Vibration Absorbers (AVA) [3] can be implemented in a straightforward manner. Design of these controllers can be accomplished with only crude models of input/ output relationships. They are also inherently robust with respect to uncertain or unmodelled dynamics. These attributes are very important for this problem, since obtaining an accurate model of a flexible antenna is difficult.

The intent of this paper is to compare vibration suppression schemes on a flexible antenna that contains piezoceramic actuators and sensors. The control laws studied are PPF and AVA. Important consideration is given to the fact that the experimental testbed exhibits the problem of closely spaced and repeated natural frequencies. The paper is organized in the following manner. First, the framework for the PPF and AVA controllers is outlined and the two techniques are compared. Theoretical stability conditions are also derived in terms of the design variables and structural parameters. Next, a description

of the flexible antenna testbed is provided with a discussion of the algorithm used to design the controllers. Results of experimental implementation is then presented for the different control schemes. The final section summarizes the important conclusions and provides direction for future research.

2. SECOND ORDER CONTROLLERS

In this section a general mathematical framework is introduced from which the stability of PPF and AVA are compared. The dynamics of a flexible structure coupled to a second order controller can be expressed as,

structure:

$$I\ddot{q} + \Lambda_p \dot{q} + \Lambda_s q = S^T B u \quad (1)$$

$$y_a = H_a S q, \quad y_v = H_v S \dot{q}, \quad y_d = H_d S q \quad (2)$$

controller

$$I\ddot{q}_c + \Lambda_{pc} \dot{q}_c + \Lambda_{sc} q_c = u, \quad (3)$$

$$y_{ac} = H_{ac} q_c, \quad y_{vc} = H_{vc} \dot{q}_c, \quad y_{dc} = H_{dc} q_c \quad (4)$$

where:

$S(n \times n)$ matrix of eigenvectors

$\Lambda_p(n \times n)$ proportional damping matrix $\text{diag}(2\zeta_i \omega_i)$

$\Lambda_{pc}(r \times r)$ controller damping matrix $\text{diag}(2\zeta_{ci} \omega_{ci})$

$\Lambda_s(n \times n)$ structure stiffness matrix $\text{diag}(\omega_i^2)$

$\Lambda_{sc}(r \times r)$ controller stiffness matrix $\text{diag}(\omega_{ci}^2)$

$q(n \times 1)$ structure modal coordinate

$q_c(r \times 1)$ controller coordinate

$H_{ac}(m \times r)$, $H_{vc}(m \times r)$, $H_{dc}(m \times r)$ controller output matrix

$H_a(s, \times n)$, $H_v(s, \times n)$, $H_d(s, \times n)$ structure output matrix

$B(n \times m)$ structure input matrix

$y_a(s, \times 1)$, $y_v(s, \times 1)$, $y_d(s, \times 1)$ system output

$y_{ac}(r \times 1)$, $y_{vc}(r \times 1)$, $y_{dc}(r \times 1)$ controller output

$u_c(r \times 1)$ controller input vector

$u(m \times 1)$ system input vector

n =structure degrees of freedom, m =number of actuators,

r =number of control filters, s_a, s_v, s_d = number of acceleration, velocity and displacement sensors

The matrices Λ_p and Λ_s are positive definite and Λ_{pc} and Λ_{sc} are chosen to be positive semidefinite. The input matrix B is defined by the location of the actuators on the structure and the measurement matrices H_{ac} , H_{vc} , and H_{dc} are defined by the location of the acceleration, velocity and displacement sensors. In general, the location of the actuators will not be the same as the location of the sensors (non collocated control). The flexible system and controller are coupled by,

$$u = (y_a - G_a y_s) + (y_b - G_b y_s) + (y_c - G_c y_s) \quad (5)$$

$$u_i = B_{a_i} y_s + B_{b_i} y_s + B_{c_i} y_s \quad (6)$$

where B_{a_i} , B_{b_i} , B_{c_i} are the controller input gain matrices and G_a , G_b , G_c are direct transmission matrices directly coupling the structure's sensors to the actuators. Combining equations (1)-(6) results in the structure plus controller closed loop system.

$$M \ddot{q} + D \dot{q} + K q = 0 \quad (7)$$

where:

$$q_i = [q^r \quad q^s]^T, \quad M_i = \begin{bmatrix} I - S^T B G_i H_i S & -S^T B H_{i2} \\ -B_{i2} H_i S & I \end{bmatrix}$$

$$D_i = \begin{bmatrix} \Lambda_a + S^T B G_i H_i S & -S^T B H_{i2} \\ -B_{i2} H_i S & \Lambda_b \end{bmatrix}$$

$$K_i = \begin{bmatrix} \Lambda_c + S^T B G_i H_i S & -S^T B H_{i2} \\ -B_{i2} H_i S & \Lambda_d \end{bmatrix} \quad (8)$$

The closed loop system, equation (7), is stable when the matrices M_i , D_i , and K_i are symmetric and positive semidefinite. By imposing the gain and symmetry constraints:

$$G_i = H_{i1} B_{i1}, \quad G_i = H_{i1} \Lambda_{i1}^{-1} B_{i1}, \quad G_i = H_{i1} \Lambda_{i1}^{-1} B_{i1} \quad (9)$$

$$\text{and} \quad (S^T B H_{i2})^T = B_{i2} H_i S \quad i=a, v, \text{ or } d \quad (10)$$

the matrices M_i , D_i , and K_i must be symmetric positive semidefinite and thus closed loop stable [3]. Juang [3] calls controllers of this form AVA and are characterized by infinite gain margins when constraint equations (9) and (10) are applied.

PPF is similar to AVA except that in PPF only position measurements are fed back and there is no direct transmission term G_i . Combining equations (1)-(6) and setting G_a , G_b , G_c , H_a , H_b , H_c , and H_{i2} each equal to a zero matrix results in the closed loop PPF equation:

$$M \ddot{q} + D \dot{q} + K q = 0 \quad (11)$$

$$\text{where} \quad q_i = [q^r \quad q^s]^T, \quad M_i = I,$$

$$D_i = \begin{bmatrix} \Lambda_a & 0 \\ 0 & \Lambda_b \end{bmatrix} \text{ and } K_i = \begin{bmatrix} \Lambda_c & -S^T B H_{i2} \\ -B_{i2} H_i S & \Lambda_d \end{bmatrix} \quad (12)$$

With PPF an inequality constraint is placed on the controller gain for stability. Here we will show that this constraint is a function of the structural stiffness matrix. Imposing the symmetry constraint equation (10) on the displacement measurements:

$$(S^T B H_{i2})^T = B_{i2} H_i S = M^T \quad (13)$$

and substituting equation (13) into the PPF closed loop stiffness matrix, equation (11), results in the symmetric matrix,

$$K_i = \begin{bmatrix} \Lambda_c & -M^T \\ -M^T & \Lambda_d \end{bmatrix} \quad (14)$$

A symmetric matrix W is positive semidefinite if [5]

$$W_i \geq 0 \quad \text{and} \quad W_i - W_i W_i^{-1} W_i \geq 0 \quad (\dagger \text{ is a pseudoinverse})$$

$$\text{where: } W = \begin{bmatrix} W_1 & W_2 \\ W_2^T & W_3 \end{bmatrix} \quad (15)$$

It follows from the above theorem and from equations (11)-(13), that the matrices in equation (10) are positive semidefinite when

$$\Lambda_c - S^T B H_{i2} \Lambda_d^{-1} B_{i2} H_i S \geq 0. \quad (16)$$

Controller design for AVA and PPF involves choosing controller parameters Λ_a and Λ_b and input matrices B_{a_i} , B_{b_i} , B_{c_i} and output gain matrices H_{a_i} , H_{b_i} , H_{c_i} for best performance. In the AVA controller the direct transmission matrix is fixed by equation (9). To ensure stability of the AVA and PPF controller, the symmetry constraint equations (10) must be imposed. The PPF controller must in addition also meet the inequality constraint (16) to ensure stability. It must be emphasized that the given stability bounds do not include the effects of unmodelled sensor and actuator dynamics which are always present. Also the symmetry constraint equation (10) involves eigenvector information which in a structure is often not accurately measured, thus leading to additional loss of control robustness in this non-collocated case.

Collocated Control

Here it is shown that with collocated feedback it is not necessary to impose the symmetry constraint equation (10). Thus the collocated controller will be more robust to a poor model. It is shown here using displacement feedback as an example that the closed loop equations for both AVA and PPF are symmetrizable (a transformation to dynamically similar system exists) when collocated feedback is used. If the actuator and displacement sensor are collocated then

$$(S^T B)^T = P, \quad H_i S = \alpha P \quad (17)$$

where α is a scalar. Combining equations (1)-(6) and (17) and using only displacement measurements (H_{a_i} , H_{b_i} , H_{c_i} and H_{i2} are zero) results in the combined structure and controller equations for collocated displacement feedback:

$$I \ddot{q} + \Lambda_a \dot{q} + \Lambda_c q = P^T H_{i2} q_s - \alpha P^T G_i P q \quad (18)$$

$$I \ddot{q}_s + \Lambda_b \dot{q}_s + \Lambda_d q_s = \alpha B_{i2} P q \quad (19)$$

In collocated feedback each sensor is able to communicate only with its associated collocated actuator resulting in sparse gain matrices. The controller input gain matrix has the block diagonal form:

$$B_m (r \times m) = \begin{bmatrix} b_1 & & & \\ & b_2 & & \\ & & \ddots & \\ & & & b_m \end{bmatrix} = \begin{bmatrix} b_{11} & & & \\ & b_{22} & & \\ & & \ddots & \\ & & & b_{mm} \end{bmatrix} \quad (20)$$

The terms in the i^{th} column vector $b_i = [b_{i1} \ b_{i2} \ b_{i3} \ \dots]^T$ are the gains associated with the i^{th} actuator. There will be m such column vectors (m is the number of actuators). The number of terms in the vector b_i will be equal to the number of control filters associated with the i^{th} actuator. Similarly the controller output gain matrix will be in block diagonal form:

$$H (m \times r) = \begin{bmatrix} h_1 & & & \\ & h_2 & & \\ & & \ddots & \\ & & & h_m \end{bmatrix} = \begin{bmatrix} h_{11} \ h_{12} \ \dots & & & \\ & h_{21} \ h_{22} \ \dots & & \\ & & \ddots & \\ & & & h_{mm} \ \dots \end{bmatrix} \quad (21)$$

where the i^{th} row vector h_i is associated with the i^{th} actuator. With collocated feedback and input/output matrices in the above mentioned block diagonal form, there is a transformation matrix T that will symmetrize equations (7) and (8). This transformation is given by:

$$q_i = T v_i \quad (22)$$

where,

$$T = \sqrt{\alpha} \text{diag} \left(\frac{b_{11}}{h_{11}} \frac{b_{12}}{h_{12}} \dots \frac{b_{1m}}{h_{1m}} \frac{b_{21}}{h_{21}} \frac{b_{22}}{h_{22}} \dots \frac{b_{2m}}{h_{2m}} \frac{b_{m1}}{h_{m1}} \frac{b_{m2}}{h_{m2}} \dots \right)^{1/2} \quad (23)$$

Because the system has been shown to be symmetrizable, the symmetry constraints given in equation (10) do not need to be imposed to ensure stability in the collocated case. For the AVA controller, as long as direct transmission equations (9)-(10) are satisfied, the closed loop system will have infinite gain margin.

For collocated PPF control, an inequality constraint on the gain is still required to ensure stability. Substituting the transformation equation (22) and (23) into the closed loop PPF equation (16) transforms the stiffness matrix (12) to the symmetric matrix

$$K_s = \begin{bmatrix} \Lambda_s & -P^T V \\ -V^T P & \Lambda_s \end{bmatrix} \quad (24)$$

where,

$$V = H_m T, \quad V^T = \alpha T^T B_m, \quad (S^T B H_m)^T = B_m^T H_m S = P^T$$

Applying the positive semidefinite test given by (15), equation (1) will be positive semidefinite if:

$$\Lambda_s - \alpha P^T H_m T \Lambda_s^{-1} T^T B_m P \geq 0 \quad (25)$$

Equation (25) can be simplified somewhat by arbitrarily fixing each element in the controller input gain matrix B_m to be equal to the square of the corresponding control filter natural frequency, for example (5 filters and 3 inputs):

$$B_m (r \times m) = \begin{bmatrix} \omega_{11}^2 & 0 & 0 \\ \omega_{12}^2 & 0 & 0 \\ 0 & \omega_{21}^2 & 0 \\ 0 & \omega_{22}^2 & 0 \\ 0 & 0 & \omega_{31}^2 \end{bmatrix} \quad (26)$$

Substituting a matrix of the form of (26) into (25) results in the simple inequality constraint on the output gain matrix:

$$\Lambda_s - \alpha P^T H_s P \geq 0 \quad (27)$$

where,

$$H_s (m \times m) = \begin{bmatrix} \sum h_{11} & & & \\ & \sum h_{22} & & \\ & & \ddots & \\ & & & \sum h_{mm} \end{bmatrix} \quad (28)$$

and the symbol $\sum h_i$ indicates a sum of the elements in the vector h_i given in equation (21).

The AVA and PPF control designs (with displacement feedback) are compared on a single degree of freedom (SDOF) undamped system [figure 1]. As can be seen from the root locus, the addition of the zeros on the real axis give the AVA controller its infinite gain margin. The asymptotic behavior of the root locus in the multiple degree of freedom (MDOF) case would be similar to SDOF case due to the interlacing of the poles and zeros in collocated feedback. Observing the controller magnitude versus frequency response it can be seen that the AVA controller does not roll off at higher frequencies. Thus in a real system the AVA gain is limited by the higher frequency dynamics. This is an important difference between the AVA and PPF controller. The PPF control gain is limited by the stiffness of the structure (equation (27)) while in the AVA controller the gain is limited by higher frequency dynamics, which are often unmodelled in the control design.

3. CONTROLLER OPTIMIZATION

The testbed for the AVA and PPF controllers is a smart flexible antenna structure [Figure 2]. Multi-Input-Multi-Output (MIMO) control capability is provided by the five collocated piezoelectric sensor/ actuator pairs which are bonded to five of the eight antenna ribs. With the exception of the inclusion of piezoelectric elements, the test antenna is similar (but smaller in scale) to the non-smart antenna which is

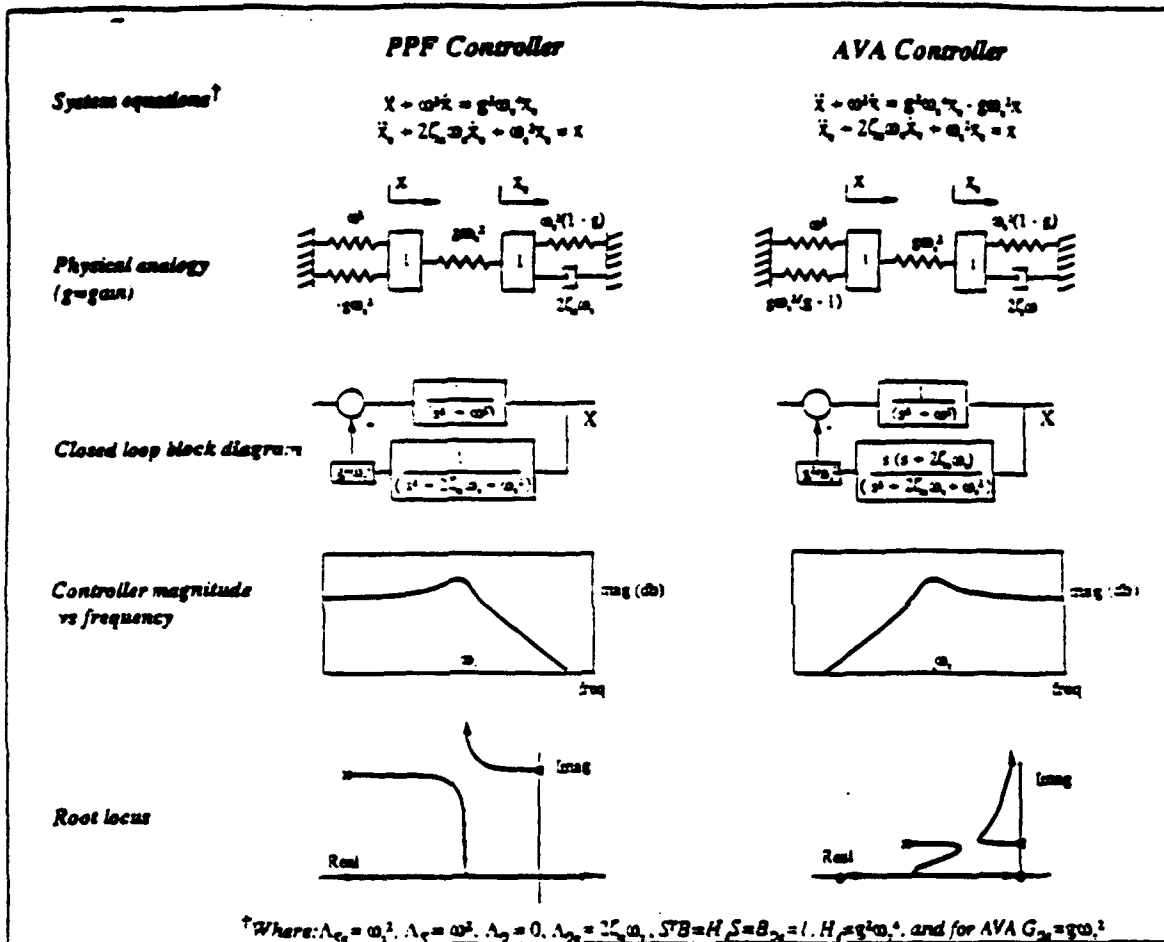


Figure 1: Comparison of PPF and AVA for the single degree of freedom case displacement feedback.

part of the CSI Evolutionary Model located at NASA Langley [4]. Each collocated sensor/ actuator is manufactured from a single sheet of piezoelectric material (.0152 x 6.4 x 2.3 cm. Piezoelectric Products material G1195). The electrode surface of the piezoceramic is separated into two electrically isolated areas (Figure 2). One electrode area serves as the actuator and the second area serves as a sensor. The control laws are implemented digitally with a sampling rate of 1000 Hz using a Systolic Systems' Optima 3 digital controller and response data is collected using a Tektronix 2630 Fourier Analyzer (Tektronix Inc., Campbell, CA).

An open loop SISO pole zero model is identified using a recursive lattice structure (RLS) identification program which is part of the Tektronix software package. In this SISO model, both the disturbance input and sensor output are at rib 1. The model includes frequencies from 0 to 20 Hz and a cluster of five closely spaced modes is identified between 9.6 and 17 Hz. Not included in this model are the repeated natural frequencies, the second cluster of modes between 30 and 40 Hz and subsequent higher modes. The first cluster corresponds to each individual rib vibrating in its first mode and the second cluster corresponds to each rib vibrating in its second mode. The repeated natural frequencies can only be identified with a

complete MIMO identification. A constrained optimization routine is used to design the controller parameters H_c , Λ_{c1} , Λ_{c2} and Λ_{c3} . The optimization minimizes the cost function:

$$J = \int_0^T (|y(t)| + w|u(t)|) dt \quad (29)$$

where $y(t)$ is the antenna response to a unit impulse and $u(t)$ is the control effort. Values for the weight w are adjusted to achieve the best trade off between minimizing the impulse response and minimizing the control effort.

In the control design each actuator is capable of having multiple filters associated with it, i.e., in the matrices $\Lambda_{c1}(r \times r)$ and $\Lambda_{c2}(r \times r)$, r is not necessarily one. Using the PPF control, the optimization is performed on the SISO model, both using one control filter and using two control filters. It is found that no significant reduction in the cost function is obtained using multiple filters. This can be attributed to the fact that the five modes are closely spaced and the model does not include higher frequency modes. Therefore, only a single filter per actuator is used in the final design. Table 1 lists the optimized parameters for the AVA and PPF controller and the optimization weight w .

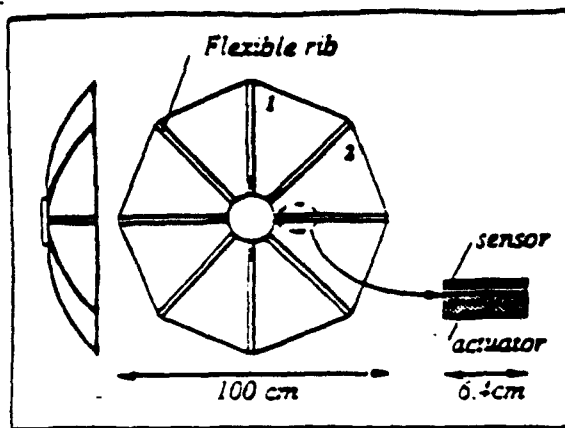


Figure 2. Schematic of the experimental smart antenna.

The optimization of the control parameters is based on the rib 1 SISO transfer function. When the MIMO control is implemented experimentally, control parameters found from the rib 1 optimization are used on all of the controlled ribs. Thus the matrices H_{rib} and B_{rib} , Λ_{rib} and Λ_{rib} are diagonal matrices respectively of the form $\text{diag}(h_1, h_2, \dots)$, $\text{diag}(b_1, b_2, \dots)$, $\text{diag}(\omega_1^2, \omega_2^2, \dots)$ and $\text{diag}(2\zeta_1\omega_1, 2\zeta_2\omega_2, \dots)$ where h_i , b_i , ω_i^2 , $2\zeta_i\omega_i$ are the control parameters from SISO rib 1 optimization.

Table 1: Optimized control parameters based on rib 1 SISO model ($\Lambda_{\text{rib}} = \omega_i^2$, $\Lambda_{\text{rib}} = 2\zeta_i\omega_i$ and $w = \text{weight}$).

	PPF	AVA
ω_i	70.2	118.9
ζ_i	0.56	0.499
w	1	2.5

4. CLOSED LOOP TEST RESULTS

Three different active control schemes are implemented on the smart antenna to compare their performance. All of the control strategies have the same objective: to increase damping in the modes contained in the 9 to 18 Hz frequency range. The first design involves a single Positive Position Feedback filter sensing and actuating on rib 1. The second design also uses collocated control on rib 1, but the compensator is an Active Vibration Absorber. Finally, a multi-input-multi-output PPF controller is implemented on ribs 1 and 2.

Single-Input-Single-Output Control

Using the parameters obtained from the optimization algorithm (shown in Table 1), a single PPF controller is implemented on the collocated sensor/actuator pair located on rib 1. Open and closed loop magnitude plots are shown below in Figure 3. This single controller increases the damping in all of the modes, illustrated by the rounded peaks of the closed loop magnitude response.

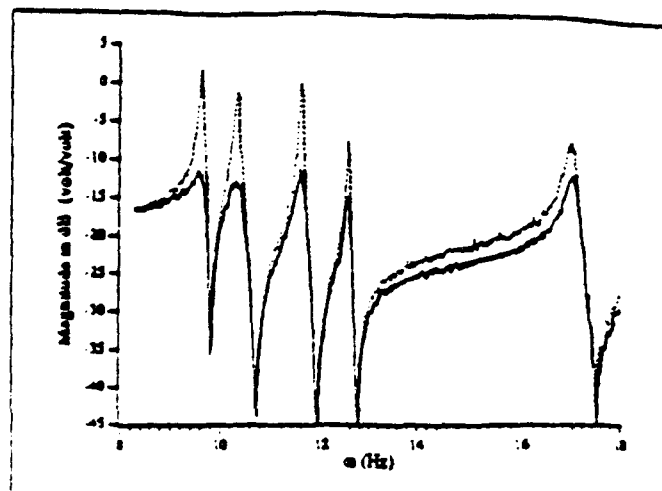


Figure 3: Experimental open (dotted) and closed loop (solid) transfer functions for SISO PPF on the smart antenna.

A second SISO controller of the AVA type is implemented using collocated control on rib 1. For this design, a high frequency instability at approximately 300 Hz occurs when the gain is set to the optimal value. The primary reason for the instability is that the digital implementation of the controller causes a phase loss at the higher frequencies. Since the magnitude of the AVA filter does not roll-off, it is sensitive to unmodelled dynamics. The system is stabilized by setting the gain to approximately half the optimal value.

The damping ratios for the closed-loop systems are obtained by curve fitting the frequency responses using the STAR Modal Analysis package (Structural Measurement Systems, Milpitas, CA). Except for the mode at 17 Hz, the PPF controller increases the damping more than the AVA filter. In the lowest two modes, the PPF controller increases the damping almost twice as much. This result is due to the fact that the gain for the AVA design is not set to its optimal value because of the 300 Hz instability. Thus, the constant gain magnitude at high frequencies limits the performance of the AVA controller.

Table 2: Closed loop natural frequencies and damping ratios for SISO AVA and PPF control. Disturbance and sensor are both at rib 1. Open loop results are shown for comparison.

Open Loop		AVA		PPF	
ω	$\zeta(\%)$	ω	$\zeta(\%)$	ω	$\zeta(\%)$
9.61	0.19	9.61	0.61	9.67	1.23
10.32	0.37	10.31	0.84	10.32	1.54
11.56	0.16	11.56	0.51	11.58	0.72
12.55	0.13	12.53	0.33	12.55	0.44
16.97	0.51	17.00	0.84	17.02	0.73

Multiple-Input-Multiple-Output

The SISO results indicate that an increase in damping is obtained using collocated PPF or AVA control. Unfortunately, controlling one rib of the antenna does not adequately address the problem of having repeated natural frequencies with linearly independent eigenvectors. This difficulty is illustrated by closing the PPF control loop around rib 1 and obtaining a transfer function between ribs 1 and 2 (Figure 4). Although it is not evident from the collocated transfer function, there are

two closely spaced modes in the region of 9.68 Hz. One of the modes is well damped and the other is still lightly damped.

The problem of controlling these repeated natural frequencies is addressed by implementing a Multi-Input-Multi-Output (MIMO) controller. Since PPF does not suffer from the high frequency instability problem of AVA, it forms the basis for the two-input-two-output design. The PPF controller designed for rib 1 is implemented using collocated feedback on both ribs 1 and 2. A closed loop transfer function between ribs 1 and 2 is also shown in Figure 4. Not only do all the modes show an increase in damping, both modes at 9.69 Hz are attenuated. Curvefitting values are consistent with this result. With only a single control loop closed, one of the modes at 9.69 Hz has only light damping. Implementing the MIMO design increases damping in this mode from 0.28 % to 1.11 % (Table 3).

Table 3: Closed loop natural frequencies and damping ratios for SISO and MIMO PPF. Disturbance located at rib 1 and sensor is at rib 2.

SISO PPF		MIMO PPF	
ω	ζ (%)	ω	ζ (%)
9.68	0.28	9.55	1.11
9.69	1.16	9.75	1.24
11.59	0.84	11.58	1.43
12.56	0.32	12.55	0.32
17.03	0.76	16.99	0.92

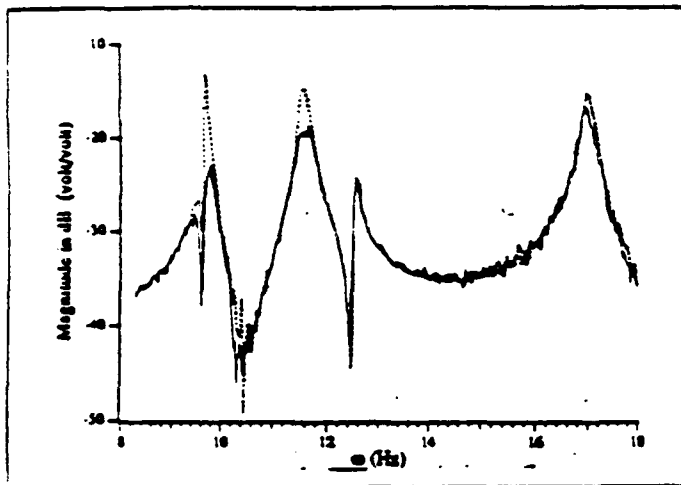


Figure 4: Transfer function between a disturbance at rib 2 and the sensor at rib 1. Dotted line is SISO PPF on rib 1, solid line is MIMO PPF on ribs 1 and 2.

5. CONCLUSIONS

A study in the control of an eight ribbed smart antenna was performed. Vibration suppression was difficult for this structure since it contained closely spaced and repeated natural frequencies. Open loop transfer functions show that six lightly damped structural modes lie in the frequency range 9 to 18 Hz. Further tests revealed that the first mode at 9.7 Hz was actually a repeated natural frequency that was only visible when exciting rib 2 and sensing at rib 1.

Two separate control strategies were studied, Positive Position Feedback and Active Vibration Absorbers. The general

framework for these second order controllers was developed and the similarities and differences of the two methods were discussed. Theoretical stability bounds were also derived, with PPF control being conditionally stable and AVA control being unconditionally stable. An important difference between the two types of control was that a PPF filter rolls off at high frequencies while the AVA controller maintains a constant gain. The roll off characteristic of PPF is an advantage since it makes it less sensitive to unmodelled dynamics. In real systems, the stability of the AVA control is determined by the high frequency response of the structure, which is often not known with any accuracy.

Both types of control were successfully implemented on the smart antenna. The performance of PPF and AVA were compared to a SISO design using one active rib. Each design consisted of only one second-order controller since numerical simulations indicated that there was no significant advantage using multiple filters. Both types of control were able to increase the damping in the target modes. PPF control produced better results since it was not limited by unmodelled dynamics. Unfortunately, the SISO controller did not adequately address the problem of repeated natural frequencies. A MIMO controller was implemented using PPF control on ribs 1 and 2. Not only did not the MIMO control improve the overall performance, it was able to add damping to a repeated mode at 9.7 Hz.

Acknowledgments

The authors are thankful for the support of AFOSR grant number 91-081 under the direction of Dr. Spencer Wu and a NASA grant number NGT 50541 under the guidance of Dr. Keith Belvin.

References

- [1] Dosch, J.J., Inman, D.J. and Garcia, E., "A Self-Sens Piezoelectric Actuator for Collocated Control," *Journal of Intelligent Materials and Structures*, Vol. 3 No. 1, January 1992.
- [2] Fanson, J.L., and Caughey, T.K., "Positive Position Feedback Control for Large Space Structures," *Proceedings 28th AIAA Structures Structural Dynamics and Materials Conference*, Monterey, CA, 1987, pp. 588-598.
- [3] Juang, J.-N., Phan, M., "Robust Controller Design for Second Order Dynamic Systems: A Virtual Passive Approach," *Proceedings 32nd AIAA Structures Structural Dynamics and Materials Conference*, 1991, pp. 1796-1805.
- [4] Belvin, W.K., L.G. Horta and K.B. Elliot, "The LaRC Phase-0 Evolutionary Model Test Bed - Design Experimental Results," *Proceedings of the 4th Ann NASA/DoD Conference on Control/Structure Interaction*, Orlando, FL, Nov., 1990.
- [5] Kerr, T.H., "Misstatements of the Test for Positive Semidefinite Matrices," *AIAA Journal of Guidance, Control, and Dynamics*, vol. 13, no. 3, 1990, pp. 571-572.

APPENDIX C
Papers Produced in the 3rd Year

CONVEX CONTROLLER DESIGN FOR VIBRATION SUPPRESSION OF A FLEXIBLE ANTENNA

Donald Leo
Research Assistant
State University of New York at Buffalo
Buffalo, NY 14260

Daniel Inman
Samuel Herrick Professor
Virginia Polytechnic Institute and State University
Blacksburg, VA 24061-0219

ABSTRACT

A procedure based on convex optimization is used to design collocated control laws for a small-scale model of a flexible antenna. The objective of the active control is to minimize the response of a single rib to a disturbance occurring at a remote location on the structure. Two separate designs are examined. The first is standard Linear Quadratic Gaussian (LQG) control, whereby the H_2 norm of the transfer matrix is minimized via the solution of two Riccati equations. Unfortunately, this type of design does not exploit the favorable attributes of sensor/ actuator collocation, resulting in control laws that are not robust to model uncertainty and structural variations. An optimization approach to H_2 optimal design is presented that bounds the phase of the control law, thereby increasing its robustness. The optimization is shown to be convex, providing important guarantees on solution accuracy and convergence. Control laws designed with both procedures are experimentally implemented on the antenna testbed. The results illustrate the advantages of designing H_2 optimal controllers that are bounded in phase.

INTRODUCTION

Active control of structures such as flexible ribbed antennae is complicated by the high modal density that results from mode localization. Mode localization is a function of the coupling between the individual ribs of the antenna and is very sensitive to structural imperfections and variations [Levine-West and Salama (1993)]. This phenomenon creates clusters of closely spaced and repeated modes, making the design of active control systems a more complicated process [Garcia, Dosch, and Inman (1992); Dosch, Leo, and Inman (1992)]. Since the mode shapes and natural frequencies of the antenna are sensitive to small structural changes, control law robustness is a priority. Increasing the robustness of the control law motivates the use of sensors and actuators that are collocated with one another, thereby assuring that all modes are in phase between the control input and the sensor output. This attribute of collocated control is exploited by designing Single-Input-Single-Output (SISO) control laws that are bounded in phase. Bounding the phase of the control law insures robustness to certain structural uncertainties such as inaccurate characterization of the structural damping.

Unfortunately, many optimal control techniques do not take advantage of the phase properties that exist when sensors and actuators are collocated with one another. One common design method is Linear Quadratic Gaussian (LQG) control, which minimizes the H_2 norm of the outputs due to white noise disturbances [Maciejowski (1989)]. The performance objective specified by LQG control is relevant to many control problems, since minimizing the H_2 norm is equivalent to minimizing the Root Mean Square response to a white noise disturbance in all inputs [Boyd and Barratt (1991)]. In general, though, LQG control can exhibit arbitrarily poor stability margins [Doyle (1978)]. Even for the case of collocated sensors and actuators, LQG synthesis can produce controllers that are sensitive to variations in the natural frequencies and damping ratios of the structure [Friedman and Bernstein (1993)].

The approach taken in this paper is to frame the LQG problem as a constrained convex optimization. The constraint on the optimization forces the phase of the SISO control law to lie within certain regions of the complex plane, essentially bounding the phase of the compensator's transfer function. When used in conjunction with collocated sensors and actuators, the control law exhibits increased stability robustness.

The constraint is applied to a convex optimization that minimizes the H_2 norm of the closed-loop transfer matrix. The optimal feedback control law is obtained via the solution of a finite dimensional optimization. Since the cost function and constraints of the optimization are convex, the global minimum can be found to any desired degree of accuracy if a feasible solution exists. Techniques for solving such optimal control problems are outlined in a recent monograph by Boyd and Barratt (1991).

CONSTRAINED LINEAR QUADRATIC GAUSSIAN SYNTHESIS

PROBLEM DESCRIPTION

Consider the block diagram of a dynamic system illustrated by Figure 1. The system is assumed to be linear and time invariant, with a set of exogenous inputs, $w(t)$, and a set of control inputs, $u(t)$. The regulated outputs are denoted $z(t)$ and the sensor outputs are denoted $y(t)$. All inputs and outputs are multivariable, with dimensions n_w , n_u , n_z , and n_y , respectively.

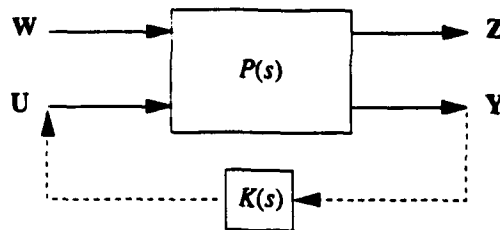


Figure 1: Block diagram of a multivariable system, illustrating the feedback connection.

The open loop system is described in the Laplace domain by a set of four transfer matrices, $P_{zw}(s)$, $P_{zu}(s)$, $P_{yw}(s)$, and $P_{yu}(s)$, where s is the Laplace variable. The subscripts denote the input/output pair of the transfer matrix. The set of equations for the open loop dynamics are

$$\begin{aligned} Z(s) &= P_{zw}(s)W(s) + P_{zu}(s)U(s) \\ Y(s) &= P_{yw}(s)W(s) + P_{yu}(s)U(s) \end{aligned} \quad (1)$$

$Z(s)$, $Y(s)$, $W(s)$, and $U(s)$ are the Laplace transforms of $z(t)$, $y(t)$, $w(t)$, and $u(t)$, respectively. By substituting the feedback connection

$$U(s) = K(s)Y(s) \quad (2)$$

into equation (1), the expression for the closed-loop transfer matrix between $z(t)$ and $w(t)$ is found to be

$$Z = \left[P_{zw} + P_{zu}K(I - P_{yu}K)^{-1}P_{yw} \right] W. \quad (3)$$

The Laplace notation has been dropped for convenience. The expression in brackets is denoted H , and represents an $n_z \times n_w$ complex matrix. The standard LQG problem is to minimize the H_2 norm of the closed loop transfer matrix by searching over all K that stabilize H . This problem can be solved by the solution of a Kalman filter problem and a linear quadratic regulator [Maciejowski (1989)]. Our objective is to constrain the controller to have a phase bounded by -180° and 0° while simultaneously minimizing the H_2 norm of certain closed loop transfer matrices.

To understand the motivation for constraining the phase of K , examine the second order equations of motion for a flexible structure. Under the assumption of modal damping, the equations of motion can always be decoupled into

$$I\ddot{r}(t) + \Delta\dot{r}(t) + \Lambda r(t) = \Phi u(t), \quad (4)$$

where $r(t)$ is the vector of modal coordinates, I is an appropriately sized identity matrix, and Φ is a vector of modal participation factors. The matrix Δ is a diagonal with entries $2\zeta_i\omega_i$, where ζ_i is the i^{th} modal

damping ratio and ω_i is the i^{th} natural frequency. The matrix Λ is also diagonal, with entries ω_i^2 . All modal damping ratios and natural frequencies are assumed to be greater than zero, therefore no rigid body or marginally stable modes exist. In this paper, we assume that only a single actuator and sensor are available for feedback control, i.e. $n_y = n_u = 1$. If collocated displacement sensors are used for feedback control, the output equation is

$$y(t) = \Phi^T r(t). \quad (5)$$

By combining equations (4) and (5), the transfer function $P_{yu}(s)$ is

$$P_{yu}(s) = \sum_{i=1}^{n_r} \frac{\phi_i^2}{s^2 + 2\zeta_i \omega_i s + \omega_i^2}, \quad (6)$$

where n_r is the number of modal coordinates, $r(t)$, and ϕ_i is the i^{th} entry of Φ . Equation (6) can be separated into real and imaginary parts by substituting $s = j\omega$ into the expression for $P_{yu}(s)$. This results in

$$P_{yu}(j\omega) = \sum_{i=1}^{n_r} \phi_i^2 \left\{ \frac{(\omega_i^2 - \omega^2) - j(2\zeta_i \omega_i \omega)}{(\omega_i^2 - \omega^2)^2 + (2\zeta_i \omega_i \omega)^2} \right\}. \quad (7)$$

The important feature of equation (7) is that the imaginary part of $P_{yu}(j\omega)$ is always negative for positive ω . This bounds the phase of the transfer function to be between -180° and 0° . Assume for a moment that the phase of the controller is also bounded between -180° and 0° . An application of the Nyquist stability criterion reveals that an encirclement of the $\{1,0\}$ point in the complex plane (remember, we have assumed positive feedback) is only possible at the point $\omega = 0$. At zero frequency, the gain of $P_{yu}(j\omega)K(j\omega)$ is

$$P_{yu}(j0)K(j0) = K(j0) \sum_{i=1}^{n_r} \frac{\phi_i^2}{\omega_i^2}. \quad (8)$$

Equation (8) must be less than one for stability, and the inverse of its value represents the gain margin of the system.

A CONVEX OPTIMIZATION APPROACH TO H_2 MINIMIZATION

We now turn to the problem of forming the H_2 control problem as a convex optimization. As mentioned before, the standard LQG solution is found by solving two Riccati equations. In order to constrain the phase of K , we will need to find convex functionals that represent the H_2 norm of the closed loop transfer matrix. To do so, we first examine the expression for H . Referring to equation (3),

$$H = P_{zw} + P_{zu}K(I - P_{yu}K)^{-1}P_{yw}. \quad (9)$$

After introducing the expression

$$Q = K(I - P_{yu}K)^{-1} \quad (10)$$

into equation (9), the closed loop transfer matrix is written as

$$H = P_{zw} + P_{zu}QP_{yw}. \quad (11)$$

Since the system is open loop stable, placing any stable matrix Q into equation (11) will result in a stable closed-loop. This is the Q (or Youla) parameterization of all stabilizing controllers [Maciejowski (1989)]. Introducing equation (10) into the expression for H transforms the H_2 minimization problem into one of

finding a stable Q that minimizes the 2-norm of the closed-loop transfer matrix. As stated, this is an infinite dimensional optimization problem, since theoretically we must search over every stable Q to find the minimizer. To transform this into a finite dimensional optimization, the approximation

$$Q = \sum_{i=1}^{n_r} x_i Q_i \quad (12)$$

is substituted into equation (11). Once this is done, the expression for the 2-norm of the transfer matrix can be written as [see pg. 271 of Boyd and Barratt (1991)]

$$\|H\|_2 = (\mathbf{x}^T \mathbf{A} \mathbf{x} + \mathbf{b}^T \mathbf{x} + c)^{\frac{1}{2}}, \quad (13)$$

where \mathbf{A} is a symmetric positive definite matrix, c is a real scalar constant greater than or equal to zero, and $\mathbf{x} = \{x_1, x_2, \dots, x_{n_q}\}^T$. Equation (13) is quadratic in the design vector \mathbf{x} , therefore it is convex. By introducing the series approximation to Q into the optimization, we have transformed the problem from a search over an infinite number of stable transfer matrices to one over a finite number of real variables. A more detailed treatment of this section is found in Boyd and Barratt (1991).

BOUNDING THE PHASE OF $K(j\omega)$: A CONVEX CONSTRAINT

The previous section established that the H_2 norm of the closed-loop transfer matrix is expressed as a quadratic function of a finite number of real variables. This section will use the same parameterization of all stabilizing controllers to define another convex function that bounds the phase of the controller, K . Solving equation (10) for K yields

$$K = \frac{Q}{1 + QP_{yu}} \quad (14)$$

The matrix notation has been dropped to emphasize that this analysis is only valid for control systems with one sensor and actuator ($n_y = n_u = 1$). Let us introduce the following notation for the real and imaginary parts of Q and P_{yu} ,

$$\begin{aligned} Q(j\omega) &= R_Q(\omega) + jI_Q(\omega) \\ P_{yu}(j\omega) &= R_P(\omega) + jI_P(\omega) \end{aligned} \quad (15)$$

Separating equation (14) into real and imaginary parts yields

$$K = \frac{[R_Q + (R_Q^2 + I_Q^2)R_P] + j[I_Q - (R_Q^2 + I_Q^2)I_P]}{(1 + R_Q R_P - I_Q I_P)^2 + (I_Q R_P + R_Q I_P)^2}, \quad (16)$$

where the ω notation has been dropped. Introducing equation (12) into equation (16), the real and imaginary parts of Q are written in vector notation as

$$\begin{aligned} I_Q &= \sum_{i=1}^{n_r} x_i I_{Q_i} = \mathbf{I}_{Q_i}^T \mathbf{x} \\ R_Q &= \sum_{i=1}^{n_r} x_i R_{Q_i} = \mathbf{R}_{Q_i}^T \mathbf{x} \end{aligned} \quad (17)$$

Upon examining equation (16), it is clear that since the denominator is simply a sum of squared terms, the sign of the real and imaginary parts of K is determined by the numerator. Substituting the previous expression into the numerator of equation (16) produces a quadratic expression in x ,

$$\begin{aligned} & \mathbf{R}_{Q_i}^T \mathbf{x} + \mathbf{R}_p \mathbf{x}^T \mathbf{E} \mathbf{x} + j(\mathbf{I}_{Q_i}^T \mathbf{x} - \mathbf{I}_p \mathbf{x}^T \mathbf{E} \mathbf{x}) \\ & \mathbf{E} = \mathbf{R}_{Q_i} \mathbf{R}_{Q_i}^T + \mathbf{I}_{Q_i} \mathbf{I}_{Q_i}^T \geq 0 \end{aligned} \quad (18)$$

Equation (18) reveals that bounding the sign of the real and imaginary parts of the controller is expressed as a quadratic constraint of the design variables x . For collocated displacement feedback, we want to bound the phase of K to lie between 0° and -180° for all positive ω , which is equivalent to

$$\mathbf{I}_{Q_i}^T \mathbf{x} - \mathbf{I}_p \mathbf{x}^T \mathbf{E} \mathbf{x} \leq 0 \text{ for all } \omega > 0. \quad (19)$$

EXPERIMENTAL TESTBED

FLEXIBLE ANTENNA MODEL

The convex optimization procedure is used to design active control laws for a small-scale model of a flexible ribbed antenna. The antenna is modeled after a similar structure that existed on the Phase 0 Evolutionary Model housed at NASA Langley Research Center [Belvin, *et al* (1990)].

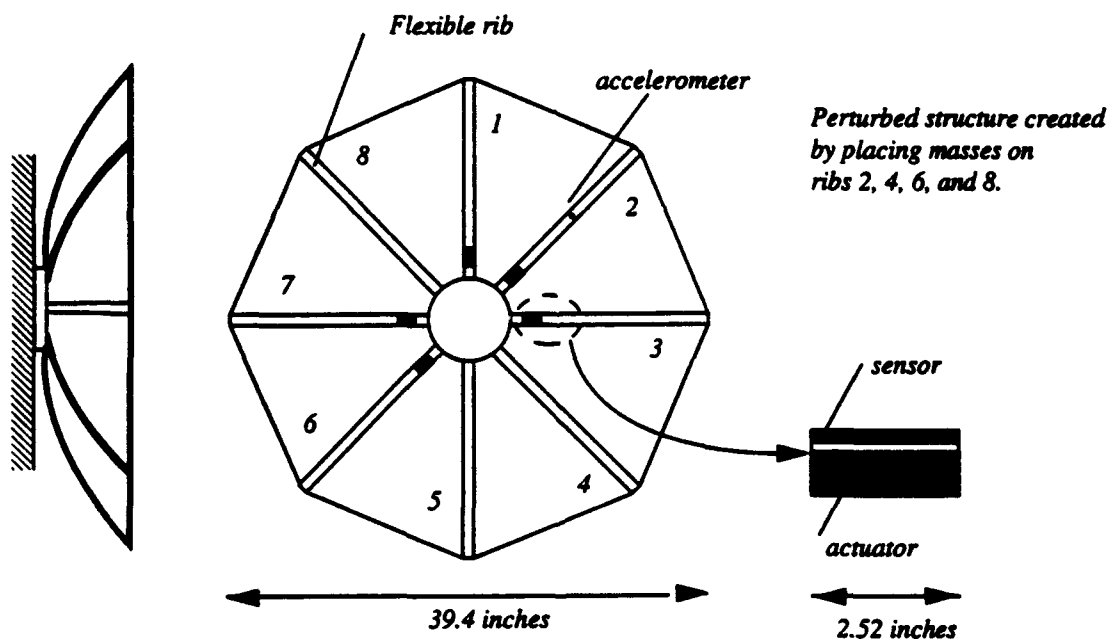


Figure 2: A schematic of the flexible antenna model illustrating the rib numbering scheme and the placement of the actuators and sensors.

The antenna model consists of eight beam-like ribs that are attached to a plastic hub [Figure 2]. The outer edges of the ribs are connected by metal wire which has been tensioned to give the antenna a parabolic shape. Five of the eight ribs have piezoceramic material [Piezoelectric Products material G1195] bonded near the clamped ends. Each ceramic is divided into two electrically isolated areas, the larger area is used as an actuator and the smaller area is used as a collocated sensor. The sensor signal from each piezoceramic is conditioned by passing it through an analog low pass filter with an input impedance of $10 \text{ M}\Omega$ and a corner frequency of $10,000 \text{ Hz}$. Due to the high input impedance, the output signal of the filter is a voltage proportional to the strain in the piezoceramic at frequencies greater than approximately 3 Hz . Strain is analogous to displacement in terms of its frequency response properties. The voltage into actuator ceramics is amplified by a Hewlett-Packard amplifier with a range of $\pm 50 \text{ volts}$.

The rest of the test equipment is as follows. Data acquisition is performed using a Tektronix 2630 Fourier Analyzer. A Kistler accelerometer is placed on rib 2 to measure vibrations. The digital control hardware consists of dSpace digital signal processing chips. The optimization routines used in the control design is written in Pro-Matlab on a Sun workstation.

CONTROLLER DESIGN

CONTROL OBJECTIVES

The objective of the active control is to reduce the vibrations of rib 2 to a disturbance occurring at a remote location on the antenna. The disturbance is provided by exciting the antenna with the actuator located on rib 1. Vibrations of rib 2 are measured with an accelerometer located at approximately half the length of the rib. The control system consists of the piezoceramic sensor/ actuator pair on rib 2.

MODELING OF THE FLEXIBLE ANTENNA

The first step in the control design is to obtain a model for the flexible antenna. In this paper, a modal approach is used, whereby the Multi-Input-Multi-Output (MIMO) is synthesized from a set of SISO transfer functions. The procedure is described in detail in Dosch, Leo, and Inman (1993). A brief overview is presented here.

First, SISO transfer functions are experimentally determined over the frequency range 5 Hz to 25 Hz. This frequency band is chosen because it contains the first eight flexible modes of the structure. This group of modes represents the motion of the antenna caused by each beam vibrating in its first mode. A second cluster of modes exists between 35 Hz and 45 Hz, but these are ignored in the modeling analysis and control design. For this paper, three SISO transfer functions are needed to produce a model for control design: input PZT rib 2/ output PZT rib 2, input PZT rib 2/ output PZT rib 1, and input PZT rib 2/ output accelerometer rib 2. These three transfer functions are modeled separately by curve fitting the individual transfer functions. This assures that the SISO models are accurate over the desired frequency range. Next, the individual transfer functions are separated into poles and residues and combined into a MIMO model. The final model is of the form

$$\begin{aligned} \ddot{\mathbf{r}} + \Delta \dot{\mathbf{r}} + \Lambda \mathbf{r} &= \Phi_{w_1} w_1 + \Phi_u u \\ \ddot{z}_2 &= \Phi_{z_2}^T \mathbf{r} + (0.085)u \\ \ddot{y} &= \Phi_y^T \mathbf{r} + (5 \times 10^{-7})u \end{aligned} \quad (20)$$

where

$$\begin{aligned} \Phi_u &= [10.1 \quad 2.5 \quad 3.8 \quad 2.8 \quad 4.2 \quad 6.4 \quad 6.4 \quad 7.9]^T \\ \Phi_{w_1} &= [-11.1 \quad 1.0 \quad -2.6 \quad 13.6 \quad 0.2 \quad 1.1 \quad -2.8 \quad 2.6]^T \\ \Phi_{z_2} &= [-1.2 \quad -0.4 \quad -1.4 \quad -0.8 \quad -0.6 \quad -1.7 \quad -1.4 \quad -1.7]^T \times 10^{-3} \\ \Delta &= \text{diag}[0.34 \quad 0.32 \quad 0.45 \quad 0.28 \quad 0.14 \quad 0.40 \quad 0.37 \quad 0.24] \\ \Lambda &= \text{diag}[1.25 \quad 0.62 \quad 0.55 \quad 0.50 \quad 0.48 \quad 0.44 \quad 0.37 \quad 0.35] \times 10^4 \end{aligned} \quad (21)$$

The direct transmission terms in equation (20) are necessary since certain transfer functions have the same number of poles and zeros in the frequency range 5 - 25 Hz. The assumption of proportional damping does introduce some error into the model, but greatly simplifies the modeling procedure. A model for the displacement of rib 2 is obtained by dividing the experimentally obtained transfer function by s^2 and placing it into the modal model shown above.

Equations (20) and (21) represent the model of the *nominal* structure. The control laws derived in the next section are also tested on a perturbed model of the antenna. The perturbed configuration is obtained by placing 15 gram masses on ribs 2, 4, 6, and 8. This has the effect of lowering the natural frequencies.

H_{ij} denotes the closed loop transfer function between z_i and w_j . The trade-off curve is obtained by solving the optimal feedback control problem

$$\begin{aligned} \min (\lambda_1 \phi_{\text{eff}}^2 + \lambda_2 \phi_{\text{perf}}^2)^{\frac{1}{2}} \\ \text{s.t. } \lambda_2 = 1 - \lambda_1 \end{aligned} \quad (25)$$

for $\lambda_1 \in (0,1)$. For each value of λ_1 , an LQG problem is solved via the two Riccati solution to obtain values of ϕ_{perf} and ϕ_{eff} . By varying λ_1 between 0 and 1, the whole design space is searched. The resulting trade-off curve is shown in Figure 4. The performance measures are normalized versus the open loop value of $\phi_{\text{perf}_ol} = 298.94 \mu\text{m}$.

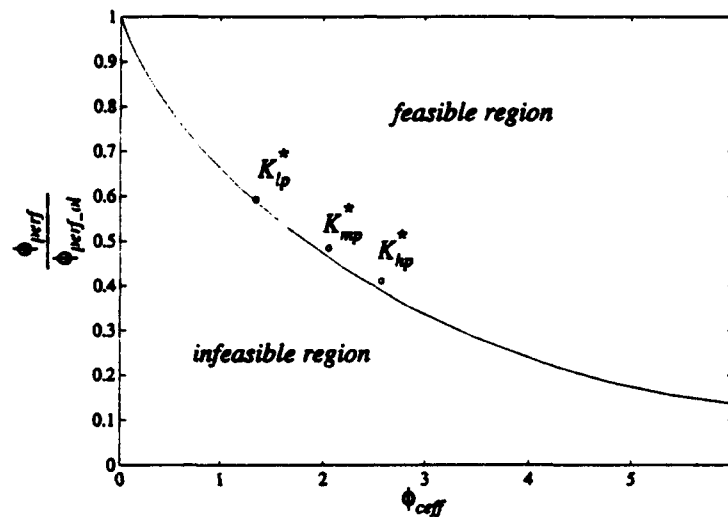


Figure 4: Trade-off curve for Linear Quadratic Gaussian control.

Figure 4 yields information regarding the achievable performance with LQG control. The trade-off curve is the boundary between feasible and infeasible solutions. All points 'above' the curve are achievable by some controller K , and none of the points 'below' the curve are achievable by any linear control law. For example, one cannot produce an 80% reduction in ϕ_{perf} (as compared to the open loop) without increasing ϕ_{eff} to at least 4.5. These guarantees on the optimal solution result from the fact that equation (25) is a convex optimization with respect to λ_1 .

Three LQG optimal controllers are chosen from the trade-off curve for implementation on the flexible antenna. Each represents an increasing level of performance and control effort. The first, K_{lp} , is designed for low performance and low control effort. The second, K_{mp} , is a controller that decreases the performance objective but uses more control effort. The final compensator, K_{hp} , exhibits the best expected performance without unduly increasing the control effort. The increase in performance obtained by implementing controllers which use more control effort is not worthwhile, as indicated by the trade-off curve for the LQG design. Table 1 lists the values of ϕ_{perf} and ϕ_{eff} for each of these control laws.

Table 1: Normalized performance measures, control effort, and size of the six optimal controllers.

LQG	$\frac{\phi_{\text{perf}}}{\phi_{\text{perf}_ol}}$	ϕ_{eff}	number of states	constr H_2	$\frac{\phi_{\text{perf}}}{\phi_{\text{perf}_ol}}$	ϕ_{eff}	number of states
K_{lp}	0.156	5.385	20	K_{lp}^*	0.412	2.573	10
K_{mp}	0.533	1.643	20	K_{mp}^*	0.487	2.051	14
K_{hp}	0.708	0.812	18	K_{hp}^*	0.595	1.346	15

CONSTRAINED H₂ MINIMIZATION

The constrained optimization approach to H₂ optimal design is also used to obtain control laws for the flexible antenna. To begin the procedure, we must first choose a set of Q functions for the approximation described by equation (12). For comparison, four sets of functions are chosen. This allows us to study the convergence properties of the optimal solution. The four sets of parameterizations are

$$\begin{aligned}
 \text{set 1: } & x_1 Q_{mp} + \sum_{i=2}^{30} x_i \left(\frac{100}{s+100} \right)^{i-1} & \text{set 3: } & x_1 Q_{mp} + \sum_{i=2}^{30} x_i \left(\frac{200}{s+200} \right)^{i-1} \\
 \text{set 2: } & x_1 Q_{hp} + \sum_{i=2}^{30} x_i \left(\frac{100}{s+100} \right)^{i-1} & \text{set 4: } & x_1 Q_{hp} + \sum_{i=2}^{30} x_i \left(\frac{200}{s+200} \right)^{i-1},
 \end{aligned} \tag{26}$$

where

$$Q_{mp} = \frac{K_{mp}}{1 - P_{yu} K_{mp}} \qquad Q_{hp} = \frac{K_{hp}}{1 - P_{yu} K_{hp}}. \tag{27}$$

Choosing the first Q function to correspond to one of the LQG optimal controllers improves the convergence properties of the solution. By choosing the functions in this manner, the controller that corresponds to the point $\mathbf{x} = [1 \ 0 \ 0 \ \dots \ 0]$ is either K_{mp} or K_{hp} , depending on parameterization. Increasing the number of basis functions beyond 30 results in only a negligible decrease in the cost function.

Once a set of Q functions is chosen, the following optimization is performed for each parameterization,

$$\begin{aligned}
 \min \phi_{perf}(\mathbf{x}) &= \left(\mathbf{x}^T \mathbf{A}_{perf} \mathbf{x} + \mathbf{b}_{perf}^T \mathbf{x} + c_{perf} \right)^{\frac{1}{2}} \\
 \text{s.t. } \phi_{ceff}(\mathbf{x}) &= \left(\mathbf{x}^T \mathbf{A}_{ceff} \mathbf{x} + \mathbf{b}_{ceff}^T \mathbf{x} + c_{ceff} \right)^{\frac{1}{2}} < \alpha \\
 \max \left[\mathbf{I}_{Q_i}^T(\omega_i) \mathbf{x} - I_p(\omega_i) \mathbf{x}^T \mathbf{E}(\omega_i) \mathbf{x} \right] &\leq -0.01.
 \end{aligned} \tag{28}$$

The optimizations are solved using a constrained ellipsoid algorithm. The termination criterion is chosen to be 1×10^{-6} , which indicates the calculated solution is within 1×10^{-6} of the actual solution.

The constraint on the phase, equation (18), is discretized with a 1000 frequency points between $\omega = 10$ and 1000 rad/s. In this sense, equation (18) can be thought of as a family of constraints, in which the maximum must be less than or equal to a constant. Since the maximum of a family of convex constraints is also convex, this method of determining the phase does not introduce any local minima into the design space. Discretizing the constraint in this manner does introduce numerical error into the optimization. For this reason, the constraint is forced to be less than -0.1, as opposed to zero. If this is not done, then the resulting optimal controller tends to violate the phase constraint at points not included in the discretization. Another option is to increase the number of frequency points (say to 2000), but this slows down the optimization considerably.

Another problem occurs for an optimization with such a large number of Q functions. Theoretically, \mathbf{A}_{perf} and \mathbf{A}_{ceff} should always be positive definite symmetric matrices, but numerical error in the solution of the Lyapunov equations causes them to have very small negative eigenvalues (on the order of -1×10^{-13}). These errors then cause problems during the solution of equation (28). To eliminate this problem, a small diagonal matrix is added to \mathbf{A}_{perf} and \mathbf{A}_{ceff} to change the lowest eigenvalue to a quantity just greater than zero (on the order of 1×10^{-13}). The optimization is then solved with the new matrices.

As in the case of LQG synthesis, three controllers with varying performance levels are designed. They are designated K_{lp}^* , K_{mp}^* , and K_{hp}^* . The amount of performance increase is controlled by varying α in equation (28). Increasing α allows for greater control effort, which in turn lets the optimization reduce the

performance objective. The values of ϕ_{perf} and ϕ_{eff} for the three controllers are listed in Table 1. They are also plotted in Figure 4 with the LQG trade-off curve. As expected, the controllers designed with the phase constraint lie 'above' the trade-off curve. They also exhibit worse performance than an LQG controller that uses the same amount of control effort. This again is to be expected, since the optimization that bounds the phase includes constraints that are not present in standard LQG synthesis.

Comparing the convergence properties of the different Q parameterizations reveals that set 1 consistently produces the lowest performance functions for a given control effort constraint (i.e. a given α). The fact that the optimization results are a function of the parameterization is not surprising, but the variation in results is unexpected. Sets 1 and 3 outperform sets 2 and 4 in all of the studies, with set 1 producing slightly lower cost functions at the optimum. Also unexpected is the fact that setting $\alpha > 2.6$ produced no change in the optimal solution. One would think that the optimal solution would lie on the control effort constraint, but this does not occur. The reason for this could be convergence difficulties in the optimization procedure.

After solving the constrained optimization, the corresponding optimal controller is obtained from the expression

$$K^* = \frac{\sum_{i=1}^{30} x_i^* Q_i}{1 + \left(\sum_{i=1}^{30} x_i^* Q_i \right) P_{yu}}, \quad (29)$$

where x_i^* are the elements of the solution to equation (28). On the average, these control laws contain 70 to 75 states. Balanced reduction [Glover (1984)] is attempted, but does not yield significant order reductions without considerably distorting the frequency response of the controller. A more straightforward pole-zero cancellation produces better results. The i^{th} pole is canceled with the j^{th} zero if

$$\frac{|p_i - z_j|}{p_i} < 0.01 \quad (30)$$

Setting the tolerance much higher than 0.01 changes the frequency response of the optimal controller considerably by canceling out pole zero combinations that are not too 'close' to one another. After canceling out pole and zeros that satisfy equation (30), the controllers are reduced to between 10 and 15 states [Table 1].

EXPERIMENTAL RESULTS

All of the control laws are implemented on the flexible antenna model to test their performance and robustness. Each is implemented in real-time on the dSpace digital control hardware sampling at 2000 Hz. This sampling rate is deemed fast enough so that no digital effects are accounted for in the controller design.

Closed-loop transfer functions are obtained by inputting white noise into the actuator on rib 1 and measuring the output of the accelerometer located at the mid span of rib 2. Closed-loop performance is measured in terms of the integral

$$\pi = \left(\int_5^{25} \left| \frac{H_{21}(j\omega)}{\omega^2} \right|^2 d\omega \right)^{\frac{1}{2}}, \quad (31)$$

where $H_{21}(j\omega)$ is the experimentally determined transfer function. Equation (31) is similar to an H_2 norm, and it is a convenient measure of the size of the transfer function over the frequency range 5 - 25 Hz. For an unstable system, π is set to ∞ .

ACTIVE CONTROL OF THE NOMINAL AND PERTURBED STRUCTURES

All six control laws are implemented on the antenna model. Table 2 summarizes the closed-loop results in terms of the performance measure, equation (31). For the nominal structure, each of the control laws designed with the constrained optimization are stable in the closed loop. For the control laws designed with standard LQG synthesis, only the low and medium performance controllers remain stable. The high performance controller causes an instability at approximately 11 Hz.

The robustness of the phase constrained controllers is even more pronounced when comparing performance on the perturbed antenna. For this case, both the medium and high performance LQG control laws are unstable in the closed-loop. The frequency of the instability is again 11 Hz. All of the controllers designed with constrained optimization remain stable. All of the control laws suffer a decrease in performance, but this is to be expected since the designs are performed with the nominal model.

Table 2: Closed loop active control results on the nominal and perturbed structures.

Nominal Structure $\pi_{ol} = 197.68 \times 10^{-6}$			
	π / π_{ol}		π / π_{ol}
K_{hp}	∞	K_{hp}^*	0.372
K_{mp}	0.521	K_{mp}^*	0.456
K_{lp}	0.673	K_{lp}^*	0.536
Perturbed Structure $\pi_{ol} = 132.05 \times 10^{-6}$			
	π / π_{ol}		π / π_{ol}
K_{hp}	∞	K_{hp}^*	0.555
K_{mp}	∞	K_{mp}^*	0.641
K_{lp}	0.803	K_{lp}^*	0.708

DISCUSSION OF THE EXPERIMENTAL RESULTS

The experimental results illustrate the utility of the phase constrained H_2 optimization procedure outlined in this paper. Constraining the optimization produces control laws that are less sensitive to modeling errors and structural variations. The instabilities caused by the high performance LQG controller indicate that it is not very robust. In controlling the unperturbed structure, LQG synthesis and constrained optimization produce similar closed-loop performance. Due to the accuracy of the nominal model used for control design, the predicted performance and the experimental results agree well. When implementing the control laws on the mass-loaded antenna, the reduction in the natural frequencies causes the medium performance LQG design to induce closed-loop instability.

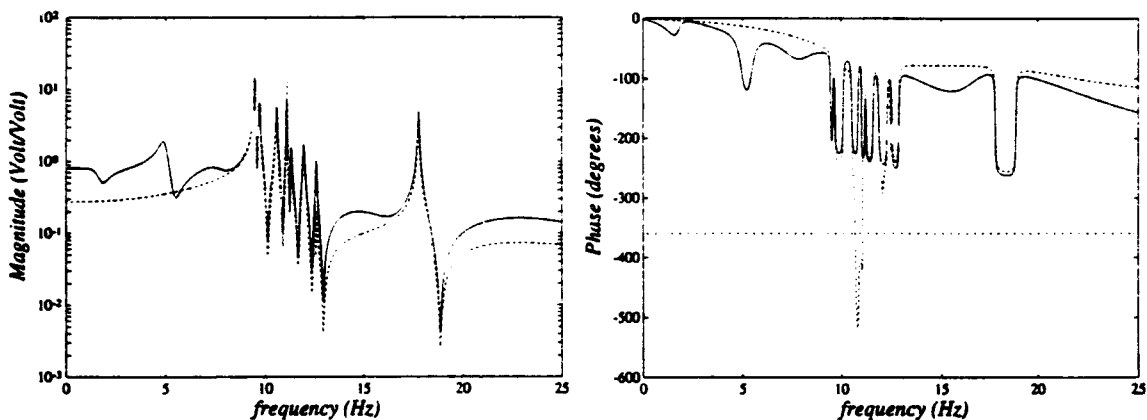


Figure 5: Magnitude and phase plots of $K_{mp}^*(j\omega)P_{yu}(j\omega)$ (solid), and $K_{mp}(j\omega)P_{yu}(j\omega)$ (dashed).

Examination of the transfer functions $K_{mp}(j\omega)P_{yu}(j\omega)$ and $K_{mp}^*(j\omega)P_{yu}(j\omega)$ illustrate the advantage of constraining the phase of the controller [Figure 5]. For the medium performance LQG design, two cross-overs of -360° occur within the frequency range 5 to 25 Hz. From the Nyquist Stability Criterion, closed-

loop instability will result if the magnitude at phase cross-over exceeds one. As the structure is perturbed, the changes in the modal parameters cause the magnitude in this frequency region to exceed one, resulting in closed-loop instability. The instabilities that occur in experiments are at a frequency near 11 Hz, precisely the region where the phase of $K_{mp}(j\omega)P_{yu}(j\omega)$ crosses -360° . In contrast, the phase of $K_{mp}^*(j\omega)P_{yu}(j\omega)$ never crosses -360° between 0 and 25 Hz, making the control law insensitive to changes in the magnitude and phase response.

CONCLUDING REMARKS

Experimental implementation of H_2 optimal controllers designed via constrained convex optimization illustrated the robustness achieved by bounding the phase of the compensator. In comparison with standard Linear Quadratic Gaussian (LQG) designs, they remained stable in the presence of structural variations and model uncertainty. The loss of performance that resulted from constraining the optimization could be compared to a trade-off curve that represented all achievable LQG solutions. In this way, convex optimization proved to be an effective method of studying the trade-offs associated with constraining the phase of the controller.

Although the results of this paper are encouraging, many questions arose regarding the convex optimization approach to control design. For example, the optimal solutions were found to be sensitive to the choice of functions used in the Q parameterization. Furthermore, the optimization seemed to exhibit convergence properties when the constraint on the control effort became large. Checking the phase constraint at discrete points (even for a fine grid) introduced errors into the control design. Finally, the pole-zero cancellation procedure used in this paper was a rather ad hoc method of order reduction, the reasons why more advanced methods were ineffective needs to be investigated. Future work involves studying these topics and also generalizing the phase constraints to control systems with more than one sensor and actuator.

ACKNOWLEDGMENTS

This research was supported by AFOSR grant number 91-0181 under the direction of Dr. Spencer Wu.

REFERENCES

- Belvin, W.K., Horta, L.G., and Elliot, K.B., "The LaRC CSI Phase-0 Evolutionary Model Test Bed - Design and Experimental Results." *Proceedings of the 4th Annual NASA/DoD Conference on Control/Structure Interaction*, Orlando, FL, November 1990.
- Boyd, S. and Barratt, C., *Linear Controller Design: Limits of Performance*, Prentice-Hall, Englewood Cliffs, NJ, 1991.
- Dosch, J., Leo, D.J., and Inman, D.J., "Comparison of Vibration Control Schemes for a Smart Antenna," *Proceedings of the 31st Conference on Decision and Control*, Tucson, AZ, Dec. 1992, pp. 1815-1820.
- Dosch, J. J., D. J. Leo and D. J. Inman, "Modeling of a Smart Antenna for Active Vibration Suppression," *Eleventh International Modal Analysis Conference*, Orlando, Florida, February, 1993, pp. 1418-1424.
- Doyle, J.C., "Guaranteed Margins for LQG Regulators," *IEEE Transactions on Automatic Control*, vol AC-23, 1978, pp. 756-757.
- Friedman, J.H., and Bernstein, D.S., "Maximum Entropy Controller Synthesis for Collocated and Non-Collocated Systems," *Second Conference on Recent Advances in Active Control of Sound and Vibration*, Blacksburg, VA, April, 1993, pp. 327-338.
- Garcia, E., Dosch, J., and Inman, D.J., "The Application of Smart Structures to the Vibration Suppression Problem," *Journal of Intelligent Material Systems and Structures*, vol. 3, no. 4, Oct. 1992, pp. 659-667.
- Glover, K., "All Optimal Hankel-norm Approximations of Linear Multivariable Systems and their L_∞ Error Bounds," *International Journal of Control*, vol. 39, 1984, pp. 1115-1193.
- Levine-West, M.B., and Salama, M.A., "Mode Localization Experiments on a Ribbed Antenna," *AIAA Journal*, vol. 31, no. 10, Oct. 1993, pp. 1929-1937.
- Maciejowski, J.M., *Multivariable Feedback Design*, Addison-Wesley, New York, 1989.

LINEAR CONTROLLER DESIGN FOR STRUCTURES WITH UNCERTAIN TRANSIENT DISTURBANCES

Donald Leo*

State University of New York at Buffalo
Buffalo, NY 14260

Daniel Inman**

Virginia Polytechnic Institute and State University
Blacksburg, VA 24061-0219

Abstract

Convex optimization techniques are developed to design feedback control laws for structures with uncertain transient inputs. The uncertain disturbances are modeled deterministically as convex sets of functions. Three types of models are considered: one which bounds the total energy of the disturbance, another which bounds the instantaneous energy, and a third that limits the maximum and minimum values of the input. Expressions for the maximum response are derived for each model. The optimal feedback control law is found via the solution of an infinite dimensional optimization, which is reduced to a finite dimensional optimization by an affine parameterization of all stabilizing controllers. The parameterization maintains convexity and converges to the unique solution as the number of terms in the approximation is increased. The techniques are illustrated on a simple model of an unconstrained flexible structure.

Introduction

The objective of many structural control problems is minimization of the response due to uncertain transient inputs. In the case of satellite design, critical scientific instruments must be isolated from disturbances caused by other payloads on the structure; an automotive application might involve minimization of cabin noise level due to engine vibration; finally, reducing peak responses of structures is imperative in the earthquake engineering community due to safety considerations and legal requirements. For all of these examples, the uncertain nature of the excitation makes obtaining an explicit model for the inputs impossible. Oftentimes the disturbances can be bounded over their duration, even if the exact nature of the signal is unknown.

Several modern control methods have been developed to deal with the problem of uncertain disturbances. H_2 theory (also called Linear

Quadratic Gaussian theory) is concerned with optimal control when white noise disturbances are present in the plant and feedback signal¹. Minimizing the H_2 norm is equivalent to minimizing the Root Mean Square (RMS) value of the output. H_∞ control minimizes the RMS gain of a system disturbed by signals with finite energy². When the disturbances are persistent, it is more appropriate to minimize the L^1 norm of the impulse response function. This problem was posed by Vidyasagar³ and solved for continuous time control systems by Dahleh and Pearson⁴.

When the disturbances are transient with known duration, it would be advantageous to include that information in the design specifications. Unfortunately, H_2 , H_∞ , and L^1 control methods are not particularly suited to deal with information concerning the duration of the disturbance. Because the definition of the 1, 2, and ∞ norms is an integral from time equals zero to infinity, these measures of the output might be overly conservative if the disturbances are transient. Also, these techniques are usually applied with frequency design specifications, which do not always correspond to exact time domain constraints.

The purpose of this paper is to develop techniques for optimal disturbance rejection of unknown but bounded transient inputs. The following two assumptions are made: the duration of the inputs is known, and the disturbances are modeled deterministically, as sets of functionals. Modeling uncertain inputs deterministically is the subject of the first part of the paper. The approach is motivated by recent applications of convex analysis in applied mechanics⁵, and results relevant to control design are presented here. Obtaining the optimal feedback controller is an infinite dimensional optimization problem over all feasible transfer matrices⁶. The optimization is reduced to one over a finite dimensional subspace through the introduction of an affine parameterization of all stabilizing controllers.

*Research Assistant, Department of Mechanical and Aerospace Engineering, Student Member AIAA

**Samuel Herrick Professor, Engineering Science and Mechanics, Associate Fellow AIAA

The techniques are illustrated on a model of a simple flexible structure.

Problem Definition And Controller Parameterization

The system under consideration is assumed to be linear, time invariant, and described by the following equations

$$\begin{aligned} \dot{\hat{x}}(t) &= A\hat{x}(t) + B_w w(t) + B_u u(t) \\ z(t) &= C_z \hat{x}(t) + D_{zw} w(t) \\ y(t) &= C_y \hat{x}(t) + D_{yw} w(t) \end{aligned} \quad (1)$$

where $A \in \mathcal{R}^{n \times n}$ is the state matrix, $w(t) \in \mathcal{R}^{n_w}$ are exogenous disturbances, $u(t) \in \mathcal{R}^{n_u}$ are control forces, $z(t) \in \mathcal{R}^{n_z}$ are regulated outputs, and $y(t) \in \mathcal{R}^{n_y}$ are sensor outputs. The block diagram for this system is shown in Figure 1.

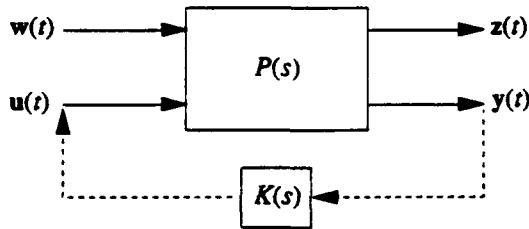


Figure 1: Block diagram for multivariable plant, illustrating the feedback connection.

In the Laplace Domain, the system is described by four transfer matrices, $P_{zw}(s)$, $P_{zu}(s)$, $P_{yw}(s)$, and $P_{yu}(s)$, where s is the Laplace variable. The subscripts denote the input/output pair of the transfer matrix. The feedback connection is

$$U(s) = K(s)Y(s), \quad (2)$$

where $K(s)$ is $n_u \times n_y$ transfer matrix of a linear time invariant controller. Optimal design of the control law is accomplished through the Q (or Youla) parameterization of all stabilizing controllers¹. First, the system is augmented by estimated state feedback [Figure 2]. The gains K_{sfb} and L_{est} are chosen such that $A - B_u K_{sfb}$ and $A - L_{est} C_y$ are stable. This could be done using Linear Quadratic Gaussian techniques, for example. The estimated state feedback is then augmented by another $n_u \times n_y$ transfer matrix, $Q(s)$. The input to $Q(s)$ is the state error, $e(t)$, and the output is injected into the system such that

$$u(t) = v(t) - K_{sfb} \hat{x}(t), \quad (2)$$

where $v(t)$ are the outputs of $Q(s)$ and $\hat{x}(t)$ are the state estimates.

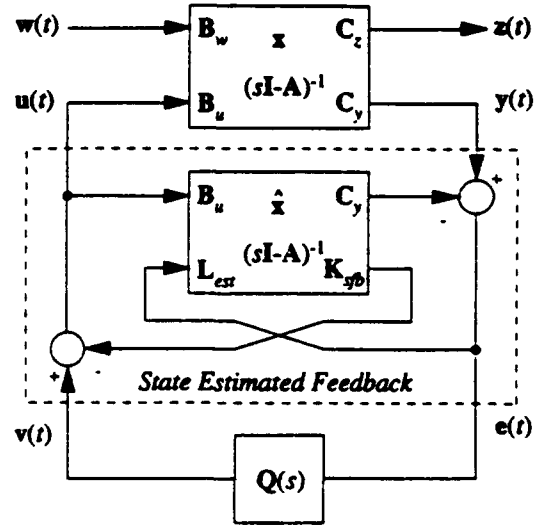


Figure 2: Estimated state feedback controller parameterization.

The augmented plant is now described by three transfer matrices, P_{zw} , P_{zw} , and P_{zv} . The transfer matrix P_{ve} is identically zero because the error states are uncontrollable from $v(t)$. The closed loop transfer matrix of the augmented plant is

$$H(s) = P_{zw}(s) + P_{zv}(s)Q(s)P_{ew}(s). \quad (3)$$

Stability of $H(s)$ is guaranteed if $Q(s)$ is a stable transfer matrix. The important feature of equation (3) is that it is affine in the free parameter $Q(s)$.

Disturbance Models

The uncertain excitations are modeled deterministically as either a finite set of known inputs or an infinite set of bounded but uncertain disturbances. The first disturbance model assumes that the uncertain excitations exist within a finite set of known inputs.

$$W_{FIN} = \{w_1(t), \dots, w_{n_i}(t)\}, \quad (4)$$

where n_i is the number of inputs. The second disturbance model bounds the maximum integral energy of the exogenous excitation.

$$W_{IEB} = \{w(t) : \int_0^T w^T(t)w(t)dt \leq \rho_I^2\} \quad (5)$$

It is assumed that the disturbance acts over a known duration, 0 to T . The scalar bound on the input energy is ρ_I^2 . A similar disturbance model is obtained by bounding the instantaneous energy of the input.

$$W_{LEB} = \{w(t) : w^T(t)w(t) \leq \rho_L^2(t)\} \quad (6)$$

The bound on the instantaneous energy is $\rho_L^2(t)$. A final disturbance model bounds the maximum and minimum values of the input, and is called the temporal envelope bound model.

$$W_{TEB} = \{w(t) : f_{Lj}(t) \leq w_j(t) \leq f_{Uj}(t)\} \quad (7)$$

The j^{th} column of $w(t)$ is denoted $w_j(t)$ and the upper and lower bounds on $w_j(t)$ are $f_{Lj}(t)$ and $f_{Uj}(t)$, respectively.

Maximum Responses To Uncertain Inputs

Assuming zero initial conditions, the regulated outputs are related to the exogenous disturbances through the convolution integral,

$$z(t) = \int_0^t h(t-\tau)w(\tau)d\tau, \quad (8)$$

where $h(t)$ is the inverse Laplace transform of $H(s)$.

Given a finite set of input disturbances, W_{FIN} , we denote the maximum response of the k^{th} output to the i^{th} disturbance as

$$\bar{z}_i^{(k)} = \int_0^{t_{max}} h^{(k)}(t_{max}-\tau)w_i(\tau)d\tau, \quad (9)$$

where $h^{(k)}(t)$ is the k^{th} row of h and t_{max} is the time at which the output attains its maximum.

For the remaining models of uncertainty, derivation of the maximum response is more involved. First consider the case of an Integral Energy Bound (IEB) excitation model (equation (5)). The maximum response of the k^{th} output to any input contained within the IEB model is found via the Cauchy-Schwarz Inequality. Referring to equation (8),

$$\int_0^t h^{(k)}(t-\tau)w(\tau)d\tau \leq \left[\int_0^t h^{(k)}(t-\tau)h^{(k)T}(t-\tau)d\tau \right]^{\frac{1}{2}} \times \left[\int_0^t w^T(\tau)w(\tau)d\tau \right]^{\frac{1}{2}} \quad (10)$$

The maximum output occurs when

$$w(\tau) \propto h^{(k)T}(t-\tau) = \gamma_I h^{(k)T}(t-\tau). \quad (11)$$

The scalar constraint γ_I is obtained by invoking the energy constraint, equation (9).

$$\gamma_I^2 \int_0^t h^{(k)}(t-\tau)h^{(k)T}(t-\tau)d\tau = \rho_I^2. \quad (12)$$

Solving for γ_I yields

$$\gamma_I = \frac{\rho_I}{\left[\int_0^t h^{(k)}(t-\tau)h^{(k)T}(t-\tau)d\tau \right]^{\frac{1}{2}}}. \quad (13)$$

The expression for the maximizing input function of the k^{th} output, $\bar{w}_I^{(k)}(t)$, for the IEB model is

$$\bar{w}_I^{(k)}(\tau) = \frac{\rho_I h^{(k)}(t-\tau)}{\left[\int_0^t h^{(k)}(t-\tau)h^{(k)T}(t-\tau)d\tau \right]^{\frac{1}{2}}}. \quad (14)$$

and the maximum output to an input constrained by equation (9) is

$$\bar{z}_I^{(k)}(t) = \rho_I \left[\int_0^t h^{(k)}(t-\tau)h^{(k)T}(t-\tau)d\tau \right]^{\frac{1}{2}}. \quad (15)$$

Through a simple substitution, equation (15) is rewritten

$$\bar{z}_I^{(k)}(t) = \rho_I \left[\int_0^t h^{(k)}(\tau)h^{(k)T}(\tau)d\tau \right]^{\frac{1}{2}}. \quad (16)$$

Next consider the disturbance model that bounds the instantaneous energy of the input, equation (6).

Following a derivation similar to that for the IEB model, the maximum response of the k^{th} output is obtained by using the Cauchy-Schwarz Inequality on the integrand of equation (8),

$$\mathbf{h}^{(k)}(t-\tau)\mathbf{w}(\tau)d\tau \leq \left[\mathbf{h}^{(k)}(t-\tau)\mathbf{h}^{(k)T}(t-\tau)d\tau \right]^{\frac{1}{2}} \times \left[\mathbf{w}^T(\tau)\mathbf{w}(\tau)d\tau \right]^{\frac{1}{2}} \quad (17)$$

The maximum occurs when

$$\mathbf{w}(\tau) = \gamma_L \mathbf{h}^{(k)T}(t-\tau), \quad (18)$$

where γ_L must satisfy

$$\gamma_L^2 \mathbf{h}^{(k)}(t-\tau)\mathbf{h}^{(k)T}(t-\tau) = \rho_L^2(\tau). \quad (19)$$

Combining equations (18) and (19) yields the maximizing input for the LEB convex model,

$$\bar{\mathbf{w}}_L(\tau) = \frac{\rho_L(\tau)\mathbf{h}^{(k)T}(t-\tau)}{\left[\mathbf{h}^{(k)}(t-\tau)\mathbf{h}^{(k)T}(t-\tau) \right]^{\frac{1}{2}}}. \quad (20)$$

The maximum output is

$$\bar{z}_L^{(k)}(t) = \int_0^t \rho_L(\tau) \left[\mathbf{h}^{(k)}(t-\tau)\mathbf{h}^{(k)T}(t-\tau) \right]^{\frac{1}{2}} d\tau. \quad (21)$$

The final disturbance model to be examined is the Temporal Envelope Bound (TEB) model, which is expressed by equation (7). For the j^{th} input, the maximum response of the k^{th} output is a function that switches between the maximum and minimum values, depending on the sign of the impulse response,

$$\bar{\mathbf{w}}_{Tj}(\tau) \begin{cases} = f_{Uj}(\tau) & \text{if } h_{kj}(t-\tau) > 0 \\ = f_{Lj}(\tau) & \text{if } h_{kj}(t-\tau) < 0 \end{cases} \quad (22)$$

The j^{th} column of $\mathbf{h}^{(k)}(t)$ is denoted $h_j^{(k)}(t)$. The maximum response to uncertain inputs bounded by equation (22) is

$$\bar{z}_T^{(k)}(t) = \sum_{j=1}^{n_w} \left\{ \int_0^t h_j^{(k)+}(t-\tau) f_{Uj}(\tau) d\tau + \int_0^t h_j^{(k)-}(t-\tau) f_{Lj}(\tau) d\tau \right\} \quad (23)$$

The superscripts $+$ and $-$ indicate if the j^{th} column of $\mathbf{h}^{(k)}(t)$ is positive or negative, respectively.

Convex Optimization Approach To Controller Design

Design of the optimal feedback control law is expressed as a constrained optimization over all feasible transfer matrices $\mathbf{h}(t)$,

$$\begin{aligned} & \min \phi(\mathbf{h}) \\ & \psi_1(\mathbf{h}) \leq 0, \dots, \psi_M(\mathbf{h}) \leq 0 \end{aligned} \quad (24)$$

where $\phi(\mathbf{h})$ is a cost function to be minimized and $\psi_i(\mathbf{h})$, $i = 1$ to M , are design constraints.

The advantage of modeling the uncertain excitations as deterministic functions is that the expressions for the maximum response are all convex with respect to $\mathbf{h}(t)$. If the cost function and all of the constraints of equation (24) are convex, it is called a *convex controller design*. Convex optimizations are by nature easier to solve than general nonlinear programming problems. If any solution to the optimization exists (i.e., the constraints are not too tight) the global minimum can be found to any desired degree of accuracy. This eliminates the choice of a stopping criterion and provides important guarantees on the accuracy of the optimal solution.

As stated in equation (24), the controller design problem is an infinite dimensional optimization. This results from the fact that there are an infinite number of transfer matrices that must be searched to obtain the optimum. A general method of solving these problems is to perform optimizations over larger and larger finite dimensional subsets. For convex controller designs, one method of doing this is to introduce a Ritz approximation of the closed loop transfer matrix. One such Ritz approximation is motivated by the Q parameterization of all stabilizing controllers (equation (3)),

$$\mathbf{H}^{(N)}(s) = \mathbf{P}_{zw}(s) + \mathbf{P}_{zv}(s) \left\{ \sum_{i=1}^N x_i \mathbf{Q}_i(s) \right\} \mathbf{P}_{ew}(s). \quad (25)$$

The functions $\mathbf{Q}_i(s)$ are arbitrarily chosen functions and each x_i is a real scalar number. Parameterizing the solution with a Ritz approximation maintains the convexity of the cost function and constraints.

Substitution of equation (25) into the optimization reduces it to a search over a finite number of real scalars. A critical feature of approximating the solution via equation (25) is the convergence

properties of the optimum. As the number of terms in the series is increased, the solution of the finite dimensional problem approaches the optimal value of the infinite dimensional problem⁶. Often times, it is possible to prove that at $N \rightarrow \infty$, the two solutions are equivalent. In practice, only a finite number of terms is required to get arbitrarily close to the optimal value.

Finite Dimensional Approximations To The Maximum Response Functions

The maximum response expressions and the Ritz series are combined to create finite dimensional approximations. Using the inverse Laplace transform on the Ritz approximation yields

$$\mathbf{h}^{(k)}(t) = \mathbf{p}_o^{(k)}(t) + \sum_{i=1}^N x_i \mathbf{p}_{x_i}^{(k)}(t), \quad (26)$$

where $\mathbf{p}_o(t)$ is the inverse transform of $\mathbf{P}_{zw}(s)$ and $\mathbf{p}_{x_i}(t)$ is the inverse transform of $\mathbf{P}_{zw}(s)\mathbf{Q}_i(s)\mathbf{P}_{sw}(s)$. For convenience, the (N) notation has been dropped. The following analysis is simplified by placing equation (26) in vector notation,

$$\mathbf{h}^{(k)}(t) = \mathbf{p}_o^{(k)}(t) + \mathbf{x}^T \mathbf{P}_x^{(k)}(t). \quad (27)$$

The design variables x_i have been placed in the vector $\mathbf{x} \in \mathcal{R}^N$, and $\mathbf{P}_x(t) \in \mathcal{R}^{N \times n_w}$ at each time t .

For the finite set disturbance model, W_{FIN} , the maximum output to the i^{th} disturbance is

$$\bar{z}_i^{(k)} = \max \left\{ c_F^{(k)}(t) + \mathbf{b}_F^{(k)T}(t) \mathbf{x} \right\}, \quad (28)$$

where,

$$\begin{aligned} c_F^{(k)}(t) &= \int_0^t \mathbf{p}_o^{(k)}(t-\tau) \mathbf{w}_i(\tau) d\tau \\ \mathbf{b}_F^{(k)}(t) &= \int_0^t \mathbf{P}_x^{(k)}(t-\tau) \mathbf{w}_i(\tau) d\tau \end{aligned} \quad (29)$$

Introducing the Ritz approximation into equation (16) reduces it to a quadratic expression in \mathbf{x} ,

$$\bar{y}_i^{(k)}(t) = \left[c_i^{(k)}(t) + \mathbf{b}_i^{(k)T}(t) \mathbf{x} + \mathbf{x}^T \mathbf{A}_i^{(k)}(t) \mathbf{x} \right]^{\frac{1}{2}}, \quad (30)$$

where,

$$\begin{aligned} c_i^{(k)}(t) &= \rho_i \int_0^t \mathbf{p}_o^{(k)}(\tau) \mathbf{p}_o^{(k)T}(\tau) d\tau \\ \mathbf{b}_i^{(k)}(t) &= \rho_i \int_0^t \mathbf{P}_x^{(k)}(\tau) \mathbf{p}_o^{(k)T}(\tau) d\tau. \\ \mathbf{A}_i^{(k)}(t) &= \rho_i \int_0^t \mathbf{P}_x^{(k)}(\tau) \mathbf{P}_x^{(k)T}(\tau) d\tau \end{aligned} \quad (31)$$

In a similar manner, the LEB disturbance model can also be expressed as a quadratic expression in \mathbf{x} ,

$$\bar{y}_L^{(k)}(t) = \left[c_L^{(k)}(t) + \mathbf{b}_L^{(k)T}(t) \mathbf{x} + \mathbf{x}^T \mathbf{A}_L^{(k)}(t) \mathbf{x} \right]^{\frac{1}{2}}, \quad (32)$$

where,

$$\begin{aligned} c_L^{(k)}(t) &= \int_0^t \rho_L(\tau) \mathbf{p}_o^{(k)}(t-\tau) \mathbf{p}_o^{(k)T}(t-\tau) d\tau \\ \mathbf{b}_L^{(k)}(t) &= \int_0^t \rho_L(\tau) \mathbf{P}_x^{(k)}(t-\tau) \mathbf{p}_o^{(k)T}(t-\tau) d\tau. \\ \mathbf{A}_L^{(k)}(t) &= \int_0^t \rho_L(\tau) \mathbf{P}_x^{(k)}(t-\tau) \mathbf{P}_x^{(k)T}(t-\tau) d\tau \end{aligned} \quad (33)$$

The Ritz approximation is also introduced into the TEB disturbance model,

$$\begin{aligned} \bar{z}_T^{(k)}(t) &= \sum_{j=1}^{n_w} \left\{ \int_0^t \left[p_{oj}^{(k)}(t-\tau) + \mathbf{x}^T \mathbf{p}_{x_j}^{(k)}(t-\tau) \right]^+ f_{Uj}(\tau) d\tau \right. \\ &\quad \left. + \int_0^t \left[p_{oj}^{(k)}(t-\tau) + \mathbf{x}^T \mathbf{p}_{x_j}^{(k)}(t-\tau) \right]^- f_{Lj}(\tau) d\tau \right\} \end{aligned} \quad (34)$$

where $(\)_j$ denotes the j^{th} column of $(\)$ and the superscripts $+$ and $-$ denote when the bracketed expression is positive or negative, respectively.

Example: Disturbance Rejection In A Flexible Structure

The optimization techniques developed in this paper are applied to the model of an unconstrained flexible structure. The model for the structure consists of two rigid body poles and a low frequency flexible mode. A block diagram of the open loop system is shown in Figure 3.

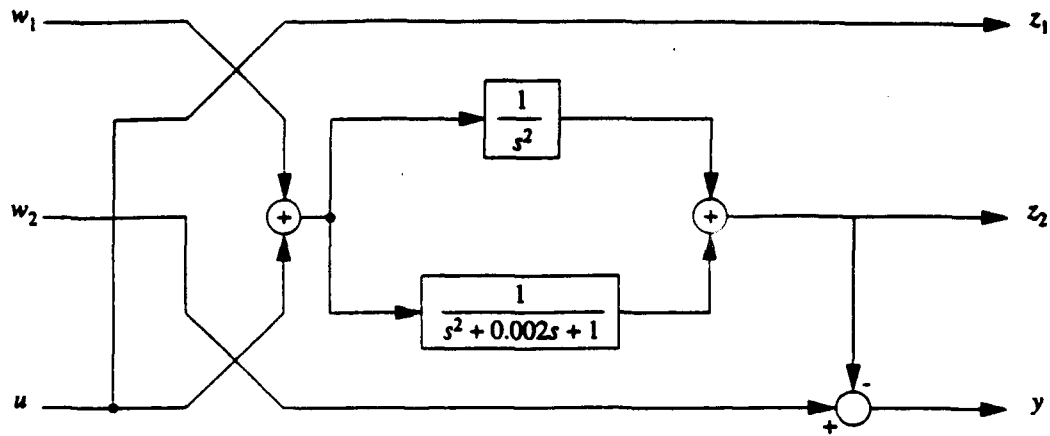


Figure 3: Open loop block diagram of an unconstrained structure with one flexible mode.

The control design is accomplished in two stages. First, Linear Quadratic Gaussian Synthesis is used to obtain an optimal estimated state feedback controller. Next, a series of convex optimizations is performed to minimize outputs to different sets of exogenous inputs. The different sets of uncertain inputs represent varying levels of previous knowledge about the disturbance set. The optimizations are used to study the performance trade-offs that exist in the design of the optimal control laws.

Linear Quadratic Gaussian Synthesis

An optimal state estimate feedback controller is designed using Linear Quadratic Gaussian synthesis. Using optimization techniques developed by Boyd and Barratt⁶, a curve is obtained that represents the trade-off between performance and control effort for LQG control [Figure 4].

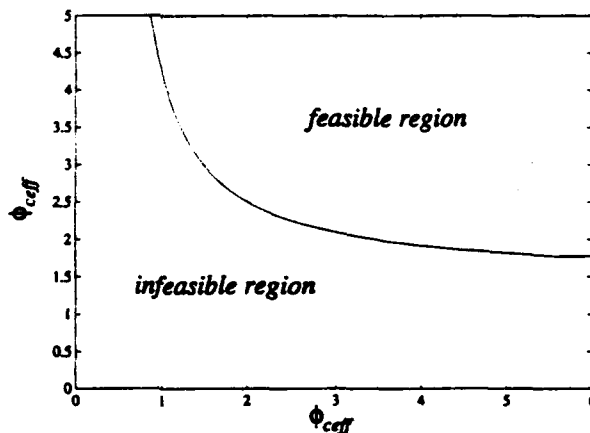


Figure 4: Trade-off curve for LQG control of the flexible structure model.

Each point along the curve is the solution of the convex optimization

$$\min (\lambda_1 \phi_{ceff}^2 + \lambda_2 \phi_{perf}^2)^{\frac{1}{2}} \quad (35)$$

$$\text{s. t. } \lambda_2 = 1 - \lambda_1$$

where

$$\phi_{perf} = (\|H_{21}\|_2^2 + \|H_{22}\|_2^2)^{\frac{1}{2}} \quad (36)$$

$$\phi_{ceff} = (\|H_{11}\|_2^2 + \|H_{12}\|_2^2)^{\frac{1}{2}}$$

$\|H_{ij}\|_2$ is the 2-norm of the closed loop transfer function between z_i and w_j . For each value of λ_1 between 0 and 1, an LQG controller is obtained through the solution of two Riccati equations¹. Points along the curve are LQG solutions for different values of λ_1 .

The trade-off curve for LQG synthesis reveals information about the achievable performance for $\|H\|_2$ minimization. The region 'above' the trade-off curve represents values of ϕ_{perf} and ϕ_{ceff} that are achievable by some control law $K(s)$. Points 'below' the curve cannot be achieved by any linear control law. For the example problem, Figure 4 illustrates that control laws that make ϕ_{ceff} greater than 5 yield very little decrease in ϕ_{perf} .

Optimal Disturbance Rejection

Once an LQG controller is designed, a set of convex optimizations is performed to augment the estimated state feedback. Three separate optimizations are

performed, each with a different model of the excitation.

If we introduce the following switching function,

$$sw(t_1, t_2) = \begin{cases} 1 & 0 \leq t \leq t_1 \\ -1 & t_1 < t \leq t_2 \\ 0 & t_2 < t \end{cases} \quad (37)$$

then the first two excitation models are defined as,

Excitation Model 1:

$$w_1(t) = \begin{cases} sw(10, 20) \\ 0 \end{cases} \quad (38)$$

Excitation Model 2:

$$w_1(t) = \begin{cases} sw(10, 20) \\ 0 \end{cases}$$

$$w_2(t) = \begin{cases} sw(5, 20) \\ 0 \end{cases} \quad (39)$$

$$w_3(t) = \begin{cases} sw(15, 20) \\ 0 \end{cases}$$

The third model for the excitation is a TEB disturbance model.

Excitation Model 3:

$$w(t) = \begin{cases} -1 \leq w_1(t) \leq 1 & 0 \leq t \leq 20 \\ w_2(t) = 0 & 0 \leq t \leq 20 \\ w_1(t) = 0 & 20 < t \\ w_2(t) = 0 & 20 < t \end{cases} \quad (40)$$

The three excitation models represent decreasing levels of knowledge about the input. For the first model, the input is known. In the second model, the input is one of three functions, each with a different switching time. The third model contains any input bounded by ± 1 over 0 to 20 seconds.

The performance objective and constraints are defined in terms of 2-norms and maximum response functions. Constraints on the H_2 norm of the closed loop transfer matrix are chosen based on the trade-off curve for LQG synthesis. The H_2 norm is obtained by letting $t \rightarrow \infty$ in equation (30) and setting $\rho_I = 1$. Thus, the 2-norm is a quadratic expression in x .

The performance objectives and constraints for the three optimizations are

Optimization 1:

$$\min \bar{z}_1^{(2)}$$

$$s.t. \quad \bar{z}_1^{(1)} < 3.0$$

$$\left(\|H_{21}\|_2^2 + \|H_{22}\|_2^2 \right)^{\frac{1}{2}} < 2.2$$

$$\left(\|H_{11}\|_2^2 + \|H_{12}\|_2^2 \right)^{\frac{1}{2}} < 5.0$$

Optimization 2:

$$\min \max\{ \bar{z}_1^{(2)}, \bar{z}_2^{(2)}, \bar{z}_3^{(2)} \}$$

$$s.t. \quad \max\{ \bar{z}_1^{(1)}, \bar{z}_2^{(1)}, \bar{z}_3^{(1)} \} < 3.0$$

$$\left(\|H_{21}\|_2^2 + \|H_{22}\|_2^2 \right)^{\frac{1}{2}} < 2.2$$

$$\left(\|H_{11}\|_2^2 + \|H_{12}\|_2^2 \right)^{\frac{1}{2}} < 5.0$$

Optimization 3:

$$\min \bar{z}_T^{(2)}(20)$$

$$s.t. \quad \bar{z}_T^{(1)}(20) < 3.0$$

$$\left(\|H_{21}\|_2^2 + \|H_{22}\|_2^2 \right)^{\frac{1}{2}} < 2.2$$

$$\left(\|H_{11}\|_2^2 + \|H_{12}\|_2^2 \right)^{\frac{1}{2}} < 5.0$$

The optimization is allowed to trade-off the 2-norm of the response and the peak value of the control effort for a decrease in the peak value of z_2 . For the LQG controller with $\phi_{ceff} = 5.0$, the value of $\phi_{perf} = 1.81$. The optimizations allow this value to increase 2.2, and it also lets the peak value of the control effort increase to 3.0.

The optimizations are performed using a constrained ellipsoid algorithm written in MATLAB⁷. The time responses are discretized over the interval 0 to 50 seconds with 2000 points. The Q parameterization is chosen to be

$$Q_i(s) = \left(\frac{1}{s+1} \right)^i \quad (41)$$

Reasons for choosing such functions are discussed in Polak and Sacludean⁸. The optimizations are

initialized at the LQG solution, $\mathbf{x} = \mathbf{0}$, and the termination criterion is set at 0.01. This guarantees that the solution is within 0.01 of the optimal value.

Discussion Of The Optimization Results

All three optimizations are performed with between 2 and 20 Q functions. The convergence histories indicate that little change in the optimal solution occurs after approximately 16 Q functions [Figure 5].

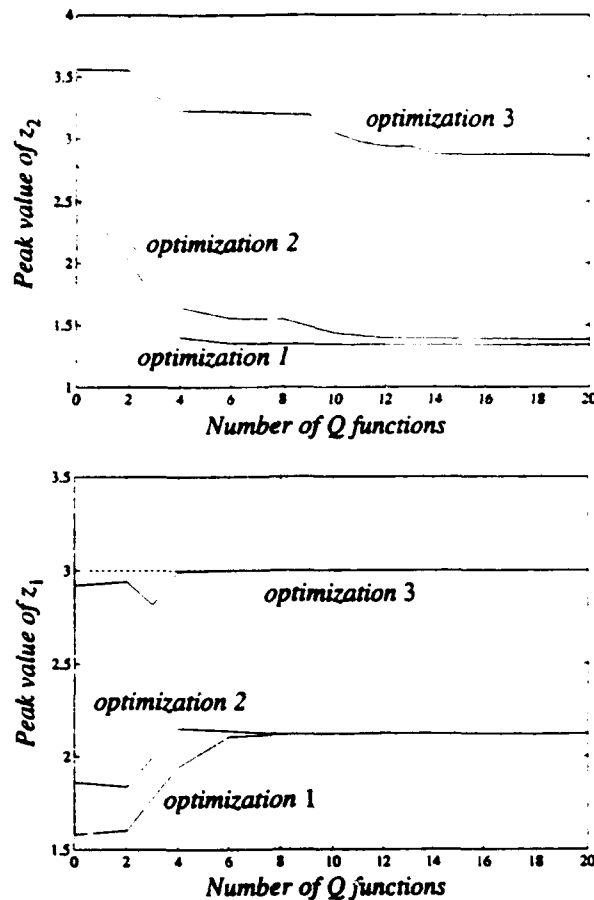


Figure 5: Convergence histories for the three optimizations. Top plot is the performance objective, bottom plot is the constraint on the peak value of $z^{(1)}$.

Quantitative results of the three optimizations are listed in Table 1. They illustrate that the achievable performance is strongly coupled to the size the disturbance model. For the first optimization, the excitation is known, resulting in a control law that can achieve a significant reduction in the peak value of $z^{(2)}$. Increasing the size of the disturbance model to three functions decreases the amount of performance reduction the optimization achieves. For the final disturbance set, the peak value at the

optimum is much higher since the assumed model for the excitation is more conservative.

The convex optimizations offer insight into the design trade-offs. In the case of the first two disturbance models, the constraint on the peak value of the control effort is not necessary. Neither optimization reaches the constraint value at the solution. Also, control laws that are excellent for one disturbance set might be poor for another. In this example, the optimal controller for the TEB disturbance model actually increases the peak response to the excitations contained within set 1 and set 2.

For all three optimizations, the constraints on the H_2 norm of the performance and control effort are limiting factors in the design. All of the optimal solutions lie on the 2-norm constraints of z_1 and z_2 .

Frequency Domain Characteristics Of The Optimal Solutions

It is instructive to examine the frequency response characteristics of the closed loop systems obtained via convex optimization. Many modern and classical design procedures involve shaping the frequency response to obtain the desired results in the time domain. In this paper, time domain information regarding the input is included in the optimization, eliminating the need to shape the frequency response.

The closed loop transfer functions for the optimal designs are compared to the LQG solution in Figure 6. Since the optimizations are minimizing the peak response of z_2 to uncertain inputs at w_1 , the only significant change occurs in H_{21} . The optimal solution is notching the frequency response to achieve reductions in the peak value of the output. The remaining closed loop transfer functions change very little, only enough to satisfy the constraints.

It is probable that a skilled designer would be able to shape the frequency response to satisfy the constraints. One advantage of the convex optimization approach is that there is no need to translate the time domain constraints into the frequency domain. The frequency response is manipulated automatically, in such a way that optimal performance is achieved while simultaneously satisfying all constraints.

Numerical Limitations

Convex optimization offers very structured methods to examine design trade-offs, but relies heavily on numerical procedures. This strong dependence on

numerical solution introduces some limitations in the optimal design of control laws. For the low order example studied in this work, the computation time is not excessive. The most demanding optimizations only take approximately 15 minutes on a Sun SPARC10 workstation. For higher order problems

with more constraints, the large number of objective and constraint evaluations (on the order of 1200 to 1500) might cause difficulties. For this reason, it is very important to make the objective and constraint evaluations as efficient as possible.

Table 1: Comparison of convex optimization results.

	Performance				Control Effort			
	$\bar{z}_1^{(2)}$	$\bar{z}_2^{(2)}$	$\bar{z}_3^{(2)}$	$\bar{z}_T^{(2)}(20)$	$\bar{z}_1^{(1)}$	$\bar{z}_2^{(1)}$	$\bar{z}_3^{(1)}$	$\bar{z}_T^{(1)}(20)$
LQG	2.52	2.80	2.28	3.56	1.58	1.86	1.64	2.92
Opt 1	1.34	2.01	1.91	4.36	2.12	2.05	2.05	3.67
Opt 2	1.38	1.38	1.38	3.85	2.01	2.01	2.16	3.90
Opt 3	2.67	2.68	2.65	2.87	1.61	1.72	1.57	3.00

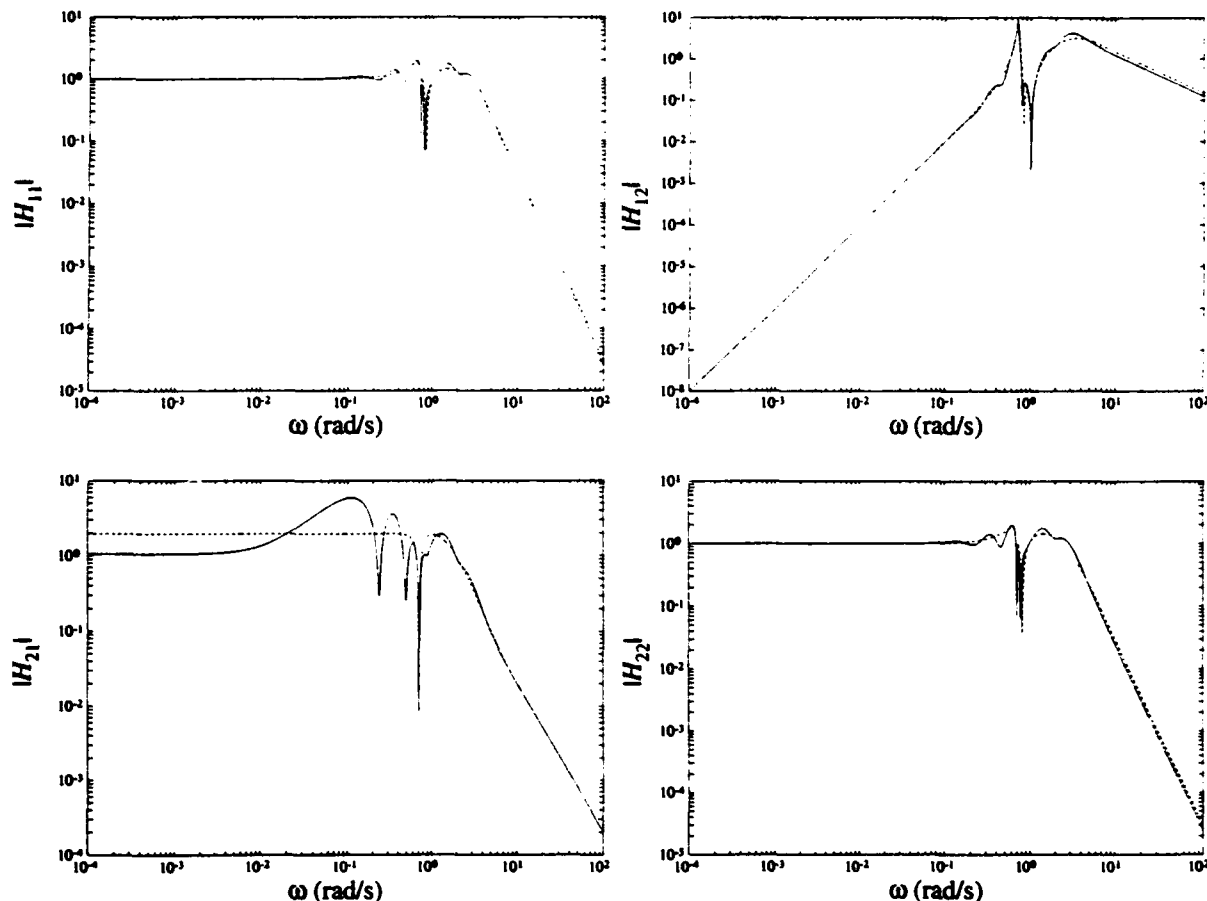


Figure 6: Closed loop transfer functions for the LQG solution (dotted), and the solution for optimization 3 (solid).

A more subtle numerical limitation involves the evaluation of the maximum response functions for the IEB, LEB, and TEB disturbance models. In

certain cases, it is straightforward to show that the maximum response monotonically increases with time. Therefore, constraining the maximum response at time T automatically constrains the response for t

$< T$. There is no such guarantee for $t > T$, though. For the flexible structure example, bounding the maximum response at $t = 20$ does not guarantee that the optimal value is not exceeded at future time. A more appropriate objective might be

$$\min \max \{z_T^{(2)}(t)\} \quad (42)$$

over the time interval 0 to 50 seconds. Unfortunately, this requires many more computations, and would increase the time of the optimization considerably. Future work on this topic might involve finding closed-form solutions for the maximum response functions.

Concluding Remarks

This paper illustrates one method of including time domain information in feedback control design. By modeling uncertain excitations deterministically, optimal control laws are obtained efficiently via convex optimization. This allows for straightforward examination of the trade-offs that exist between achievable performance and the design constraints.

In the presence of uncertain inputs, the achievable performance is a function of the model chosen to represent the disturbances. As one would expect, more conservative input models yield more conservative control laws. One method of reducing the conservativeness of a control law might be to investigate the allowable inputs and include any available time domain information in the optimal feedback design.

Acknowledgments

This research was supported by AFOSR grant number 91-081 under the direction of Dr. Spencer Wu. The authors would also like to thank Professor Yakov Ben-Haim for his comments regarding early drafts of this manuscript.

References

1. Maciejowski, J.M., *Multivariable Feedback Design*, Addison-Wesley Publishing, Wokingham, England, 1989.
2. Doyle, J.C., Francis, B.A., and Tannebaum, A.R., *Feedback Control Theory*, MacMillan Publishing, New York, 1992.
3. Vidyasagar, M., "Optimal Rejection of Persistent Bounded Disturbances," *IEEE Transactions on Automatic Control*, vol. AC-31, 1986, pp. 527-534.

4. Dahleh, M., and Pearson, J.B., "L¹ Optimal Compensators for Continuous Time Systems," *IEEE Transactions on Automatic Control*, vol. AC-32, no. 10, October 1987, pp. 889-895.

5. Ben-Haim, Y., and Elishakoff, I., *Convex Models of Uncertainty in Applied Mechanics*, Elsevier, Amsterdam, 1990.

6. Boyd, S., and Barratt, C., *Linear Controller Design - Limits of Performance*, Prentice Hall, Englewood Cliffs, N.J., 1991.

7. *MATLAB User's Guide*, The MathWorks, Inc., 1993.

8. Polak, E., and Sacludean, S.E., "On the Design of Linear Multivariable Feedback Systems via Constrained Nondifferentiable Optimization in H_∞ Spaces," *IEEE Transactions on Automatic Control*, vol. AC-34., no. 3, March, 1989, pp. 268-276.

COMPARISON OF LINEAR AND NONLINEAR CONTROL ON A DISTRIBUTED PARAMETER SYSTEM

Ralph W. Rietz

Department of Mechanical and Aerospace Engineering
State University of New York, Buffalo
Buffalo, New York

Daniel J. Inman

Department of Engineering Science and Mechanics
Virginia Polytechnic Institute and State University
Blacksburg, Virginia

ABSTRACT

The performance of a single link, very flexible manipulator using two different position control systems was studied. A standard PD feedback control was considered along with PD plus position times velocity feedback. An analytical model of the plant was identified and computer simulations using the two controllers were performed. The results clearly showed a decrease in control effort for the system using nonlinear control when compared to a similar response for the system using PD control. Experimental results on a slewing beam system verified this result. The system using the proposed nonlinear feedback control required significantly less energy to complete the same maneuver as the system using the standard PD feedback control. Other measures of performance (e.g. rise time, settling time, overshoot) were slightly improved when the nonlinear feedback was added to the controller.

INTRODUCTION

Slewing motion, the rotation of a structure or manipulator about an axis, forms the basis for many robot and satellite maneuvers. The work presented here concerns the single axis slew maneuver of a flexible structure. Numerous researchers have modeled slewing structures and designed linear control schemes for them. The slewing flexible structure is typically approximated as a rigid hub connected to a flexible appendage. Cannon and Schmitz (1984) modeled and performed experiments with a single link, very flexible beam. They considered the noncolocated control problem, where the tip position was sensed and controlled from an actuator located at the other end of the beam. Similarly, Juang, Horta and Robertshaw (1986) experimented with a slewing beam and a solar panel. They compared the experimental results with analytical predictions and found good agreement. Other researchers investigated the interaction between the actuator and structure of slewing structures. Garcia (1989) modeled a slewing beam and considered the effect which different gear ratios between the motor and the beam had on the system. Sah (1990) performed

similar work, providing a method to select the parameters of a slewing system through a nondimensional analysis. Finally, Garcia and Inman (1991) considered the effect of integrated sensing and actuation along a slewing beam to control the flexibility of the structure.

Why consider nonlinear control? The strongest argument for using nonlinear control is that it can significantly improve the performance over linear control schemes. This can be shown in simulations, where the step response rise time, settling time and overshoot are significantly smaller than the response when linear control is used. Lewis (1953) showed the response of a second order system can be improved by constructing a variable damping. He used position times velocity feedback to eliminate overshoot and improve the settling time of a positional servomechanism. More recently, Castelazo and Lee (1990) proposed using the same type of feedback to improve the response of a slewing beam system. They considered a nonlinear feedback, where state positions and state velocities were multiplied. A heuristic method was proposed to tune the nonlinear feedback gains and the resulting performance was better than the performance provided by an optimal linear controller. They provided simulation results for a slewing beam to verify the method. Others, such as Kuo and Wang (1990), have proposed using nonlinear controllers to improve the robustness of a more complicated two link manipulator.

Initially, the purpose of this work was to experimentally verify the simulation results found by Castelazo and Lee. However, to insure global stability, their proposed feedback required a simple modification. Also, full state feedback is difficult to implement and as a result, proportional plus derivative feedback control, which lends itself well to experimentation, was chosen for this purpose. Angular position and angular velocity are easily measured on the experimental apparatus. The nonlinear feedback consisted of the angular position times the angular velocity and the objective was to show that the system using nonlinear feedback provided better results than the system using the best available linear feedback.

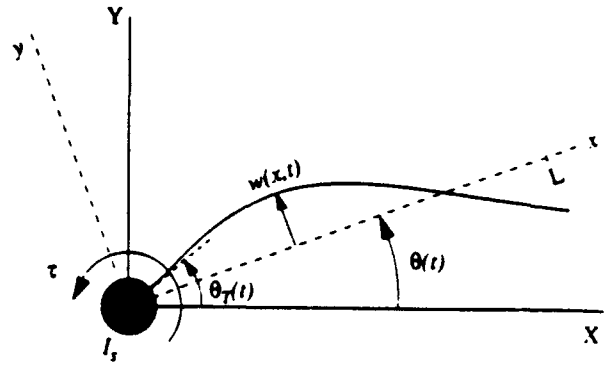
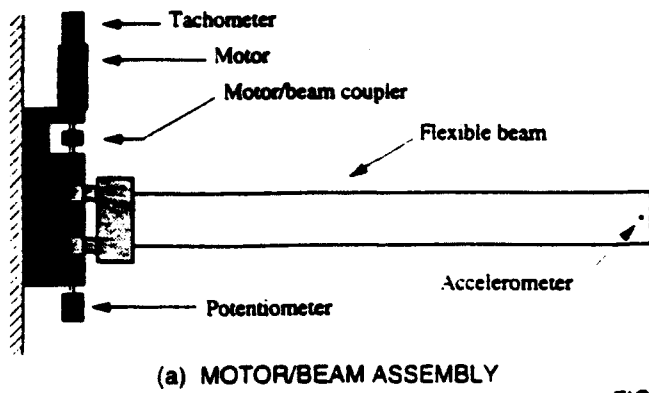


FIGURE 1

THEORY AND MODELING

The experimental apparatus consisted of an armature controlled DC motor connected to a very flexible aluminum beam, Figure 1. The slewing equations of motion [Garcia (1989)] can be developed using Hamilton's principle and performing simple mechanical and circuit analyses of the motor assembly. The equations of motion are written as

$$M\ddot{q} + D\dot{q} + Kq = B_r e_s \quad (1)$$

where, using the definition

$$\Phi(x) = [1 \quad \phi_1'(x) \quad \dots \quad \phi_n'(x)]^T$$

$$M = \begin{bmatrix} I_b + I_s & I_1 + I_s \phi_1'(0) & \dots & I_n + I_s \phi_n'(0) \\ & M_1 & 0 & \dots & 0 \\ & & M_2 & & \vdots \\ \text{symm.} & & & \ddots & 0 \\ & & & & M_n \end{bmatrix}$$

$$D = b_v \Phi(0) \Phi^T(0)$$

$$K = \begin{bmatrix} 0 & \dots & 0 \\ \omega_1^2 M_1 & 0 & \dots & 0 \\ & \ddots & & \vdots \\ \text{symm.} & & & 0 \\ & & & & \omega_n^2 M_n \end{bmatrix}$$

$$B_r = \left(\frac{N_g K_m}{R_a} \right) \Phi(0)$$

$$q = [\theta \quad q_1 \quad \dots \quad q_n]^T$$

and

$$I_b = \int_0^L \rho A x^2 dx$$

$$I_s = N_g^2 I_m$$

$$I_i = \int_0^L \rho A x \phi_i dx$$

$$M_i = \int_0^L \rho A \phi_i^2 dx + I_s (\phi_i'(0))^2$$

$$\omega_i^2 = - \frac{EI \phi_i''(0)}{I_s \phi_i'(0)}$$

$$b_v = N_g^2 \left(c_v + \frac{K_g K_m}{R_a} \right)$$

Also, $\phi_i(x)$ are the mode shapes of the inertia-free beam, $q_i(t)$ are the generalized coordinates, N_g is the gear ratio between the motor and the beam, ρ is the beam density, A is the beam cross sectional area, x is measured along the beam, c_v is the equivalent viscous damping in the model, I_m is the motor inertia, and K_g , K_m and R_a are motor parameters.

A pole zero model of the slewing beam system of Figure 1 was also identified. A Fourier analyzer manufactured by Tektronix, Inc. (model # 2630) was used to collect data for the experimental model. The natural frequencies and damping ratios of the pole zero model are given in Table 1 below. This model was used in the simulations to be presented since it was obtained from test data of the system used in the experiments.

OUTPUT FEEDBACK

Simulations will be presented where the identified pole zero model of the slewing beam (Table 1) was used as the system

TABLE 1 EXPERIMENTAL NATURAL FREQUENCIES AND DAMPING RATIOS

mode(i)	ω_{ie} (Hz)	ζ_{ie} (%)
1	5.0	1.3
2	15.4	1.4
3	30.8	1.7
4	51.8	1.1
5	79.6	1.1

plant. Using a potentiometer and a tachometer mounted at the slewing axis and an accelerometer mounted at the beam tip, this single input multiple output model of the slewing beam system was identified. In the experimental slewing beam system, only angular position and angular velocity at the slewing axis were made available to the controller. For this reason, a proportional plus derivative (PD) controller was studied. A block diagram of the closed loop system is shown in Figure 2.

The dashed box indicates the operations performed in the analog computer in the experiments. In Figure 2, the motor armature voltage, e_a , can be represented as

$$e_a = \bar{k}_p(\theta_{ref} - \theta_T) - N_s \bar{k}_d \dot{\theta}_T - N_s \bar{k}_{nl} |\theta_T| \dot{\theta}_T$$

$$= \bar{k}_p(\theta_{ref} - \Phi^T(0)q) - \bar{k}_d \Phi^T(0)\dot{q} - \bar{k}_{nl} |\Phi^T(0)q| \Phi^T(0)\dot{q} \quad (2)$$

There are no gears present in the system. The controller was designed to return the system from an initial angular displacement of 30° to equilibrium in the shortest time possible. The best response was defined as the response where the tip position settled in the shortest time without exceeding the constraints of the motor and controller. The motor was limited to a maximum of 30 V and 15 A and the controller saturated at 10 V.

Setting $k_{nl} = 0$, a simple PD control system is obtained. In search of the ideal response, a tradeoff exists where the magnitudes of the feedback gains are limited by the constraints of the system. Increasing the proportional gain beyond a certain value caused the motor and controller to saturate. Also, beyond certain values of k_d the settling time of the beam tip increased, which was also undesirable.

The nonlinear feedback consists of the absolute value of the angular position at the slewing axis times the angular velocity at the slewing axis adjusted by a feedback gain. The variable (nonlinear) damping proposed here provides very little additional damping at the beginning of the control maneuver. As the target position is approached, the damping increases. If the best response of the linear feedback system exhibited overshoot, it could be decreased or eliminated by increasing the nonlinear feedback gain, k_{nl} . In this case, increasing k_{nl} caused the settling time to decrease initially, then increase as k_{nl} became large and the system exhibited an overdamped response. If the system using linear feedback showed a critically damped response, then increasing k_{nl} increased the settling time. In this case, when k_{nl}

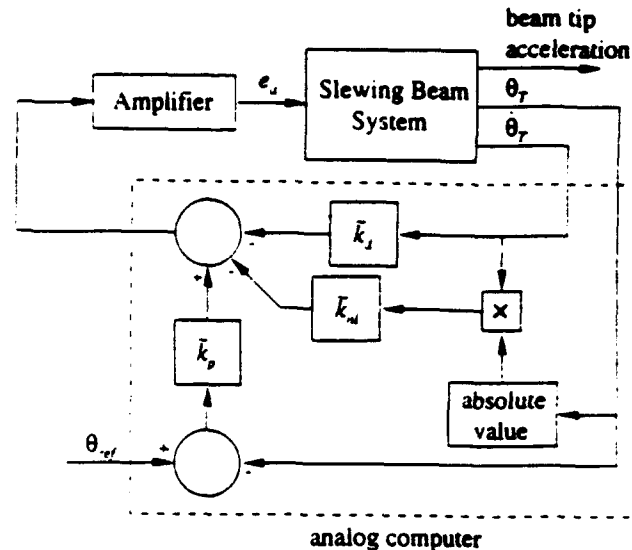


FIGURE 2 CLOSED LOOP PD PLUS NONLINEAR FEEDBACK CONTROL SYSTEM

was small, there was no visible effect on the time response of the beam tip, however, the control effort decreased. In other words, it was possible to obtain the same time response using less energy when the nonlinear feedback was added to the control system.

The best simulation results are given below. First, a response with the fastest settling time which remained within the physical constraints of the system was obtained using PD control. Then, nonlinear feedback was added to the system until the most desirable effects were obtained. The angular position at the slewing axis versus time is shown in Figure 3. The acceleration of the beam tip versus time is shown in Figure 4. The dotted line represents the PD control and the solid line is the response of the PD plus nonlinear control. The addition of the nonlinear feedback eliminated the overshoot and reduced the magnitude of the acceleration at the beam tip. The settling time did not change, however the improvements in the overshoot and acceleration make the result using the nonlinear feedback control more favorable.

Figure 5 is a plot of the instantaneous power versus time where the upper curve is for the linear feedback and the lower curve is the result using nonlinear feedback. Integrating, the energy required to execute the control maneuvers was obtained and tabulated in Table 2. A significant savings in energy resulted through the addition of a simple nonlinear feedback to the standard PD controller. An improved response was obtained and 30.6% less energy was used in the nonlinear feedback case.

The simulations presented above used a model obtained from data of the experimental system and therefore, they provide the most optimistic result that the simulated observations can be implemented on a real system.

EXPERIMENTAL RESULTS

Simulations provide valuable information concerning the dynamics of systems before any experiments are performed. The experimental results are presented here. First, a PD controller

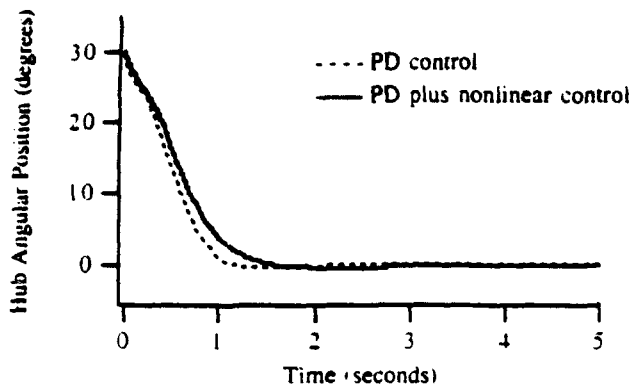


FIGURE 3 ANGULAR POSITION AT THE SLEWING AXIS VERSUS TIME

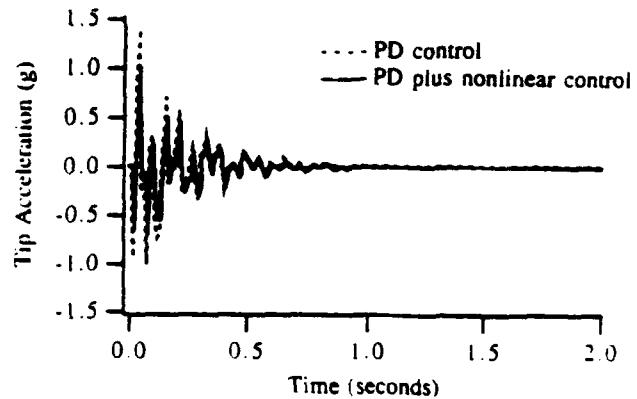


FIGURE 4 ACCELERATION OF THE BEAM TIP VERSUS TIME

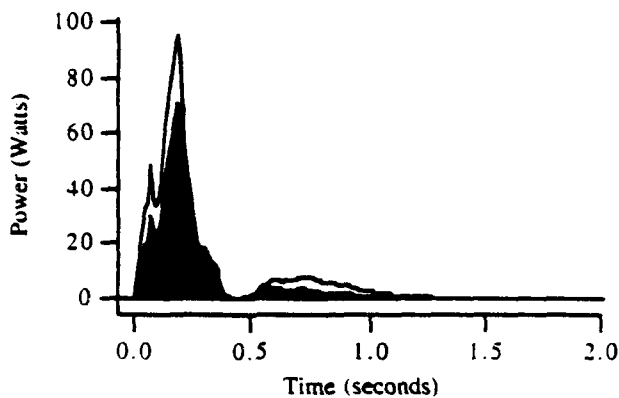


FIGURE 5 INSTANTANEOUS POWER VERSUS TIME FOR THE LINEAR AND NONLINEAR FEEDBACK CASES USING THE IDENTIFIED PLANT MODEL

TABLE 2 TOTAL ENERGY INPUT TO THE MOTOR FOR THE SIMULATED 30° SLEWING MANEUVER USING THE IDENTIFIED PLANT MODEL

Linear	17.4 J
Nonlinear	12.1 J
% reduction	30.6 %

computer manufactured by Electronic Associates, Inc. was used to implement the controllers. A block diagram of the closed loop system was given in Figure 2.

The controller gains were adjusted until the fastest settling time was obtained. The time responses are shown below for the PD controlled slewing beam. The beam is given an angular displacement of 30° and slewed to 0°. A plot of angular position versus time is shown in Figure 6, the beam tip acceleration versus time is shown in Figure 7.

These experimental responses are comparable to the simulated responses. In general, the experimental result shows less damping than the simulation. The overshoot is larger and the settling time is also larger than the simulation predicted. The reason for this is that the derivative gain used was smaller than that used in the simulations. A smaller gain was required since higher gains degraded the performance and caused the amplifier to saturate. The settling times of the angular position at the slewing axis and of the beam tip are found in Figures 6 and 7 and they were approximately 2 seconds each.

The time responses for the system using the nonlinear feedback are also shown. Angular position at the slewing axis versus time is plotted in Figure 8, Figure 9 shows a plot of the beam tip acceleration versus time. Figures 8 and 9 show that the settling times of the angular position and tip acceleration are approximately 2 seconds.

The instantaneous power versus time curves for the system using the linear and nonlinear feedback controllers is given in Figure 10. The upper curve is the result obtained from the PD controlled system and the lower curve represents the nonlinear feedback case. The instantaneous power versus time curve was obtained by multiplying the time histories of the motor voltage

was constructed for the slewing beam and an experiment was performed. Then, the nonlinear feedback was added to the controller and another experiment was performed.

It is important to note that this study was initially conducted to verify through experimentation that the proposed nonlinear feedback control could be used to improve the time responses of the slewing beam system. However, within the physical constraints of the system, the improvements in the time responses were small. A natural extension of this investigation was to determine the cost of the change in performance. This is where more significant results were found. The purpose now is to show that it is possible to reduce the energy requirements of this system with no loss in performance. We have found through simulations and through experimentation that even when there is no visual improvement in the performance as measured with respect to settling time or rise time or overshoot, there is a significant improvement in energy consumption when the proposed nonlinear control is used in addition to the linear control.

The controllers were implemented in the same manner as in the simulations. The beam tip acceleration was measured and used as an indicator of the closed loop performance. An EAI 2000 analog

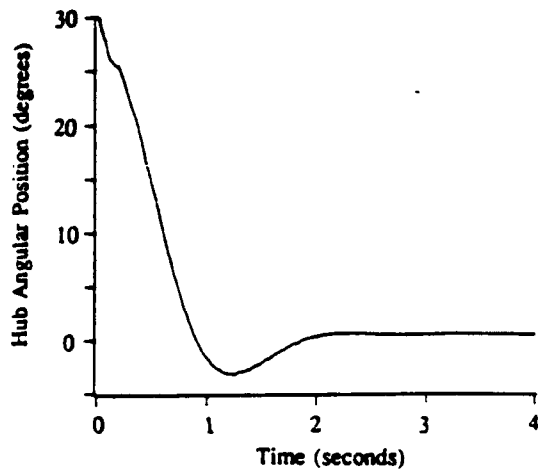


FIGURE 6 ANGULAR POSITION AT THE SLEWING AXIS VERSUS TIME (LINEAR FEEDBACK)

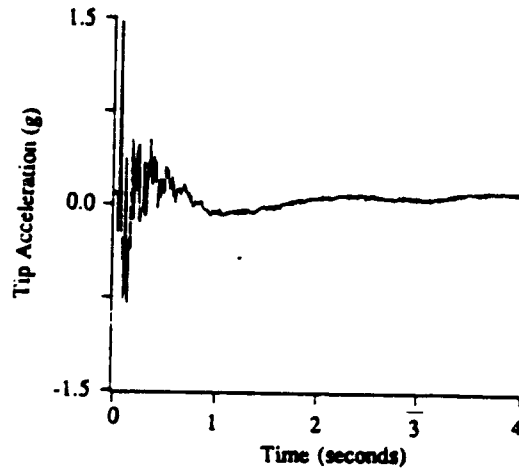


FIGURE 7 BEAM TIP ACCELERATION VERSUS TIME (LINEAR FEEDBACK)

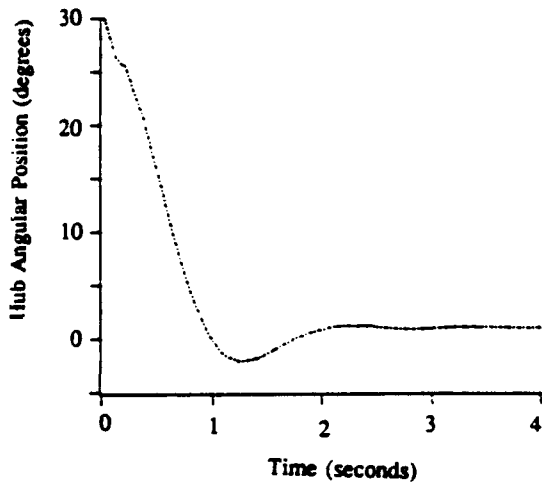


FIGURE 8 ANGULAR POSITION AT THE SLEWING AXIS VERSUS TIME (NONLINEAR FEEDBACK)

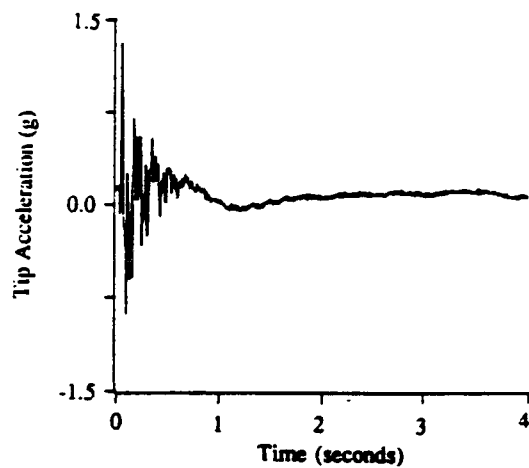


FIGURE 9 BEAM TIP ACCELERATION VERSUS TIME (NONLINEAR FEEDBACK)

and current together. Integrating under the power curve gives the total energy input to the motor for the control maneuver. For the PD controlled system, the energy input was 16.3 J. The total energy input to the motor for the nonlinear feedback system was 13.7 J.

When the PD feedback gains were lowered, an underdamped response was obtained which remained well below the system constraints. As a result of the lower PD gains, the nonlinear feedback gain could be set to larger values and significant improvements in overshoot and settling time were obtained. Thus, it was verified that the proposed nonlinear feedback control could be used to improve the closed loop performance of the linear system. The plots are not included here since the objective of this work was to find the best experimental PD controller, then add as much nonlinear feedback as possible (before saturating the amplifier) and compare the energy requirements of each system.

Consider the experimental time responses shown above. The angular position and beam tip acceleration settled in 2 seconds for

both the linear and nonlinear control systems implemented. There was a small decrease in overshoot in the angular position for the nonlinear feedback result, but this is not readily apparent in the figures shown. In general, the angular position plot shows an underdamped response for both the linear and nonlinear feedback results. Considering the time responses of the beam tip acceleration, the nonlinear feedback result shows a small decrease in magnitude of the peak accelerations. This is the same result noticed in the simulations.

Finally, consider the power plot shown in Figure 10. From the figure, it appears that the system using nonlinear feedback required less energy than the system using the linear feedback alone. The peak magnitude of the instantaneous power input to the system decreased by approximately 10%. Integrating under the instantaneous power versus time curves gives the total energy input to the motor during the control maneuver. The results are shown in Table 3. A 15.6% decrease in energy resulted for the system using nonlinear control than for the system

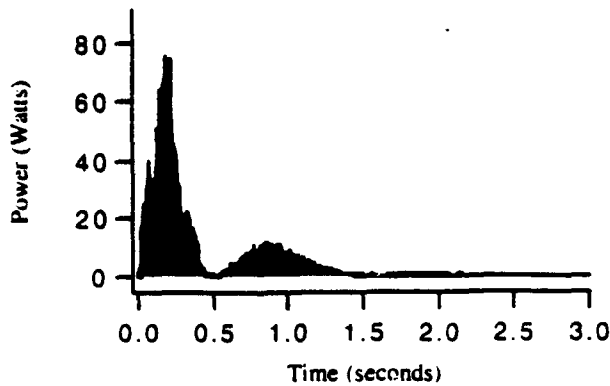


FIGURE 10 EXPERIMENTAL INSTANTANEOUS POWER VERSUS TIME FOR THE LINEAR AND NONLINEAR FEEDBACK CASES

using linear control, while the performance was virtually the same for both control methods. Therefore, it is possible to add nonlinear feedback of the form proposed here to a linearly controlled system and save energy, while obtaining the same performance in every other respect.

CONCLUSIONS

Initially, the purpose of this work was to experimentally verify that a specific nonlinear feedback control could be used to improve the time response of a closed loop system using linear control. A slewing beam system was chosen to implement the nonlinear control.

Simulation results showed only small improvements in the time responses (settling time and overshoot) for the nonlinear system within the system constraints. However, it was noticed that the control effort required by the system using nonlinear control was less than that required by the system using the linear control. The objective then changed to experimentally verify that this type of nonlinear control used less energy than the linear control when all other measures of performance were virtually unchanged.

Experiments proved that the addition of the proposed nonlinear feedback improved the performance by lowering the energy required to execute the slewing maneuver. The best performance for the linear control was an underdamped response. Adding the nonlinear feedback showed no significant improvement in performance. However, when the control efforts were compared, the nonlinearly controlled system required much less energy than the system using linear control. The conclusion reached was that the nonlinear feedback control proposed here can significantly save energy, even when no other change in performance is perceived.

REFERENCES

Cannon, Jr., R. H., and Schmitz, E., 1984, "Initial Experiments on the End-Point Control of a Flexible One-Link Robot," *The International Journal of Robotics Research*, Vol. 3, No. 3, pp. 62-75.

Castelazo, I. A., and Lee, H., 1990, "Nonlinear Compensation for Flexible Manipulators," *Journal of Dynamic Systems, Measurement, and Control*, Vol. 112, pp. 62-68.

TABLE 3 TOTAL ENERGY INPUT TO THE MOTOR FOR THE EXPERIMENTAL 30° SLEWING MANEUVER

Linear	16.3 J
Nonlinear	13.7 J
% reduction	15.6 %

Chen, C. T., 1984, *Linear System Theory and Design*, New York, NY, Holt, Rinehart and Winston.

Crassidis, A., 1992, "An Experimental Study of a Slewing System with the Inclusion of Coulomb Friction," Master's Thesis, Department of Mechanical and Aerospace Engineering, State University of New York at Buffalo.

Franklin, G. F., Powell, J. D., and Emami-Naeini, A., 1991, *Feedback Control of Dynamic Systems*, Second Edition, Menlo Park, CA, Addison-Wesley Publishing.

Garcia, E., 1989, "On the Modeling and Control of Slewing Flexible Structures," Ph.D. Dissertation, Department of Mechanical and Aerospace Engineering, State University of New York at Buffalo.

Garcia, E., and Inman, D. J., "Advantages of Slewing an Active Structure," *Journal of Intelligent Material Systems and Structures*, Vol. 1, No. 3, pp. 261-272.

Inman, D. J., 1989, *Vibration, with Control, Measurement, and Stability*, Englewood Cliffs, NJ, Prentice Hall.

Inman, D. J., 1990, "Control/Structure Interaction: Effects of Actuator Dynamics," *Mechanics and Control of Large Flexible Structures*, (ed. Junkins, J. L.), AIAA Press, pp.507-535.

Juang, J. N., Horta, L. G., and Robertshaw, H. H., 1986, "A Slewing Control Experiment for Flexible Structures," *AIAA Journal of Guidance, Control, and Dynamics*, Vol. 9, No. 5, pp.599-607.

Hagedorn, P., 1988, *Non-Linear Oscillations*, Second Edition, Translated and edited by W. Stadler, New York, NY, Oxford University Press.

Hagedorn, P., 1989, *Technische Schwingungslehre Band 2 Lineare Schwingungen kontinuierlicher mechanischer Systeme*, New York, NY, Springer-Verlag.

Kuo, B. C., 1987, *Automatic Control Systems*, Fifth Edition, Englewood Cliffs, NJ, Prentice Hall.

Kuo, C. Y., and Wang, Shay-Ping T., "Nonlinear Robust Hybrid Control of Robotic Manipulators," *Journal of Dynamic Systems, Measurement, and Control*, Vol. 112, pp. 49-54.

Leo, D. J., 1992, "Active Control of a Slewing Frame," Master's Thesis, Department of Mechanical and Aerospace Engineering, State University of New York at Buffalo.

Lewis, J. B., 1953, "The Use of Nonlinear Feedback To Improve the Transient Response of a Servomechanism," *AIEE Transactions*, Vol. 71, Part II, pp. 449-453.

Nieswander, R. S., and MacNeal, R. H., 1953, "Optimization of Nonlinear Control Systems by Means of Nonlinear Feedbacks," *AIEE Transactions*, Vol. 72, Part I, pp. 262-272.

Palm III, W. J., 1986, *Control Systems Engineering*, New York, NY, John Wiley & Sons.

Rietz, R. W., 1992, "Nonlinear Feedback Control of a Slewing Flexible Structure," Master's Thesis, Department of Mechanical and Aerospace Engineering, State University of New York at Buffalo.

Sab, J. J., 1990. "On the Interaction Between Actuator and Slewing Structure." Ph.D. Dissertation, Department of Mechanical and Aerospace Engineering, State University of New York at Buffalo.

Shames, I. H., and Dym, C. L., 1985, *Energy and Finite Element Methods in Structural Mechanics*, New York, NY, Hemisphere Publishing Corporation.

Sokolnikoff, I. S., and Redheffer, R. M., 1966, *Mathematics and Physics of Modern Engineering*, Second Edition, New York, NY, McGraw-Hill.

Tektronix, 1988, *TurboPac User's Guide*, Campbell, CA.

Thomson, W. T., 1988, *Theory of Vibrations with Applications*, Third Edition, Englewood Cliffs, NJ, Prentice Hall.

Robust Identification and Vibration Suppression of a Flexible Structure

John L. Crassidis*

Donald J. Leo†

D. Joseph Mook‡

Daniel J. Inman§

Abstract

A robust vibration suppression design involving the use of H_∞ optimal control theory is studied for a complex flexible structure. The digital control architecture involves non-colocated feedback utilizing active piezoceramic actuators and position sensor data. The modal properties of the multi-input-multi-output structure are first determined from experimental data in order to obtain an identified state-space model. This model forms the basis for the H_∞ vibration suppression design. Performance specifications are developed which obtain adequate damping in the structure while maintaining controller integrity without the destabilization of higher modes. A controller optimized for these H_∞ performance specifications is implemented on the actual test structure. Experimental structural perturbations are also examined in order to determine the robustness of the vibration suppression design. The experimental study indicates that the H_∞ design substantially increases damping in the targeted frequency region and conforms to predicted analytical simulations.

* Research Assistant, Department of Mechanical and Aerospace Engineering, Member AIAA, State University of New York at Buffalo, Buffalo NY, 14260.

† Research Assistant, Department of Mechanical and Aerospace Engineering, Member AIAA, State University of New York at Buffalo, Buffalo NY, 14260.

‡ Associate Professor, Department of Mechanical and Aerospace Engineering, Senior Member AIAA, State University of New York at Buffalo, Buffalo NY, 14260.

§ Samuel Herrick Professor, Department of Engineering Science and Mechanics, Member AIAA, Virginia Polytechnic Institute and State University, Blacksburg, VA, 24061.

Introduction

Space structures are generally very flexible and have many degrees of freedom in both the bending and torsional modes. The problem of controlling these structures has been investigated vigorously in the past (see, e.g. [1-3]), by utilizing both active and passive damping control techniques. Previous work has demonstrated the potential of using active strut elements to improve the vibrational response of a structure⁴. The application of these active elements to a non-colocated structural control problem can enhance system performance while tailoring the input/output properties of the structure.

The H_∞ control strategy, as compared to classical control techniques, provides new techniques and perspectives in designing control systems. This is accomplished by shaping the frequency response characteristics of a plant according to pre-specified performance specifications in the form of weighting functions. The H_∞ design process is chosen since: (1) it supplies robust stability to model and sensor uncertainties; (2) it achieves performance requirements efficiently; (3) it handles both disturbance and controller saturation problems easily; and (4) it works not only on simple single-input-single-output (SISO) systems but also on multi-input-multi-output (MIMO) systems⁵. Therefore, frequency response criteria can easily be shaped to desired specifications.

In recent years the implementation of robust stabilization and control based on H_∞ control theory has been investigated for different structures (see, e.g. [6-7]). However, most of these studies are limited to analytical simulations. A common procedure first involves the generation of a finite element model for the structure. Colocated rate feedback is often implemented in order to damp certain modes and to facilitate a reduced order model used in the H_∞ design process. However, experimental implementation of colocated velocity feedback can lead to stability problems if a priori precautions of actuator dynamics are not taken⁸⁻⁹. In particular, the control of low frequency modes could destabilize the intermediate and higher modes. Also, the closed-loop response characteristics are sensitive to the plant model used in the H_∞ design. If significant error exists between the nominal model and the actual system, then experimental results could drastically differ from analytical simulations.

Recent experimental verification of applying an H_∞ design for active vibration suppression has shown more practical solutions to this control problem. Fanson et al² have demonstrated that a non-colocated robust control approach can provide satisfactory performance characteristics in structures with and without passive damping. However, differences exist between experimental results and theoretical responses, due to significant error between the nominal (finite element) model and the actual structure. Stroughton and Voth¹⁰ have shown that a colocated robust control design for a highly damped structure could be developed. This design is insensitive to fairly large errors in specific structural modes. However, the controller is of high order which imposes extensive computational burden. The intent of this paper is to develop a low order H_∞ controller which provides structural damping in a flexible structure using non-colocated sensors and actuators. Non-colocated control of a flexible structure is difficult to achieve since low damping and non-minimum phase characteristics are inherent in the system.

In recent years, several time domain techniques have become useful for structural testing (see, e.g. [11-13]). In most circumstances, time domain identification algorithms have advantages over conventional frequency domain algorithms, including: higher testing speed, better resolution of modes in high modal density bandwidths, and lower cost of instrumentation¹⁴. Therefore, time domain techniques for flexible structure realization and identification are useful in determining state-space models, which are required for the H_∞ control design. In most circumstances, the identification of SISO models from experimental data can easily be obtained. However, since transmission zeros impose strict mathematical constraints on system matrices, minimal realizations of MIMO systems are usually difficult to obtain experimentally. Possible sources of error include: sensor and instrumentation noise, slight nonlinearities inherent in the structure, and/or background vibration. Therefore, for system identification of flexible structures, multiple experiments are usually performed in order to improve mathematical models. However, this requires extensive computational time and effort.

The identification algorithm used in this paper identifies accurate (near minimal) realizations of a structure from only one set of experimental data. This algorithm combines an optimal state estimation

routine, known as the Minimum Model Error (MME) estimator¹⁵⁻¹⁶, with the Eigensystem Realization Algorithm¹⁷ (ERA) in order to provide robust features for MIMO identification. In several previous studies, this algorithm has been successfully applied to numerous applications, including; e.g., nonlinear estimation¹⁸, and robust realization/identification of mode shapes in damped structures¹⁹⁻²⁰.

The μ -synthesis approach²¹ utilizes robust performance techniques in order to alleviate deviations in the nominal model. However, this methodology usually results in high order controllers if the nominal model has a large number of uncertainties. Also, the choice of uncertainty weights requires some level of iteration and intuition in order to achieve the required performance characteristics. The design procedure in this paper involves the determination of an accurately identified model from experimental data, so that the use of uncertainty weighting can be minimized.

Robustness, with respect to parameter and structural changes, is an important aspect to any control design. The use of multiplicative and additive uncertainty singular value relationships can help determine which modes are sensitive to structural variations⁵. Of particular interest is the suppression (damping) of lower modes without the destabilization of high frequency modes. The aid of accurate model representations, using the MME/ERA identification algorithm, can lead to a clearer coherence between experimental results and theoretical predictions. Therefore, model and structural uncertainties can be studied in order to test the robustness and sensitivity of the H_∞ controller on the closed-loop system.

The organization of this paper proceeds as follows. First, a brief overview of the H_∞ control theory and design methodology is summarized. Then, the experimental implementation and system hardware for the structure are shown. The identified model is then realized into state-space form by using the combined MME/ERA identification algorithm. This model is incorporated with H_∞ performance specifications for vibration suppression and controller frequency-response shaping. Two designs are presented. One design stresses active damping in the first two modes of the structure, while the other design stresses robust stability over a higher system bandwidth. Each of these control designs are experimental implemented and results are compared to theoretical computer simulations.

H_∞ Overview

This section gives a brief overview of the fundamental theory of H_∞ control design. The H_∞ norm of a transfer function matrix represents the maximum energy in the output signal from the transfer function due to any input of unit energy. Therefore, minimizing the H_∞ norm of a transfer function is equivalent to minimizing the energy in the output signal due to the inputs⁵.

In order to demonstrate the fundamental aspects of H_∞ control theory, consider a system with controller $F(s)$ and plant $G(s)$. The sensitivity function $(I - FG)^{-1}$ is defined as the transfer function from the output disturbance $D(s)$ to the plant output $Y(s)$. Then, if a stabilizing controller (F) is chosen such that $\| (I - FG)^{-1} \|_\infty$ is minimized, the energy of the plant output due to a disturbance of bounded energy is minimized. Similarly, the output controller function $F(I - FG)^{-1}$ is the transfer function from the reference input $R(s)$ to the controller output $U(s)$. Minimizing $\| F(I - FG)^{-1} \|_\infty$ constrains controller output energy and also maximizes allowable additive plant uncertainty⁵. Finally, the complementary sensitivity function $FG(I - FG)^{-1}$ is the transfer function from the reference input to the plant output. Minimizing $\| FG(I - FG)^{-1} \|_\infty$ tailors plant output energy to input reference commands. The H_∞ design process considers these closed-loop performances to pre-specified weighting functions, denoted as $\gamma W_1(j\omega)$, $W_2(j\omega)$, and $W_3(j\omega)$. The H_∞ optimization problem is to find a stabilizing controller $F(s)$ that minimizes:

$$\left\| \begin{array}{c} \gamma W_1(I - FG)^{-1} \\ W_2 F(I - FG)^{-1} \\ W_3 FG(I - FG)^{-1} \end{array} \right\|_\infty \quad (1)$$

Equation (1) also shapes the frequency loop transfer function $L(s) = G(s)F(s)$ by penalizing the sensitivity function to reject plant disturbances, and high frequency $L(s)$ by penalizing the complementary sensitivity to cope with model uncertainties, while maintaining controller output to desired specifications. The solution of the H_∞ control problem involves an iteration on the γ term of the

specified disturbance weighting function. As γ is increased the sensitivity function ($S(s)$) decreases, while the complementary sensitivity function ($(I - S)$) approaches the W_3^{-1} weighting function.

H_∞ Design with Active Damping

The mixed sensitivity approach²² in Equation (1) shows a clear trade-off between performance and robustness of a multi-variable system. However, this methodology does not enable a practical design approach for active damping, since plant dynamics are usually canceled with compensator dynamics. This section expands upon the fundamental H_∞ control formulation in order to provide a means of incorporating active damping into a structure with inherently low structural damping ratios (well below 0.50% critical).

Consider the block diagram of a MIMO plant in Figure 1. Let the MIMO plant ($G(s)$) be partitioned into "disturbance" ($G_1(s)$) and "plant/actuator" ($G_2(s)$) transfer functions, i.e.:

$$Y(s) = G_1(s)U_{1a}(s) + G_2(s)U_2(s) \quad (2)$$

The partitioned transfer functions have ideally the same characteristic polynomial, and differ only in numerator dynamics. The inputs in Figure 1 are: $U_{1a}(s)$, any disturbance input into the structure (non-colocated with the actuator; and $U_{1b}(s)$, a fictitious input used to simulate the sensor uncertainty. The "augmented" plant with control compensator is shown in Figure 2.

Figure 1 Multi-Input-Multi-Output Block Diagram

Figure 2 Augmented Closed-Loop System

The open-loop transfer function matrix of the augmented plant is:

$$\begin{bmatrix} y_{1a} \\ y_{1b} \\ y_{1c} \\ \dots \\ y_2 \end{bmatrix} = \begin{bmatrix} W_1 G_1 & W_1 & -W_1 G_2 \\ 0 & 0 & W_2 \\ 0 & 0 & W_3 G_2 \\ \dots & \dots & \dots \\ G_1 & I & -G_2 \end{bmatrix} \begin{bmatrix} u_{1a} \\ u_{1b} \\ \dots \\ u_2 \end{bmatrix} \quad (3)$$

where u_2 and y_2 are controller output and input, respectively. The sensitivity function between the disturbance input and the plant output now becomes:

$$\frac{e}{u_{1a}} = \frac{G_1}{I - FG_2} \quad (4)$$

Therefore, active damping can be accomplished, since pole locations of the closed-loop transfer function in Equation (4) are shifted by the controller (F) and plant/actuator transfer functions. From Figure 2, the characteristics of the weighting function $W_1(s)$ determines the amount of damping and frequency response dynamics of the closed-loop systems. The complementary sensitivity (sensor uncertainty) function and controller/limiter function remain unchanged from the previous section. Also, once the augmented plant in Equation (3) is formed, numerical algorithms for the computation of the optimal controller can be utilized. This controller solution is determined by the two-Riccati algorithm²³ using the Robust Control Toolbox²⁴ for Matlab.

Experimental Hardware

A clamped frame serves as a testbed for the experimental H_∞ control implementation. The structure consists of 39 elements connected at 18 nodes. All but two of the structural members are made from thin-walled circular aluminum tubing with an outer diameter of 0.25" and a wall thickness of 0.05". Each member is pinned and bolted into the nodes to eliminate looseness in the joints. The frame

is configured in a planar fashion so that the only significant deformation occurs perpendicular to the structure (see Figure 3).

Figure 3 Flexible Frame Testbed

Two of the structural members are flat aluminum bars layered with piezoceramics. Either of these struts can excite the frame since a voltage applied across the piezoceramics produces a moment on the frame. The strut on the bottom of the frame has four ceramics glued to it and serves as the control actuator. The other flat strut is configured with the same number of piezoceramics and acts as a disturbance source. Each of these active members has a thickness of 0.25" and a width of 1.0625". The piezoceramics are Model G-1195 from Piezo Electric Products with dimensions 2.5" x 0.75" x 0.01".

The sensor is a Philtec (model 88NE3) optical displacement sensor placed near node 18 at the free end of the frame. This sensor is non-located with both the control actuator and the disturbance source. Frequency analysis and data acquisition are performed using a Tektronix 2630 Fourier Analyzer. Control laws are implemented on an Optima 3 digital controller, sampling at a rate of 500 Hz. This sampling rate allows the maximum allowable performance for the H_∞ controller design. Finally, two Hewlett Packard (model 6924A) amplifiers are used to magnify the control and disturbance signals.

Robust System Estimation and Identification

An accurate state-space model of the testbed is required in order to perform an optimal control design. In this work, the Eigensystem Realization Algorithm¹⁷ (ERA) is combined with the Minimum Model Error¹⁵ (MME) optimal estimator in order to update a finite element (nominal) model to conform with experimental data. The finite element model provides a fairly accurate representation of the frame at the lower modes, as shown in Figures 4 and 5. However, the higher modes are not modeled accurately. This could cause the destabilization of higher modes when implementing the controller onto the actual structure.

Figure 4 Experimental, Analytical, and Identified Magnitude Plots (1st input)

Figure 5 Experimental, Analytical, and Identified Magnitude Plots (2nd input)

The ERA method is effective for developing accurate state-space models when noise levels are low in nature. However, difficulties arise when higher noise levels are present in the output measurements. These effects can make a minimal state-space model of a MIMO system extremely difficult to obtain, since transmission zeros also constrain the realization. For the identification of the testbed the ERA is able to identify the natural frequencies and damping ratios fairly accurately using an average of three different time histories. But, a near minimal MIMO realization of the testbed could not be obtained. By combining the ERA with the MME estimator, which utilizes the minimal state-space MIMO finite element model, improved modal identification is achieved with near minimal MIMO realizations.

In this section, the MME algorithm is briefly reviewed for the case of linear time-variant state-space models. A more detailed derivation of the algorithm may be found in Reference 15. The MME algorithm assumes that the state estimates are given by a nominal (pre-specified) model and an unmodeled error vector, shown as:

$$\begin{aligned}\dot{\underline{x}}(t) &= A_m(t) \underline{x}(t) - B_m(t) u(t) - \underline{d}(t) \\ \underline{y}(t) &= C_m(t) \underline{x}(t) - D_m(t) u(t)\end{aligned}\tag{5}$$

where $A_m(t)$, $B_m(t)$, $C_m(t)$, $D_m(t)$ are time-variant nominal state matrices from the finite element model, $u(t)$ is a $(p \times 1)$ known forcing input, $\underline{d}(t)$ is an $(n \times 1)$ un-modeled (to-be-determined) model error vector, $\underline{x}(t)$ is the $(n \times 1)$ state estimate vector, and $\underline{y}(t)$ is the $(q \times 1)$ estimated output. For the remainder of this paper, the state-space (model) matrices are assumed time-variant, but are shown without the time argument (t) .

State-observable discrete time-domain measurements are assumed for Equation (5) in the following form:

$$\underline{y}(t_k) = \underline{g}_k(\underline{x}(t_k), t_k) + \underline{v}_k\tag{6}$$

where $\underline{\hat{y}}(t_k)$ is an $(q \times 1)$ measurement vector at time t_k , g_k is an accurate model of the measurement process, ν_k represents measurement noise, and m is the total number of measurement output sets. The measurement noise process is assumed to be a zero-mean, Gaussian distributed process of known covariance, R .

In the MME, the optimal state estimates are determined on the basis that the measurement-minus-estimate error covariance matrix must match the measurement-minus-truth error covariance matrix. This condition is referred to as the "covariance constraint", approximated by:

$$\left\{ \left[\underline{\hat{y}}(t_k) - \underline{\hat{y}}(t_k) \right] \left[\underline{\hat{y}}(t_k) - \underline{\hat{y}}(t_k) \right]^T \right\} \approx R \quad (7)$$

Therefore, the estimated measurements are required to fit the actual measurements with approximately the same error covariance as the actual measurements fit the truth.

A cost functional, consisting of the weighted sum square of the measurement-minus-estimate residuals plus the weighted sum square of the model correction term, is next minimized:

$$J = \sum_{k=1}^m \left\{ \left[\underline{\hat{y}}(t_k) - \underline{\hat{y}}(t_k) \right]^T R^{-1} \left[\underline{\hat{y}}(t_k) - \underline{\hat{y}}(t_k) \right] \right\} - \int_{t_0}^{t_f} \underline{d}(\tau)^T W \underline{d}(\tau) d\tau \quad (8)$$

where W is a weight matrix determined by satisfying the covariance constraint. If the measurement residual covariance is larger than R , then the measurement estimate is not close to the actual system measurements. Therefore, W should be decreased in order to less penalize the model correction ($\underline{d}(t)$). However, if the estimate covariance is too low, then W should be increased in order to allow more model correction. The model error corrects the finite element model in order to estimate the output

using experimental measurements. Therefore, the model error term tends to update the finite element model to conform to actual system responses.

The necessary conditions for the minimization of J , with respect to the model correction term $\underline{d}(t)$, leads to the following Two-Point-Boundary-Value-Problem TPBVP¹⁵:

$$\begin{aligned}\dot{\underline{x}}(t) &= A_m \underline{x}(t) - B_m u(t) - \underline{d}(t) \\ \dot{\underline{\lambda}}(t) &= -A_m^T \underline{\lambda}(t) \\ \underline{d}(t) &= -\frac{1}{2} W^{-1} \underline{\lambda}(t) \\ \underline{\lambda}(t_k^-) &= \underline{\lambda}(t_k^-) - 2 C_m^T R^{-1} [\underline{\hat{y}}(t_k) - \underline{\hat{y}}(t_k)]\end{aligned}\tag{9}$$

where $\underline{\lambda}(t)$ is a vector of co-states (Lagrange multipliers). Also, the co-state equation is updated at each measurement interval. The boundary conditions are selected such that either $\underline{\lambda}(t_0^-) = \underline{0}$ or $\underline{x}(t_0)$ is specified for the initial time and either $\underline{\lambda}(t_f^-) = \underline{0}$ or $\underline{x}(t_f)$ is specified at the final time. The solution of the TPBVP involves the determination of a linear Riccati equation and a linear differential equation¹⁶.

Modified Eigensystem Realization Algorithm

The ERA method is a modal synthesis technique based on the concept of singular value decomposition (see Reference 17 for more details). This procedure is capable of accurately identifying the model properties of systems involving perfect or low-noise measurements. In this section the ERA is expanded to include the state and output estimates given by the MME estimator.

Consider the discrete-time linear dynamic equation:

$$\begin{aligned}\underline{x}(k+1) &= A \underline{x}(k) + B \underline{u}(k) \\ y(k) &= C \underline{x}(k) + D \underline{u}(k)\end{aligned}\tag{10}$$

where \underline{x} is a $(n \times 1)$ state vector, \underline{u} is a $(p \times 1)$ input vector, y is a $(q \times 1)$ output vector, and A , B , and C are $(n \times n)$, $(n \times p)$ and $(q \times n)$ constant matrices, respectively. A solution to Equation (10) is

given by the Markov parameters from a unit impulse response:

$$Y(k) = CA^{k-1}B \quad X(K) = A^{k-1}B \quad (11)$$

The first step in the modified ERA is to form an $(r \times s)$ block Hankel matrix composed of the impulse response data from the MME:

$$H(k-1) = \begin{bmatrix} Z(k) & \dots & Z(k-m_{s-1}) \\ \vdots & \ddots & \vdots \\ Z(k-l_{r-1}) & \dots & Z(k+l_{r-1}+m_{s-1}) \end{bmatrix} \quad (12)$$

where r and s are arbitrary integers satisfying the inequalities $rq \geq n$ and $sp \geq n$, and l_i ($i = 1, 2, \dots, r-1$) and m_j ($j = 1, 2, \dots, s-1$) are arbitrary integers. The vector Z consists of the estimated output and states given by the MME estimator, i.e. $\underline{z} = [\underline{\hat{x}} \ \hat{y}]^T$. The singular value decomposition of H may be expressed as $H = PD_nQ$. The ERA then forms the discrete-time, reduced-order model realization of dimension n in the following form:

$$\begin{aligned} A &= D_n^{-1/2} P_n^T H(1) Q_n D_n^{-1/2} \\ B &= D_n^{1/2} Q_n^T E_p \\ C &= E_q^T P_n D_n^{1/2} \\ D &= Y(0) \end{aligned} \quad (13)$$

where P_n and Q_n are formed from the first n columns of P and Q from the singular value decomposition, and D_n is the diagonal matrix of singular values. E_p^T is $[I_p, 0]$, and E_q^T is $[I_q, 0]$, where I_p and I_q are identity matrices of order p and q , respectively, and 0 is the zero matrix.

The modal damping ratios and damped natural frequencies are calculated by observing the real and imaginary parts of the eigenvalues, after a transformation from the z -plane to the s -plane is completed¹⁷. The physical mode shapes of the system are determined using the realized eigenvectors (Φ) of the ERA

state matrices. The physical mode shapes are given by $\Psi = C_m \Phi$. Physical state matrices can be determined by using this mode shape matrix and the continuous eigenvalue matrix:

$$A_m = \Psi \Lambda \Psi^{-1} \quad B_m = \Psi \begin{bmatrix} \frac{e^{\lambda_1 \Delta t}}{\lambda_1} & 0 & \dots & 0 \\ 0 & \ddots & & 0 \\ \vdots & & \ddots & \vdots \\ 0 & 0 & \dots & \frac{e^{\lambda_n \Delta t}}{\lambda_n} \end{bmatrix}^{-1} \Psi^{-1} B \quad (14)$$

where Λ is the continuous eigenvalue matrix, derived from a discrete to continuous eigenvalue transformation of the ERA state matrix. Therefore, an identification of system parameters is possible by using the physical state matrices shown in Equation (14).

Combined Realization Algorithm

The combined MME/ERA algorithm enables the realization of a MIMO model in the presence of significant model error, process noise, and measurement noise. In order to obtain impulse response data, the test structure is excited using a random input with a bandwidth of 0–50 Hz. An inverse and regular Fourier transformation is applied on this data to obtain the impulse response time histories. Also, only one set of data for each input is taken for the identification. Therefore, extensive and repetitive computational analysis is attenuated by using the combined MME/ERA method, since averaging of multiple sets of data is not needed. This is an important aspect due to the difficulty of obtaining multiple sets of experimental data for orbiting space structures.

A block diagram illustrating the steps of the robust realization algorithm is shown in Figure 6. First, the finite element model is used as the assumed model in the MME estimator. Next, the MME estimation problem is solved, using the covariance constraint to determine an optimal weighting matrix. The continuous estimated state histories produced from the MME are then re-sampled. Finally, these estimated time histories are processed, in order to realize an accurate model of the system parameters, using the modified version of the ERA. These steps may be repeated if necessary in order to further

smooth the measurements and improve the identification process. However, accurate identification results for this testbed required only one iteration through the MME estimation process.

Figure 6 Block Diagram of the Combined Realization Algorithm

The modal properties for the first eleven flexible modes of the frame are shown in Table 1. The frame has all of the characteristics of a large flexible structure. It is modally dense, with eleven modes in the first 60 Hz bandwidth. Also, inherent damping in the structure is low, with modes having damping ratios less than 0.50%. The combined algorithm also identifies the frequency response characteristics of the in-room fluorescent lighting at about 60 Hz.

Table 1 Poles of the Identified Model

Mode	ω (Hz)	ζ (%)
1	1.91	0.46
2	4.00	0.25
3	10.14	0.21
4	15.80	0.20
5	23.10	0.13
6	29.67	0.17
7	37.06	0.13
8	48.36	0.45
9	49.00	0.36
10	54.55	0.25
11	56.08	0.27
lights	60.00	0.00
real	0.20	

Magnitude Bode plots of the MME/ERA identification results are compared to experimental frequency response characteristics in Figures 4 and 5 (also shown is the finite element model frequency plot). The MME/ERA produced a near minimal realization (24th order) for the first eleven modes. This MIMO model is extremely accurate with good agreement to experimental frequency response results. Also, the modal amplitude coherence¹⁷ (MAC) factors are substantially improved when using

the combined MME/ERA algorithm. Therefore, this MIMO state-space model forms the basis for the robust control design.

Robust Control Design

In this section the concepts and limitations for the selection of the proper weighting functions used in the H_∞ design are presented. The appropriate selection of weighting functions over the desired frequency range is not explicitly related to the performance objectives in a straightforward manner. Numerous trial selections are usually required in order to obtain desired performance objectives.

The goal of the H_∞ design is to reshape the open-loop dynamics in order to provide vibration suppression in the frequency region considered. Therefore, the sensitivity function in Equation (4) is utilized to reshape these desired frequency characteristics and provide adequate damping to the structure. The complementary sensitivity function is used as an uncertainty weight for the sensor output. After careful consideration and numerous trials, a set of proper inverse weighting functions is obtained. The inverse weighting functions for the sensitivity and complementary sensitivity functions are shown in Figure 7. The W_1^{-1} function weights the sensitivity function along the zero decibel region over a desired frequency. Damping can be added to the system by decreasing the overall magnitude of this weighting function (accomplished by increasing γ in the control solution formulation). The W_3^{-1} frequency function invokes a higher weight at lower frequencies with a first order roll-off at higher frequencies. This limits the low frequency noise from the sensor so that it is not amplified through the controller.

Figure 7 Magnitude Plots of the Inverse Weighting Functions

The inverse weighting function for the controller output is also shown in Figure 7. The desired characteristics of the controller is to obtain an attenuated controller response at lower *and* higher frequencies. This results in a third-order weighting function that simulates a band-pass filter. The choice of this weighting function insures that the controller does not destabilize higher frequency modes and also attenuates control signals at lower frequencies.

The selection of these weighting functions provides adequate damping in the closed-loop system. An optimal H_∞ controller solution, using the γ iteration technique, is determined with these weighting functions. The controller is found to be proper and rational. Since the augmented state-space model, derived from Equation (3), is 29th order, the subsequent H_∞ controller is also 29th order. The Schur balanced model reduction method²⁴ is used to reduce this controller. The size of the resulting controller is 15th order. The frequency response characteristics of the control design is shown in Figure 8. The controller size is the maximum allowable order for the digital computer implementation. The next section summarizes the closed-loop results and shows a comparison between analytical simulations and experimental results.

Figure 8 Magnitude Plot of the Robust Controller

Experimental Control Results

In this section, the H_∞ controller is experimentally implemented onto the testbed in order to test the validity of the identification and control techniques previously described. Results show that the performance objectives can be met with a significant increase in damping for more than one mode. Model uncertainties are also experimentally investigated and the results are compared to theoretical predictions.

The initial H_∞ controller design (shown in Figure 8) is found to substantially increase the damping in the first two modes without the destabilization of higher modes. Digital implementation of this controller onto the testbed increases the damping in the first mode (bending) by a factor of about 14 ($\zeta_{cl} = 6.32\%$) and the second mode (torsional) by a factor of about 30 ($\zeta_{cl} = 7.51\%$). These results are summarized in Table 2 (the table also gives results for perturbed systems and a second control design, each described later). Slight damping is also provided in higher frequency modes. The closed-loop transfer function between the disturbance input and position sensor for the first two modes is shown in Figure 9. The H_∞ controller is able to significantly provide active damping in the targeted frequency region. Figure 10 shows the position sensor output to a random noise input (bandwidth of 0–5 Hz)

applied at the disturbance strut. Both open-loop and closed-loop responses are shown. Without the H_∞ controller, the vibration of the frame does not settle out for well over 80 seconds. Closing the loop not only attenuates the level of vibration by over 75%, but the increase in damping also reduces the settling time to less than 4 seconds. In fact, the closed-loop response has a magnitude near to the noise level of the sensor.

Table 2 System Results for Two Controller Designs and Perturbations

	System	Nominal	1 st Perturbed	2 nd Perturbed
	ω_n $\zeta(\%)$	ω_n $\zeta(\%)$	ω_n $\zeta(\%)$	ω_n $\zeta(\%)$
Initial Controller	1) 1.91 0.46	1) 1.95 6.32	1) 1.95 6.55	unstable
	2) 4.00 0.25	2) 4.41 7.51	2) 4.44 6.57	unstable
Second Controller	1) 1.91 0.46	1) 1.91 1.94	1) 1.91 1.93	1) 1.59 1.56
	2) 4.00 0.25	2) 4.12 2.56	2) 4.11 2.50	2) 3.93 2.62

Figure 9 Closed-Loop and Open-Loop Transfer Function Magnitude Plots

Figure 10 Closed-Loop and Open-Loop Time Responses

With the nominal design complete, model and structural uncertainties are next studied in order to test the robustness and sensitivity of the H_∞ controller on the closed-loop system. This is accomplished by varying the modal properties of the frame, while utilizing the controller designed for the *nominal* system. The net effect on the structure is to incorporate multiplicative perturbations into the system. The H_∞ norm of a system can be used to measure the stability margins of the nominal control design in the face of these perturbations. Applying small gain theory⁵ to this uncertainty case, a sufficiency test for stability robustness with a multiplicative uncertainty input is given as:

$$\bar{\sigma}(\Delta_m(s)) < \frac{1}{\bar{\sigma}[F(s)(I + G(s)F(s))]^{-1}} \quad (15)$$

where $\Delta_m(s)$ denotes multiplicative uncertainties and $\bar{\sigma}$ denotes the maximum singular value over

the desired frequency region. Therefore, a multiplicative uncertainty bound over all frequencies can be used to determine which frequency is most sensitive to multiplicative perturbations. A plot of the theoretical uncertainty bound for the initial control design using the nominal plant is shown in Figure 11. From this figure, the frequency which is most sensitive to plant perturbations is the 23 Hz mode. Therefore, this mode is most likely to become unstable in the face of perturbations on the frame.

Figure 11 Theoretical Multiplicative Uncertainty Bound

Multiplicative perturbations are accomplished experimentally by varying the modal properties of the frame, while utilizing the initial (nominal) control design. The natural frequencies and mode shapes are altered by placing weights at various points along the frame. These weights have a mass of approximately 3–5% of the mass of the total structure. The first perturbation is to place the weights on nodes 4 and 5 on the testbed (see Figure 3). The second perturbation is to place the weights on nodes 16 and 17 on the testbed. The resulting changes in natural frequencies for these perturbations are shown in Table 3. The first perturbation has an average deviation of about 10% from the nominal natural frequencies. The second perturbation has an average deviation of about 15%. The most significant changes occur at higher frequencies. Therefore, the nominal H_∞ controller can be tested for stability and performance using the experimentally perturbed systems. The controller is first used with the weights on nodes 4 and 5. Results for the closed-loop damping ratios are shown in Table 2. Even with an average of 10% changes from the nominal system, robust stability and performance is achieved, with equal damping ratios as the nominal system. Closed-loop results for the second perturbation show that the system becomes unstable. However, as theory predicts from the multiplicative uncertainty plot (Figure 11), the closed-loop system becomes unstable at a frequency of about 23 Hz (shown in Figure 12). Therefore, with the aid of accurate system models, the sensitivity of the H_∞ controller can be investigated and adjusted in order to compensate for perturbations *without* implementing the controller to the actual frame.

Figure 12 Experimental Instability using the First Perturbed System

Table 3 Natural Frequencies of the Perturbed Models

Mode number	ω (Hz) (nom.)	ω (Hz) (1st pert.)	ω (Hz) (2nd pert.)
1	1.91	1.88	1.59
2	4.00	4.00	3.88
3	10.14	9.78	9.41
4	15.80	15.28	15.03
5	23.10	22.66	21.38
6	29.67	25.09	24.03
7	37.06	29.03	27.97
8	48.36	32.12	35.47
9	49.00	44.25	39.72
10	54.55	47.25	46.16

The second controller design provides more robust stability, but decreases performance slightly. This controller is derived by simply decreasing the γ term during the H_∞ solution. The experimental closed-loop results for the nominal, first perturbation, and second perturbation systems are shown in Table 2. The magnitude frequency response and time responses to a random input are also shown in Figures 9 and 10, respectively. The nominal design increases damping by a factor of about 4 in the first mode and by a factor of about 10 in the second mode. This damping is less than the first controller design; however, the multiplicative uncertainty bound allows a greater perturbation at 23 Hz, as opposed to the initial controller design. Closed-loop results indicate that robust stability and performance is maintained for both perturbation systems (see Table 2). The second perturbation system remains stable and has approximately the same increase in damping as the first perturbation and nominal design, using the second controller.

The control of the frame is next tested by placing the sensor at various nodes along the frame. The sensor is next mounted at node 15 and the H_∞ control design is repeated. Results indicate that significant damping is again achieved in the first two modes with good agreement between theory and experiment.

The control design for all cases involved SISO control of one node. The final control design is a MIMO controller with sensors placed at nodes 15 and 18. Theoretical results indicate that no significant increase in damping is achieved for the MIMO design. This is most likely due to the frame being controlled only by one strut. If multiple controller actuators are used, then greater possibilities of MIMO control can be achieved. The MME/ERA identification algorithm is extremely useful for designing MIMO feedback loops, since accurate (near minimal) realizations of MIMO systems are possible. Therefore, the extension to more complicated flexible frames can easily be accomplished using H_∞ control.

Finally, the increase in system performance is achieved without the use of any supplementary (low authority) control. In many circumstances, passive damping elements and colocated control loops are first implemented in the design. The H_∞ controller is then used to further improve stability and performance. The results in this paper illustrate that system performance can be significantly improved and maintained in the face of modest perturbations, without the use of supplementary control. Therefore, eliminating the need for supplementary active or passive damping decreases the complexity of the overall control problem.

Conclusions

A controller using H_∞ optimal control theory was designed and experimentally implemented to provide vibration suppression on a flexible frame structure. Time domain data was first used to obtain an accurate MIMO model. The identification algorithm combined the Minimum Model Error estimator with the Eigensystem Realization Algorithm in order to update a finite element model to conform with experimental data. Eleven flexible modes were found to be inside the frequency range of 0–60 Hz, all with damping ratios of less than 0.5% critical. This MIMO model formed the basis for the H_∞ control design.

A formulation designed to add active damping to the structure was determined for the control design. The closed-loop response characteristics of the structure was shaped by careful choice of three weighting functions. The first weight constrained sensor noise uncertainty. The second weight was

designed to roll-off the controller at low and high frequencies. The last weight controlled the amount of active damping in the structure. Experimental implementation of the H_∞ controller on the flexible frame validated the control formulation. Two control designs were considered. The first design provided significant damping in the first two modes, but was sensitive to structural perturbations. The second design provided damping to a lesser degree, but supplied robust stability over significant perturbations to the structure. Results also indicate that with accurate model representations, the H_∞ controller can provide not only robust stability, but robust performance to modest system perturbations.

The difficult problem of designing a non-colocated controller for a flexible structure was handled well using H_∞ control theory. The framework in which the controller was designed was greatly simplified due to the accuracy of the identified state-space model. Reducing the complexity of the problem allowed a physical basis for choosing weighting functions. Therefore, the amount of effort needed to obtain and implement an H_∞ controller was greatly decreased.

References

- [1] Cannon, R.H., and Rosenthal, D.E., "Experiments in Control of Flexible Structures with Non-Colocated Sensors and Actuators," *AIAA Journal of Guidance, Control and Dynamics*, Vol. 7, No. 5, Sept.-Oct. 1984, pp. 546-553.
- [2] Fanson, J.L., Lurie, B.J., O'Brien, J.F., Chu, C-C., and Smith, R.S., "System Identification and Control of the JPL active Structure," *Proceedings of the 32nd Structures, Structural Dynamics, and Materials Conference*, Baltimore, MD, April, 1991.
- [3] Wie, B., Horta, L., and Sulla, J., "Classical Control System Design and Experiment for the Mini-Mast Truss Structure," *AIAA Journal of Guidance, Control and Dynamics*, Vol. 14, No. 4, July-Aug. 1991, pp. 778-784.

- [4] Fanson, J.L., Chu, C-C., Smith, R.S., and Anderson, E.H., "Active Member Control of a Precision Truss Structure with an H_∞ Performance Objective." *Proceedings of the AIAA Dynamics Specialists Conference*, Long Beach, CA, 1990.
- [5] Tsen, Fu-Min, "Optimal Design Techniques of H_∞ Control," Ph.D. Thesis, State University of New York at Buffalo, December, 1991.
- [6] Kashani, R., Melkote, S., and Sorgenfrei, A., " H_∞ Control of a Smart Structure Helicopter Rotor Blade," *Proceedings of the ASME Design Technical Conferences*, Miami, FL, 1991.
- [7] Safonov, M.G., Chiang, R.Y., and Flashner, H., " H_∞ Robust Control Synthesis for a Large Space Structure," *AIAA Journal of Guidance, Control and Dynamics*, Vol. 14, No. 3, May-June 1991, pp. 513-519.
- [8] Goh, C.J., and Caughey, T.K., "On the Stability Problem Caused by Finite Actuator Dynamics in the Colocated Control of Large Space Structures," *International Journal of Control*, Vol. 41, No. 3, pp. 787-802.
- [9] Inman, D.J., "Control/Structure Interaction: Effects of Actuator Dynamics," *Mechanics and Control of Large Flexible Structures*, (ed. Junkins, J.L.), AIAA Press, 1990, pp. 507-535.
- [10] Stroughton, R.M., and Voth, C.T., "Vibration Suppression for a Large Space Structure Using H_∞ Control," *Proceedings of the AIAA Guidance, Navigation, and Control Conference*, New Orleans, LA, 1991.
- [11] Ibrahim, S.R., and Mikulcik, E.C., "A Method for the Direct Identification of Vibration

Parameters from the Free Response," *Shock and Vibration Bulletin*, No. 47, Pt. 4, Sept. 1977, pp. 183-198.

[12] Yeh, F-B., and Yang, C-D., "New Time-Identification Technique." *AIAA Journal of Guidance, Control and Dynamics*, Vol. 8 No. 4, Jul-Aug. 1987, pp. 463-470.

[13] Billings, S.A., "Identification of Nonlinear Systems-A Survey." *IEE Proceedings*, Vol. 127, Pt. D, No. 6, 1980, pp. 272-285.

[14] Roemer, M., "Robust System Realization/Identification via Optimal State Estimation," Ph.D. Dissertation, State University of New York at Buffalo, 1991.

[15] Mook, D.J., and Junkins, J.L., "Minimum Model Error Estimation for Poorly Modeled Dynamic Systems." *AIAA Journal of Guidance, Control and Dynamics*, Vol. 11, No. 3, May-June 1988, pp. 256-261.

[16] Crassidis, J.L., Mason, P.A.C., and Mook, D.J., "A Riccati Solution for the Minimum Model Error Algorithm." to appear in the *AIAA Journal of Guidance, Control and Dynamics*.

[17] Juang, J.-N., and Pappa, R.S., "An Eigensystem Realization Algorithm [ERA] for Modal Parameter Identification and Model Reduction," *AIAA Journal of Guidance, Control and Dynamics*, Vol. 8, No. 5, Sept.-Oct. 1985, pp. 620-627.

[18] Stry, G.I., and Mook, D.J., "Experimental Study of Nonlinear Dynamic System Identification." to appear in *Nonlinear Dynamics*.

- [19] Roemer, M.J., and Mook, D.J., "Robust Modal Identification/Estimation of the Mini-Mast Testbed," *AIAA Journal of Guidance, Control and Dynamics*, Vol. 15, No. 3, May-June 1992, pp. 642-647.
- [20] Roemer, M.J., and Mook, D.J., "Enhanced Realization/Identification of Physical Modes," *A.S.C.E. Journal of Aerospace Engineering*, Vol. 3, No. 2, April 1990, pp. 128-139.
- [21] Balas, G.J., Packard, A.K., and Harduvel, J.T., "Application of μ -Synthesis Techniques to Momentum Management and Attitude Control of the Space Station," *Proceedings of the AIAA Guidance, Navigation, and Control Conference*, New Orleans, LA, 1991.
- [22] Francis, B.A., Helton, J.W., and Zames, G., " H_∞ Optimal Control for Linear Multivariate Systems," *IEEE Transactions on Automatic Control*, Vol. AC-29, Oct. 1984, pp. 888-900.
- [23] Doyle, J.C., Khargonekar, P.P., and Francis, B.A., "State-Space Solutions to Standard H_2 and H_∞ Control Problems," *IEEE Transactions on Automatic Control*, Vol. AC-34, Aug. 1984, pp. 831-847.
- [24] Chiang, R.Y., and Safonov, M.G., *Robust-Control Toolbox*, Mathworks, South Natick, MA, 1988.

Figure 1 Multi-Input-Multi-Output Block Diagram

Figure 2 Augmented Closed-Loop System

Figure 3 Flexible Frame Testbed

Figure 4 Experimental, Analytical, and Identified Magnitude Plots (1st input)

Figure 5 Experimental, Analytical, and Identified Magnitude Plots (2nd input)

Figure 6 Block Diagram of the Combined Realization Algorithm

Figure 7 Magnitude Plots of the Inverse Weighting Functions

Figure 8 Magnitude Plot of the Robust Controller

Figure 9 Closed-Loop and Open-Loop Transfer Function Magnitude Plots

Figure 10 Closed-Loop and Open-Loop Time Responses

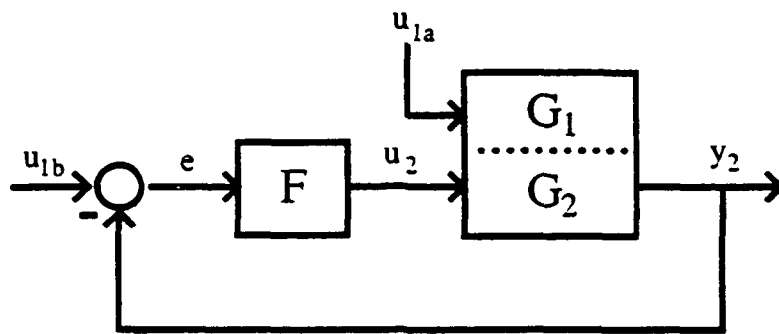
Figure 11 Theoretical Multiplicative Uncertainty Bound

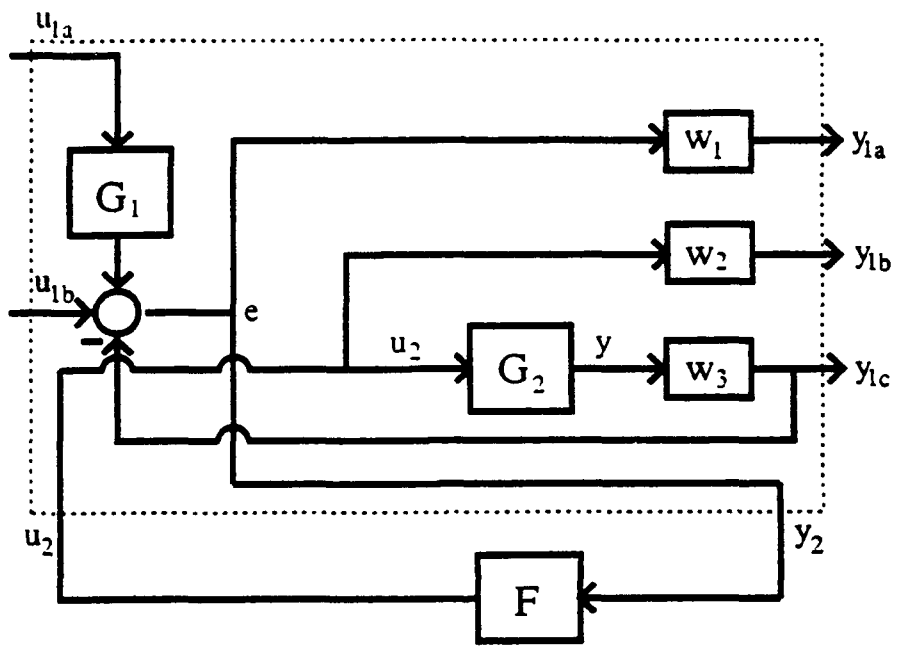
Figure 12 Experimental Instability using the First Perturbed System

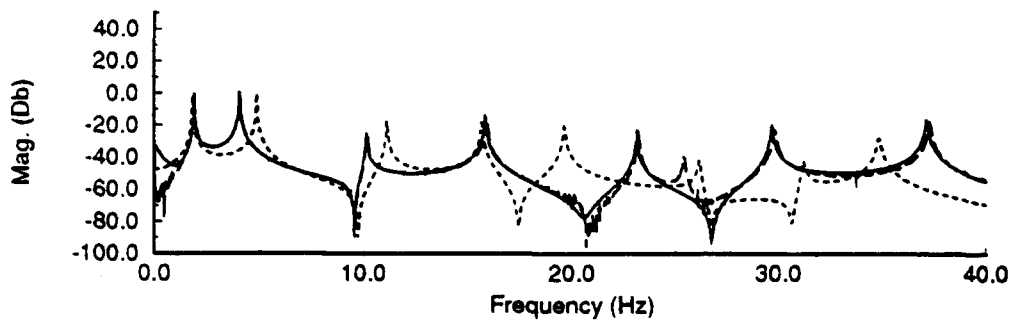
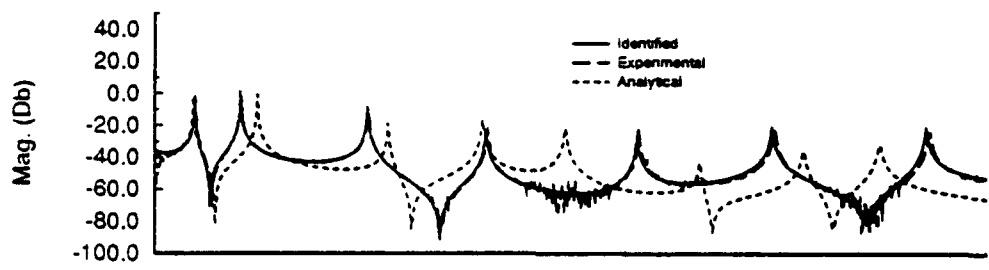
Table 1 Poles of the Identified Model

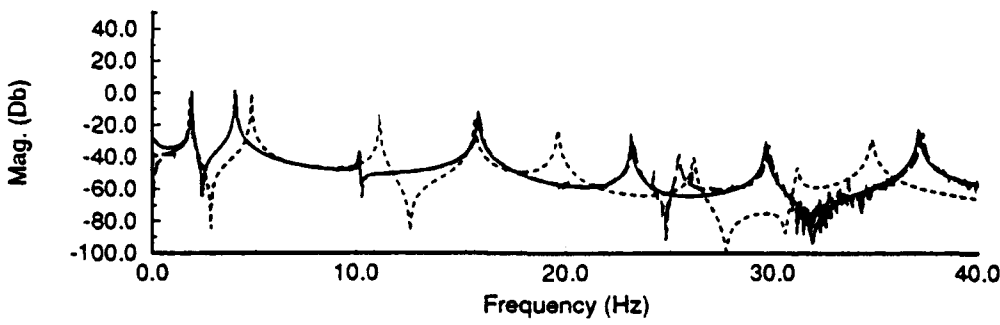
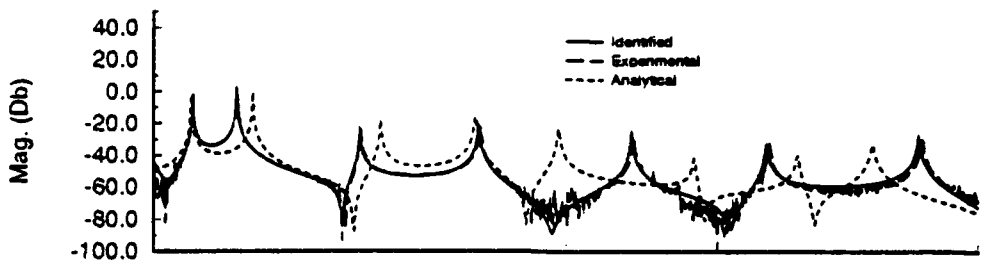
Table 2 System Results for Two Controller Designs and Perturbations

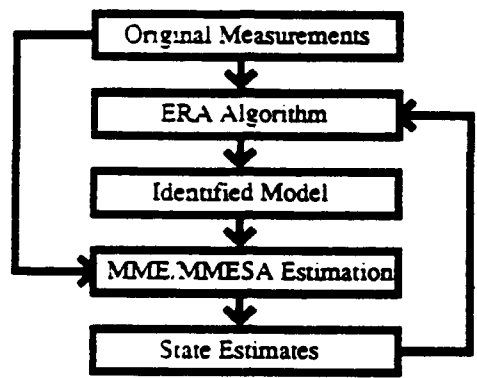
Table 3 Natural Frequencies of the Perturbed Models

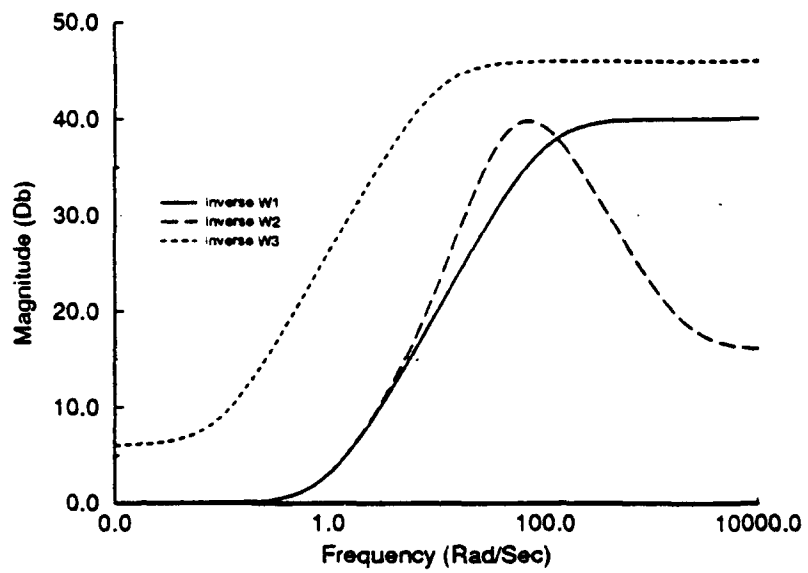


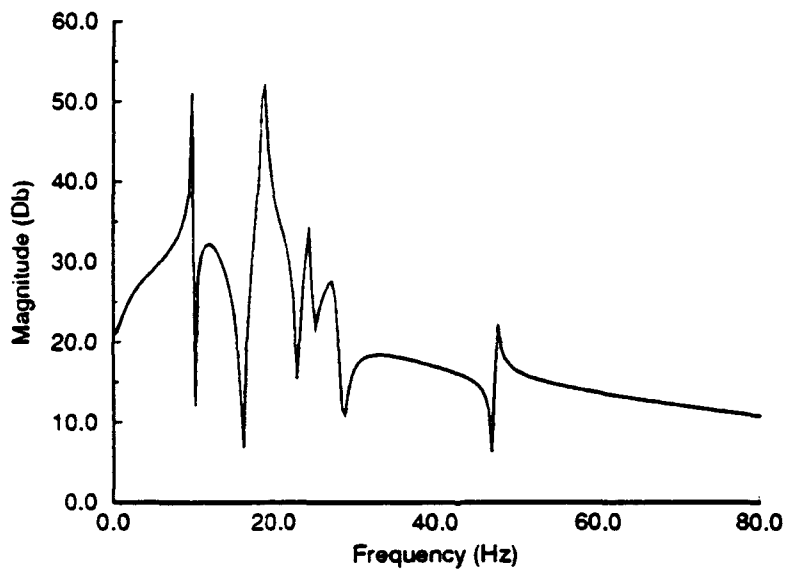


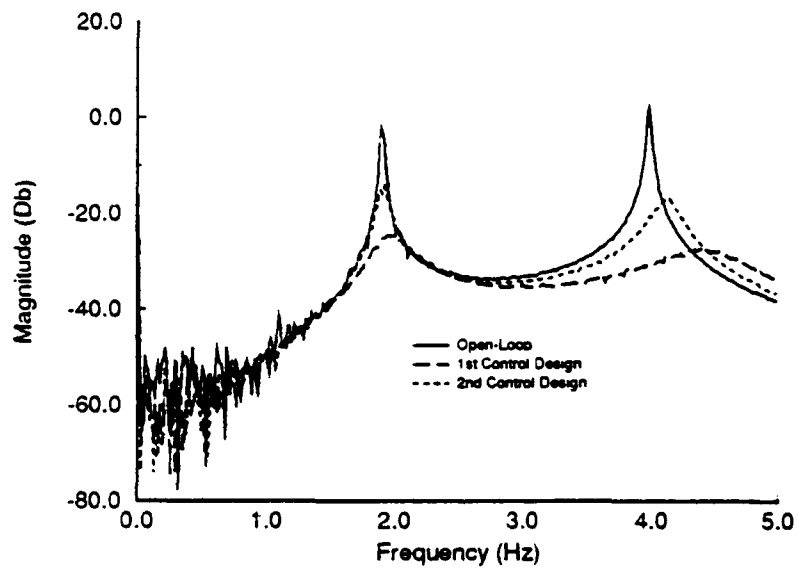


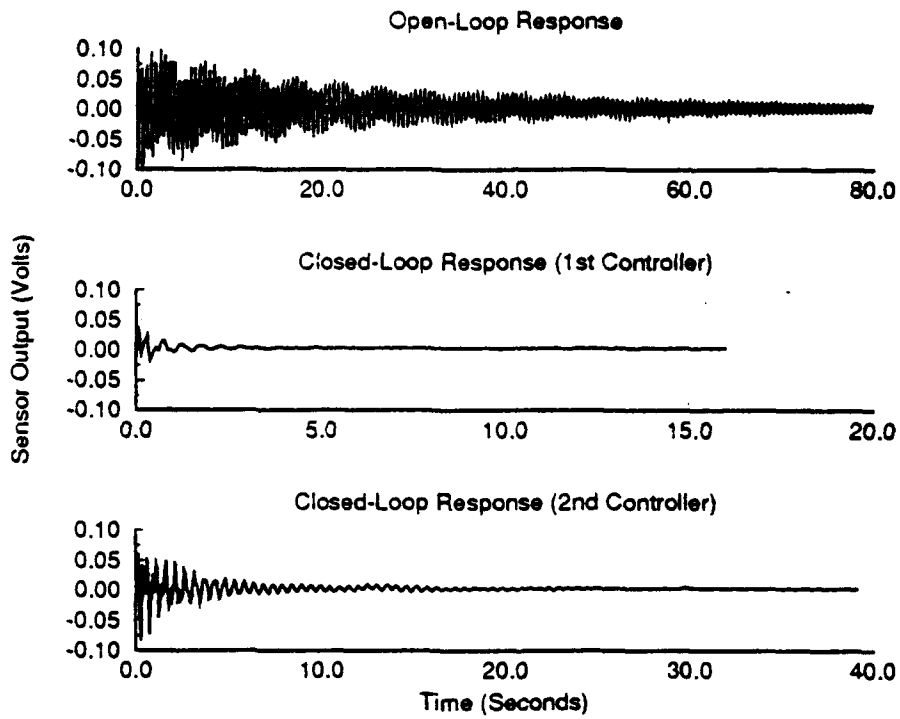


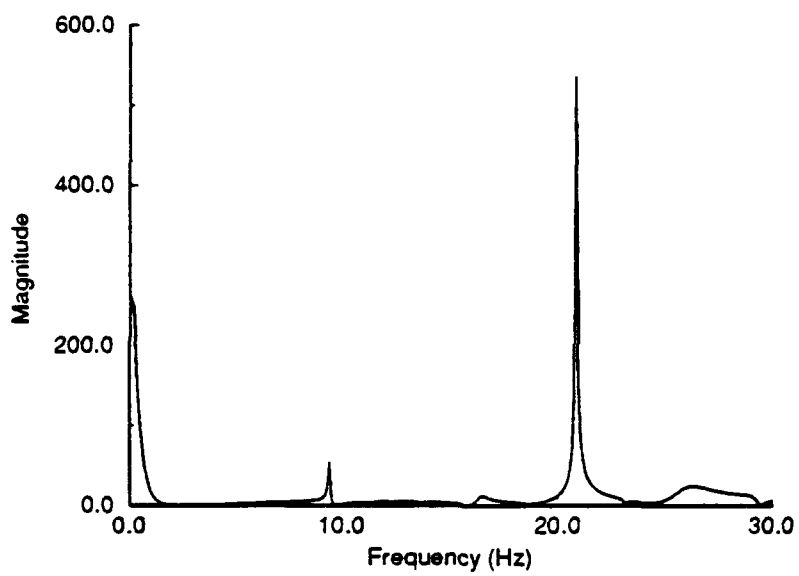


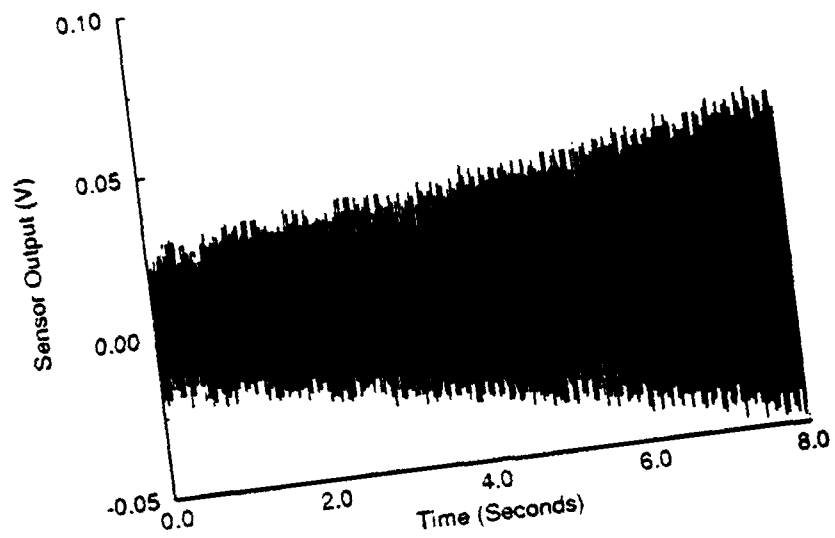












ACTIVE CONTROL OF A SLEWING FRAME USING SMART STRUCTURES

Donald J. Leo*, Daniel J. Inman**

**Research Assistant, Department of Mechanical and Aerospace Engineering
State University of New York at Buffalo, Buffalo, NY, 14260*

***Samuel Herrick Professor, Department of Engineering Science and
Mechanics, Virginia Polytechnic Institute and State University, Blacksburg, VA,
24061*

ABSTRACT

A testbed consisting of a flexible frame slewed by a dc motor is modeled for active vibration suppression. This presents a challenging control problem since the primary action of slewing induces both bending and torsional vibrations in the structure. Inserted into the frame are two active members that can be used as colocated sensor/actuators in feedback control loops. A theoretical study is conducted to obtain control laws that simultaneously slew the frame and suppress the residual vibrations. Simulation results indicate that the dc motor is effective in slewing the frame and suppressing the bending motion but not the torsional motion. Hence, the torsional vibrations are suppressed using the active members in colocated feedback loops.

INTRODUCTION

Slewing a flexible structure involves vibration suppression as well as accurate pointing and tracking. For simple structures such as flexible beams, both of these objectives can be obtained using a feedback loop consisting of the slewing actuator and angular rate and position sensors (Garcia [1]). A variety of control laws have been presented, some based on optimal control theory (Juang, *et al* [2]), others designed with Lyapunov methods (Junkins, *et al* [3], Fujii, *et al* [4]). For a structure that exhibits more complicated dynamics, slewing the structure and suppressing vibrations calls for a more sophisticated control

system. The increase in controller complexity is necessary since it is likely that not all of the flexible modes are easily controlled using the slewing actuator. A straightforward approach is to take advantage of recent developments in *smart structure control* and integrate active members into the slewing structure. Integrating active members into the structure provides additional sensors and actuators for feedback control and has been shown to improve performance (Garcia and Inman [5]). Vibration suppression and accurate pointing is accomplished using Multiple-Input-Multiple-Output (MIMO) control.

This approach is taken in the design of a control system for a slewing flexible frame. This is a challenging control problem since the slewing motion excites bending and torsional vibrations in the structure. Previous results illustrate the need for multiple control loops, since the torsional motion is difficult to suppress with the slewing actuator (Leo and Inman [6]). The ability to implement MIMO control is provided by replacing two passive members of the frame with active elements. The active members can be used in conjunction with the slewing actuator in non-colocated control loops, or they can be used as independent colocated sensor/actuators. This paper discusses the merits of each approach with regards to design, robustness, and performance.

MODELING OF THE SLEWING FRAME

The slewing frame is modeled as a set of second order ordinary differential equations of the form

$$\mathbf{M} \begin{Bmatrix} \ddot{\mathbf{r}}(t) \\ \ddot{\theta}(t) \end{Bmatrix} + \mathbf{D} \begin{Bmatrix} \dot{\mathbf{r}}(t) \\ \dot{\theta}(t) \end{Bmatrix} + \mathbf{K} \begin{Bmatrix} \mathbf{r}(t) \\ \theta(t) \end{Bmatrix} = \mathbf{B}_m i_a(t) + \sum_{i=1}^2 \mathbf{B}_{pi} v_{ai}(t) \quad (1)$$

where \mathbf{M} , \mathbf{D} , and \mathbf{K} are the $(n+1) \times (n+1)$ mass, damping and stiffness matrices derived from a finite element model consisting of the first n elastic modes of the frame. The modal coordinates are denoted $\mathbf{r}(t)$ and the rotation of the structure's rigid body about its axis is $\theta(t)$. The overdot represents differentiation with respect to time. Three inputs to the system exist: the slewing actuator and two active members. The $(n+1) \times 1$ forcing vectors for these actuators are \mathbf{B}_m , \mathbf{B}_{p1} , and \mathbf{B}_{p2} , respectively. The slewing actuator is a dc motor with armature current $i_a(t)$, v_{a1} and v_{a2} are the actuator voltages across the active members. The input to the motor is the armature voltage, $e_a(t)$. The relationship between the input voltage and the armature current is

$$L_a \frac{d}{dt} [i_a(t)] + R_a i_a(t) = -K_b \dot{\theta}_s(t) + e_a(t) \quad (2)$$

The parameters L_a and R_a are the inductance and resistance of the dc motor, and K_b is the back-*emf* constant. The angular rate of the slewing frame is denoted $\dot{\theta}_s(t)$. It differs from $\dot{\theta}(t)$ because it is the summation of the rigid body rotation and the rotation due to flexibility. The sensor outputs of the system are the angular rate and position of the frame, $\dot{\theta}_s(t)$ and $\theta_s(t)$, and the output signals of

the active members, $v_{ps1}(t)$ and $v_{ps2}(t)$. The outputs are can be related to the system coordinates and inputs by the expressions

$$\begin{aligned} \theta_s(t) &= \mathbf{C}_p \begin{Bmatrix} \mathbf{r}(t) \\ \theta(t) \end{Bmatrix} & \dot{\theta}_s(t) &= \mathbf{C}_v \begin{Bmatrix} \dot{\mathbf{r}}(t) \\ \dot{\theta}(t) \end{Bmatrix} \\ v_{ps1}(t) &= \mathbf{B}_{ps1}^T \begin{Bmatrix} \mathbf{r}(t) \\ \theta(t) \end{Bmatrix} + K_{fd1} v_{a1}(t) & v_{ps2}(t) &= \mathbf{B}_{ps2}^T \begin{Bmatrix} \mathbf{r}(t) \\ \theta(t) \end{Bmatrix} + K_{fd2} v_{a2}(t) \end{aligned} \quad (3)$$

where \mathbf{C}_p and \mathbf{C}_v are the $1 \times (n+1)$ output vectors corresponding to the angular position and rate, respectively. Since each active member is a colocated sensor/actuator, the output vector is simply the transpose of the input vector. The impedance mismatch between the active members and the structure is modeled as a feedthrough term, K_{fdi} , coupling the output directly to the input. The piezoceramics on the active members are coupled to ground through a resistor, thus creating a high-pass filter. The sensor signals from the active members, $v_{s1}(t)$ and $v_{s2}(t)$, are related to $v_{ps1}(t)$ and $v_{ps2}(t)$ by the following expression

$$V_{si}(s) = \frac{\tau_i s}{\tau_i s + 1} V_{psi}(s) = G_{hp}(s) V_{psi}(s) \quad (4)$$

where s is the Laplace operator and τ_i is the circuit's time constant. The model is displayed graphically in Figure 1. A complete derivation of this model is presented in Leo [7].

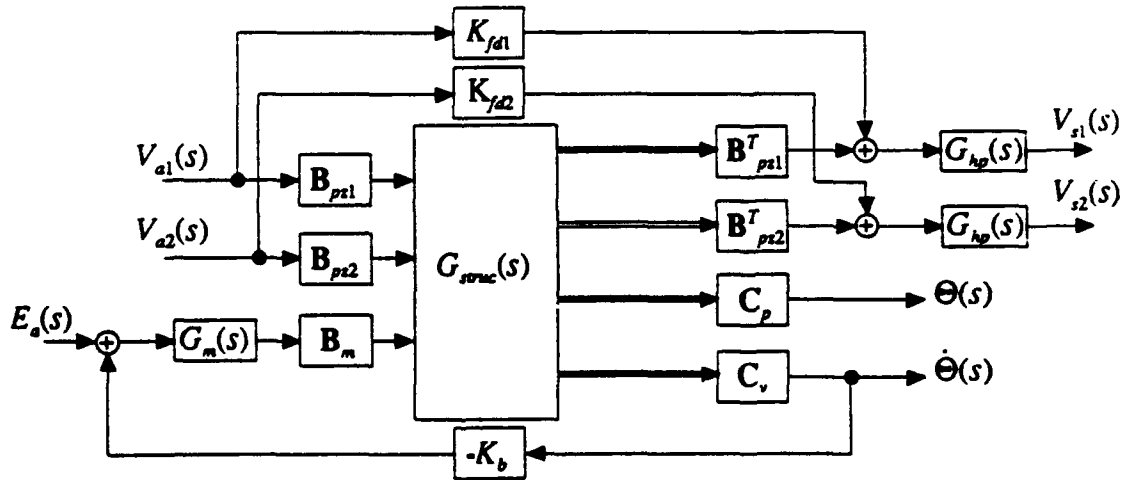


Figure 1: Block diagram of the slewing frame model.

In Figure 1, the following notation is used:

$$\begin{aligned} G_m(s) &= \frac{1}{L_s s + R_s} \\ G_{struct}(s) &= \{\mathbf{M}s^2 + \mathbf{D}s + \mathbf{K}\}^{-1} \end{aligned} \quad (5)$$

THE SLEWING FRAME TESTBED

A frame slewed by a dc motor is presented as a testbed for experiments in the control of slewing flexible structures. Due to its configuration, the action of rotating the frame about an axis causes both bending and torsional vibrations. The frame consists of individual elements of thin-walled circular aluminum tubing. Each member is 0.635 cm in diameter and has a wall thickness of 0.124 cm. The elements are joined at octagonal nodes that are also made of aluminum. Each member is pinned and bolted into the node to eliminate looseness in the joints. The frame is mounted onto the larger steel shaft by bolting two of the nodes into aluminum clamps.

The slewing actuator is an Electro-Craft 670 dc motor. The shaft of the motor is coupled to a steel shaft with a diameter of 0.635 cm, which in turn is connected to another steel shaft of diameter 1.270 cm. The smaller shaft can easily be removed so that gears can be placed between the motor and the structure. A tachometer housed inside the motor measures angular rate, and a potentiometer attached to the bottom of the larger steel shaft produces a signal proportional to angular position. The whole slewing rig is attached to a large concrete block that serves as ground. Figure 2 is a diagram of the slewing frame testbed.

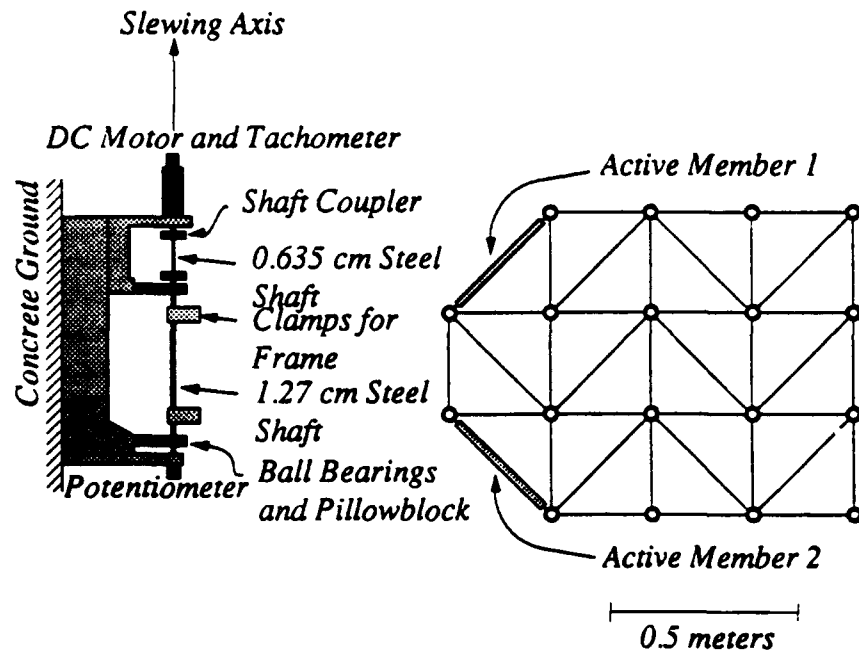


Figure 2: Slew frame testbed showing the location of the active members, angular rate and position sensors, and the dc motor.

Two of the passive elements of the frame have been replaced by active elements. The active members are flat aluminum bars that have four strips of piezoceramic material bonded to each side (see Figure 3). The piezoceramics are model G-1195 from Piezo Electric Products and have dimensions 6.350 cm

x 1.905 cm x 0.025 cm. Each ceramic is glued to the member with Duro Depend II adhesive. All of the piezoceramics are electrically coupled to one another to create one sensor/ actuator. On both active members, the aluminum beam is used as a ground for the underside of all the ceramics.

The parameters for the dc motor and the active members are listed in Table 1.

Table 1: Parameters for the slewing actuator and active members.

back emf constant	K_b	0.11298	V/rad/sec
feedthrough	K_{fd}	0.024	
motor inductance	L_a	0.002	H
motor resistance	R_a	0.63	Ohms
piezo thickness	t_{ps}	3.175 e-3	m
member thickness	t_s	2.54 e-4	m
circuit time constant	τ_s	0.275	seconds

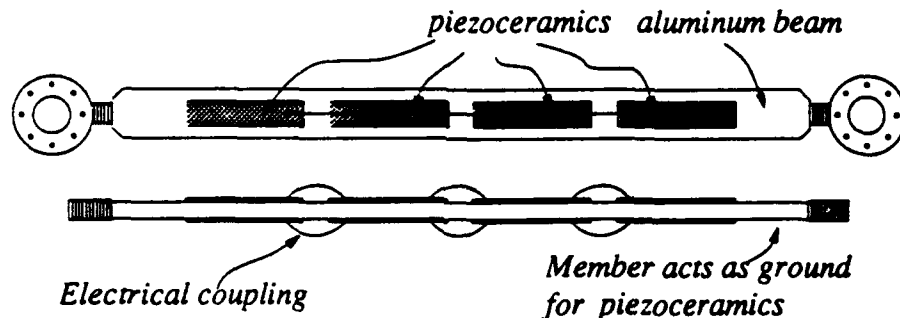


Figure 3: Piezoceramic active member.

CONTROL SIMULATIONS

The objective of this study is to develop control schemes for the slewing frame. The primary action of the frame is a rotation about its slewing axis, which, due to the flexibility and low inherent damping of the structure, induces vibrations that do not decay for a considerable amount of time. Using the model developed in this paper, control laws are designed that simultaneously slew the frame and suppress the vibrations. The simulations involve designing a controller that provides satisfactory step response. Important performance criteria include minimizing the settling time and overshoot of the frame's hub position, as well as suppressing the structural vibrations induced during the maneuver.

Consider the case of designing a controller to obtain satisfactory step response of the frame's hub position. The input command to the motor corresponds to a 15° slewing maneuver. Three designs are studied. The first is a simple Proportional-Derivative controller using the slewing actuator and angular rate and position feedback. The second control law has a non-colocated control loop using active member 2 in addition to the PD compensator. The final control

scheme involves two separate colocated controllers, one loop closed around the motor and the other loop closed around active member 2. All designs are performed using the nominal model shown in the previous section. Robustness is checked by closing the control loops around models that have slightly higher and lower natural frequencies [see Table 2]. While not an exhaustive search, this check indicates how well the controllers can tolerate uncertainty.

Table 2: First three natural frequencies (in Hz) for the nominal model and the perturbed models used for stability analysis during the simulations.

	Nominal	Model 1	Model 2
1st torsional	4.21	4.33	4.09
1st bending	7.17	7.33	7.00
2nd torsional	13.90	14.30	13.53

Proportional-Derivative Control

The procedure for designing this type of controller is rather straightforward, since both angular rate and position measurements are available. The form for the control law is

$$e_a(t) = K_p [\theta_{ref} - \theta(t)] - K_v \dot{\theta}(t) \quad (6)$$

where $\theta(t)$ and $\dot{\theta}(t)$ are the outputs of the potentiometer and tachometer, respectively. The reference voltage, θ_{ref} , commands a 15° slew. After iterating on the controller gains, values of $K_p = 2.5$ and $K_v = 40$ produce a satisfactory step response without exceeding the voltage limits on the motor (see Figure 4). The overshoot of the hub position is less than 5 % and the settling time is approximately 4 seconds.

The importance of examining this control design lies in its inability to suppress the torsional motion of the frame. This results in substantial residual vibrations after the end of the slewing maneuver, as illustrated by the output of active member 2 in Figure 4. This problem is due to the pole-zero cancellation that occurs in the transfer function between the motor and the tachometer/potentiometer outputs. As listed in Table 3, the PD compensator successively adds damping to the first bending mode, but leaves the torsional modes lightly damped. The ability to suppress the bending motion of the frame is due to the large interaction between the motor and the structure, as evidenced in the open loop magnitude plots.

Proportional-Derivative Compensation with Supplementary Non-Colocated Control

A natural extension of simple PD control is to use an active member as a non-colocated sensor for a supplementary feedback loop. The function of the supplementary control is to suppress the torsional motion of the frame while the PD compensator provides a satisfactory step response. Using the active member in this manner leads to the design of a control law for a non-colocated sensor and actuator. Similar actuator/sensor arrangements have been used in

the past (Juang, *et al.*, [2]), but with different design strategies and on structures that did not exhibit torsional vibrations.

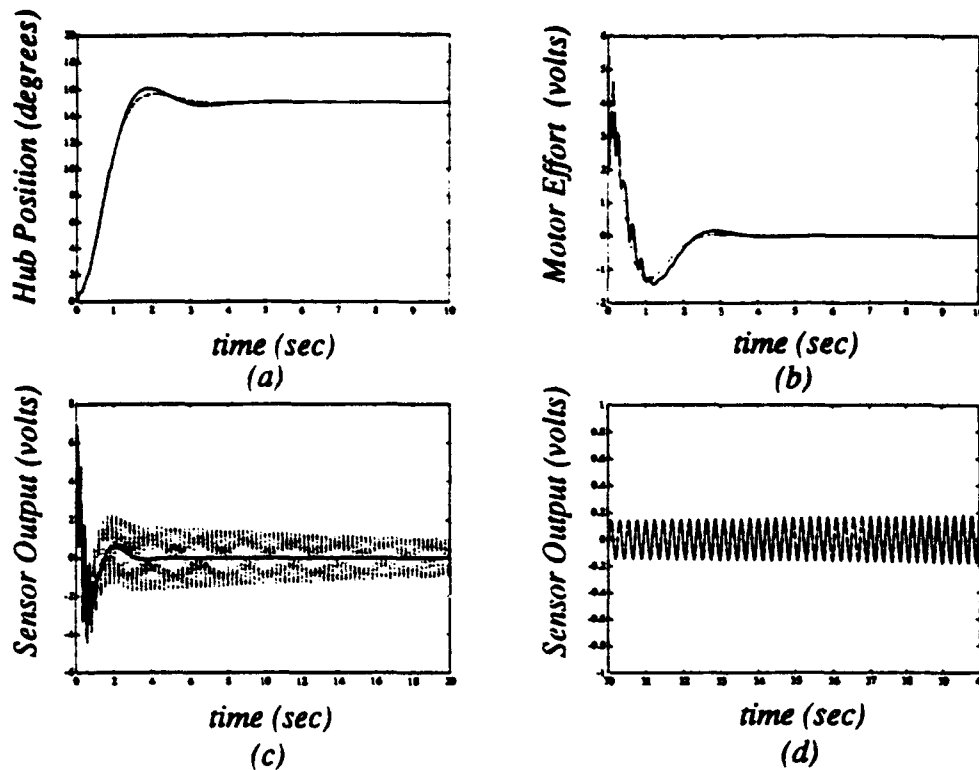


Figure 4: Simulated step responses for the slewing frame with PD control (dotted) and PD with supplementary GSF feedback (solid). (a) Hub position. (b) Motor control voltage. (c) Output of active member 1. (d) Output of member 2 showing instability due to model error.

Control law development is performed using a method called Generalized Structural Filtering (GSF). A detailed treatment of the GSF method is presented in Wie and Byun [8]. In its basic form, Generalized Structural Filtering is a classical control approach to active vibration suppression in that frequency domain and root locus techniques are used to find a suitable compensator. The design for the slewing frame is accomplished in the following manner. First, the model is used to find the transfer function between the motor input and the output of active member 2, with the PD control loop closed. Closing the first loop is important since it greatly effects the dynamics of the structure. The first stage of the design involves introducing a fourth order Butterworth Lowpass Filter into the forward loop with a corner frequency of 20 Hz. This attenuates the high frequency content of the signal but causes substantial phase lag in the target region, 0 to 20 Hz. Following the procedure outlined in Wie and Byun [8], a lead filter is then placed in the compensator to recover phase around the frequency of the first torsional mode (4 Hz). Finally, parameters of a non-minimum phase second order filter are chosen to actively damp the first torsional mode. The final form for the control law is

$$e_a(t) = 2.5[\theta_{ref} - \theta(t) - v_{gsf}(t)] - 40\dot{\theta}(t) \quad (7)$$

where $v_{gsf}(t)$ is the output of the GSF compensator. In the Laplace domain, it takes the form

$$V_{gsf}(s) = \frac{0.025 \left(\frac{s}{-15.8 \pm j42.1} + 1 \right) \left(\frac{s}{20} + 1 \right)}{\left(\frac{s}{48.1 \pm j116} + 1 \right) \left(\frac{s}{116 \pm j48.1} + 1 \right) \left(\frac{s}{14 \pm j37.5} + 1 \right) \left(\frac{s}{40} + 1 \right)} V_{z2}(s) \quad (8)$$

A root locus plot for the GSF design is shown in Figure 5a. From the roots locus, a gain of 0.025 is chosen since it increases the damping in the first torsional mode. An important feature of the root locus is that the damping in the first bending mode is being decreased as a result of the supplementary control loop. This is an unattractive feature of this method. The time responses of the slewing frame with supplementary control are shown in Figure 4. The rigid body response has slightly greater overshoot due to the added control effort in the motor. The motor voltages with and without supplementary control are similar, although a higher frequency component is added to the input due to the GSF compensator (Figure 4b). The marked difference with this control scheme is the suppression of the residual vibrations in the frame. With the supplementary control, the structural vibrations are negligible at the end of the slewing maneuver, which contrasts sharply with the case when there is only PD compensation (Figure 4c). The addition of the non-colocated GSF controller enables the suppression of the first torsional mode of the frame.

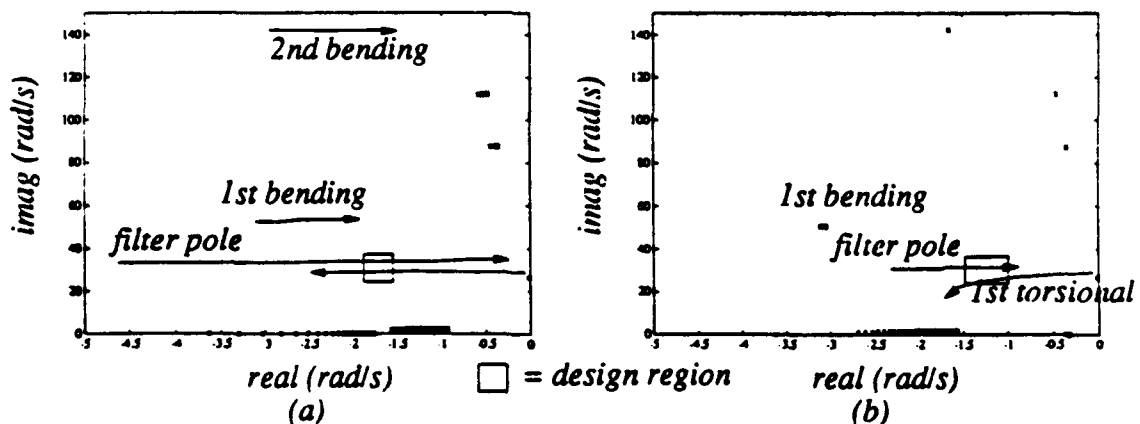


Figure 5: Root locus plots for the GSF design (a) and the PPF design (b). The PPF controller does not exhibit the spillover into the higher modes that occurs in the GSF compensation.

The robustness of this control strategy is checked by closing the loop around the perturbed models shown in Table 2. For both cases, an instability in the first torsional mode results. This is illustrated in Figure 4d, where it shows that the

frame is still vibrating almost forty seconds after the slewing maneuver is over. This vibration is due to the mode at 4 Hz being marginally stable. Checking the robustness in this manner indicates that the non-colocated control design is sensitive to the uncertainties that are bound to exist in the model. Attempts at redesigning the control law in light of these results could be made, but a more practical approach to achieving performance and robustness specifications is detailed in the next section.

Proportional-Derivative Compensation with Supplementary Colocated Control

The final design for satisfactory step response uses active member 2 as both a sensor and an actuator to provide vibration suppression. As in the previous case, a PD compensator is used to slew the frame, with the colocated control loop acting as supplementary feedback. The control law chosen for the active member is Positive Position Feedback. Much like the GSF method, Positive Position Feedback (PPF) consists of second order filters tuned to suppress specific structural modes. For a detailed treatment of the design procedure, the reader is referred to Fanson and Caughey [9]. PPF control is chosen since it is easy to design and is robust with respect to unmodeled dynamics (Goh and Caughey [10]). It has also been experimentally implemented in previous work (Fanson and Caughey [9]). In the Laplace domain, the form of the PPF controller is

$$V_s(s) = \left\{ \sum_{i=1}^{N_f} \frac{\omega_{fi}^2}{s^2 + 2\zeta_{fi}\omega_{fi}s + \omega_{fi}^2} \right\} V_r(s) \quad (9)$$

The parameters for the filter design are found using root locus techniques (see Figure 5b). The design procedure for PPF control is more straightforward than for the GSF method and requires much less iteration. In this case, the first torsional mode is targeted for suppression. An important feature of the control law is that the spillover into the high frequency modes of the system is almost negligible due to the controller roll-off. This contrasts with the GSF design, which decreases the damping in the first bending mode. After performing the analysis, the following control law is obtained

$$e_a(t) = 2.5[\theta_{ref} - \theta(t)] - 40\dot{\theta}(t)$$

$$V_{a2}(s) = \frac{1.6(31)^2}{s^2 + 2(0.08)(31)s + (31)^2} V_{s2}(s) \quad (10)$$

The first part of equation (10) is simply the PD compensator designed in the previous section, the second part is the PPF controller using active member 2 as a colocated sensor/ actuator. A simulated slewing maneuver is shown in Figure 6. The hub position response and motor voltage are essentially the same with and without PPF control. This is to be expected since the feedback loop is independent of the motor. With the supplementary control loop, the structural vibrations in the frame are suppressed by the time the slewing maneuver is over (Figure 6c). The damping out of the torsion is not as fast as with the GSF controller, but this is due to the fact that the motor is a much more powerful

actuator. During the design, the achievable damping was limited by the peak value of the active member control effort, which is approximately 100 volts (Figure 6d).

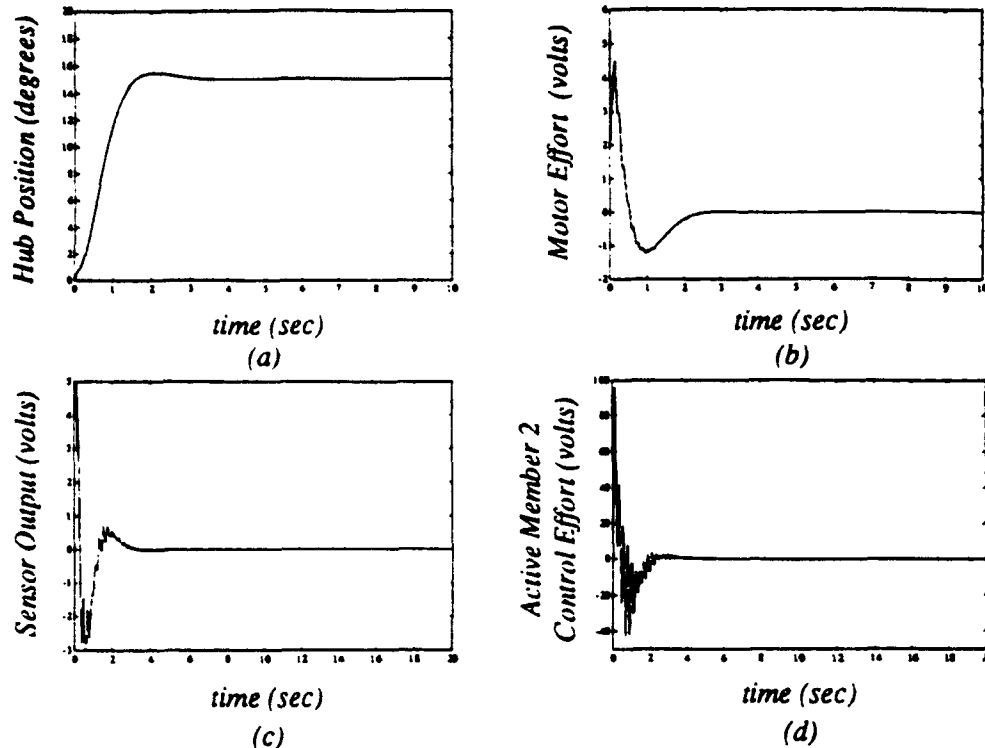


Figure 10: Simulated time responses for PD control with supplementary PPF feedback. (a) Hub position. (b) Motor control voltage. (c) Sensor output of active member 1. (d) Active member 2 control voltage.

The robustness tests are performed on this control scheme. The test is to close the feedback loops around the perturbed models listed in Table 2. For both cases, the system remains stable. This represents a major advantage over the non-colocated control, which results in an unstable system in the presence of model error.

Table 3: Comparison of the results for the three separate simulations.

Control Law	PD	PD + GSF	PD + PPF
Damping (%)			
1st torsional	0.2	8.2	4.8
1st bending	6.1	4.8	6.1
2nd torsional	0.4	0.5	0.4
Rigid Body Response			
settling time (seconds)	4 seconds	4 seconds	4 seconds
overshoot (degrees)	0.7	1.1	0.4
Stability Robustness ¹	Yes	No	Yes

¹ Defined as being stable with the perturbed models listed in Table 2.

Discussion of the Simulation Results

These simulations indicate the inability of a motor control law to suppress the torsional motion of the slewing frame. This is a result of a pole-zero cancellation that occurs between the motor input and the angular rate and position sensors. Physically, this means that the interaction between the input torque and the torsional modes is small. These modes can be suppressed, though, by integrating actuators and sensors into the structure. In one control law, the active member is used solely as a sensor in a non-colocated feedback loop. This achieves the desired vibration suppression, but is difficult to design and does not maintain stability in the presence of model error. Another approach is to use the active member in a colocated feedback loop, taking advantage of the piezoelectrics ability to actuate. This leads to a rather simple design that has negligible spillover into the higher modes. It is also more robust with respect to model uncertainty. The results of these simulations are consistent with initial experiments on the slewing frame (Leo and Inman [6]).

CONCLUSIONS AND FUTURE WORK

Integrating active members into complicated slewing structures is an effective means of suppressing vibrations during and after maneuvers. This is the result of a modeling and simulation study of a slewing frame. The distinctive feature of the slewing frame is that the torsional modes cannot be controlled using feedback loops consisting of the slewing actuator and angular rate and position sensors. Vibration suppression is achieved by using active members as sensors in non-colocated feedback loops, but this yields a difficult design that is sensitive to model error. A superior approach is to use the active members in colocated feedback loops with robust control laws such as Positive Position Feedback. When used in conjunction with a simple Proportional-Derivative compensator, this design produces satisfactory slewing maneuvers and simultaneously suppresses the structural vibrations.

Future work on this topic includes experimentally implementing active control schemes and studying the effects of actuator and sensor dynamics. The problem of controlling the slewing frame is well suited to the study of MIMO control systems.

ACKNOWLEDGMENT

This work is supported by AFOSR grant number 91-0181 under the direction of Dr. Spencer Wu.

REFERENCES

1. Garcia, E., "On the Modeling and Control of Slewing Flexible Structures," PhD Dissertation, Dept. of Mechanical and Aerospace Engineering, State University of New York at Buffalo, 1989.

2. Juang, J.N., and Horta, L.G., Robertshaw H.H., "A Slewing Control Experiment for Flexible Structures," *AIAA J. of Guidance, Control, and Dynamics*, v9, n5, pp. 599-607, 1986.
3. Junkins, J.L., Rahman, Z., and Bang, H., "Near-Minimum-Time Maneuvers of Flexible Vehicles: A Lyapunov Control Law Design Method," *Mechanics and Control of Large Flexible Structures* (ed. Junkins, J.L.), AIAA Press, pp. 565-593, 1990.
4. Fujii, H., Ohtsuka, T., Udou, S., "Mission Function Control for a Slew Maneuver Experiment," *AIAA J. of Guidance, Control, and Dynamics*, v.14, n5, pp. 986-1000. 1991.
5. Garcia, E., and Inman, D.J., "Advantages of Slewing an Active Structure," *J. of Intelligent Material Systems and Structures*, v1, n3, pp. 261-272, 1990.
6. Leo, D.J., and Inman, D.J., "Control of a Flexible Frame in Slewing," *Proc. of the American Control Conference*, 1992.
7. Leo, D.J., "Active Control of a Slewing Frame," M.S. Thesis, Dept. of Mechanical and Aerospace Engineering, State University of New York at Buffalo, 1992.
8. Wie, B., and Byun, K.W., "New Generalized Structural Filtering Concept for Active Vibration Control Synthesis," *J. of Guidance, Control, and Dynamics*, v12, n2, pp. 147-155, 1989.
9. Fanson, J.L., and Caughey, T.K., "Positive Position Feedback Control for Large Space Structures," *Proc. of the 28th Structural, Dynamics, and Materials Conference*, pp. 588-98, 1987.
10. Goh, C.J., and Caughey, T.K., "On the Stability Problem Caused by Finite Actuator Dynamics in the Colocated Control of Large Space Structures," *Int. J. of Control*, v 41 n3, pp. 787-802, 1985.



The American Society of
Mechanical Engineers

Reprinted From
DE-Vol. 58, Intelligent Structures,
Materials, and Vibrations
Editors: Mo Shahinpoor, and H. S. Tzou
Book No. G00819 - 1993

VIBRATION SUPPRESSION BY MODULATION OF ELASTIC MODULUS USING SHAPE MEMORY ALLOY¹

Daniel J. Segalman
Sandia National Labs.
Albuquerque, New Mexico

Gordon G. Parker
Dept. of Mechanical and
Aerospace Engineering
State University of New York
Buffalo, New York

Daniel J. Inman
Department of Engineering Science and Mechanics
Virginia Polytechnic Institute and State University
Blacksburg, Virginia

ABSTRACT

A method is proposed for suppressing the resonances that occur as an item of rotating machinery is spun-up from rest to its operating speed. This proposed method invokes "stiffness scheduling" so that the resonant frequency of the system is shifted during spin-up so as to be distant from the excitation frequency. A strategy for modulating the stiffness through the use of shape memory alloy is also presented.

INTRODUCTION

Most common applications of "smart materials" actuators involves obliging them to undergo some generalized displacement in response to a specified stimulus. A slightly different approach is suggested in this paper. Here, we consider an application in which a modulus rather than a displacement is manipulated. Further, we present a class of problems for which such a smart material can be used to address very simply a problem of rotating equipment.

The first portion of this paper proposes a method of fabricating a material whose modulus can be changed substantially through the application of a specified stimulus. The particular implementation presented here indirectly exploits the large deformation associated with shape memory alloys to achieve the desired modulation of stiffness.

The next portion of this paper discusses a class of vibration problems for which such materials have a serious potential for vibration suppression. These are problems, such as the spinning up of rotating machinery, in which the excitation at any time lies within a narrow frequency band, and that band moves through the frequency spectrum in a predictable manner.

Finally, an example problem is examined and the utility of this approach is discussed.

A SMART MATERIAL WITH MODULATED ELASTIC MODULUS

Here we present an approach for modulating the elastic moduli of materials by introducing a reinforcing material whose contribution to the stiffness of the composite can be turned on and off. We first consider an elastic matrix structure through which an array of holes has been drilled. Then strands of shape memory alloy (SMA) are threaded through the holes and knobs (or knots) are placed at the ends of the strands, leaving just a little slack. (See Figure 1 and Figure 2.) Since the SMA can move freely through the matrix, it contributes nothing to the stiffness of the composite structure.

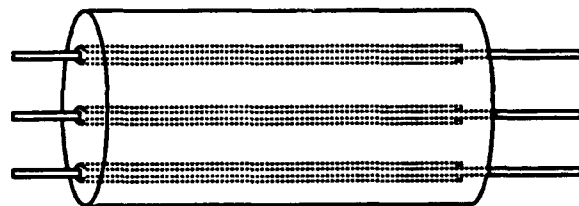


FIGURE 1. THE MATRIX MATERIAL WITH HOLES THROUGH WHICH SMA IS THREADED. THE FREE MOVEMENT OF THE SMA WITH RESPECT TO THE MATRIX PREVENTS IT FROM CONTRIBUTING TO THE STIFFNESS OF THE COMPOSITE STRUCTURE.

We now take advantage of a fundamental feature of shape memory alloy: when shape memory alloy is subjected to a change of temperature it is caused to jump to an equilibrium phase appropriate to that temperature. In particular, it can be switched from the extended, stress-free state shown in Figure 2 to the shortened state

¹ Work supported by the U.S. Department of Energy at Sandia National Laboratories under Contract DE-AC0476DP00789

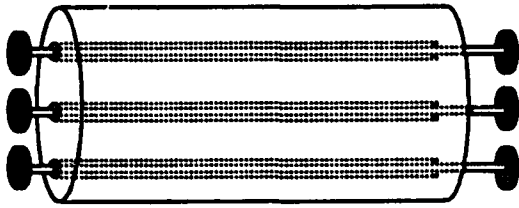


FIGURE 2. THE MATRIX MATERIAL WITH HOLES THROUGH WHICH SMA IS THREADED. EVEN THOUGH THERE ARE KNOBS ON THE ENDS OF THE SMA STRANDS, THERE IS STILL ENOUGH SLACK TO PERMIT FREE MOVEMENT. AGAIN, THE FREE MOVEMENT OF THE SMA WITH RESPECT TO THE MATRIX PREVENTS IT FROM CONTRIBUTING TO THE STIFFNESS OF THE COMPOSITE.

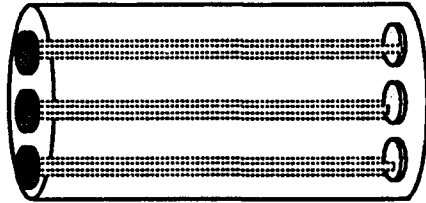


FIGURE 3. THE MATRIX MATERIAL WITH HOLES THROUGH WHICH SMA IS THREADED. THE SMA HAS BEEN ACTIVATED, CAUSING A JUMP TO A PHASE WITH A SHORTER EQUILIBRIUM LENGTH, TAKING UP ALL SLACK. THE KNOBS ARE NOW PRESSING AGAINST THE MATRIX MATERIAL, COMPLETELY COUPLING EXTENSIONAL DEFORMATIONS OF THE TWO MATERIALS.

shown in Figure 3. In the shortened state, all slack is taken up, the knobs are pulled into the matrix, and the SMA is in tension.

This state, in which the SMA is contracted, the knobs fully couple the extensional deformation of the SMA to that of the matrix material. One may now use any one of the standard formulae to estimate the extensional modulus of the composite structure. A good review of alternative methods of performing these calculations is presented by Christensen (1991). A first approximation of the stiffening effect of the SMA is obtained by assuming uniform strains within the composite. This analysis results in a stiffness increase proportional to the relative stiffness of the SMA and the matrix material, to the ratios of the cross sectional areas of the SMA and the matrix materials, and to the percentage of the SMA strands that have been activated to contract.

The phase transformations of the SMA is reversible, so that a return to the previous temperature will result in a return to the configuration shown in Figure 2. By raising and dropping temperature, one can cause repeated reversals in the stiffness of the composite. The issue of response time becomes primarily an issue of the rates of heating and cooling. Heating is usually achieved by running a current through the SMA itself while cooling is usually achieved through convective and diffusive processes. However, response times can be accelerated by using more aggressive cooling techniques (Zerkus 1992).

It is important to note that the effect that is being targeted here is to modulate stiffness rather than to impose a deformation, as has been done often before; see Lagoudas and Tadjbakhsh (1992). A. Baz et al (1992) have used shape-memory alloy embedded in a composite to achieve a more gradual modulation in stiffness, exploiting primarily the modulus change accompanying phase change.

Because applications described below require a change in modulus just from one stage of a transient spinning process to another, rather than within each rotation, particularly fast response times are not necessary.

It should be noted that the strategy presented above for modulating the stiffness of a composite structure could be applied with materials other than shape memory alloy, so long as those materials can be caused to undergo large static deformation through some outside stimulus. Classes of such materials besides shape memory alloys include thermo-elastic, piezo-electric, and magnetostrictive materials.

A further note should observe that the crude configuration shown above could be extended by placing the SMA near the surface of a beam, and staggered along the length of the beam. This configuration, shown in Figure 4, permits effective modulation of the bending modulus of the beam. If the beam is originally in a spiral configuration, one now has a spring whose stiffness is modulated.

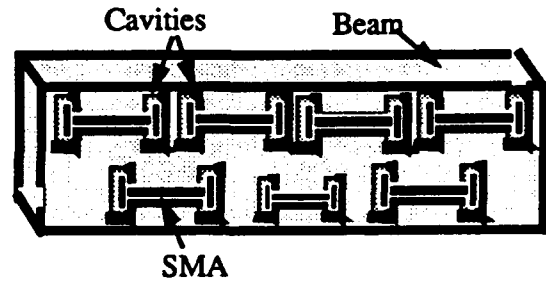


FIGURE 4. A STAGGERED CONFIGURATION OF SMA FILLERS IN AN ELASTIC MATRIX.

APPLICATION TO A CLASS OF VIBRATION PROBLEMS

General Problem Description

The vibration suppression capabilities of the smart material described above will be demonstrated by application to a class of rotating vibration problems. This class of problems is defined by the excitation frequency of the system being an integer multiple, n , of the angular velocity of the system so that during spin-up, the excitation frequency passes through the natural frequency of the system.

Paradigm Problem Description

We consider here the simplest such case, that of a rigid disk pinned to a rigid shaft. The connection includes a keyway so that the disk must rotate with the shaft, though it may wobble from side to side. A torsional spring serves to restore the disk to its normal configuration. This simple model, used in other dynamics analysis

by Chen and Bogy(1992), is meant to account in a very approximate way for shaft or disk flexibility. The disk rotates between frictionless spring loaded plates. A number, n , of small sinusoidally shaped projections on the surface of the disk cause a sinusoidal excitation. The torsional spring is oriented such that a line connecting the peaks of the projections on the disk would be perpendicular to the axis of rotation of the torsional spring. This system is shown in Figure 5.

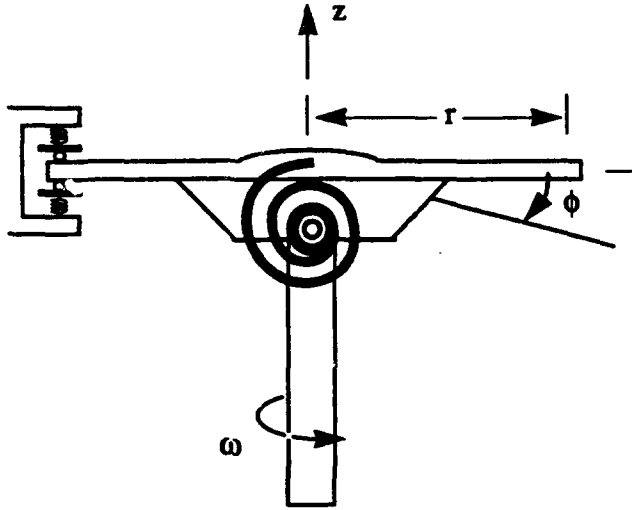


FIGURE 5. DISK/SHAFT SYSTEM.

The governing equations can be derived in many ways (the authors have used the method presented by Segalman and Dohrmann (1990). The equation for the angle ϕ , by which the disk is off normal is:

$$I_{yy}\ddot{\phi} + c\dot{\phi} + \phi(\beta k + I_{yy}\omega^2) = A \sin(n\omega t) \quad (1)$$

The multiplier β is ordinarily unity, but will be used later on as a "stiffening" multiplier. An interesting feature of this system is that the excitation frequency at resonance is:

$$\omega^2 = \frac{k}{I_{yy}} - \frac{(c/2I_{yy})^2}{n^2 - 1} \quad (2)$$

so that excitation will pass through the damped natural frequency of the system only for n greater than one.

The following quantities are used to make the equation of motion dimensionless:

$$\omega_o = \sqrt{\frac{k_o}{I_{yy}}} \quad \text{natural frequency for the nonspinning system.}$$

$$\alpha = \frac{\omega}{\omega_o} \quad \text{dimensionless frequency}$$

$$T = \omega_o t \quad \text{dimensionless time}$$

$$\xi = \frac{c}{2I_{yy}\omega_o} \quad \text{dimensionless damping ratio}$$

$$\bar{A} = \frac{A}{\omega_o^2 I_{yy}} \quad \text{dimensionless excitation amplitude}$$

$$\Phi(T) = \phi\left(\frac{t}{\omega_o}\right) \quad \text{dimensionless deflection amplitude}$$

The dimensionless equation of motion is:

$$\Phi'' + 2\xi\Phi' + (\beta + \alpha^2)\Phi = \bar{A} \sin(n\alpha T) \quad (3)$$

Stiffness modulation will be affected by changing β , representing a gain factor for stiffness.

The spin-up profile for the class of problems considered is:

$$\omega = \begin{cases} rt & 0 < t < t_o \\ rt_o & t > t_o \end{cases} \quad (4)$$

This spin-up profile causes the differential equation of motion to contain coefficients which are explicit functions of time, and the forcing sinusoid to be a function of t^2 . The ramping nature of the forcing function contains a narrow band of frequencies about the instantaneous frequency of $nr t$. This results in the system's damped natural frequency being excited prior to the intersection of the instantaneous excitation frequency and the system's damped natural frequency.

SMART MATERIAL APPLICATION – STIFFNESS SCHEDULING

Stiffness scheduling is defined as adapting the stiffness of the structure to reduce disturbance sensitivity. (This approach has been investigated by Viderman and Porat (1987) and by Nagaya et al (1987), in which the stiffnesses at the supports of rotors are modulated.) Since the smart material described above can take on two distinct elastic moduli, the system will have two distinct damped natural frequencies. If the frequency responses for these two systems can be sufficiently separated, then the frequency response of the smart system can be greatly reduced.

Here we consider a system with the following dimensionless parameters:

$$\xi = 0.02$$

$$n = 2$$

$$\bar{A} = 0.1$$

$$\alpha = \begin{cases} rT & 0 < T < 200.0 \\ 200r & T > 200.0 \end{cases}$$

$$r = 0.005$$

A fourth order Runge-Kutta method was used to integrate the governing equation for this system for three cases:

- the dimensionless stiffness is set to a higher value;
- the dimensionless stiffness β is set to a relatively low value;
- and dimensionless stiffness is appropriately switched during the ramp up of spin.

RESULTS

Figure 6 shows the dimensionless tilt as a function of dimensionless time for the case where the torsional spring is held in a stiffer mode throughout: $\beta = 4$. For that case, a large resonance behavior is seen near a dimensionless time of 120. A beating occurs for a while after the shaft reaches its terminal speed. More significantly, a fairly large oscillation remains at long times, after the disk has reached terminal speed.

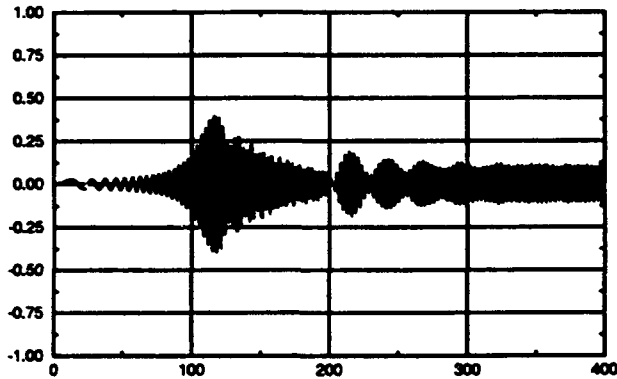


FIGURE 6. STIFFENING ACTUATOR TURNED ON THROUGHOUT SPIN-UP.

Figure 7 shows the corresponding curve for the case of $\beta = 1$. As expected, the resonance-like behavior occurs earlier in the process, when the excitation frequencies are lower. It is important that the behavior at long times manifests much lower amplitudes than is the case with the stiffer spring. This difference occurs because the natural frequency in this case is further from the steady state forcing frequency.

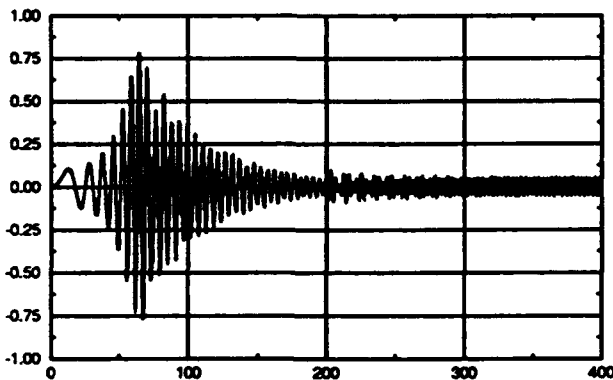


FIGURE 7. STIFFENING ACTUATOR TURNED OFF THROUGHOUT SPIN.

Figure 8 shows the dimensionless tilt as a function of dimensionless time where the stiffness parameter, β , is initially held at a value of 1.0 and instantaneously changed to a value of 4.0 at dimensionless time 98.0.

Note that the maximum amplitude in the resonance regime is slightly more than halved and that the long term oscillations are substantially lower in amplitude than those of the stiff system. Of course, this high frequency response is due to the stiffness of the

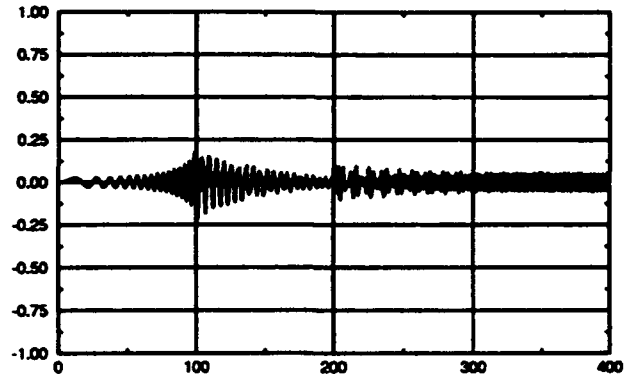


FIGURE 8. AMPLITUDE RESPONSE WITH STIFFNESS SCHEDULING.

structure at long times being that of the material shown in Figure 7, and the forced response at those frequencies are similar.

CONCLUSIONS

The smart material described here can be used in conjunction with stiffness scheduling to give a reduction in vibration amplitude for a class of rotating systems where the excitation is proportional to the spin rate. The time at which to change stiffness is based on the spin-up profile being known in advance. This permits the best switching time to be chosen based on the frequency components of the excitation and the stiffness switching transients.

FUTURE WORK

A control law for choosing the stiffness switching time is being developed which does not require exact knowledge of the spin-up profile. Further, basic work in the materials issues of such actuators must be done.

REFERENCES

- Baz, A., Poh, S., Ro, J., Mutua, M., Gilheany, J., 1992, "Active Control of Nitinol-Reinforced Composite beam", *Intelligent Structural Systems*, H.S. Tsou and G.L. Anderson editors, Kluwer Academic Publishers, the Netherlands, pp. 169-212.
- Chen, J-S. and Bogy, D.B., 1992, "Mathematical Structure of Modal Interactions in a Spinning Disk-Stationary Load System", *Journal of Applied Mechanics, Transactions of the ASME*, Vol. 59, pp. 390-397.
- Christensen, R.M., 1991, *Mechanics of Composite Materials*, Krieger Publishing Company, Malabar, Florida.
- Lagoudas, D.C. and Tadjbakhsh, I.G., 1992, "Active Flexible rods with embedded SMA fibers", *Smart Materials and Structures I*, pp. 162-167.
- Nagaya, K., Takeda, S., Psukui, Y., Kumaido, T., 1987, "Active Control Method for Passing Through Critical Speeds of Rotating Shafts by Changing Stiffness of the Supports With Use of Memory Metals", *Journal of Sound and Vibration*, Vol. 113, pp. 307-315.
- Segalman, D.J. and Dohrmann, C.R., 1990, "Dynamics of Rotating Flexible Structures by a Method of Quadratic Modes", Sandia Report: SAND90-2737.

Videman, Z. and Porat, I., 1987, "An Optimal Control Method for Passage of a Flexible Rotor Through Resonances", *Journal of Dynamic Systems Measurement and Control*, Vol. 109, pp. 216-223.

Zerkus, M. and Akers, J., 1992, "Thermoelectrically Controlled Shape Memory Alloy Actuators", *Proceedings of the Conference on Recent Advances in Adaptive and Sensory Materials and their Applications*, held at Virginia Polytechnic Institute and State University, Blacksburg, Virginia, April 27-29.